

Comprehensive glycoprofiling of oral tumours associates *N*-glycosylation with lymph node metastasis and patient survival.

Carolina Moretto Carnielli ¹, Thayná Melo de Lima Moraes ², Fábio Malta de Sá Patroni ³, Ana Carolina Prado Ribeiro ^{4,5}, Thaís Bianca Brandão ⁴, Evandro Sobroza ⁴, Leandro Luongo Matos ⁶, Luiz Paulo Kowalski ^{7,8}, Adriana Franco Paes Leme ^{1*}, Rebeca Kawahara ^{9,10##}, Morten Thaysen-Andersen ^{9,10,11##}

¹ Laboratório de Espectrometria de Massas, Laboratório Nacional de Biociências (LNBio), Centro Nacional de Pesquisa em Energia e Materiais (CNPEM), Campinas, 13083-970 SP, Brazil.

² Oral Pathology, Department of Oral Diagnosis, Piracicaba Dental School, University of Campinas, Brazil.

³ Molecular Biology and Genetic Engineering Center, University of Campinas, Campinas, Brazil.

⁴ Serviço de Odontologia Oncológica, Instituto do Câncer do Estado de São Paulo, ICESP-FMUSP, São Paulo, 01246-000 SP, Brazil.

⁵ Universidade Brasil, Fernandópolis, 15600-000 SP, Brazil.

⁶ Serviço de Cirurgia de Cabeça e Pescoço, Instituto do Câncer do Estado de São Paulo, ICESP-FMUSP, São Paulo, 01246-000 SP, Brazil.

⁷ Departamento de Cirurgia de Cabeça e Pescoço e Otorrinolaringologia, A.C. Camargo Cancer Center, São Paulo, SP, 01509-900, Brazil.

⁸ Departamento de Cirurgia de Cabeça e Pescoço, Faculdade de Medicina, Universidade de São Paulo - USP, São Paulo, SP, 01246-903, Brazil.

⁹ School of Natural Sciences, Macquarie University, Sydney, NSW-2109, Australia

¹⁰ Biomolecular Discovery Research Centre, Macquarie University, Sydney, NSW-2109, Australia

¹¹ Institute for Glyco-core Research (iGCORE), Nagoya University, Nagoya, 464-8601, Japan

These authors contributed equally to this work.

*Joint corresponding authors.

E-mails: adriana.paesleme@lnbio.cnpem.br; rebeca.kawaharasakuma@mq.edu.au; morten.andersen@mq.edu.au

Abstract

While altered protein glycosylation is regarded a trait of oral squamous cell carcinoma (OSCC), its heterogeneous glycoproteome and dynamics with disease progression remain unmapped. To this end, we here employ an integrated multi-omics approach comprising unbiased and quantitative glycomics and glycoproteomics applied to a valuable cohort of resected tumour tissues from OSCC patients with (n = 19) and without (n = 12) lymph node metastasis. While all tumour tissues displayed uniform *N*-glycome profiles suggesting relatively stable global *N*-glycosylation during lymph node metastasis, glycoproteomics and advanced correlation analysis notably uncovered altered site-specific *N*-glycosylation and

previously unknown associations with several key clinicopathological features. Importantly, focused analyses of the multi-omics data unveiled two *N*-glycans and three *N*-glycopeptides that were closely associated with patient survival. This study provides novel insight into the complex OSCC tissue *N*-glycoproteome forming an important resource to further explore the underpinning disease mechanisms and uncover new prognostic glyco-markers for OSCC.

Teaser

Deep survey of the dynamic landscape of complex sugars in oral tumours paves a way for new prognostic disease markers.

ABBREVIATIONS

ACN: acetonitrile; DTT: dithiothreitol; EIC: extracted ion chromatogram; EPPS: *N*-(2-hydroxyethyl)piperazine-*N'*-(3-propanesulfonic acid); FA: formic acid; FDR: false discovery rate; FFPE: formalin-fixed paraffin-embedded; FWHM: full width half maximum; HCD: higher energy collision-induced dissociation; HLB: hydrophilic – lipophilic-balanced; IAA: iodoacetamide; LC: liquid chromatography; LTQ: linear trap quadrupole; MS: mass spectrometry; N0: absence of lymph node metastasis; N+: presence of lymph node metastasis; NCE: normalised collision energy; OSCC: oral squamous cell carcinoma; PGC: porous graphitised carbon; PMSF: phenylmethylsulfonyl fluoride; PSM: peptide-to-spectrum match; PVDF: polyvinylidene fluoride; SPE: solid phase extraction; TFA, trifluoroacetic acid; TIC: total ion chromatogram; ZIC-HILIC: zwitterionic hydrophilic interaction liquid chromatography.

MAIN TEXT

Introduction

Oral squamous cell carcinoma (OSCC) is the most common type of head and neck cancer (1). With more than 377,000 new cases and 170,000 deaths annually worldwide, OSCC is an aggressive disease with a dishearteningly low five-year survival rate of 50% (2, 3), mainly due to lymph node metastasis and loco-regional failures. OSCC prognostication is currently based on the clinical staging system of tumour-lymph node-metastasis (TNM system) of the disease. However, this system has several flaws, as patients assigned with the same TNM stage may present with different clinical features and experience different outcomes (4, 5). Thus, identification of molecular signatures that may assist in a more precise staging and prognosis of patients with OSCC is urgent needed.

Histopathological analysis of formalin-fixed paraffin-embedded (FFPE) tissues remains the principal method for diagnosis and prognosis of OSCC patients (6, 7). FFPE tissue slides preserve the cellular morphology and molecular features of the tumour tissues, and have therefore been explored as a source for biomarker investigations (8, 9). We recently used sensitive mass spectrometry (MS)-based proteomics to map different areas of FFPE tissues from OSCC patients, which revealed key proteins with potential prognostic value as demonstrated by their associations with various clinicopathological parameters; the prognostic value of these proteins was also demonstrated by targeted proteomics of saliva from OSCC patients with and without lymph node metastasis (10). Our findings also revealed that specific glycoproteins i.e. ITGAV and COL6A1 from the tumour stroma, and COL1A2 from tumour cells associate with lymph node metastasis and type of disease treatment, which collectively point to the involvement of protein glycosylation in OSCC and suggest that glycoproteomics may augment OSCC prognostication.

Despite the growing list of candidate biomarkers reported for oral cancer, none has to date been implemented to aid the clinical decision-making, but further evaluation studies are underway

98 and may eventually provide a path towards clinically robust biomarkers for improved disease
99 management (11).

100 Evidence is emerging that not only the protein abundance, but also the glycosylation
101 patterns and levels of the underlying glycosylation enzymes, are altered in OSCC (12, 13).
102 Moreover, glycosylation changes have previously been associated with altered adhesion behaviour,
103 migration and metastasis of oral cancer cells as well as OSCC disease progression (13–15).
104 Aberrant *N*-glycosylation of E-cadherin, a key marker of epithelial mesenchymal transition in
105 cancer development (16), and reduced adhesion of human salivary epidermoid carcinoma cells were
106 found to result from the overexpression of dolichol-P-dependent *N*-acetylglucosamine-1-phosphate
107 transferase (DPAGT1), an enzyme that initiates the synthesis of the lipid-linked oligosaccharide
108 precursor for protein *N*-glycosylation in the endoplasmic reticulum (17). Overexpression of
109 DPAGT1 detected in specimens from resected OSCC tumours in the oral cavity was also found to
110 be associated with an aberrant activation of the canonical Wnt signalling pathway that contributes
111 to the development and progression of many human cancers (14, 18, 19). Moreover, site-specific
112 glycoprofiling of a gingival carcinoma cell line uncovered elevated sialylation and reduced
113 fucosylation relative to a non-cancerous oral epithelial cell line from gingiva (20). The study also
114 revealed that B7-H3 (also known as B7 homolog 3 or CD276 isoform 1) knockdown suppresses
115 tumour cell proliferation, and that B7-H3 restoration enhances tumour growth. Finally, elevated
116 sialidase activity was observed in saliva of oral cancer patients as compared to healthy individuals
117 and patients with precancerous conditions (21). While these studies collectively indicate that
118 aberrant protein glycosylation is linked to the onset and progression of oral cancer, altered
119 glycosylation has not previously been associated with patient prognosis including lymph node
120 metastasis status and survival outcome.

121 Herein, we employ an integrative glyco-centric multi-omics approach to quantitatively
122 profile the heterogenous *N*-glycoproteome in tumour tissues from OSCC patients with (N+) or
123 without (N0) lymph node metastasis to establish the glycan fine structures, their site-specific
124 microheterogeneity, and their disease dynamics. Our study is the first to unpick the OSCC *N*-
125 glycoproteome; we report on novel associations between altered *N*-glycosylation and key clinical
126 features including lymph node metastasis and patient survival, and provide a comprehensive
127 resource to further explore the underpinning disease mechanisms and uncover new disease markers
128 for OSCC.

131 Results

132 Comprehensive *N*-glycoprofiling of OSCC tumours from patients with and without lymph 133 node metastasis

134 This study applied an integrative MS-driven multi-omics approach comprising both
135 quantitative glycomics and glycoproteomics to comprehensively profile the protein *N*-glycosylation
136 in FFPE tumour tissues surgically removed from 31 patients operated with curative intent due to
137 OSCC, including patients with (N+, $n = 19$) and without (N0, $n = 12$) lymph node metastasis, Figure
138 1 and Supplementary Figure S1. See Supplementary Table S1-S2 for patient metadata and overview
139 of the generated LC-MS/MS datasets, respectively.

141 Comparative *N*-glycome profiling of OSCC tissues from N+ and N0 patients

142 State-of-the-art quantitative *N*-glycomics of proteins extracted from the OSCC tumour
143 tissues was used to profile, with glycan fine structural resolution, a total of 83 *N*-glycan structures
144 spanning 52 *N*-glycan compositions (denoted Glycan 1-52 with isomers denoted a, b, c...). See
145 Supplementary Figure S2 for a map of the identified *N*-glycan structures and Supplementary Table
146 S3 and Supplementary File S1 for tabulated glycomics data and spectral evidence, respectively.

147 Mainly complex (38.7-61.5%), oligomannosidic (18.3-36.5%) and paucimannosidic (9.8-
148 31.9%) *N*-glycans were identified across the OSCC tumour tissues, Figure 2A and Supplementary
149 Figure S3. Despite minor fold-change differences between N+ and N0 patients (-0.82 to 0.94), no
150 prominent differences were observed in the *N*-glycan type distribution nor in the common *N*-glycan
151 structural features such as the degree of branching and levels of fucosylation and sialylation (all p
152 ≥ 0.05), Figure 2B. Uniform global *N*-glycosylation across the N0 and N+ tissues was further
153 demonstrated using pair-wise *N*-glycome correlation analysis, PCA and hierarchical clustering
154 analysis, Supplementary Figure S4 and Supplementary Table S4.

155 Despite notable *N*-glycome similarities, differential expression was observed for six
156 individual *N*-glycan structures ($p < 0.05$) including one down-regulated *N*-glycan (Glycan 34) and
157 five up-regulated *N*-glycans (Glycan 20a, Glycan 40a, Glycan 45b, Glycan 46a, Glycan 49b) in N+
158 compared to N0 tissues, Supplementary Table S3. Interestingly, these differentially expressed *N*-
159 glycans were able to accurately stratify the N0 and N+ patients with confidence using a logistic
160 regression model (AUC values ranging from 67.5-85.5%), and, in part, also by a random forest
161 model (AUC values from 49.1% to 70.2%), Supplementary Figure S5.

162 **Comparative *N*-glycoproteome profiling of OSCC tumour tissues from N+ and N0 patients**

163 Guided by the acquired *N*-glycomics data, we then explored the glycoproteome complexity
164 of the OSCC tumour tissues using our recently developed glycomics-informed glycoproteomics
165 method (22). A total of 3,117 unique *N*-glycopeptides (i.e. glycopeptides carrying a discrete glycan
166 composition at a discrete site) displaying 55 different *N*-glycan compositions from 419 different
167 source *N*-glycoproteins spanning a wide dynamic range were profiled across the OSCC tissue
168 cohort, Figure 3A and Supplementary Table S5-S6.

169 In line with the *N*-glycome data, most *N*-glycopeptides carried complex/hybrid (67.9%) or
170 oligomannosidic (28.6%) *N*-glycans, Figure 3B. The under-representation of paucimannosidic *N*-
171 glycopeptides in the glycoproteomics data (1.8%) relative to the considerable levels found in the
172 *N*-glycome (18.4%) can likely be attributed to inefficient HILIC-SPE enrichment of these less
173 hydrophilic *N*-glycopeptides (unpublished observation). Recapitulating findings from the *N*-
174 glycome data, the glycoproteomics data did not reveal any consistent differences in the *N*-glycan
175 type distribution, Figure 3C, and the global *N*-glycoproteome, Supplementary Figure S6, between
176 the N0 and N+ patients. Providing further insights into the OSCC tumour tissue *N*-glycoproteome
177 complexity, the glycoproteomics data also revealed that most *N*-glycosites (70%) carried more than
178 one discrete *N*-glycan composition (25% of sites were decorated with ≥ 5 glycan compositions)
179 while most *N*-glycoproteins (58%) were identified with only one occupied *N*-glycosylation site,
180 Figure 3D.

181 Despite the relatively uniform *N*-glycoproteome across the N0 and N+ patients, a total of
182 79 *N*-glycopeptides from 56 source *N*-glycoproteins were found to be quantitatively altered between
183 the two patient groups ($p < 0.05$) including 57 *N*-glycopeptides from 43 source *N*-glycoproteins that
184 were elevated and 22 *N*-glycopeptides from 14 source *N*-glycoproteins of lower abundance in N+
185 relative to N0 tissues, Supplementary Table S5. Excitingly, all 79 *N*-glycopeptides demonstrated a
186 notable potential to stratify N0 and N+ OSCC patients (AUC-ROC $> 60\%$ by logistic regression
187 model), Supplementary Table S7. In support, a high proportion of these *N*-glycopeptides (50 *N*-
188 glycopeptides, 63.3%) were also found to stratify the patient groups with an AUC-ROC $> 60\%$ using
189 a random forest model.

190 ***N*-glycosylation-guided clustering of OSCC patients**

191 To further investigate the relatively subtle yet consistent differences in *N*-glycosylation
192 found within the investigated OSCC tumour tissue cohort, the obtained *N*-glycome and *N*-
193 glycoproteome data were then interrogated using advanced data analysis and visualisation methods.
194
195

196 Unsupervised hierarchical clustering of the *N*-glycome data revealed two major tumour
197 clusters (T-C1 and T-C2) and two major *N*-glycan clusters (NG-C1 and NG-C2), Figure 4A. Within
198 the NG-C1 cluster, altered distribution of all *N*-glycan classes were found between T-C1 and T-C2,
199 while in NG-C2 differences in the distribution of paucimannosidic and complex *N*-glycans, but not
200 oligomannosidic *N*-glycans, were observed between the two tumour clusters ($p < 0.05$) (note that
201 the other glycan classes were not observed in NG-C2), Figure 4B.

202 Similarly, unsupervised hierarchical clustering of the *N*-glycoproteome data revealed two
203 main tumour clusters (T-C1 and T-C2) and two *N*-glycopeptide clusters (IG-C1 and IG-C2), Figure
204 5A. Differences in expression of highly truncated, oligomannosidic and complex/hybrid *N*-glycans
205 were identified between T-C1 and T-C2 in IG-C1, while only the highly truncated *N*-glycans
206 exhibited differences between the two tumour clusters in IG-C2, Figure 5B.

207 To explore potential biological roles of the source *N*-glycoproteins identified within each
208 *N*-glycopeptide cluster, pathway enrichment analyses were performed. Extracellular matrix
209 organisation was the most enriched biological process in both *N*-glycopeptide clusters (FDR
210 adjusted $p = 9.4 \times 10^{-36}$ in IG-C1 and $p = 3.6 \times 10^{-45}$ in IG-C2), followed by platelet degranulation
211 in IG-C1 (FDR adjusted $p = 1.1 \times 10^{-20}$) and neutrophil degranulation in IG-C2 (FDR adjusted $p =$
212 2.0×10^{-21}) when comparing T-C1 and T-C2, Supplementary Figure S7A. We then tested for
213 differential *N*-glycan class distribution within these highly enriched pathways, which demonstrated
214 altered expression of highly truncated *N*-glycans decorating proteins involved with platelet
215 degranulation within IG-C1, and showed altered pauci- and oligomannosidic *N*-glycosylation on
216 proteins involved in neutrophil degranulation within IG-C2, Supplementary Figure S7B.

217 **Associations between *N*-glycoproteome components, clinical features and biological processes**

218 The six *N*-glycans and 79 *N*-glycopeptides found to be differentially expressed in N0 and
219 N+ patients were then evaluated for associations with a range of clinical features.

220 Unsupervised hierarchical clustering of the expression data of the six *N*-glycan structures
221 revealed two new distinct tumour groups that displayed differences in vascular invasion ($p = 0.049$,
222 Fisher's Exact Test) and lymph node (N) status ($p = 0.039$, Pearson Chi-Square test), Figure 6A-B.
223 In contrast, the two tumour groups formed by the 79 *N*-glycopeptides differed in terms of N status
224 ($p = 0.0078$), tumour size ($p = 0.0169$, both Fisher's Exact Test) and type of treatment received by
225 the OSCC patient ($p = 0.0354$, Pearson Chi-Square), Figure 6C-D.

226 To investigate whether *N*-glycosylation was associated to specific biological processes,
227 cellular compartments and molecular function, we searched for enriched gene ontology (GO) terms
228 within the IG-C1 and IG-C2 *N*-glycopeptide clusters. This analysis revealed significant enrichment
229 of extracellular matrix organisation and cell-matrix adhesion in IG-C1, while 'negative regulation
230 of blood coagulation' and 'fibrinolysis' were enriched in IG-C2, Figure 6E. Proteins from IG-C1
231 were enriched in 'focal adhesion' and 'collagen-containing extracellular matrix' compartments, and
232 were involved in 'protease binding' and 'cell-matrix adhesion mediator activity', whereas proteins
233 from IG-C2 showed trends of being of platelet and secretory granule origins, and involved in protein
234 binding.
235

236 **Specific OSCC *N*-glycans and *N*-glycopeptides associate with key clinical outcomes**

237 In total 25 of the 79 *N*-glycopeptides that displayed differential abundance between N0 and
238 N+ patients were found to correlate with distinct clinicopathological features, Supplementary
239 Figure S8. Amongst them were five *N*-glycopeptides all carrying Glycan 40a (but arising from five
240 different source glycoproteins), which associated with lymph node status and surgical margin
241 involvement (23), Figure 7A. Surprisingly, three of the source *N*-glycoproteins (BTN3A1,
242 SIGLEC1 and PLTP) were not identified in the global proteomics data, Supplementary Table S6.
243 Moreover, while the *N*-glycopeptide from COL6A3 was less abundant in tumours from N+ patients,
244 the source glycoprotein was found in higher levels in these individuals. Finally, ITGB6, whose
245

glycopeptide was more abundant in N+ patients, displayed reduced protein abundance in this condition, observations that collectively indicate separate protein and glycan regulation in OSCC, Figure 7B.

Notably, Kaplan-Meier plots showed that relatively high levels of Glycan 40a and Glycan 46a were associated with a relatively poor patient survival, Figure 7C. The potential prognostic value of Glycan 40a and 46a was supported by their ability to stratify N0 and N+ patients as demonstrated by high ROC-AUC values (AUC 78.1 for Glycan 40a and AUC 85.5 for Glycan 46a, both by logistic regression model), Supplementary Figure S5.

Similarly, three *N*-glycopeptides that displayed abundance differences between N0 and N+ showed an association with patient survival, Figure 7D. Specifically, higher abundance of a fibronectin peptide (P02751) carrying an M9 oligomannosidic *N*-glycan (Glycan 14) was found to associate with lower patient survival, while reduced levels of a CD59 peptide (P13987) carrying a fucosylated complex *N*-glycan (Glycan 35) and an afamin peptide (P43652) carrying a related non-fucosylated *N*-glycan variant (Glycan 31) were associated with lower patient survival. These three *N*-glycopeptides also demonstrated an ability to stratify N0 and N+ patients as demonstrated by ROC analysis, Supplementary Figure S9.

Taken together, unbiased and global as well as targeted interrogations of our quantitative *N*-glycome and *N*-glycoproteome data pointed to previously unknown associations between OSCC tumour *N*-glycosylation and key clinical outcomes including, most importantly, lymph node metastasis and patient survival.

Discussion

Previous studies have investigated the glycosylation patterns in oral cancer within diverse biological specimens including in cell lines (12, 20), tumour tissues (24), saliva (13, 21, 25), blood (13), plasma (26) and serum (27, 28) in attempts to uncover changes related to cell transformation (12) and with disease progression (13). Most of those studies evaluated the total levels of specific glycans or glycan features (13, 21, 24, 26) using relatively simple analytical techniques such as lectin-based strategies (24, 26, 27) and MALDI-MS profiling (12, 20, 27, 28) not able to survey the glycoproteome in an unbiased and quantitative manner with glycan fine structure and site-specific information (29). Our study is the first to use integrated glycomics and glycoproteomics to provide detailed insights into the heterogenous *N*-glycoproteome of OSCC tumour tissues obtained from a valuable cohort of patients with and without lymph node metastasis, a principal prognostic factor in OSCC (3, 30, 31).

To allow for a comprehensive examination of the global *N*-glycosylation of OSCC tumour tissues using our glycomics-informed glycoproteomics method (22), we firstly obtained quantitative *N*-glycomics data which served to establish a detailed *N*-glycome profile and inform a customised *N*-glycan database to aid the challenging downstream glycoproteomics data analysis. Intuitively, tailoring the glycan database reduces the search space resulting in lower glycopeptide FDRs and reduced search times (32) and ultimately more accurate quantitative information of the protein carriers, site occupancy (macroheterogeneity), and site distribution (microheterogeneity) of *N*-glycosylation, Figure 1 and Supplementary Figure S1.

We found surprisingly few global differences in the *N*-glycome between the N+ and N0 patient groups including in the *N*-glycan class distribution and *N*-glycosylation features (core fucosylation, sialylation and branching) suggesting a relative stable glycosylation machinery during lymph node metastasis, Figure 2B. Related studies have reported more dramatic glycan differences including altered sialylation, fucosylation and branching when comparing OSCC patients with healthy donors (24, 28) suggesting that disease onset rather than disease progression (involving lymph node metastasis) has a stronger influence on glycan remodelling.

295 Six sialic acid-capped *N*-glycans (displayed in Figure 6A) showed different expression
296 between N+ and N0 tumour tissues. These six *N*-glycans appeared structurally (and thus
297 biosynthetically) unrelated, suggesting that alteration in the abundance and/or activity of multiple
298 glycosylation enzymes from a diversity of cellular/tissue origins may contribute to the subtle glycan
299 remodelling observed upon lymph node metastasis. While their altered expression patterns remain
300 mechanistically unexplained, the six differentially expressed *N*-glycans exhibited an interesting
301 capacity to accurately stratify the N+ and N0 patient groups with confidence (AUC values > 60%),
302 Supplementary Figure S5.

303 Bisecting GlcNAcylated *N*-glycans were consistently observed in the OSCC tumour tissue
304 *N*-glycome (albeit at relatively low abundance) as confirmed by their early PGC-LC elution and
305 prominent D- and D-GlcNAc fragment ions (33). Aberrant expression of bisecting *N*-glycans has
306 repeatedly been reported as a feature of human cancers (34) including in colorectal cancer (35),
307 prostate cancer (22), breast cancer (36) and, importantly, in oral cancer (37). Contrasting these
308 reports, our *N*-glycome and *N*-glycoproteome data did not reveal any differences in bisecting
309 GlcNAcylation across the N0 and N+ tumour tissues indicating that bisecting GlcNAc is not
310 involved directly in the risk of lymph node metastasis in OSCC.

311 With a total of 3,117 identified *N*-glycopeptides from 419 source glycoproteins, the OSCC
312 tumour tissue *N*-glycoproteome displayed an extreme complexity and dynamic range, Figure 3.
313 Recapitulating the stable *N*-glycome, no striking global *N*-glycoproteome differences were
314 observed between the N0 and N+ tumour tissues. Only 79 *N*-glycopeptides (~2.5%) were found to
315 be altered between the N0 and N+ patient groups and, similarly to the regulated *N*-glycans, these
316 appeared biosynthetically unrelated spanning all *N*-glycan classes and belonging to different source
317 proteins supporting that lymph node metastasis is a complex process that is not limited to the
318 dysregulation of only a single glycosylation enzyme from a single cellular origin. Importantly, the
319 79 *N*-glycopeptides demonstrated a notable potential to accurately stratify N+ from N0 patients,
320 Supplementary Table S7.

321 Seeking to mine the information-rich *N*-glycome and *N*-glycoproteome data further,
322 unsupervised clustering revealed distinct tumor clusters that displayed interesting differences in the
323 *N*-glycan class distribution including pauci- and oligomannosidic *N*-glycans, Figure 4A-B. While
324 less explored relative to the more widely recognised cancer-associated changes in the
325 complex/hybrid-type *N*-glycans and related features such as fucosylation and sialylation (15, 38,
326 39), we and others have recently shown that both pauci- and oligomannosylation are important *N*-
327 glycan features altered in a wide range of human cancers (40, 41). The altered expression of these
328 mannose-terminating *N*-glycans across the tumour clusters implies regulation, and possibly
329 functional involvement, of the family of α -mannosidases (40, 42) and β -hexosaminidases (43, 44)
330 in OSCC, speculations which require further exploration.

331 Through enrichment analysis, we investigated biological functions of the glycoproteins
332 localising to each glycopeptide cluster, and observed extracellular matrix (ECM) organisation, and
333 platelet and neutrophil degranulation being enriched processes, Supplementary Figure S7. ECM
334 remodelling has repeatedly been linked to cancer development and progression, including changes
335 in the abundance and composition of ECM components, post-translational modifications (e.g.
336 glycosylation) (38, 45), and proteolytic activity, with several studies pointing to tumour-driven
337 changes in the ECM supporting tumour growth, tumour cell migration and metastatic processes
338 (46, 47). Further, platelet degranulation has been associated with cancer metastasis, possibly
339 through the release of platelet factors that can enhance vascular permeability, and consequently
340 promote tumour cell extravasation (48, 49). Finally, elevated neutrophil degranulation observed in
341 a subset of the OSCC tumour tissues not only aligns with robust literature pointing to the
342 involvement of neutrophils in tumour progression (50), but also provide a possible mechanistic
343 explanation for the *N*-glycan differences observed between the tumour clusters including altered
344 expression of paucimannosidic and highly truncated (chitobiose core) *N*-glycans. Neutrophils are

namely known to store and upon activation secrete bioactive and highly unusual *N*-glycoproteins carrying paucimannosidic and chitobiose core type *N*-glycans as we have demonstrated (51–54). Infiltration of neutrophils in tumours (tumour-associated neutrophils) has been described in many cancers (55), including oral cancer, in which high neutrophil counts have been associated with poor clinical outcomes (56). In an early study, Wang *et al.* (57) identified that tongue squamous cell carcinomas exhibiting high neutrophil infiltration displayed increased lymph node metastasis, more advanced clinical stage and increased risk of tumour recurrence.

Interesting associations between key clinical features and two well-separated *N*-glycan- and *N*-glycopeptide-guided tumour clusters were identified through advanced clustering analysis. In addition to the association with the lymph node status, the *N*-glycan-guided tumour clusters informed by Glycan 20a, Glycan 34, Glycan 40a, Glycan 45b, Glycan 46a, and Glycan 49b were associated with vascular invasion, Figure 6A-B. Likewise, the two *N*-glycopeptide-informed tumour clusters contained patients that exhibited different tumour size and that received different treatments, Figure 6C-D. Moreover, correlation analysis of the 79 differentially expressed *N*-glycopeptides revealed associations with 1) the presence of perineural invasion, an important indicator of poor prognosis in oral cancer (58), 2) extracapsular extension, which is associated with poor prognosis and increased risk of recurrence and survival in head and neck cancers (1, 59), 3) the WPOI (worst pattern of invasion) score used for histological risk assessment in oral cancer (60), amongst other key clinical patient features, Supplementary Table S8 and Supplementary Figure S8.

Amongst the 25 *N*-glycopeptides associated with clinicopathological features, five were identified to carry Glycan 40a (a mono- α 2,6-sialylated core fucosylated complex-type *N*-glycan), Figure 7A. One of the five Glycan 40a-carrying glycopeptides belongs to BTN3A1 (butyrophilin subfamily 3 member A1 or CD277) and was identified to associate with lymph node status. BTN3A1 plays a well-known role in T-cell activation and in the adaptive immune response, and altered BTN3A1 expression has been reported in different human cancers including in head and neck squamous cell carcinoma and in breast cancer (61). Remarkably, BTN3A1 was not detected in our OSCC proteome profile, Figure 7B, but only identified in HILIC-enriched glycoproteome analysis, highlighting the importance of employing multi-omics approaches to obtain a comprehensive coverage and holistic insights in the disease complexity and dynamics.

Interestingly, focused analysis of the *N*-glycome and *N*-glycoproteome data demonstrated an association between two *N*-glycans (Glycan 40a and 46a, both mono- α 2,6-sialylated core fucosylated complex-type *N*-glycans) and three seemingly unrelated neutral *N*-glycopeptides and low patient survival rate, Figure 7C-D. Powered by our glycomics-assisted glycoproteomics method, the identification of several survival-associated glycans and glycopeptides expands on similar findings made in colorectal cancer (62) and gastric cancer (63), and represents an extremely exciting discovery as it opens for previously unexplored avenues to better prognosticate, monitor and manage patients diagnosed with OSCC.

In summary, this is the first study to report on the complexity and dynamics of the OSCC tumour tissue *N*-glycoproteome in patients with and without lymph node metastasis. Our comprehensive and quantitative *N*-glycomics and *N*-glycoproteomics data have unveiled a range of previously unknown associations between protein *N*-glycosylation in OSCC tumour tissues and key patient clinical features and survival outcome, and provide an important publicly-available resource to explore the underpinning disease mechanisms and to uncover potential prognostic glyco-markers for OSCC.

Materials and Methods

OSCC tumour tissues

The study was approved by the Ethics Review Board of the Cancer Institute of São Paulo (ICESP), Octavio Frias de Oliveira, ICESP, São Paulo, SP, Brazil, and Plataforma Brasil (protocol CAAE 61402116.8.0000.0065). Informed consent was obtained from all patients included in the

395 study. The methods and experimental protocols were performed in accordance with the approved
396 guidelines and regulations. Surgically removed oral squamous cell carcinoma (OSCC) tissues
397 provided as formalin-fixed paraffin-embedded (FFPE) tissues from a 31-patient cohort collected
398 over a two-year period (2017-18) were investigated. In total, 19 patients presented lymph node
399 metastasis (N+) and 12 patients presented without lymph node metastasis (N0) as determined by
400 histopathology. See Supplementary Table S1 for key clinicopathological data.

401 402 **Tissue sample preparation**

403 Eight histological sections (each 10 µm thick) were prepared for each of the 31 OSCC FFPE tissues.
404 Paraffin blocks were cut using a microtome and the tumour area was assigned by a trained
405 pathologist for manual excision. A total tumour area of 7-8 cm² were excised from 3-8 histological
406 sections from each tumour tissue sample and transferred to a microtube for deparaffinization and
407 protein extraction using a published protocol with modifications (64). For paraffin removal, 1 mL
408 xylene was added to each sample, mixed for 1 min and centrifuged at 12,000 x g for 15 min at room
409 temperature. The pellet was washed with 1 mL ethanol, mixed for 30 s, centrifuged as above and
410 dried in a vacuum concentrator. Samples were resuspended in 300 µL lysis buffer containing 0.1
411 M *N*-(2-hydroxyethyl)piperazine-*N'*-(3-propanesulfonic acid) (EPPS), 0.1 M dithiothreitol (DTT),
412 1 x protease inhibitor cocktail (cOmplete ULTRA Tablets, Mini, EDTA-free, Roche; 1:10), pH 8.5.
413 SDS was added to a final concentration of 4% (w/v) and the samples incubated for 60 min at 99°C
414 with agitation (400 rpm). Samples were then centrifuged at 15,000 x g for 30 min at 4°C and
415 submitted to ice-cold acetone precipitation with three-fold (v/v) excess acetone for 16 h at -20°C.
416 Following centrifugation at 15,000 x g for 30 min at 4°C, protein pellets were resuspended in 30
417 µL buffer containing 8 M urea, 50 mM EPPS, protease inhibitor cocktail, 1 mM sodium fluoride,
418 1 mM sodium orthovanadate, 1 mM phenylmethylsulfonyl fluoride (PMSF), 1 mM EDTA, pH 8.5.
419 Protein concentrations were determined by a bicinchoninic acid (BCA) protein assay kit (Thermo
420 Fisher Scientific, Waltham, MA) and stored at -20°C until further handling.

421 422 ***N*-glycan release**

423 Glycans were prepared as described (65). Briefly, the protein extracts (15 µg/sample) were
424 blotted on a primed 0.45 µm polyvinylidene fluoride (PVDF) membrane (Merck-Millipore). Protein
425 spots were stained using Direct Blue (Sigma-Aldrich, Australia), excised and transferred to a flat
426 bottom polypropylene 96-well plate (Corning Life Sciences, Australia), blocked with 1% (w/v)
427 polyvinylpyrrolidone in 50% (v/v) methanol and washed with MilliQ water. The *N*-glycans were
428 then released using 10 U recombinant *Elizabethkingia miricola* *N*-glycosidase F (Promega, V4831,
429 10 U/µL) for 16 h at 37°C. The detached *N*-glycans were reduced with 1 M sodium borohydride in
430 50 mM aqueous potassium hydroxide for 3 h at 50°C. The reaction was stopped using glacial acetic
431 acid and the *N*-glycans desalted sequentially using strong cation exchange (AG 50W X8, Bio-Rad),
432 C18 and porous graphitised carbon (PGC, Thermo Fisher Scientific) solid phase extraction. The
433 desalted *N*-glycan samples were stored at -20°C until analysis.

434 435 ***N*-glycome profiling**

436 *N*-glycomics data were acquired using an established PGC-LC-MS/MS method (65, 66),
437 see Supplementary Table S2 for experimental overview and details of all generated 'omics datasets.
438 The *N*-glycans were separated on an UltiMate 3000 HPLC system (Dionex, Sunnyvale, CA, USA)
439 interfaced with a linear ion trap quadrupole (LIT) Velos Pro (Thermo Scientific, San Jose, CA,
440 USA). The glycan samples (3 µL injection volume) were loaded on a PGC HPLC capillary column
441 (Hypercarb KAPPA, 5 µm particle size, 200 Å pore size, 180 µm inner diameter x 100 mm length,
442 Thermo Scientific) operated at 50°C with a constant flow rate (4 µL/min) supplemented with a post-
443 column make-up flow supplying pure acetonitrile (ACN) delivered by the HPLC system. Aqueous
444 ammonium bicarbonate (10 mM), pH 8.0 (solvent A) and 10 mM ammonium bicarbonate in 70%

445 ACN (solvent B) were used as mobile phases with the following 86 min-gradient: 8 min at 2.6% B,
446 2.6-13.5% B over 2 min, 13.5-37.3% B over 55 min, 37-64% B over 10 min, 64-98% B over 1 min,
447 5 min at 98% B, 98-2.6% B over 1 min and 4 min at 2.6% B. The ESI source was operated in
448 negative ion polarity mode with source potential of 3.6 kV. Full MS1 scans were acquired in the
449 range m/z 570-2,000 using 1 microscan, m/z 0.25 full width half maximum (FWHM) resolution, 5
450 $\times 10^4$ automatic gain control (AGC) and 50 ms maximum accumulation time. MS/MS data were
451 acquired using m/z 0.35 FWHM resolution; 2×10^4 AGC, 300 ms maximum accumulation time,
452 and 2 m/z precursor ion isolation window. The five most abundant precursors in each MS1 full scan
453 were selected for collision-induced dissociation (CID)-based MS/MS using a normalised collision
454 energy (NCE) of 33% with an activation Q of 0.250 and 10 ms activation time. To prevent
455 instrument bias, the injection order of the glycan samples from the OSCC patient cohort was
456 randomised (67), using the *psych* package (68) under R (v3.6.0).

457 458 **N-glycan data analysis**

459 Xcalibur v2.2 (Thermo Scientific) was used to browse and interrogate the raw LC-MS/MS
460 data. Putative glycan precursor ions were extracted using RawMeat v2.1 (Vast Scientific) (22, 69).
461 Common contaminants not matching known N-glycan compositions and redundant precursors were
462 manually removed. The monoisotopic precursors were searched against GlycoMod (70) with a
463 mass tolerance of 0.5 Da to identify putative monosaccharide compositions. Only compositions
464 containing Hex, HexNAc, dHex, NeuAc, and NeuGc were considered and N-glycans already
465 reported in the UniCarbKB database were prioritised. The N-glycan fine structures were manually
466 elucidated using monoisotopic mass, absolute and relative PGC-LC retention time and MS/MS
467 fragmentation patterns as described (33, 71). EIC-based relative quantification of the identified N-
468 glycans was performed using Skyline v.20.1.0.31 as described (22, 72). GlycoWorkBench v2.1 (73)
469 was used to aid the manual annotation of the glycan fragment spectra and to generate glycan
470 cartoons. Poorly expressed N-glycans with a relative abundance below 0.1% were excluded from
471 the relative quantitation due to poor spectral signal-to-noise ratios.

472 473 **Protein digestion and peptide desalting**

474 Protein samples (35 μ g/sample) were reduced with 5 mM DTT (final concentration) for 25
475 min at 56°C and alkylated using 14 mM iodoacetamide (IAA) for 30 min at room temperature in
476 the dark. Urea was added to a final concentration of 1.6 M in 50 mM ammonium bicarbonate and
477 1 mM calcium chloride prior to digestion with 1 μ g sequencing grade porcine trypsin (Promega)
478 for 16 h at 37°C (74). The reaction was quenched with a final concentration of 0.4% (v/v)
479 trifluoroacetic acid (TFA). The resulting peptides were desalted using Oasis HLB 1 cc (30 mg) SPE
480 cartridges (Waters) using an established protocol with modifications (74). Columns were activated
481 with 1 mL methanol, washed twice with 1.5 mL 1% formic acid (FA) in 70% ACN (both v/v) and
482 equilibrated with 1.5 mL 1% (v/v) aqueous FA prior to sample loading. After washing twice with
483 1.5 mL 1% (v/v) aqueous FA, peptides were eluted twice with 250 μ L 1% FA in 70% ACN (both
484 v/v) and dried.

485 486 **TMT labelling of peptides**

487 A reference sample was prepared to allow for quantitative comparisons across multiple TMT
488 experiments by pooling 3 μ g digested protein from each sample. In total, 25 μ g from this pool and
489 25 μ g protein extract from each sample were used for TMT labelling (22). The peptide samples
490 were randomised before being labelled using three separate TMT-11plex sets. The reference sample
491 was consistently labelled with the 131 Da (131C) reporter ion channel in all three sets. In total, 30
492 peptide samples were labelled with TMT for quantitative proteomics including 12 N0 and 18 N+
493 samples (one random N+ sample from the sample cohort was excluded in TMT experimental design
494 due to limited channels available), Supplementary Table S2. For the TMT labelling, 100 μ L 100

495 mM triethylammonium bicarbonate buffer (final concentration) was added to each peptide sample
496 that was labelled individually with 0.4 mg TMT-11plex mass tags (Thermo) in 41 μL anhydrous
497 ACN over a 1 h incubation period at room temperature. The labelling reactions were quenched
498 using 8 μL 5% (v/v) hydroxylamine for 15 min at room temperature. After TMT labelling, all
499 peptide samples were mixed 1:1:1 (w/w/w), desalted using HLB SPE cartridges (Waters) and dried.
500 Aliquots of the TMT-labelled peptide mixtures from the three TMT-11plex experiments were
501 analysed without any pre-fractionation by LC-MS/MS, Supplementary Table S2.

502

503 **Glycopeptide enrichment**

504 TMT-labelled peptides (from 275 μg protein extract from 10 tumour tissue samples + one
505 pool) was reconstituted in 50 μL loading/washing solvent containing 1% TFA in 80% ACN (both
506 v/v). Five microliters (~ 18 μg protein digest) were allocated to the proteome analysis. The
507 remaining peptides were loaded onto primed custom-made HILIC SPE micro-columns packed with
508 ZIC-HILIC resin (10 μm particle size, 200 \AA pore size, kindly provided by Sequant/Merck, Umea,
509 Sweden) onto supporting C8 disks (Empore) in p10 pipette tips (75). The flow-through fractions
510 were collected. The HILIC-SPE micro-columns were then washed with 50 μL loading/washing
511 solvent and the wash fraction combined with the flow-through fraction for separate downstream
512 analysis, as this fraction contained the non-glycosylated peptides. The retained *N*-glycopeptides
513 were eluted in three sequential steps, firstly with 50 μL 0.1% (v/v) aqueous TFA, followed by 50
514 μL 25 mM aqueous ammonium bicarbonate and then 50 μL 50% (v/v) ACN. The three *N*-
515 glycopeptide fractions were combined to form the enriched glycopeptide mixture, which was dried
516 and desalted on a primed Oligo R3 reversed phase SPE micro-column. R3 resin suspended in ACN
517 was packed into a p10 pipette tips, washed three times with 50 μL ACN, and then washed with
518 0.1% (v/v) aqueous TFA before sample loading. The sample loading was repeated once to ensure
519 high recovery ahead of three washing steps with 0.1% (v/v) aqueous TFA and elution with 50 μL
520 0.1% TFA in 50% ACN (both v/v) and then with 50 μL 0.1% TFA in 70% ACN (both v/v). The
521 desalted glycopeptide fractions were combined, dried and stored at -20°C (22).

522

523 **High-pH reversed phase prefractionation**

524 The HILIC enriched *N*-glycopeptides and HILIC flow-through fractions containing the non-
525 glycosylated peptides were resuspended separately in 50 μL 25 mM aqueous ammonium
526 bicarbonate for high pH pre-fractionation using Oligo R2 reversed phase SPE micro-columns
527 packed on supporting C18 discs (Empore) in standard p10 pipette tips. The SPE micro-columns
528 were primed three times with 50 μL ACN and then washed with 50 μL 25 mM aqueous ammonium
529 bicarbonate. Samples were loaded on the columns followed by two washing steps with 50 μL 25
530 mM aqueous ammonium bicarbonate. The peptides were eluted in three fractions i.e. fraction 1: 25
531 mM ammonium bicarbonate in 10% (v/v) ACN; fraction 2: 25 mM ammonium bicarbonate in 20%
532 (v/v) ACN, and fraction 3: 25 mM ammonium bicarbonate in 60% (v/v) ACN. Each eluted fraction
533 was dried and resuspended in 0.1% (v/v) aqueous FA for separate LC-MS/MS analysis.

534

535 **(Glyco)proteome profiling by LC-MS/MS**

536 Approximately 1 μg (glyco)peptide material was injected per LC-MS/MS run. The
537 (glyco)peptides were loaded on a trap column (2 cm length x 100 μm inner diameter) custom packed
538 with ReproSil-Pur C18 AQ 5 μm resin (Dr. Maisch, Ammerbuch-Entringen, Germany) and
539 separated at a constant flow rate of 250 nL/min on an analytical column (Reprosil-Pur C18-Aq, 25
540 cm length x 75 μm inner diameter, 3 μm particle size, Dr. Maisch, Ammerbuch-Entringen,
541 Germany) using an UltiMate™ 3000 RSLCnano System. The mobile phases were 0.1% FA in
542 99.9% (both v/v) ACN (solvent B) and 0.1% (v/v) aqueous FA (solvent A). The gradient was 2-
543 30% B over 100 min, 30-50% B over 18 min, 50-95% B over 1 min and 9 min at 95% B. The
544 nanoLC was connected to a Q-Exactive HF-X Hybrid Quadrupole-Orbitrap mass spectrometer

(Thermo Fisher Scientific) operating in positive ion polarity mode. The Orbitrap acquired full MS1 scans with an AGC of 3×10^6 ions and 50 ms maximum accumulation time. Full MS1 scans were acquired at high-resolution (60,000 FWHM at m/z 200) in the m/z 350-1,800 range. The 20 most abundant precursor ions were selected from each MS1 full scan using data-dependent acquisition and were fragmented utilising higher energy collision-induced dissociation (HCD) with a NCE of 35%. Only multicharged precursors ($z \geq 2$) were selected for fragmentation. Fragment spectra were acquired at 45,000 resolution with an AGC of 1×10^5 and 90 ms maximum accumulation time using a precursor isolation window of m/z 1.0 and a dynamic exclusion of 30 s after a single isolation and fragmentation of a given precursor ion.

***N*-glycoproteomics data analysis**

The HCD-MS/MS data of intact *N*-glycopeptides were searched with Byonic v2.6.46 (Protein Metrics Inc, CA, USA) (76) using 10/20 ppm as the precursor/product ion mass tolerance, respectively. Cys carbamidomethylation (+57.021 Da) and TMT (+229.163 Da) at N-term and lysine (K) were considered fixed modifications. Trypsin specific cleavages were considered with a maximum of two missed cleavages allowed per peptide. The following variable modifications were considered: Met oxidation (+15.994 Da), and *N*-glycosylation of sequon-localised Asn with a glycomics-informed *N*-glycan database comprising the *N*-glycan compositions identified in the OSCC tissue *N*-glycome data (Supplementary Table S3) and HexNAc₁, HexNAc₁Fuc₁ and HexNAc₂ that were manually added to the database. A maximum of two common modifications and a maximum of one rare modification were allowed. The HCD-MS/MS data were searched against a protein database composed of all reviewed UniProtKB human proteins (20,300 sequences, released December 11, 2019). All searches were filtered to <1% false discovery rate (FDR) at the protein level and 0% at the peptide level by using a protein decoy database (77). Only *N*-glycopeptides confidently identified with PEP 2D scores < 0.001 were considered (22). Glycopeptides identified with low confidence, and those in the reverse database and contaminant database were excluded. The identified *N*-glycopeptides were quantified using the ‘Report Ion Quantifier’ available as a node in Proteome Discoverer v2.2 (Thermo Scientific) and the reporter ion intensities from the MS/MS scans were extracted from the QuantSpectra table (22). Glycopeptides were manually grouped by summing the reporter ion intensities from the glycopeptide spectral matches (glycoPSMs) belonging to the same UniProtKB identifier, same glycosylation site within the protein, and same glycan composition. The abundances of the unique glycopeptides from each channel were first normalised by dividing each unique glycopeptide reporter ion intensity by the reference reporter intensity (from the peptide pool, see above) within that specific experiment and further normalised by the total sum intensity of each channel to correct for any inter-sample variation in the total yield during the labelling reactions.

Proteomics data analysis

LC-MS/MS-based proteomics data were acquired of both unenriched peptide samples not subjected to glycopeptide enrichment as well as to the HILIC flow-through fractions. All data were processed using MaxQuant v1.6.12.0 (78). The HCD-MS/MS data were searched against the reviewed UniProtKB Human Protein Database (20,300 sequences, released December 11, 2019) using the Andromeda search engine (79) with a tolerance of 4.5 ppm for precursor ions and 20 ppm for product ions. Report fragment ions “10plex TMT” were enabled in the quantification settings and the enzyme specificity was set to trypsin with a maximum of two missed cleavages permitted. Carbamidomethylation of Cys (+57.021 Da) was considered a fixed modification, and oxidation of Met (+15.994 Da) and protein N-terminal acetylation (+42.010 Da) were considered variable modifications. Both the protein and peptide identifications were filtered to 1% FDR. Processing and statistical analyses (Student’s t-test) of the resulting data table (MaxQuant output) were performed in Perseus v1.6.14.0 (78). Proteins identified using the reverse database, proteins only

595 identified through modified peptides and proteins identified from the MaxQuant contaminant
596 database were excluded (except human keratins, which were not excluded since they are of interest
597 in the study of squamous tissues (80)). The identified proteins were quantified by their reporter ion
598 intensities using at least one razor/unique peptide per protein. Protein abundances of each channel
599 were first normalised by dividing the reporter ion intensity by the reference protein reporter ion
600 intensity (131C channel of peptide pool) within that specific LC-MS/MS run and further normalised
601 by dividing by the sum of total intensity of each channel to correct for any inter-sample variation
602 in the total yield during the labelling reactions.

603 604 **Statistical analysis**

605 For the glycome profiling and glycosylation site analyses, statistical significance was
606 assessed using unpaired two-tailed Student's t-tests in which $p < 0.05$ was used as the confidence
607 threshold. For the glycoproteome profiling, the statistical significance of the summed intensities of
608 the glycopeptides grouped based on their *N*-glycan classes or tissue cluster was assessed using
609 unpaired two-tailed Student's t-tests in which $p < 0.05$ was used as the confidence threshold. For
610 data visualisation, heat maps with z-score values of normalised intensities were generated using the
611 open-source statistical programming language R.

612 613 **Clinical association and survival analysis**

614 Linear regression analysis was performed using the R code to evaluate the linear
615 relationship between glycan or glycopeptide abundance and the following clinicopathological
616 variables: age (>63 or ≤ 63 , mean age of patient cohorts chosen as the threshold), sex, smoking
617 habit, alcohol consumption, tumour size, lymph node metastasis (N+, N0), clinical stage, type of
618 treatment (surgery, surgery and radiotherapy, or a combination of surgery, radiation and
619 chemotherapy), disease-free survival, presence of the worst pattern of invasion (60), presence of
620 inflammatory infiltrate, and perineural invasion. Linear regressions with $p < 0.05$ were considered
621 significant. The Pearson product-moment correlation coefficient (R) was also calculated to
622 measure the strength of the association between variables. Only associations with $R < -0.5$ or $0.5 <$
623 R with at least six valid values per group and at least three valid values per clinical feature were
624 considered (81). For cluster analysis and associations to clinical features, Fisher's Exact Test (for
625 two group comparisons) or Pearson Chi-Square test (for comparisons of more than two groups)
626 were performed using IBM SPSS Statistics v 28.0.0.0 (190). Furthermore, a survival analysis was
627 calculated on GraphPad Prism v.9.1.2 using the Kaplan-Meier methodology and compared with the
628 log-rank test, evaluating the survival probability comparing a higher and lower abundance of
629 specific glycoproteins, glycopeptides and glycans.

630 631 **ROC curve analysis by logistic regression and random forest models**

632 The potential of select *N*-glycans and *N*-glycopeptides to stratify N0 and N+ patients was
633 evaluated by the area-under-the-curve (AUC) of the constructed receiver operating characteristic
634 (ROC) curves generated using random forest and logistic regression models. The area-under-the-
635 curve (AUC-ROC) with a 95% confidence interval was used for comparison. Optimal cut-off by
636 highest sensitivity (true positive rate) as a function of the specificity (false positive rate) was
637 calculated, and 60% was chosen as the decision threshold. For all statistical comparisons, an
638 ANOVA $p < 0.05$ was considered as significance threshold. The data analysis was performed using
639 the package pROC (82) and the R environment version 3.6.0.

640 641 **Enrichment analysis of gene ontology (GO) terms**

642 GO enrichment analysis was performed using the DAVID (83) or Enrichr (84) with
643 corrected $p < 0.05$ chosen as the significance threshold. The entire human proteome GO annotation
644 file was used as a reference set.

645
646
647
648
649
650
651
652
653
654
655
656
657
658
659
660
661
662
663
664
665
666
667
668
669
670
671
672
673
674
675
676
677
678
679
680
681
682
683
684
685
686
687
688
689
690
691
692
693
694

References

1. D. E. Johnson, B. Burtneß, C. R. Leemans, V. W. Y. Lui, J. E. Bauman, J. R. Grandis, Head and neck squamous cell carcinoma. *Nat. Rev. Dis. Prim.* 2020 61. **6**, 1–22 (2020).
2. H. Sung, J. Ferlay, R. L. Siegel, M. Laversanne, I. Soerjomataram, A. Jemal, F. Bray, Global Cancer Statistics 2020: GLOBOCAN Estimates of Incidence and Mortality Worldwide for 36 Cancers in 185 Countries. *CA. Cancer J. Clin.* **71**, 209–249 (2021).
3. A. S. Ho, S. Kim, M. Tighiouart, C. Gudino, A. Mita, K. S. Scher, A. Laury, R. Prasad, S. L. Shiao, J. E. Van Eyk, Z. S. Zumsteg, Metastatic lymph node burden and survival in oral cavity cancer. *J. Clin. Oncol.* **35**, 3601–3609 (2017).
4. A. Almangush, A. A. Mäkitie, A. Triantafyllou, R. de Bree, P. Strojjan, A. Rinaldo, J. C. Hernandez-Prera, C. Suárez, L. P. Kowalski, A. Ferlito, I. Leivo, Staging and grading of oral squamous cell carcinoma: An update. *Oral Oncol.* **107**, 104799 (2020).
5. M. Sharma, P. Sah, S. Sharma, R. Radhakrishnan, Molecular changes in invasive front of oral cancer. *J. Oral Maxillofac. Pathol.* **17**, 240 (2013).
6. A. Almangush, R. D. Coletta, I. O. Bello, C. Bitu, H. Keski-Säntti, L. K. Mäkinen, J. H. Kauppila, M. Pukkila, J. Hagström, J. Laranne, S. Tommola, Y. Soini, V.-M. Kosma, P. Koivunen, L. P. Kowalski, P. Nieminen, R. Grénman, I. Leivo, T. Salo, A simple novel prognostic model for early stage oral tongue cancer. *Int. J. Oral Maxillofac. Surg.* **44**, 143–150 (2015).
7. F. Chasma, R. Pedr King, S. Y. Ker, Are there diagnostic alternatives to histopathology in detecting oral cancer? *Evidence-Based Dent.* 2022 231. **23**, 24–25 (2022).
8. P. Ostasiewicz, D. F. Zielinska, M. Mann, J. R. Wisniewski, Proteome, phosphoproteome, and N-glycoproteome are quantitatively preserved in formalin-fixed paraffin-embedded tissue and analyzable by high-resolution mass spectrometry. *J. Proteome Res.* **9**, 3688–3700 (2010).
9. A. Mangé, P. Chaurand, H. Perrochia, P. Roger, R. M. Caprioli, J. Solassol, Liquid chromatography-tandem and MALDI imaging mass spectrometry analyses of RCL2/CS100-fixed, paraffin-embedded tissues: Proteomics evaluation of an alternate fixative for biomarker discovery. *J. Proteome Res.* **8**, 5619–5628 (2009).
10. C. M. Carnielli, C. C. S. Macedo, T. De Rossi, D. C. Granato, C. Rivera, R. R. Domingues, B. A. Pauletti, S. Yokoo, H. Heberle, A. F. Busso-Lopes, N. K. Cervigne, I. Sawazaki-Calone, G. V. Meirelles, F. A. Marchi, G. P. Telles, R. Minghim, A. C. P. Ribeiro, T. B. Brandão, G. de Castro, W. A. González-Arriagada, A. Gomes, F. Penteado, A. R. Santos-Silva, M. A. Lopes, P. C. Rodrigues, E. Sundquist, T. Salo, S. D. da Silva, M. A. Alaoui-Jamali, E. Graner, J. W. Fox, R. Della Coletta, A. F. Paes Leme, Combining discovery and targeted proteomics reveals a prognostic signature in oral cancer. *Nat. Commun.* **9**, 3598 (2018).
11. J. Pillai, T. Chincholkar, R. Dixit, M. Pandey, A systematic review of proteomic biomarkers in oral squamous cell cancer. *World J. Surg. Oncol.* 2021 191. **19**, 1–28 (2021).
12. Y. T. Chen, Y. M. Chong, C. W. Cheng, C. L. Ho, H. W. Tsai, F. H. Kasten, Y. L. Chen, C. F. Chang, Identification of novel tumor markers for oral squamous cell carcinoma using glycoproteomic analysis. *Clin. Chim. Acta.* **420**, 45–53 (2013).
13. B. N. Vajaria, K. A. Patel, P. S. Patel, Role of aberrant glycosylation enzymes in oral cancer progression. *J. Carcinog.* **17** (2018), doi:10.4103/JCAR.JCAR_7_18.
14. G. Liu, P. K. Sengupta, B. Jamal, H. Y. Yang, M. P. Bouchie, V. Lindner, X. Varelas, M. A. Kukuruzinska, N-glycosylation induces the CTHRC1 protein and drives oral cancer cell migration. *J. Biol. Chem.* (2013), doi:10.1074/jbc.M113.473785.
15. C. Reily, T. J. Stewart, M. B. Renfrow, J. Novak, Glycosylation in health and disease. *Nat.*

- 695 *Rev. Nephrol.* (2019), , doi:10.1038/s41581-019-0129-4.
- 696 16. M. Iwatsuki, K. Mimori, T. Yokobori, H. Ishi, T. Beppu, S. Nakamori, H. Baba, M. Mori,
697 Epithelial–mesenchymal transition in cancer development and its clinical significance.
698 *Cancer Sci.* **101**, 293–299 (2010).
- 699 17. M. Nita-Lazar, V. Noonan, I. Rebutini, J. Walker, A. S. Menko, M. A. Kukuruzinska,
700 Overexpression of DPAGT1 leads to aberrant N-glycosylation of E-cadherin and cellular
701 discohesion in oral cancer. *Cancer Res.* (2009), doi:10.1158/0008-5472.CAN-08-4512.
- 702 18. B. Jamal, P. K. Sengupta, Z. N. Gao, M. Nita-Lazar, B. Amin, S. Jalisi, M. P. Bouchie, M.
703 A. Kukuruzinska, Aberrant amplification of the crosstalk between canonical Wnt signaling
704 and N-glycosylation gene DPAGT1 promotes oral cancer. *Oral Oncol.* (2012),
705 doi:10.1016/j.oraloncology.2012.01.010.
- 706 19. T. Zhan, N. Rindtorff, M. Boutros, Wnt signaling in cancer. *Oncogene* (2017), ,
707 doi:10.1038/onc.2016.304.
- 708 20. J.-T. Chen, C.-H. Chen, K.-L. Ku, M. Hsiao, C.-P. Chiang, T.-L. Hsu, M.-H. Chen, C.-H.
709 Wong, Glycoprotein B7-H3 overexpression and aberrant glycosylation in oral cancer and
710 immune response. *Proc. Natl. Acad. Sci.* (2015), doi:10.1073/pnas.1516991112.
- 711 21. B. N. Vajaria, K. R. Patel, R. Begum, J. B. Patel, F. D. Shah, G. M. Joshi, P. S. Patel,
712 Salivary Glyco-sialylation changes monitors oral carcinogenesis. *Glycoconj. J.* (2014),
713 doi:10.1007/s10719-014-9561-7.
- 714 22. R. Kawahara, S. Recuero, M. Srougi, K. R. M. Leite, M. Thaysen-Andersen, G. Palmisano,
715 The complexity and dynamics of the tissue glycoproteome associated with prostate cancer
716 progression. *Mol. Cell. Proteomics* (2020), doi:10.1074/mcp.ra120.002320.
- 717 23. D. A. Mitchell, A. Kanatas, C. Murphy, P. Chengot, A. B. Smith, T. K. Ong, Margins and
718 survival in oral cancer. *Br. J. Oral Maxillofac. Surg.* **56**, 820–829 (2018).
- 719 24. M. H. Shah, S. D. Telang, P. M. Shah, P. S. Patel, Tissue and serum α 2-3- and α 2-6-
720 linkage specific sialylation changes in oral carcinogenesis. *Glycoconj. J.* **25**, 279–290
721 (2008).
- 722 25. N. Sinevici, S. Mittermayr, G. P. Davey, J. Bones, J. O’Sullivan, Salivary N-glycosylation
723 as a biomarker of oral cancer: A pilot study. *Glycobiology* (2019),
724 doi:10.1093/glycob/cwz046.
- 725 26. S. C. Chang, W. L. Lin, Y. F. Chang, C. T. Lee, J. S. Wu, P. H. Hsu, C. F. Chang,
726 Glycoproteomic identification of novel plasma biomarkers for oral cancer. *J. Food Drug*
727 *Anal.* **27**, 483–493 (2019).
- 728 27. Y.-L. Wong, R. Anand, K. M. Yuen, W. M. W. Mustafa, M. T. Abraham, K. K. Tay, Z. A.
729 A. Rahman, Y. Chen, Identification of potential glycoprotein biomarkers in oral squamous
730 cell carcinoma using sweet strategies. *Glycoconj. J.* (2021), doi:10.1007/s10719-021-
731 09973-z.
- 732 28. S.-Y. Guu, T.-H. Lin, S.-C. Chang, R.-J. Wang, L.-Y. Hung, P.-J. Fang, W.-C. Tang, P.
733 Yu, C.-F. Chang, Serum N-glycome characterization and anti-carbohydrate antibody
734 profiling in oral squamous cell carcinoma patients. *PLoS One.* **12**, e0178927 (2017).
- 735 29. M. Thaysen-Andersen, D. Kolarich, N. H. Packer, Glycomics & Glycoproteomics: From
736 Analytics to Function. *Mol. Omi.* **17**, 8–10 (2021).
- 737 30. C. Grandi, M. Alloisio, D. Moglia, S. Podrecca, L. Sala, P. Salvatori, R. Molinari,
738 Prognostic significance of lymphatic spread in head and neck carcinomas: therapeutic
739 implications. *Head Neck Surg.* **8**, 67–73 (1985).
- 740 31. L. P. Kowalski, A. Sanabria, Elective neck dissection in oral carcinoma: a critical review of
741 the evidence. *Acta Otorhinolaryngol. Ital.* **27**, 113 (2007).
- 742 32. R. Kawahara, A. Chernykh, K. Alagesan, M. Bern, W. Cao, R. J. Chalkley, K. Cheng, M.
743 S. Choo, N. Edwards, R. Goldman, M. Hoffmann, Y. Hu, Y. Huang, J. Y. Kim, D. Kletter,
744 B. Liquet, M. Liu, Y. Mechref, B. Meng, S. Neelamegham, T. Nguyen-Khuong, J. Nilsson,

- 745 A. Pap, G. W. Park, B. L. Parker, C. L. Pegg, J. M. Penninger, T. K. Phung, M. Pioch, E.
746 Rapp, E. Sakalli, M. Sanda, B. L. Schulz, N. E. Scott, G. Sofronov, J. Stadlmann, S. Y.
747 Vakhrushev, C. M. Woo, H. Y. Wu, P. Yang, W. Ying, H. Zhang, Y. Zhang, J. Zhao, J.
748 Zaia, S. M. Haslam, G. Palmisano, J. S. Yoo, G. Larson, K. H. Khoo, K. F. Medzihradzsky,
749 D. Kolarich, N. H. Packer, M. Thaysen-Andersen, Community evaluation of
750 glycoproteomics informatics solutions reveals high-performance search strategies for
751 serum glycopeptide analysis. *Nat. Methods* 2021 1811. **18**, 1304–1316 (2021).
- 752 33. J. L. Abrahams, M. P. Campbell, N. H. Packer, Building a PGC-LC-MS N-glycan retention
753 library and elution mapping resource. *Glycoconj. J.* **35**, 15–29 (2018).
- 754 34. H. E. Miwa, Y. Song, R. Alvarez, R. D. Cummings, P. Stanley, The bisecting GlcNAc in
755 cell growth control and tumor progression. *Glycoconj. J.* (2012), doi:10.1007/s10719-012-
756 9373-6.
- 757 35. M. K. Sethi, M. Thaysen-Andersen, J. T. Smith, M. S. Baker, N. H. Packer, W. S.
758 Hancock, S. Fanayan, Comparative N-glycan profiling of colorectal cancer cell lines
759 reveals unique bisecting GlcNAc and α -2,3-linked sialic acid determinants are associated
760 with membrane proteins of the more metastatic/aggressive cell lines. *J. Proteome Res.* **13**,
761 277–288 (2014).
- 762 36. L. Cheng, L. Cao, Y. Wu, W. Xie, J. Li, F. Guan, Z. Tan, Bisecting N-Acetylglucosamine
763 on EGFR Inhibits Malignant Phenotype of Breast Cancer via Down-Regulation of
764 EGFR/Erk Signaling. *Front. Oncol.* **10** (2020), doi:10.3389/FONC.2020.00929.
- 765 37. Y. Wang, Q. Li, L. Niu, L. Xu, Y. Guo, L. Wang, C. Guo, Suppression of G6PD induces
766 the expression and bisecting GlcNAc-branched N-glycosylation of E-Cadherin to block
767 epithelial-mesenchymal transition and lymphatic metastasis. *Br. J. Cancer* (2020),
768 doi:10.1038/s41416-020-1007-3.
- 769 38. A. Magalhães, H. O. Duarte, C. A. Reis, Aberrant Glycosylation in Cancer: A Novel
770 Molecular Mechanism Controlling Metastasis. *Cancer Cell.* **31**, 733–735 (2017).
- 771 39. O. M. T. Pearce, H. Läubli, Sialic acids in cancer biology and immunity. *Glycobiology.* **26**,
772 111–128 (2016).
- 773 40. S. Chatterjee, J. Ugonotti, L. Y. Lee, A. Everest-Dass, R. Kawahara, M. Thaysen-
774 Andersen, Trends in oligomannosylation and α 1,2-mannosidase expression in human
775 cancers. *Oncotarget.* **12**, 2188–2205 (2021).
- 776 41. S. Chatterjee, L. Y. Lee, R. Kawahara, J. L. Abrahams, B. Adamczyk, M. Anugraham, C.
777 Ashwood, Z. Sumer-Bayraktar, M. T. Briggs, J. H. L. Chik, A. Everest-Dass, S. Förster, H.
778 Hinneburg, K. R. M. Leite, I. Loke, U. Möglinger, E. S. X. Moh, M. Nakano, S. Recuero,
779 M. K. Sethi, M. Srougi, K. Stavenhagen, V. Venkatakrishnan, K. Wongtrakul-Kish, S.
780 Diestel, P. Hoffmann, N. G. Karlsson, D. Kolarich, M. P. Molloy, M. H. Muders, M. K.
781 Oehler, N. H. Packer, G. Palmisano, M. Thaysen-Andersen, Protein Paucimannosylation Is
782 an Enriched N-Glycosylation Signature of Human Cancers. *Proteomics.* **19**, 1900010
783 (2019).
- 784 42. Y. Xiang, K. Karaveg, K. W. Moremen, Substrate recognition and catalysis by GH47 α -
785 mannosidases involved in Asn-linked glycan maturation in the mammalian secretory
786 pathway. *Proc. Natl. Acad. Sci. U. S. A.* **113**, E7890–E7899 (2016).
- 787 43. J. Ugonotti, R. Kawahara, I. Loke, Y. Zhu, S. Chatterjee, H. C. Tjondro, Z. Sumer-
788 Bayraktar, S. Neelamegham, M. Thaysen-Andersen, N-acetyl- β -D-hexosaminidases
789 mediate the generation of paucimannosidic proteins via a putative noncanonical truncation
790 pathway in human neutrophils. *Glycobiology.* **32**, 218–229 (2022).
- 791 44. K. T. Schjoldager, Y. Narimatsu, H. J. Joshi, H. Clausen, Global view of human protein
792 glycosylation pathways and functions. *Nat. Rev. Mol. Cell Biol.* 2020 2112. **21**, 729–749
793 (2020).
- 794 45. G. Marsico, L. Russo, F. Quondamatteo, A. Pandit, Glycosylation and Integrin Regulation

- 795 in Cancer. *Trends in Cancer*. **4**, 537–552 (2018).
- 796 46. C. Bonnans, J. Chou, Z. Werb, Remodelling the extracellular matrix in development and
797 disease. *Nat. Rev. Mol. Cell Biol.* **15**, 786–801 (2014).
- 798 47. J. Winkler, A. Abisoye-Ogunniyan, K. J. Metcalf, Z. Werb, Concepts of extracellular
799 matrix remodelling in tumour progression and metastasis. *Nat. Commun.* **2020 111**. **11**, 1–
800 19 (2020).
- 801 48. A. Braun, H. J. Anders, T. Gudermann, E. Mammadova-Bach, Platelet-Cancer Interplay:
802 Molecular Mechanisms and New Therapeutic Avenues. *Front. Oncol.* **11**, 2576 (2021).
- 803 49. M. Schlesinger, Role of platelets and platelet receptors in cancer metastasis. *J. Hematol.*
804 *Oncol.* **2018 111**. **11**, 1–15 (2018).
- 805 50. F. Mollinedo, Neutrophil Degranulation, Plasticity, and Cancer Metastasis. *Trends*
806 *Immunol.* **40**, 228–242 (2019).
- 807 51. H. C. Tjondro, J. Ugonotti, R. Kawahara, S. Chatterjee, S. Chen, F. Soltermann, H.
808 Hinneburg, B. L. Parker, V. Venkatakrishnan, I. Loke, R. Dieckmann, O. C. Grant, J.
809 Bylund, A. Rodger, R. J. Woods, A. Karlsson-Bengtsson, W. B. Struwe, M. Thaysen-
810 Andersen, Hyper-truncated Asn355- and Asn391-glycans modulate the activity of
811 neutrophil granule myeloperoxidase. *J. Biol. Chem.* **296** (2021),
812 doi:10.1074/JBC.RA120.016342.
- 813 52. V. Venkatakrishnan, R. Dieckmann, I. Loke, H. C. Tjondro, S. Chatterjee, J. Bylund, M.
814 Thaysen-Andersen, N. G. Karlsson, A. Karlsson-Bengtsson, Glycan analysis of human
815 neutrophil granules implicates a maturation-dependent glycosylation machinery. *J. Biol.*
816 *Chem.* **295**, 12648–12660 (2020).
- 817 53. I. Loke, N. H. Packer, M. Thaysen-Andersen, Complementary LC-MS/MS-Based N-
818 Glycan, N-Glycopeptide, and Intact N-Glycoprotein Profiling Reveals Unconventional
819 Asn71-Glycosylation of Human Neutrophil Cathepsin G. *Biomolecules.* **5**, 1832–1854
820 (2015).
- 821 54. I. Loke, O. Østergaard, N. H. H. Heegaard, N. H. Packer, M. Thaysen-Andersen,
822 Paucimannose-Rich N -glycosylation of Spatiotemporally Regulated Human Neutrophil
823 Elastase Modulates Its Immune Functions . *Mol. Cell. Proteomics* (2017),
824 doi:10.1074/mcp.m116.066746.
- 825 55. M. E. Shaul, Z. G. Fridlender, Tumour-associated neutrophils in patients with cancer. *Nat.*
826 *Rev. Clin. Oncol.* **2019 1610**. **16**, 601–620 (2019).
- 827 56. M. Domnich, J. Riedesel, E. Pylaeva, C. H. L. Kürten, J. Buer, S. Lang, J. Jablonska, Oral
828 Neutrophils: Underestimated Players in Oral Cancer. *Front. Immunol.* **0**, 2529 (2020).
- 829 57. N. Wang, Y. Feng, Q. Wang, S. Liu, L. Xiang, M. Sun, X. Zhang, G. Liu, X. Qu, F. Wei,
830 Neutrophils infiltration in the tongue squamous cell carcinoma and its correlation with
831 CEACAM1 expression on tumor cells. *PLoS One.* **9** (2014),
832 doi:10.1371/JOURNAL.PONE.0089991.
- 833 58. I. Chatzistefanou, J. Lubek, K. Markou, R. A. Ord, The role of perineural invasion in
834 treatment decisions for oral cancer patients: A review of the literature. *J. Craniomaxillofac.*
835 *Surg.* **45**, 821–825 (2017).
- 836 59. S. K. Rajappa, U. Maheshwari, D. Ram, V. P. B. Koyyala, G. Mandal, R. Kumar, A. K.
837 Dewan, G. Vishwakarma, Extracapsular extension in oral cavity cancers-predictive factors
838 and impact on recurrence pattern and survival. *Int. J. Oral Maxillofac. Surg.* **48**, 989–994
839 (2019).
- 840 60. M. Brandwein-Gensler, M. S. Teixeira, C. M. Lewis, B. Lee, L. Rolnitzky, J. J. Hille, E.
841 Genden, M. L. Urken, B. Y. Wang, Oral squamous cell carcinoma: histologic risk
842 assessment, but not margin status, is strongly predictive of local disease-free and overall
843 survival. *Am. J. Surg. Pathol.* **29**, 167–78 (2005).
- 844 61. F. Liang, C. Zhang, H. Guo, S. H. Gao, F. Y. Yang, G. B. Zhou, G. Z. Wang,

- 845 Comprehensive analysis of BTN3A1 in cancers: mining of omics data and validation in
846 patient samples and cellular models. *FEBS Open Bio.* **11**, 2586–2599 (2021).
- 847 62. S. W. de Vroome, S. Holst, M. R. Gironde, Y. E. M. van der Burgt, W. E. Mesker, R. A. E.
848 M. Tollenaar, M. Wuhner, Serum N-glycome alterations in colorectal cancer associate with
849 survival. *Oncotarget.* **9**, 30610 (2018).
- 850 63. K. Kodar, J. Stadlmann, K. Klaamas, B. Sergejev, O. Kurtenkov, Immunoglobulin G Fc
851 N-glycan profiling in patients with gastric cancer by LC-ESI-MS: relation to tumor
852 progression and survival. *Glycoconjugate J.* **29**, 57–66 (2011).
- 853 64. T. Zhao, C. Zhang, W. Ma, Y. Xiong, J. Yao, G. Yan, G. Chen, H. Lu, A practical
854 approach to enrich intact tryptic N-glycopeptides through size exclusion chromatography
855 and hydrophilicity (SELIC) using an acrylamide-agarose composite gel system. *Anal.*
856 *Chim. Acta* (2019), doi:10.1016/j.aca.2019.01.044.
- 857 65. P. H. Jensen, N. G. Karlsson, D. Kolarich, N. H. Packer, Structural analysis of N- and O-
858 glycans released from glycoproteins. *Nat. Protoc.* (2012), doi:10.1038/nprot.2012.063.
- 859 66. H. Hinneburg, S. Chatterjee, F. Schirmeister, T. Nguyen-Khuong, N. H. Packer, E. Rapp,
860 M. Thaysen-Andersen, Post-Column Make-Up Flow (PCMF) Enhances the Performance of
861 Capillary-Flow PGC-LC-MS/MS-Based Glycomics. *Anal. Chem.* (2019),
862 doi:10.1021/acs.analchem.8b05720.
- 863 67. A. L. Oberg, O. Vitek, Statistical design of quantitative mass spectrometry-based
864 proteomic experiments. *J. Proteome Res.* **8** (2009), pp. 2144–2156.
- 865 68. W. Revelle, Package “psych” - Procedures for Psychological, Psychometric and
866 Personality Research. *R Packag.* (2015).
- 867 69. C. Ashwood, C. H. Lin, M. Thaysen-Andersen, N. H. Packer, Discrimination of Isomers of
868 Released N- and O-Glycans Using Diagnostic Product Ions in Negative Ion PGC-LC-ESI-
869 MS/MS. *J. Am. Soc. Mass Spectrom.* (2018), doi:10.1007/s13361-018-1932-z.
- 870 70. C. A. Cooper, E. Gasteiger, N. H. Packer, GlycoMod - A software tool for determining
871 glycosylation compositions from mass spectrometric data. *Proteomics* (2001),
872 doi:10.1002/1615-9861(200102)1:2<340::AID-PROT340>3.0.CO;2-B.
- 873 71. A. V. Everest-Dass, D. Kolarich, M. P. Campbell, N. H. Packer, Tandem mass spectra of
874 glycan substructures enable the multistage mass spectrometric identification of
875 determinants on oligosaccharides. *Rapid Commun. Mass Spectrom.* **27**, 931–939 (2013).
- 876 72. K. J. Adams, B. Pratt, N. Bose, L. G. Dubois, L. St. John-Williams, K. M. Perrott, K. Ky,
877 P. Kapahi, V. Sharma, M. J. Maccoss, M. A. Moseley, C. A. Colton, B. X. Maclean, B.
878 Schilling, J. W. Thompson, Skyline for Small Molecules: A Unifying Software Package for
879 Quantitative Metabolomics. *J. Proteome Res.* (2020), doi:10.1021/acs.jproteome.9b00640.
- 880 73. A. Ceroni, K. Maass, H. Geyer, R. Geyer, A. Dell, S. M. Haslam, GlycoWorkbench: A tool
881 for the computer-assisted annotation of mass spectra of glycans. *J. Proteome Res.* (2008),
882 doi:10.1021/pr7008252.
- 883 74. J. Villén, S. P. Gygi, The SCX/IMAC enrichment approach for global phosphorylation
884 analysis by mass spectrometry. *Nat. Protoc.* **3**, 1630–1638 (2008).
- 885 75. S. Mysling, G. Palmisano, P. Hojrup, M. Thaysen-Andersen, Utilizing ion-pairing
886 hydrophilic interaction chromatography solid phase extraction for efficient glycopeptide
887 enrichment in glycoproteomics. *Anal. Chem.* (2010), doi:10.1021/ac100530w.
- 888 76. M. Bern, Y. J. Kil, C. Becker, Byonic: Advanced peptide and protein identification
889 software. *Curr. Protoc. Bioinforma.* (2012), doi:10.1002/0471250953.bi1320s40.
- 890 77. M. W. Bern, Y. J. Kil, Two-dimensional target decoy strategy for shotgun proteomics. *J.*
891 *Proteome Res.* (2011), doi:10.1021/pr200780j.
- 892 78. J. Cox, M. Mann, MaxQuant enables high peptide identification rates, individualized
893 p.p.b.-range mass accuracies and proteome-wide protein quantification. *Nat. Biotechnol.*
894 **26**, 1367–1372 (2008).

- 895 79. J. Cox, N. Neuhauser, A. Michalski, R. A. Scheltema, J. V. Olsen, M. Mann, Andromeda:
896 A Peptide Search Engine Integrated into the MaxQuant Environment. *J. Proteome Res.* **10**,
897 1794–1805 (2011).
- 898 80. M. Vaidya, C. Dmello, S. Mogre, Utility of Keratins as Biomarkers for Human Oral
899 Precancer and Cancer. *Life* 2022, Vol. 12, Page 343. **12**, 343 (2022).
- 900 81. L. X. Neves, D. C. Granato, A. F. Busso-Lopes, C. M. Carnielli, F. M. de Sá Patroni, T. de
901 Rossi, A. K. Oliveira, A. C. P. Ribeiro, T. B. Brandão, A. N. Rodrigues, P. A. Lacerda, M.
902 Uno, N. K. Cervigne, A. R. Santos-Silva, L. P. Kowalski, M. A. Lopes, A. F. Paes Leme,
903 Peptidomics-driven strategy reveals peptides and predicted proteases associated with oral
904 cancer prognosis. *Mol. Cell. Proteomics.* **20** (2021), doi:10.1074/MCP.RA120.002227.
- 905 82. X. Robin, N. Turck, A. Hainard, N. Tiberti, F. Lisacek, J. C. Sanchez, M. Müller, pROC:
906 An open-source package for R and S+ to analyze and compare ROC curves. *BMC*
907 *Bioinformatics* (2011), doi:10.1186/1471-2105-12-77.
- 908 83. D. W. Huang, B. T. Sherman, R. A. Lempicki, Systematic and integrative analysis of large
909 gene lists using DAVID bioinformatics resources. *Nat. Protoc.* **4**, 44–57 (2009).
- 910 84. E. Y. Chen, C. M. Tan, Y. Kou, Q. Duan, Z. Wang, G. Meirelles, N. R. Clark, A. Ma'ayan,
911 Enrichr: interactive and collaborative HTML5 gene list enrichment analysis tool. *BMC*
912 *Bioinformatics.* **14**, 128 (2013).
- 913 85. J. A. Vizcaíno, E. W. Deutsch, R. Wang, A. Csordas, F. Reisinger, D. Ríos, J. A. Dienes,
914 Z. Sun, T. Farrah, N. Bandeira, P.-A. Binz, I. Xenarios, M. Eisenacher, G. Mayer, L. Gatto,
915 A. Campos, R. J. Chalkley, H.-J. Kraus, J. P. Albar, S. Martinez-Bartolomé, R. Apweiler,
916 G. S. Omenn, L. Martens, A. R. Jones, H. Hermjakob, ProteomeXchange provides globally
917 coordinated proteomics data submission and dissemination. *Nat. Biotechnol.* **32**, 223–226
918 (2014).
- 919 86. Y. Watanabe, K. F. Aoki-Kinoshita, Y. Ishihama, S. Okuda, GlycoPOST realizes FAIR
920 principles for glycomics mass spectrometry data. *Nucleic Acids Res.* **49**, D1523–D1528
921 (2021).
- 922
- 923

924 Acknowledgments

925 We thank Dr. Sami Yokoo for the assistance with tissue recovery and Dr. Daniela Granato
926 for assistance with sample digestion. We also thank Dr Edward S.X. Moh and Dr Krishnatej
927 Nishtala for assistance with the acquisition of glycomics data.

928

929 Funding

930 Fundação de Amparo à Pesquisa do Estado de São Paulo (FAPESP) grant 2018/02180-0
931 (CMC)

932 Fundação de Amparo à Pesquisa do Estado de São Paulo (FAPESP) grant 2019/17840-8
933 (CMC)

934 Fundação de Amparo à Pesquisa do Estado de São Paulo (FAPESP) grant 2018/18496-6
935 (AFPL)

936 Cancer Institute NSW Grant ECF181259 (RK)

937 Australian Research Council (ARC) Future Fellowship grant (FT210100455) (MTA)

938 Macquarie University Enterprise Partnership Scheme (175232162) (MTA)

939

940

941 Author contributions

942 Conceptualisation: CMC, AFPL, RK, MTA

943 Collected the clinical samples: ACPR, TBB, ES, LLM

944 Prepared tissues slides and assigned tumour area: TMLM

945 Methodology: CMC, AFPL, RK, MTA
946 Investigation: CMC, RK
947 Visualisation: CMC, FP, RK
948 Supervision: AFPL, RK, MTA
949 Writing-original draft: CMC
950 Writing-review & editing: AFPL, RK, LPK, MTA

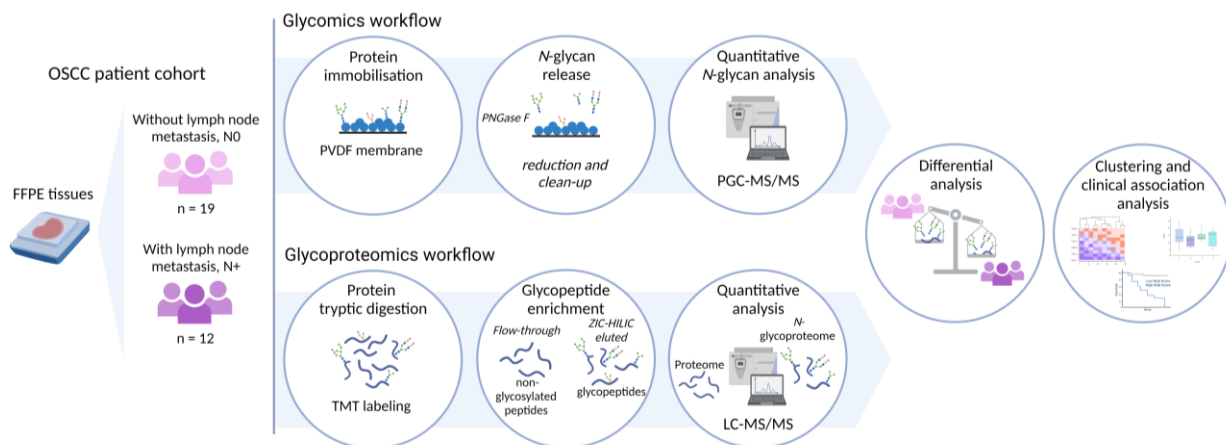
951 **Competing interests**

952 The authors declare no conflict of interest.

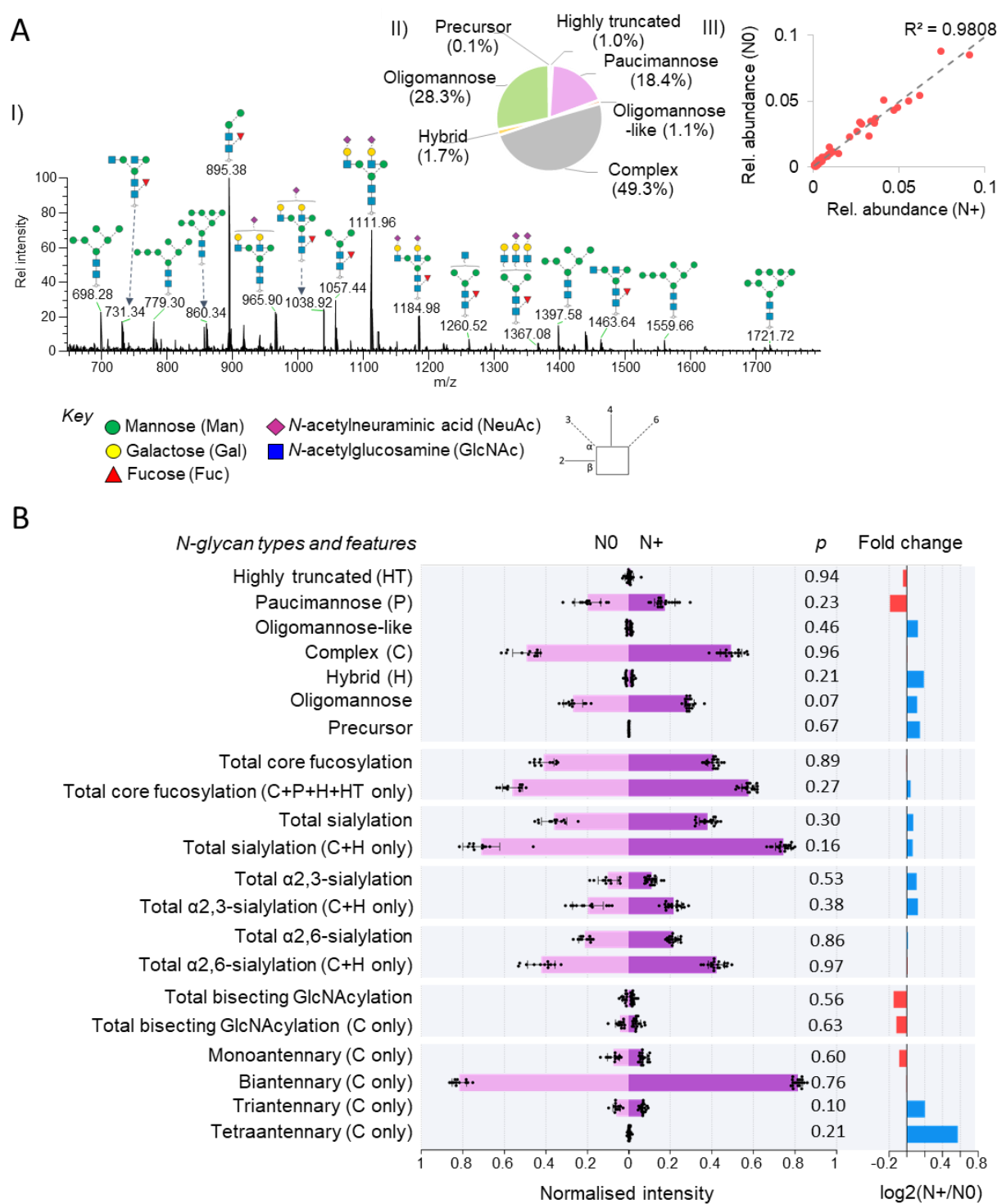
953 **Data and materials availability:**

954 All proteomics and glycoproteomics LC-MS/MS raw data files supporting the conclusions
955 presented herein have been deposited to the ProteomeXchange Consortium via the PRIDE
956 (85) partner repository with the dataset identifier PXD037134. All glycomics LC-MS/MS
957 raw data files are available via the GlycoPOST (86) with the identifier GPST000296.
958
959
960
961

962 **Figures and Tables**



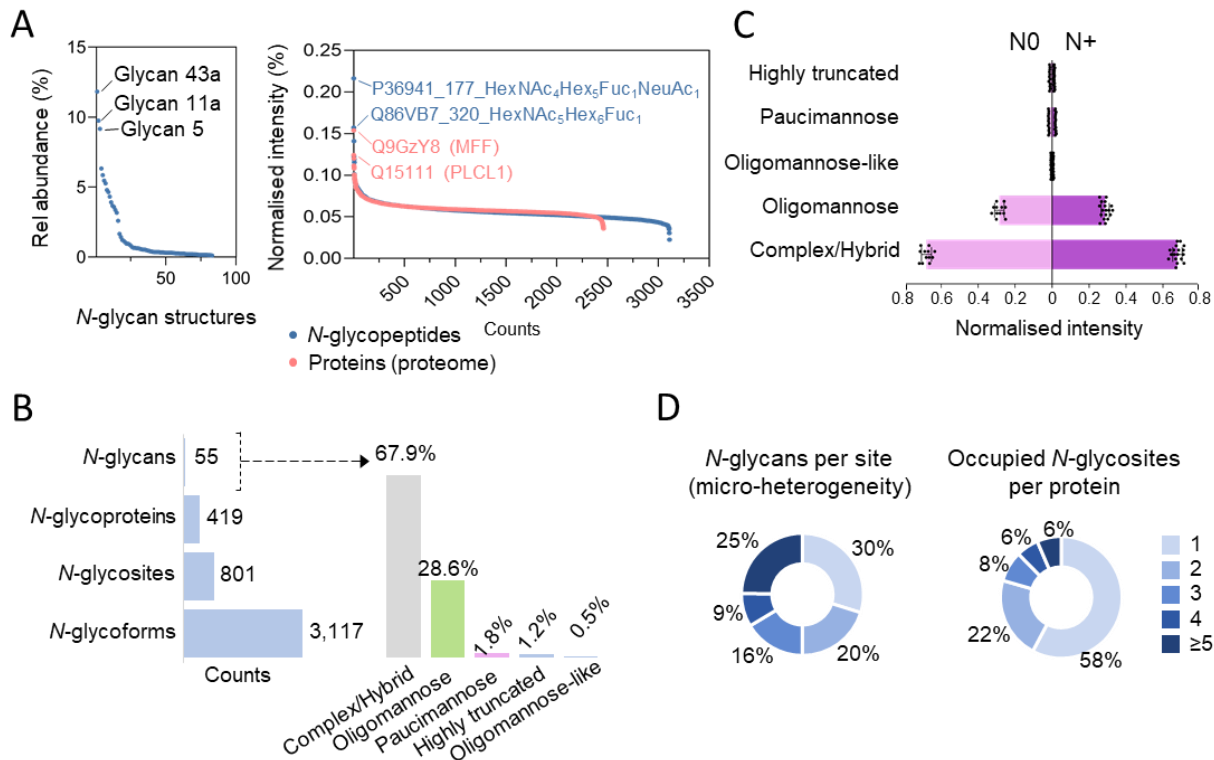
965 **Figure 1. Study overview.** Protein *N*-glycosylation was investigated using quantitative glycomics
966 (top) and glycoproteomics (bottom) from resected tumour tissues from 31 OSCC patients with (N+,
967 n = 19) or without (N0, n = 12) lymph node metastasis. The resulting *N*-glycome and *N*-
968 glycoproteome data were quantitatively compared between patient groups using advanced
969 statistical tests including clustering analysis and associations to a range of clinicopathological
970 features were explored using patient metadata.



971

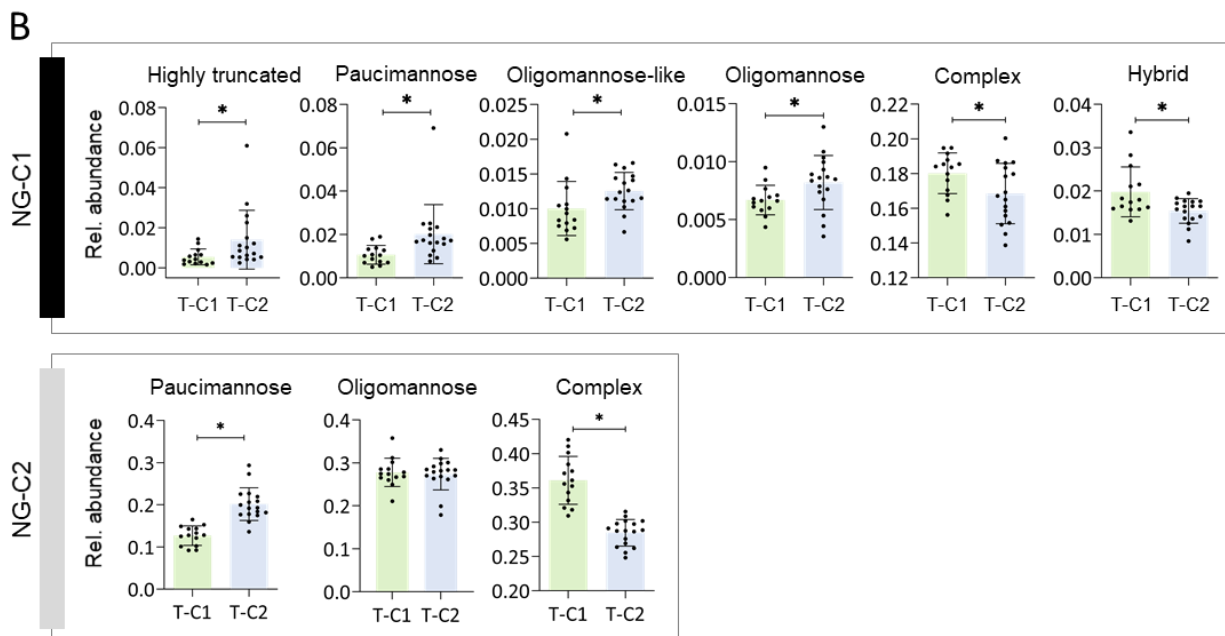
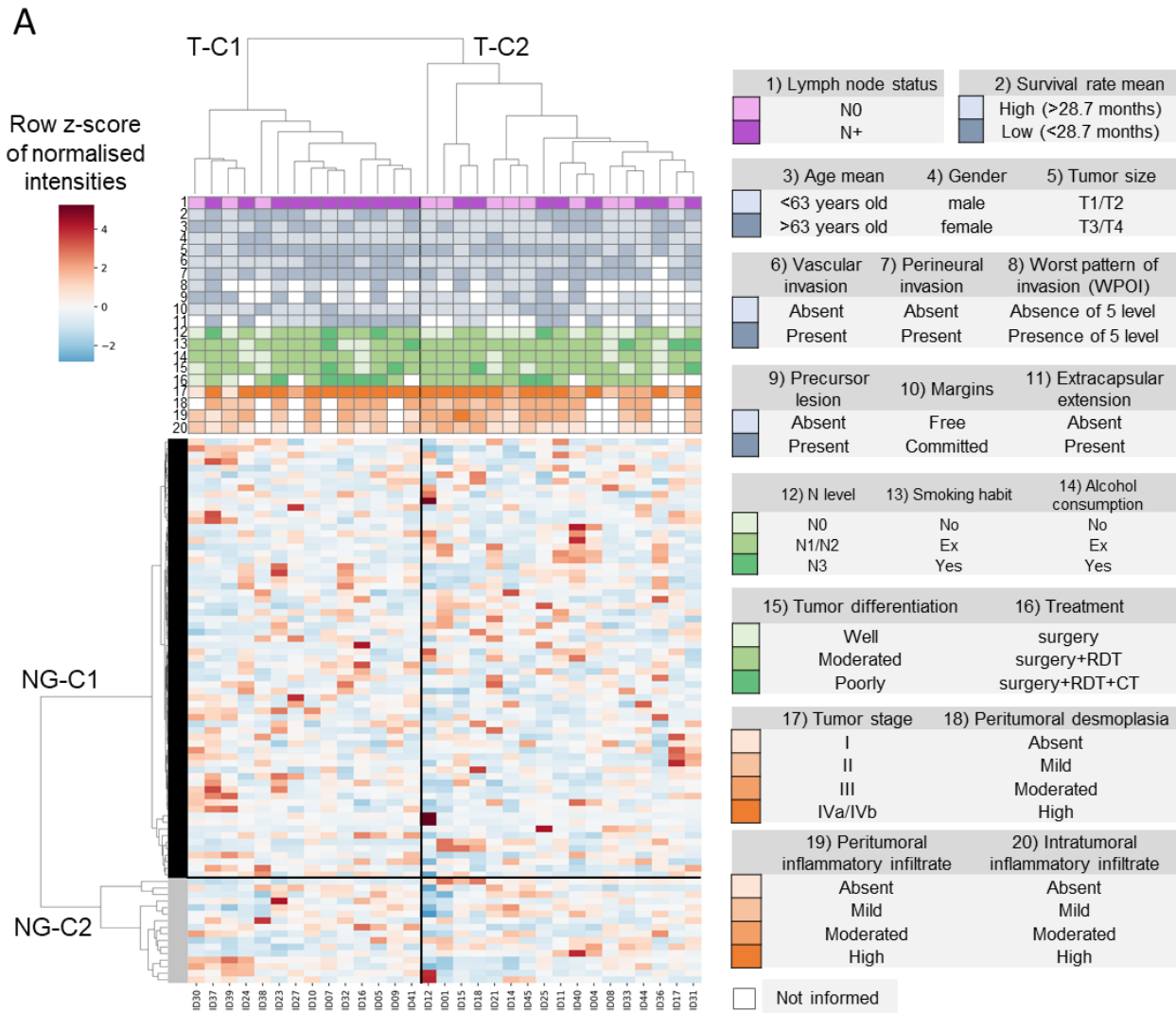
972 **Figure 2. Stable *N*-glycome in OSCC tumour tissues.** A) I- The OSCC tumour tissue *N*-glycome
 973 predominantly comprises complex, oligomannosidic and paucimannosidic *N*-glycans as shown by
 974 an exemplar summed MS1 spectrum. II- Overall distribution of *N*-glycan classes. III- Similar *N*-
 975 glycan distribution within N+ and N0 tissues as demonstrated by a high correlation coefficient (R^2).
 976 B) Quantitative comparison of *N*-glycan types and other key structural features between N0 and N+
 977 including total core fucosylation levels (calculated both out of the entire *N*-glycome and out of only
 978 structures able to carry core fucosylation) and total sialylation levels including α 2,3- or α 2,6-
 979 sialylation, bisecting GlcNAcylation and degree of branching (mono-, bi- or triantennary *N*-
 980 glycosylation). While minor fold-change differences were observed (right), no significant
 981 differences were consistently found between N0 and N+. HT: highly truncated, P: paucimannose,

982 H: hybrid, C: complex, see Supplementary Figure S2 for structures and classification. Data are
983 plotted as means and error bars represent their standard deviation (n = 19, N+ and n = 12, N0).
984 Statistical test: two-sided Student's t test.



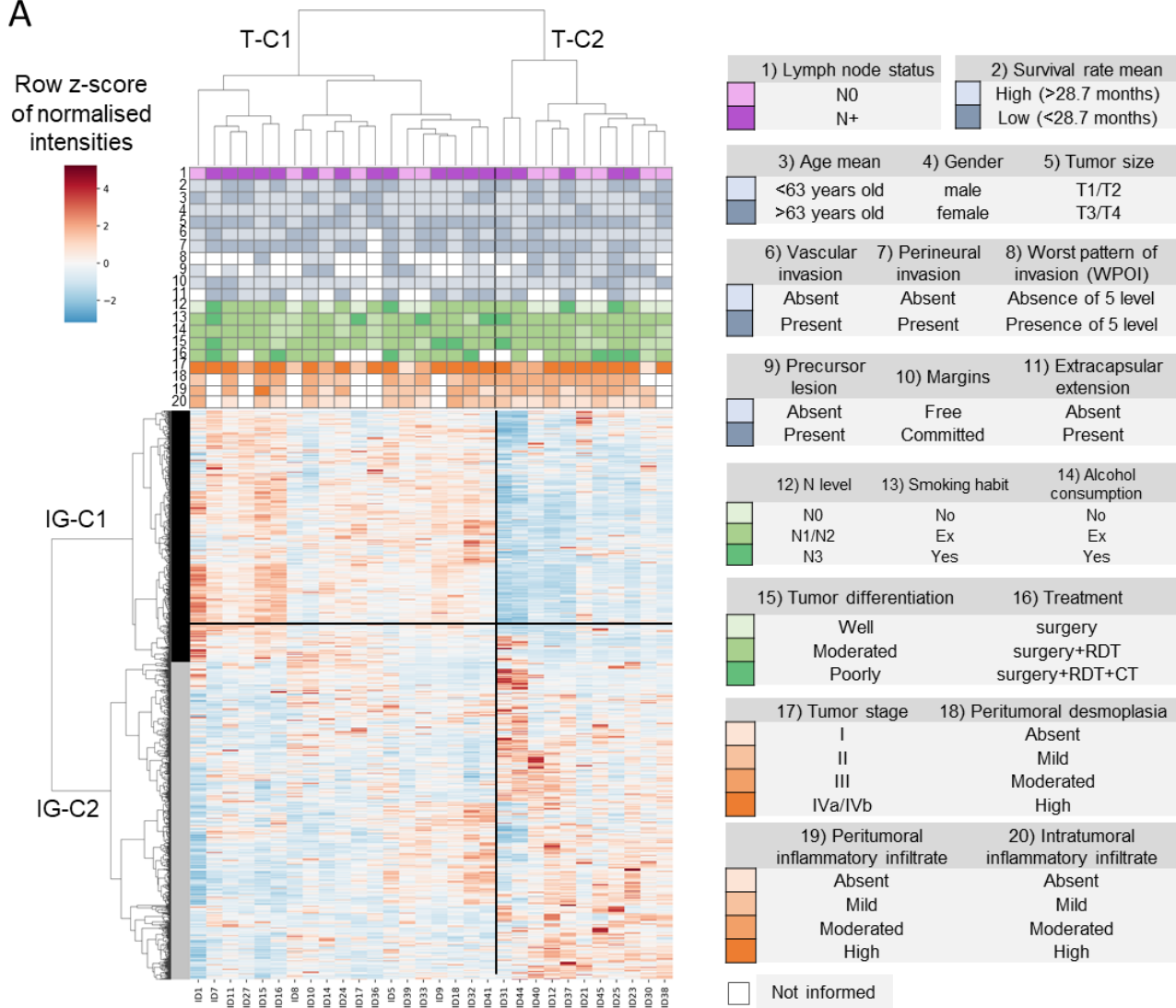
985

986 **Figure 3. Overview of the N-glycoproteome profile of OSCC tumour tissues.** A) Abundance
 987 range of identified N-glycan compositions (left) and identified N-glycopeptides (both from the
 988 acquired N-glycoproteome data) and proteins (from the proteome data). The most abundant N-
 989 glycans, N-glycopeptides and proteins are labelled in each graph. B) Overview of the N-
 990 glycoproteome of the investigated OSCC tumor tissues including the N-glycan compositions (and
 991 their distribution across the N-glycan classes, right), source N-glycoproteins, N-glycosites, and
 992 unique N-glycoforms (unique protein + unique site + unique glycan) identified in the ZIC-HILIC-
 993 enriched fractions. C) Comparison between the distribution of N-glycan classes in the NO and N+
 994 tumour tissues. D) Site-specific N-glycan micro-heterogeneity (top) and occupied sites per protein
 995 (bottom) in the OSCC tumour tissues. HT: highly truncated, P: paucimannose, O: oligomannose,
 996 O-L: oligomannose-like, C/H: complex and hybrid (grouped since these cannot reliably be
 997 distinguished through glycoproteomics data).

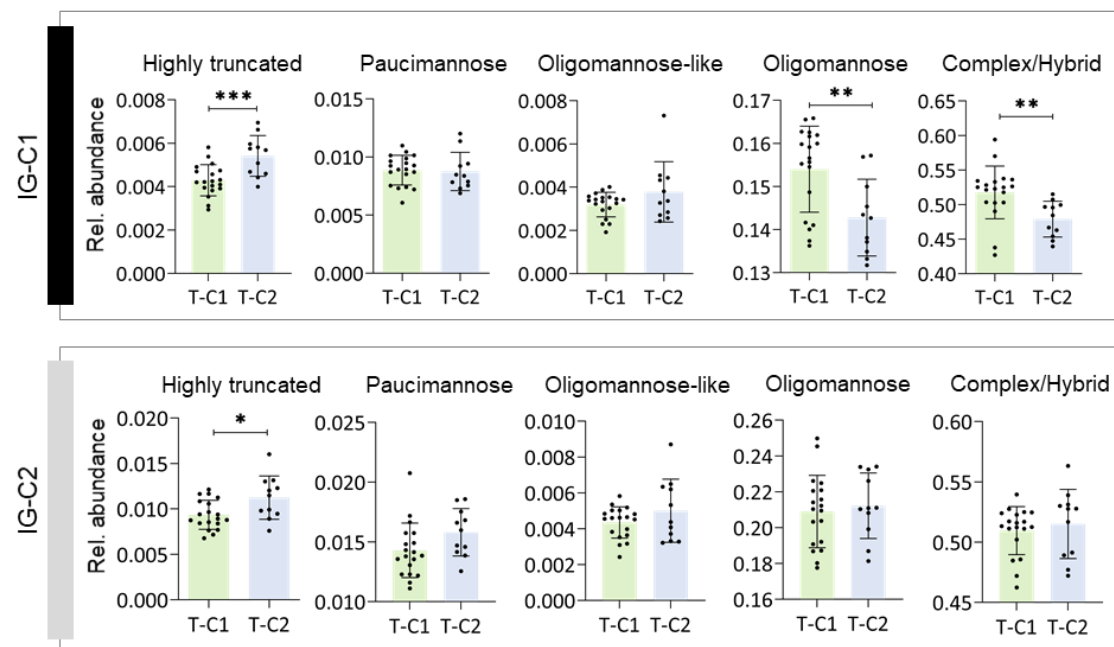


999 **Figure 4. *N*-glycome-driven clustering of OSCC tumour tissues.** A) Unsupervised hierarchical
1000 clustering analysis of the OSCC tumour tissue *N*-glycome data from N0 and N+ patients, performed
1001 with the 'cluster map' function in the Saborne package under Python using Euclidean distance and
1002 Ward linkage. Two major tumour clusters (T-C1 and T-C2) and two major *N*-glycan clusters (NG-
1003 C1 and NG-C2) were observed. Clinical and patient data are presented on top of the heat map and
1004 expanded to the right. B) Relative abundance of the *N*-glycan types between T-C1 (green bars) and
1005 T-C2 (blue bars) in NG-C1 (top) and NG-C2 (bottom), respectively. Student's t test, two-sided, $\alpha =$
1006 0.05, * $p < 0.05$, ** $p < 0.01$, *** $p < 0.001$.

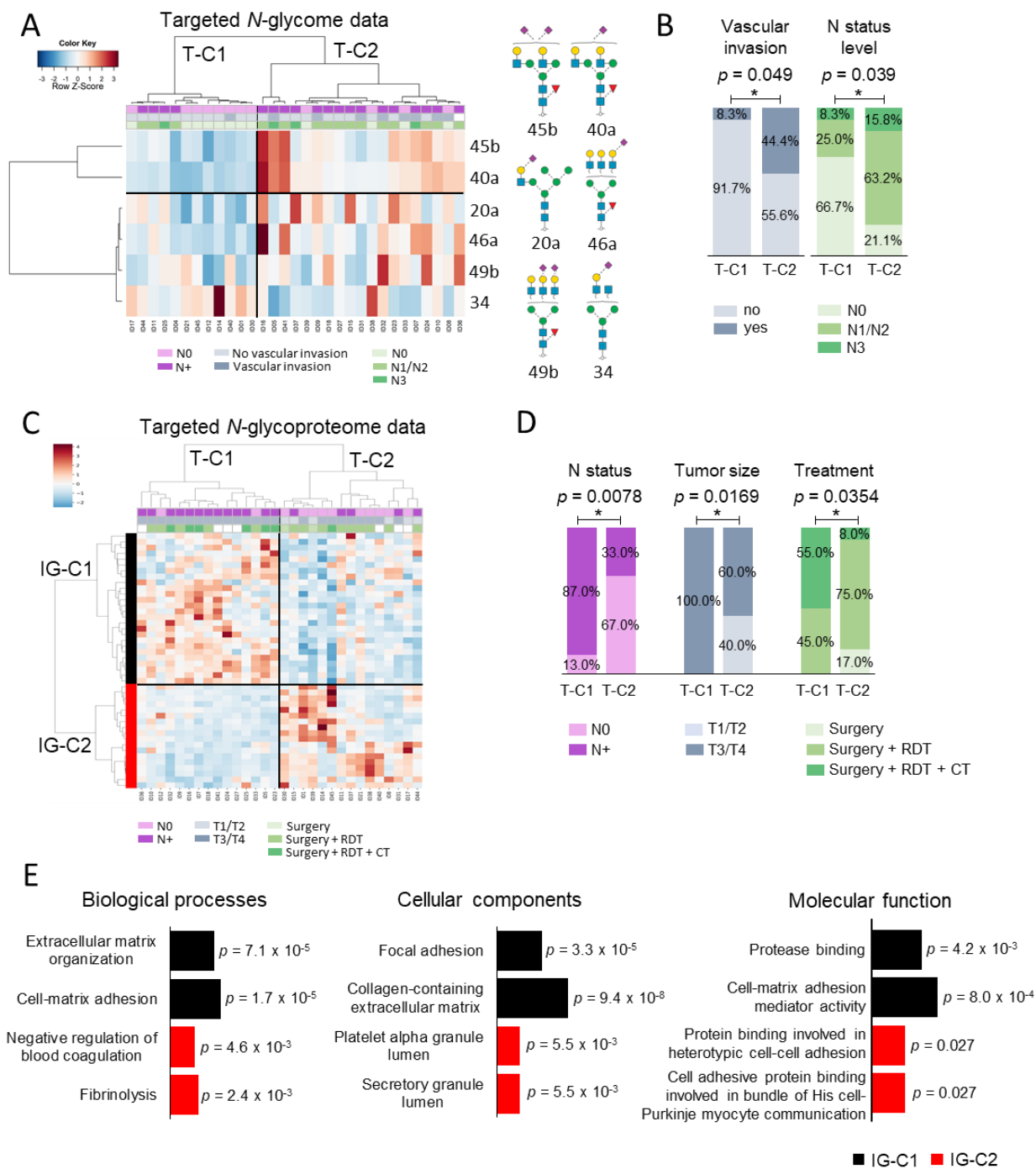
A



B



1008 **Figure 5. *N*-glycoproteome-driven clustering of OSCC tumour tissues.** A) Unsupervised
1009 hierarchical clustering analysis of *N*-glycopeptides identified in the tumor tissues from N0 and N+
1010 patients, performed with the ‘cluster map’ function in the Saborne package under Python using
1011 Canberra distance and Ward linkage. Two major tumor clusters i.e. T-C1 and T-C2 and two major
1012 *N*-glycopeptide clusters i.e. IG-C1 and IG-C2 were observed. Clinical and patient data are presented
1013 on top of the heat map, and expanded to the right. B) Relative abundance of *N*-glycan classes
1014 between tumor clusters (T-C1 in green, and T-C2 indicated in blue) in IG-C1 (top) and IG-C2
1015 (bottom). Student's t test, two-sided, $\alpha = 0.05$, * $p < 0.05$, ** $p < 0.01$, *** $p < 0.001$.



1016

1017

1018

1019

1020

1021

1022

1023

1024

1025

1026

1027

Figure 6. *N*-glycan and *N*-glycopeptide-guided tumour clusters associate with clinical features. A) Unsupervised hierarchical clustering analysis of six *N*-glycans found to be differentially abundant in OSCC tumour tissues from N0 and N+ patients. Plots are made with the 'heatmap.3' function under the R environment using Euclidean distance and Ward linkage. B) Cluster association analysis with clinical features ($p < 0.05$, Fisher's Exact Test for two group comparisons; or Pearson Chi-Square test for more than two group comparisons) performed using IBM SPSS Statistics. C) Unsupervised hierarchical clustering analysis of 79 *N*-glycopeptides found to be differentially expressed between the N0 and N+ tumour tissues. Plots were performed with the 'cluster map' function in the Saborne package under Python using Ward and correlation for clustering. D) Cluster association analysis with clinical features. E) The two most enriched Gene Ontology biological processes, cellular components and molecular function in the IG-C1 (black)

1028 and IG-C2 (red) glycopeptide clusters. An adjusted p value is indicated for each term in the
1029 enrichment analysis performed using the Enrichr tool. Fisher's Exact Test or Pearson Chi-Square
1030 test, $*p < 0.05$. RDT: radiotherapy; CT: chemotherapy.

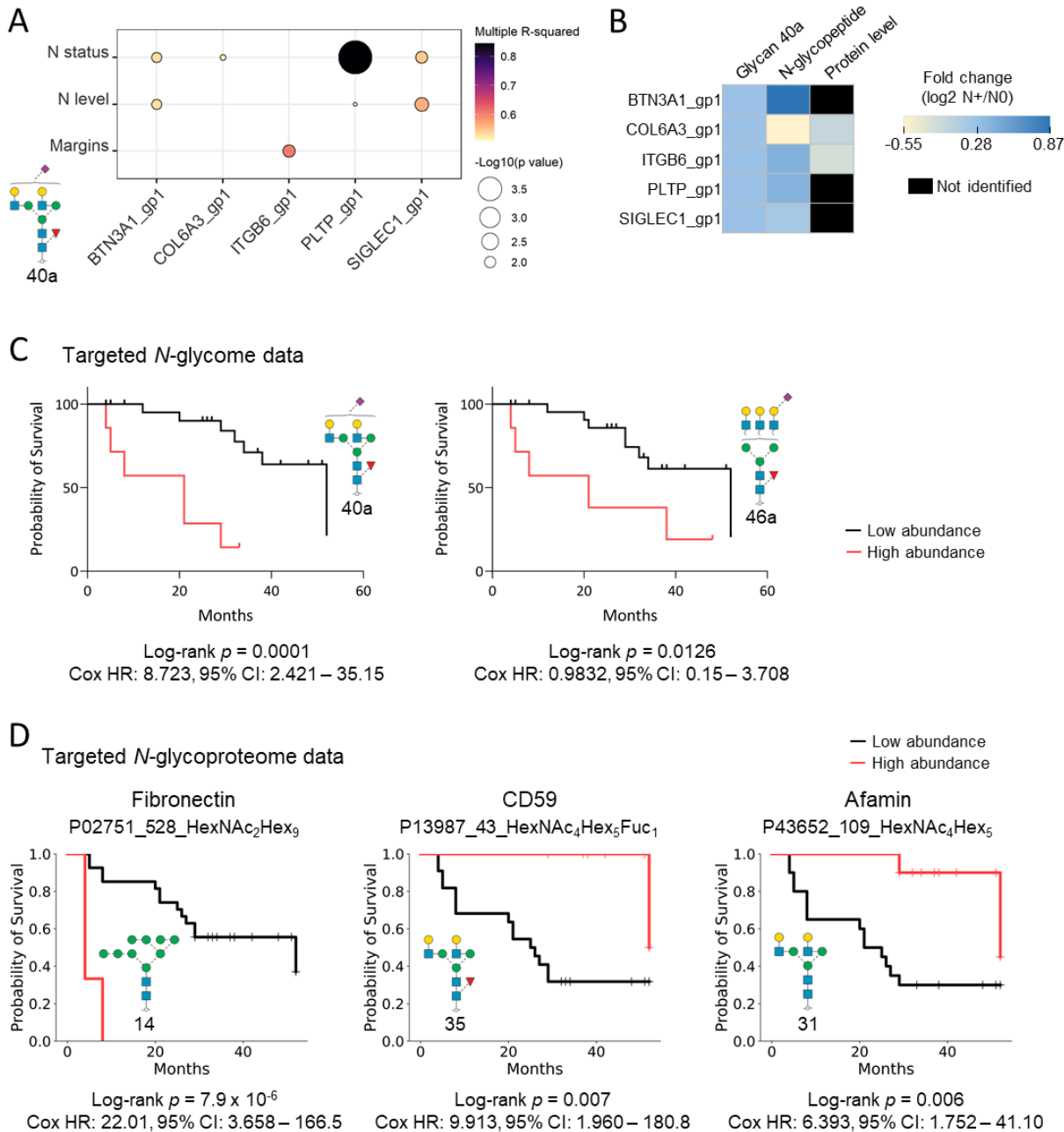


Fig. 7. N-glycan and N-glycopeptide levels are associated with clinical outcomes in OSCC. A) Five out of 25 N-glycopeptides that associated with clinicopathological features were found to carry Glycan 40a. B) Distribution of fold change values ($\log_2 N^+/N^0$) of Glycan 40a, glycopeptides carrying Glycan 40a and their source glycoproteins in the OSCC patient cohort. C) Glycan-guided Kaplan-Meier survival analysis. Patients with relative high levels of Glycan 40a and Glycan 46b presented worse overall survival ($p < 0.05$, log-rank test). D) Glycopeptide-guided Kaplan-Meier survival analysis. Left: Relative high abundance of a HexNAc₂Hex₉ glycopeptide from fibronectin was associated with relatively low patient survival (elevated glycopeptide levels found in N+ samples). Middle-right: Relative low abundance of N-glycopeptides from CD59 and afamin, respectively, were associated with a relatively low patient survival (reduced levels in N+ samples).

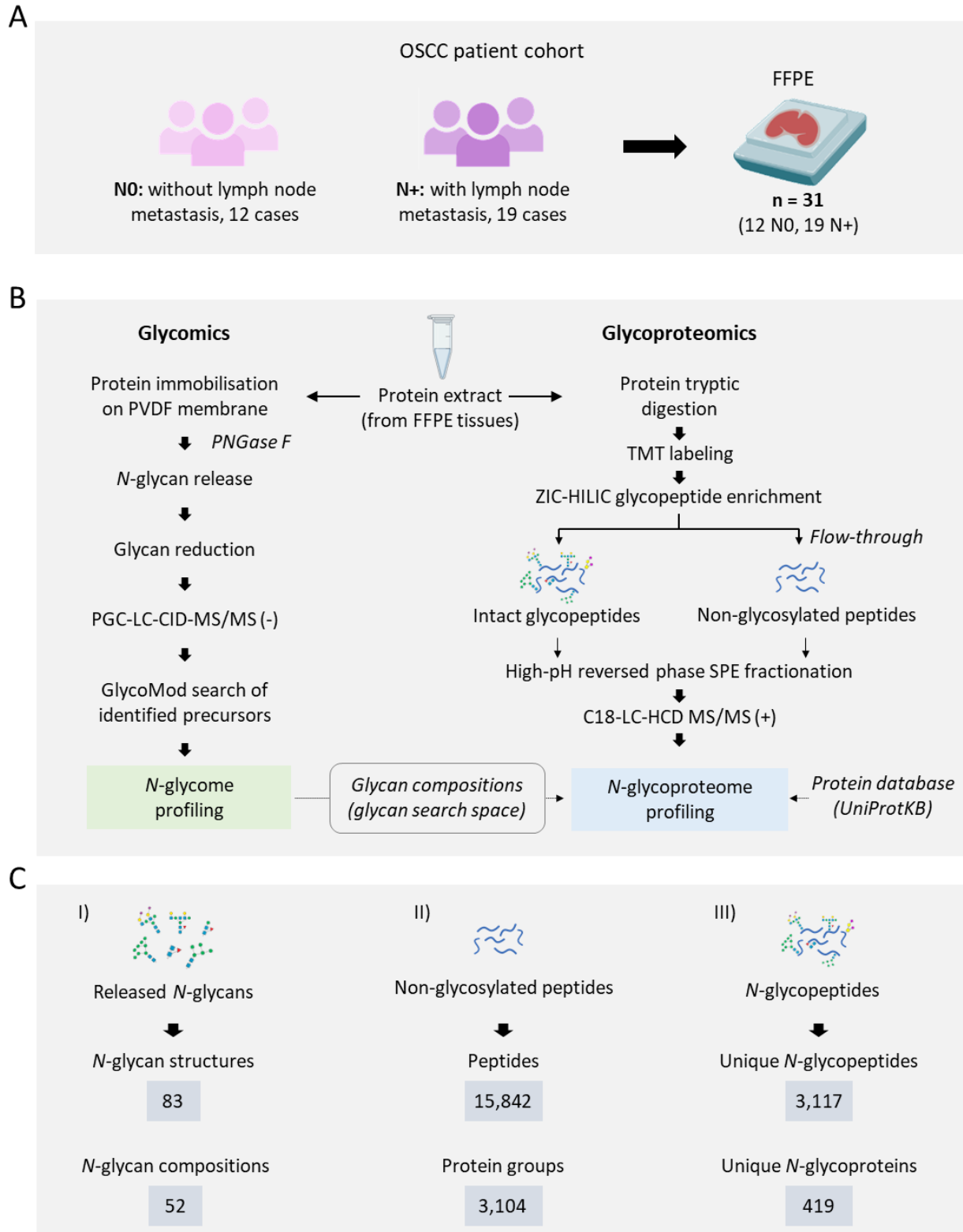
Supplementary Materials

Please see the attached Supplementary Materials.

Supplementary Materials for
Comprehensive glycoprofiling of oral tumours associates *N*-glycosylation with lymph node metastasis and patient survival

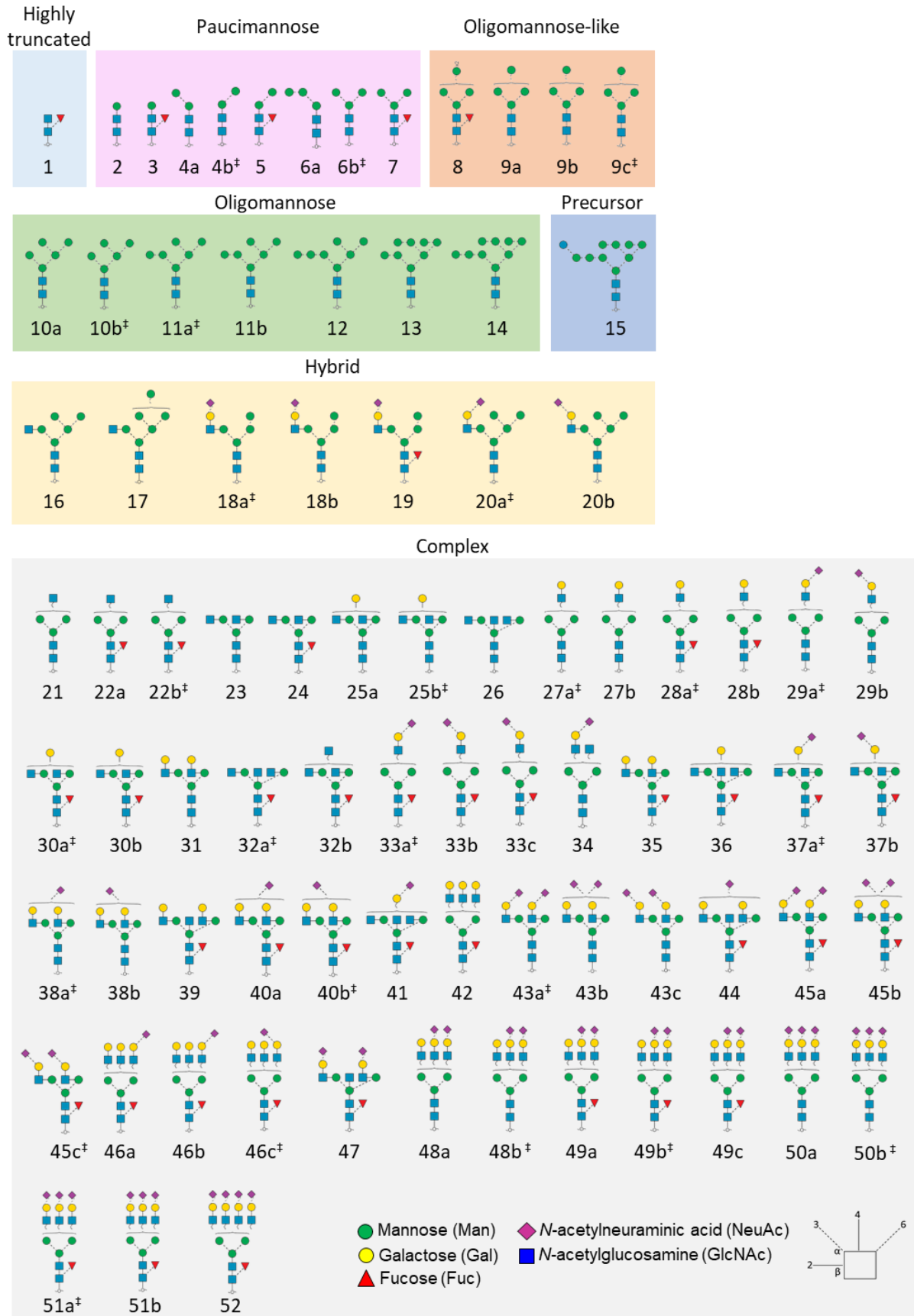
Carolina Moretto Carnielli, Thayná Melo de Lima Morais, Fábio Malta de Sá Patroni, Ana Carolina Prado Ribeiro, Thaís Bianca Brandão, Evandro Sobroza, Leandro Luongo de Matos, Luiz Paulo Kowalski, Adriana Franco Paes Leme, * Rebeca Kawahara, * Morten Thaysen-Andersen *

*Joint corresponding authors. Emails: adriana.paesleme@lnbio.cnpem.br; rebeca.kawaharasakuma@mq.edu.au; morten.andersen@mq.edu.au

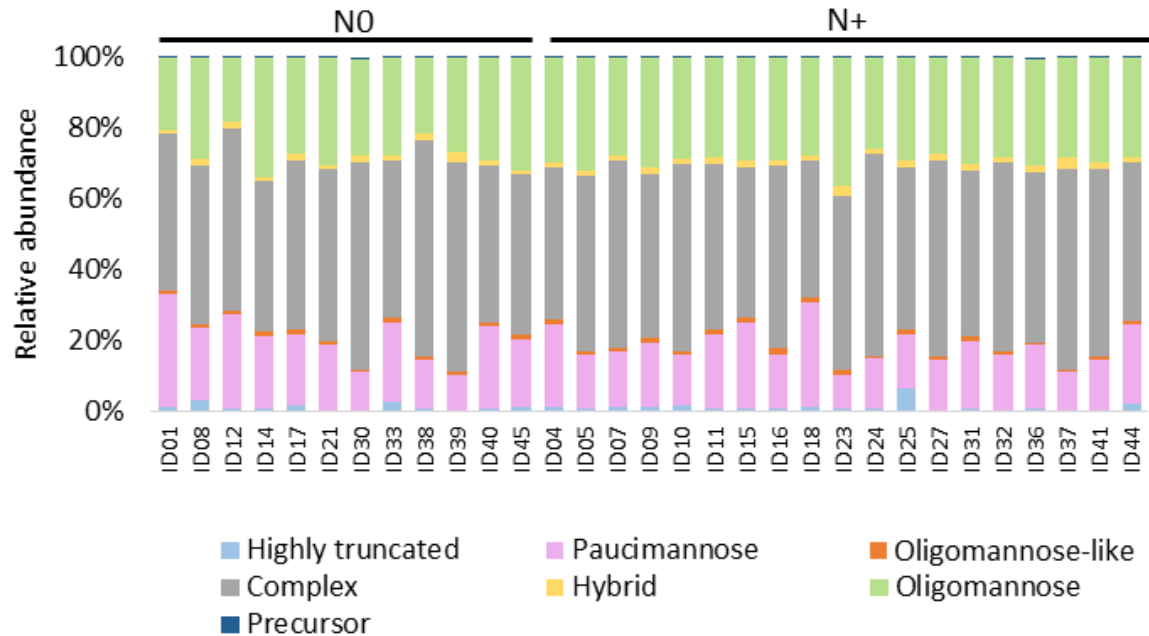


Supplementary Figure S1. Study design and overview of the integrated glycomics and glycoproteomics approach. A) Overview of the sample cohort comprising resected tumour

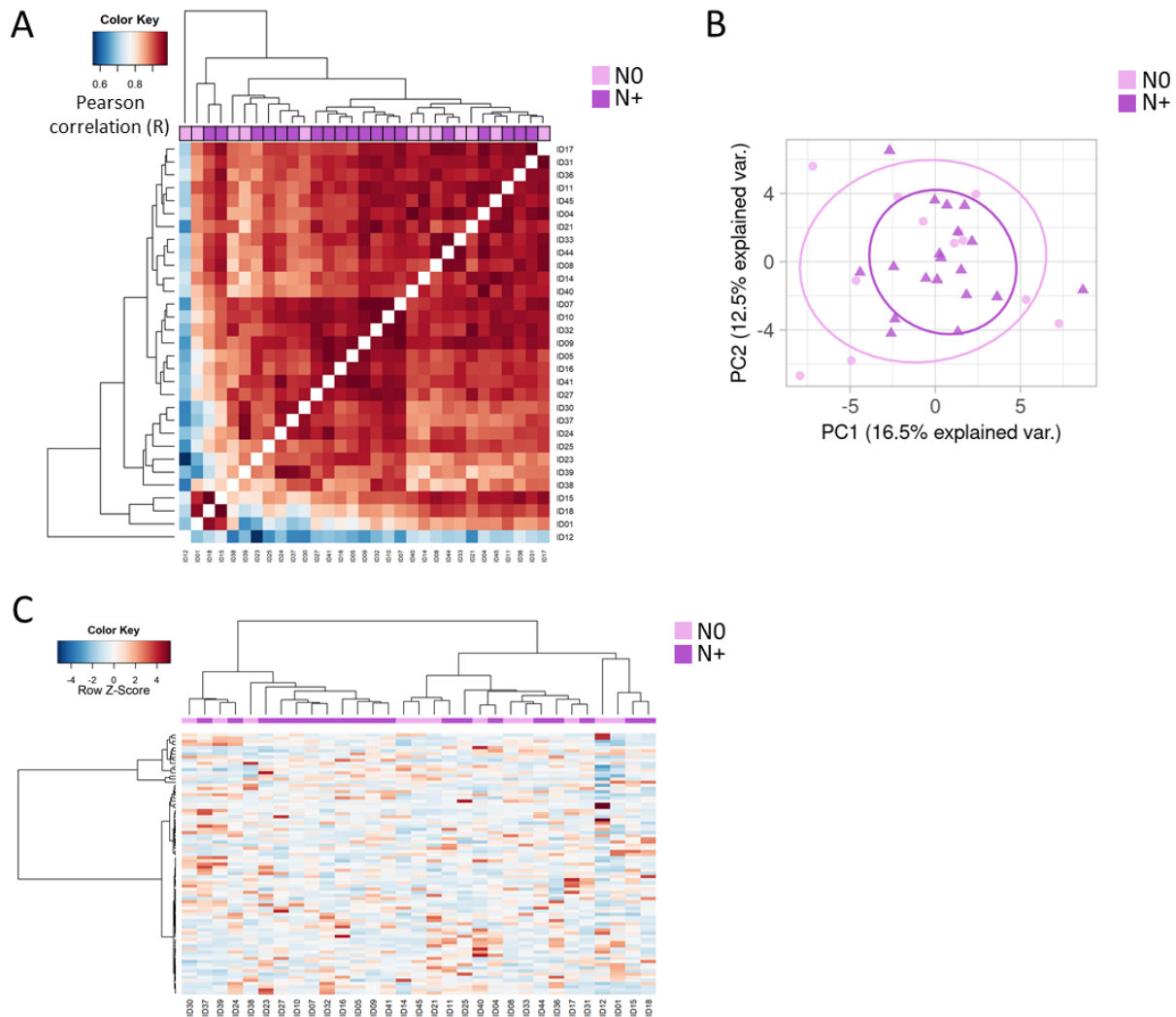
tissues (FFPE slides) from N0 and N+ OSCC patients. B) Overview of the integrated glycomics and glycoproteomics workflows. C) Total number of identifications for I) the *N*-glycome profiling including the *N*-glycan structures (including isomeric variants) and compositions, II) proteome profiling including the unique peptides and corresponding source proteins identified in the non-enriched (ZIC-HILIC flowthrough) fraction, III) *N*-glycoproteome profiling including the unique intact *N*-glycopeptides and corresponding source *N*-glycoproteins identified after ZIC-HILIC enrichment.



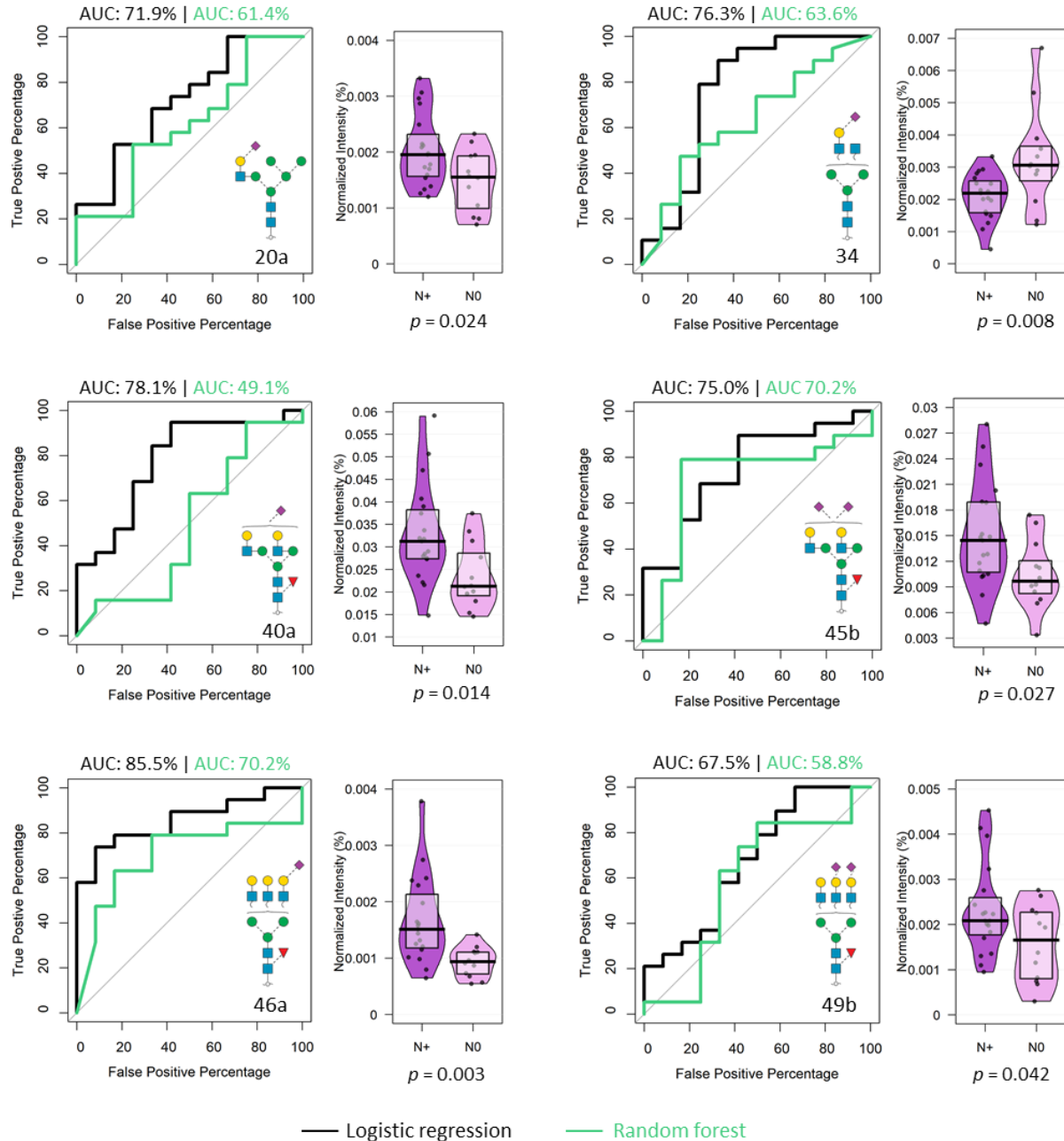
Supplementary Figure S2. *N*-glycome map of the investigated OSCC tissues. Map of the confidently identified *N*-glycan isomers and the assigned glycan identifiers used consistently in this study (Glycan 1-52). The *N*-glycan isomers observed for each composition are denoted with lower case letters (a, b, c...). ‡The most abundant *N*-glycan isomer.



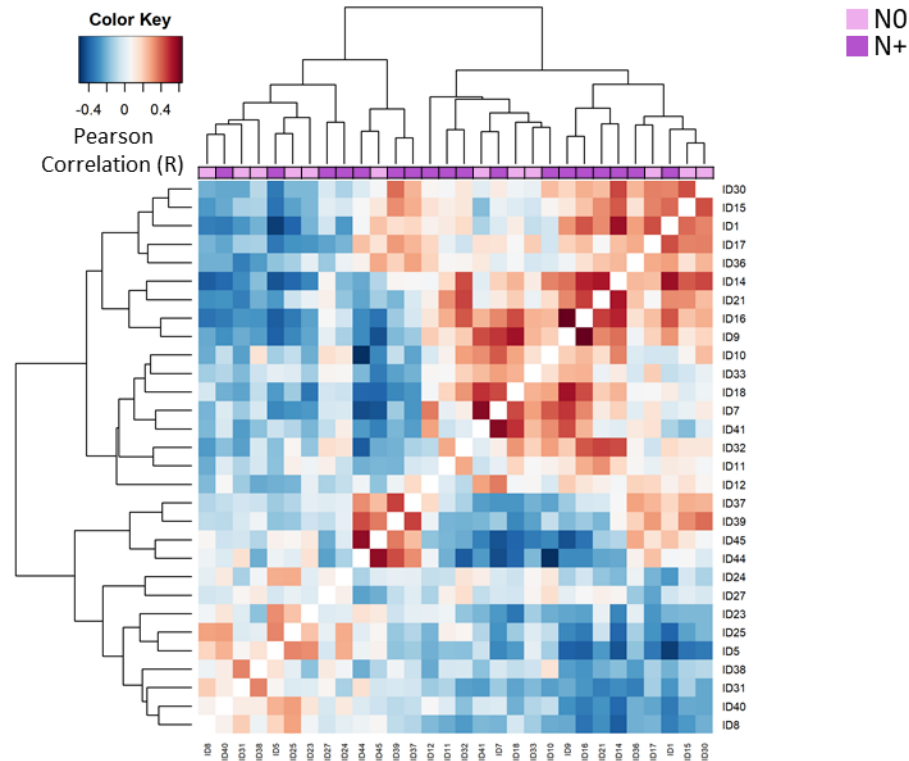
Supplementary Figure S3. *N*-glycan type distribution across the studied OSCC tumour tissue samples. Relative abundance of the identified *N*-glycan types within each N0 and N+ sample classified into highly truncated, paucimannose, complex, hybrid, oligomannose, oligomannose-like and precursor-type *N*-glycans, see Supplementary Figure S2 for *N*-glycan structures and classification.



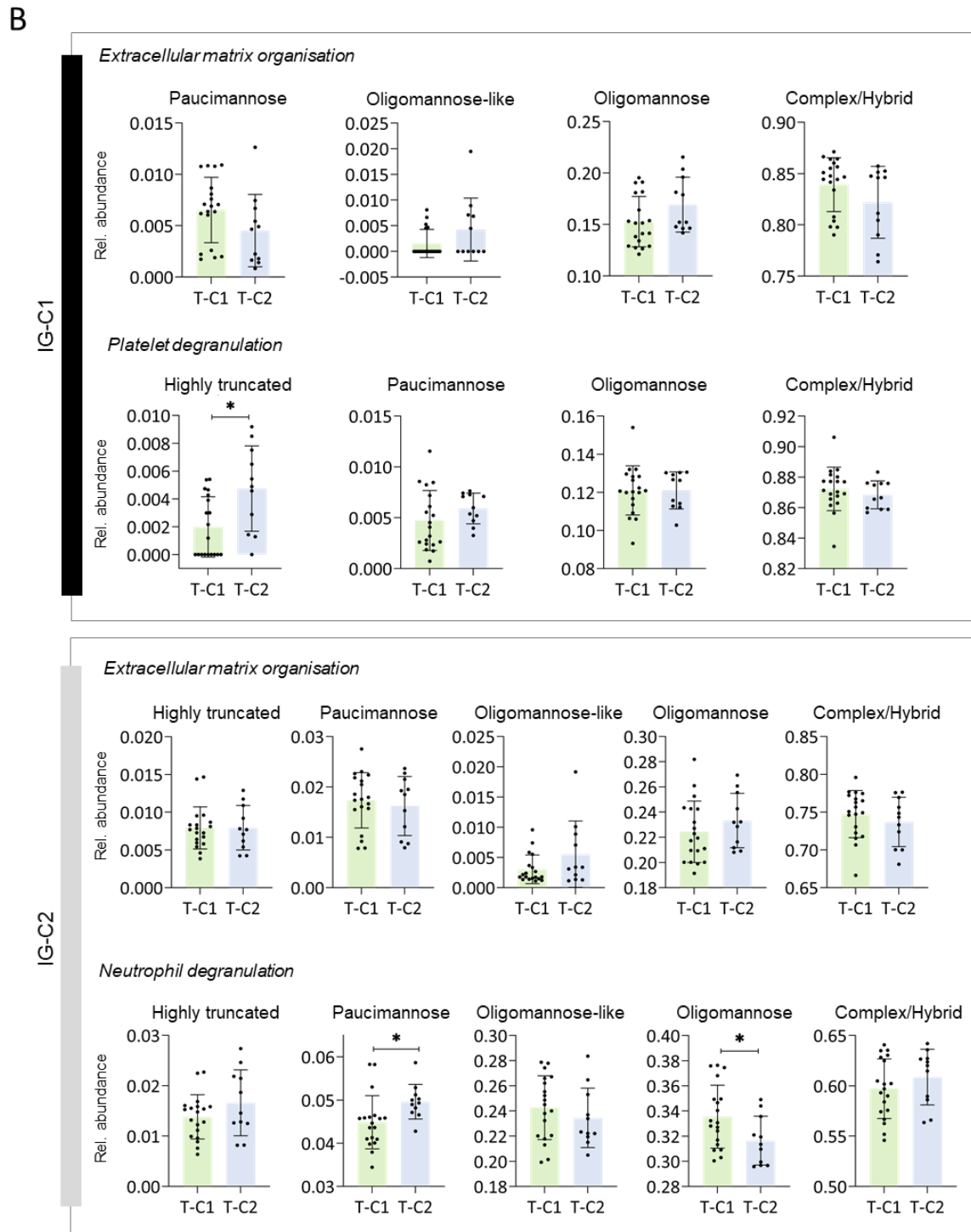
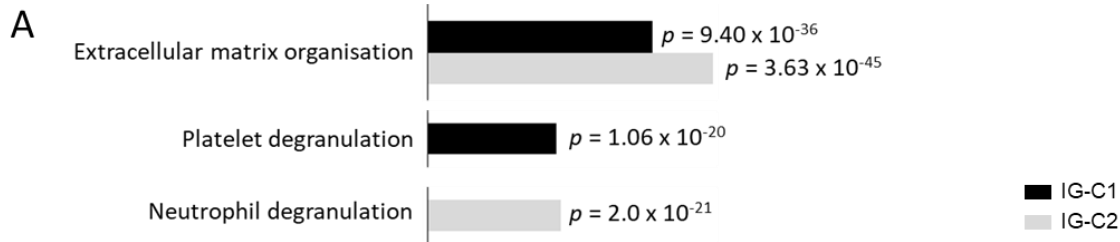
Supplementary Figure S4. Uniform global *N*-glycosylation across the N0 and N+ OSCC tumour tissues. A) Heat map profile of Pearson correlation coefficients (R) derived from pairwise comparison of the quantitative *N*-glycome datasets comprising 83 *N*-glycan structures collected from the investigated OSCC tissue cohort. Relative *N*-glycan abundance values were used to calculate the correlation coefficient using the Perseus software, and the heat map was constructed using the R language with the function ‘heatmap.3’. The dendrogram was created using Euclidean distance with complete linkage. B) Principal component analysis of the *N*-glycome data, showing no distinct separation of the N0 and N+ patient groups. C) Unsupervised hierarchical clustering analysis of the *N*-glycome from the 12 N0 and 19 N+ samples performed with heatmap function under the R environment using Euclidean distance and Ward linkage.



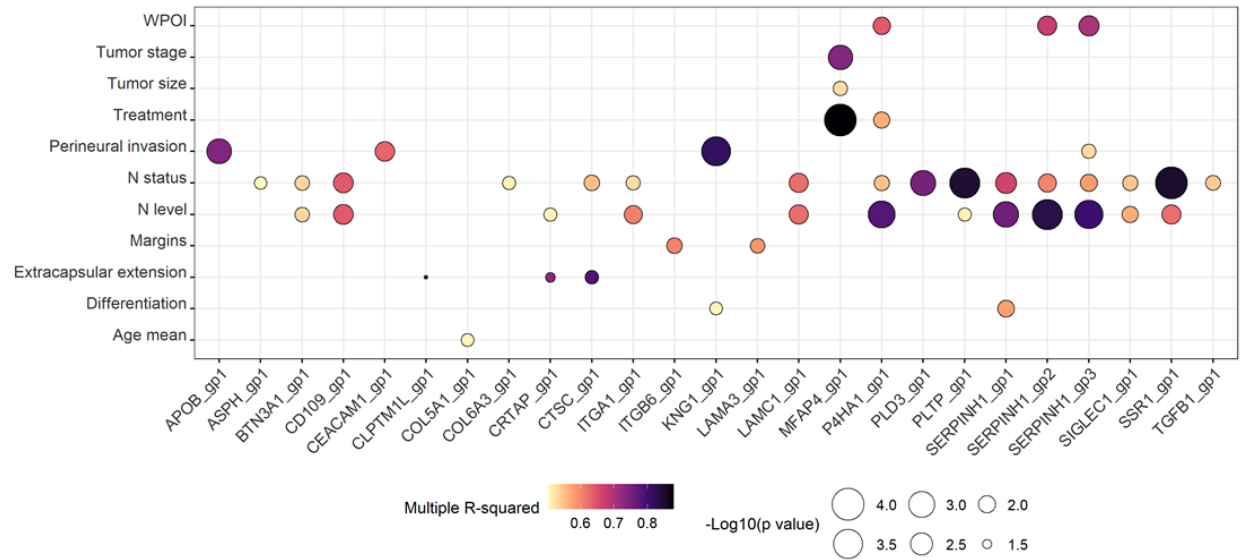
Supplementary Figure S5. Tumour tissue N-glycans show potential for OSCC patient stratification. Five N-glycans (Glycan 20a, 40a, 45b, 46a and 49b) displaying increased expression in N+ tissues, and one N-glycan (Glycan 34) displaying decreased level in N+ tissues (relative to N0, see violin plots in purple) show a potential to stratify the N0 and N+ patient groups with an AUC-ROC > 60% using the logistic regression model (black trace). Four of those N-glycans were also able to stratify the N0 and N+ patient groups by using a random forest model (AUC-ROC > 60%, green trace). AUC-ROC: area-under-the-curve of the receiver operating characteristic. $p < 0.05$ was used as a threshold to denote statistical significance in the applied Student's t-tests.



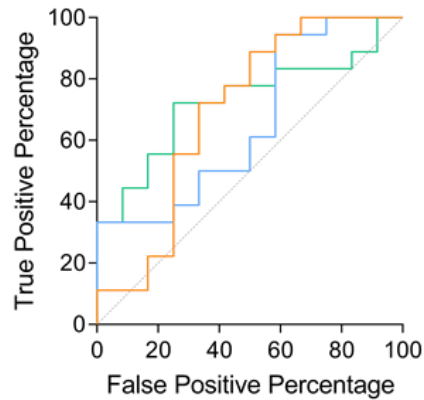
Supplementary Figure S6. Correlation analysis of the *N*-glycoproteome data from N+ and N0 tumour tissues. Heat map of Pearson correlation coefficients (R) derived from pairwise comparisons of the tissue *N*-glycoproteome data collected across the N+ and N0 OSCC tumour tissues. Normalised intensity values of glycopeptides were used to calculate the correlation coefficient using the Perseus software, and the heat map was constructed using the R language with the function ‘heatmap.3’. The dendrogram was generated using Euclidean distance with complete linkage.



Supplementary Figure S7. Enriched biological processes and altered glycan class distribution in the *N*-glycopeptide clusters. A) The most enriched biological processes in both *N*-glycopeptide clusters (IG-C1 and IG-C2). B) *N*-glycan class distribution of *N*-glycoproteins involved in the two most enriched biological processes in IG-C1 and IG-C2 within the T-C1 and T-C2 tumour clusters (Figure 5). Student's t test, two-sided, $\alpha = 0.05$, * $p < 0.05$, ** $p < 0.01$, *** $p < 0.001$.



Supplementary Figure S8. Association of specific N-glycopeptides with distinct clinicopathological features. In total 25 of the 79 N-glycopeptides that displayed differential abundance between the N0 and N+ patients (plotted on the x axis) were found to associate with a range of clinicopathological features (plotted on the y axis) as measured using Pearson correlation (R). Minimum correlation coefficient $+0.7/-0.7$, multiple $R^2 > 0.5$.



	Glycopeptide	Source protein	AUC (%)
—	P02751_528_HexNAc ₂ Hex ₉	Fibronectin	72.7
—	P13987_43_HexNAc ₄ Hex ₅ Fuc ₁	CD59	65.7
—	P43652_109_HexNAc ₄ Hex ₅	Afamin	69.4

Supplementary Figure S9. ROC analysis of three *N*-glycopeptides associated with patient survival. *N*-glycopeptides that displayed differential abundance between the N0 and N+ patients and associations with patient survival were evaluated for their potential to stratify patients with and without lymph node metastasis using a logistic regression model. Three *N*-glycopeptides from three different source glycoproteins (fibronectin, green trace; CD59, blue trace; afamin, orange trace) displayed an AUC-ROC > 60%. AUC-ROC: area-under-the-curve of the receiver operating characteristic.

Supplementary Table S1-8. (provided as a separate .xlsx file)
Information of data composition and analysis.

Supplementary File S1. (provided as a separate .pptx file)
Spectral evidence of the reported *N*-glycans observed from the OSCC tissue samples.

Supplementary File S1

for

Comprehensive glycoprofiling of oral cancer tumours associates *N*-glycosylation with lymph node metastasis and patient survival

Carolina Moretto Carnielli ¹, Thayná Melo de Lima Morais ², Fábio Malta de Sá Patroni ³, Ana Carolina Prado Ribeiro ^{4,5}, Thaís Bianca Brandão ⁴, Evandro Sobroza ⁴, Leandro Luongo Matos ⁶, Luiz Paulo Kowalski ^{7,8}, Adriana Franco Paes Leme ^{1*}, Rebeca Kawahara ^{9,10#*}, Morten Thaysen-Andersen ^{9,10,11#*}

Affiliations

¹ Laboratório de Espectrometria de Massas, Laboratório Nacional de Biociências (LNBio), Centro Nacional de Pesquisa em Energia e Materiais (CNPEM), Campinas, 13083-970 SP, Brazil.

² Oral Pathology, Department of Oral Diagnosis, Piracicaba Dental School, University of Campinas, Brazil.

³ Molecular Biology and Genetic Engineering Center, University of Campinas, Campinas, Brazil.

⁴ Serviço de Odontologia Oncológica, Instituto do Câncer do Estado de São Paulo, ICESP-FMUSP, São Paulo, 01246-000 SP, Brazil.

⁵ Universidade Brasil, Fernandópolis, 15600-000 SP, Brazil.

⁶ Serviço de Cirurgia de Cabeça e Pescoço, Instituto do Câncer do Estado de São Paulo, ICESP-FMUSP, São Paulo, 01246-000 SP, Brazil.

⁷ Departamento de Cirurgia de Cabeça e Pescoço e Otorrinolaringologia, A.C. Camargo Cancer Center, São Paulo, SP, 01509-900, Brazil.

⁸ Departamento de Cirurgia de Cabeça e Pescoço, Faculdade de Medicina, Universidade de São Paulo - USP, São Paulo, SP, 01246-903, Brazil.

⁹ School of Natural Sciences, Macquarie University, Sydney, NSW-2109, Australia

¹⁰ Biomolecular Discovery Research Centre, Macquarie University, Sydney, NSW-2109, Australia









¹¹ Institute for Glyco-core Research (iGCORE), Nagoya University, Nagoya, 464-8601, Japan

These authors contributed equally to this work.

*Joint corresponding authors.

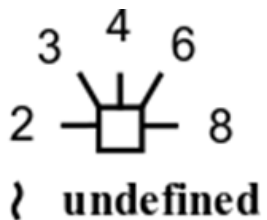
E-mails: adriana.paesleme@lnbio.cnpem.br; rebeca.kawaharasakuma@mq.edu.au; morten.andersen@mq.edu.au

Annotation and Fragmentation Key

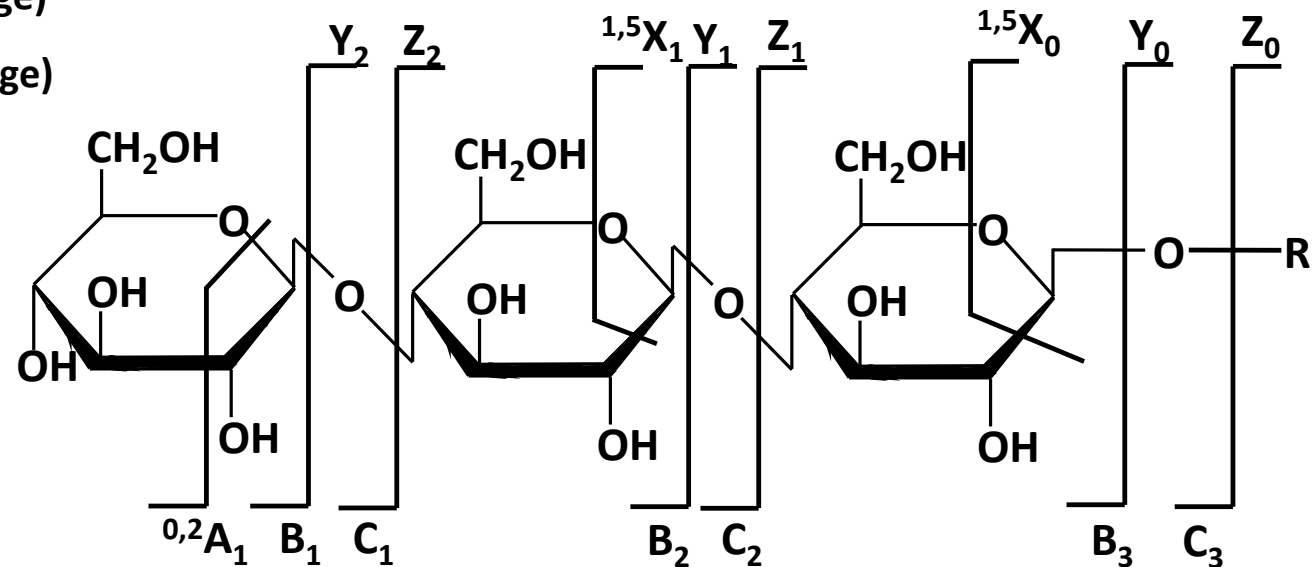
-  Mannose (162.0528 Da)
-  Galactose (162.0528 Da)
-  N-Acetylglucosamine (203.0794 Da)
-  N-Acetylgalactosamine (203.0794 Da)
-  N-Acetylneuraminic acid (291.0954 Da)
-  N-Glycolylneuraminic acid (307.0903 Da)
-  Fucose (146.0579 Da)
-  Cross-ring fragment (unspecified)

 Indicates mostly Y ions (includes oxygen of glycosidic linkage)

 Indicates mostly Z ions (excludes oxygen of glycosidic linkage)



Note: All glycans contain reducing end which is not depicted in the *N*-glycan structure cartoon

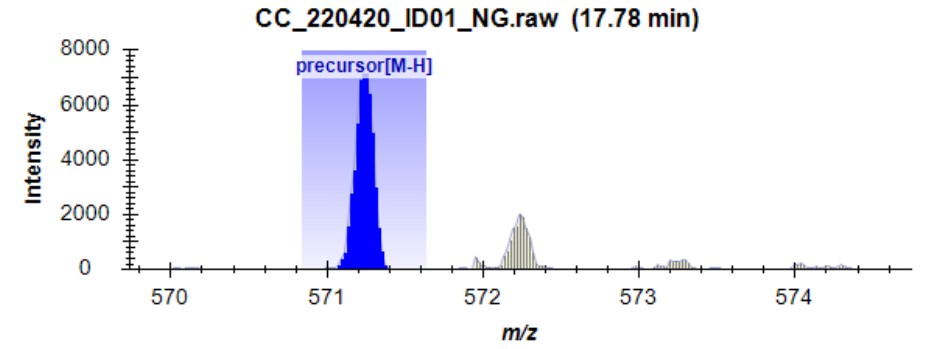
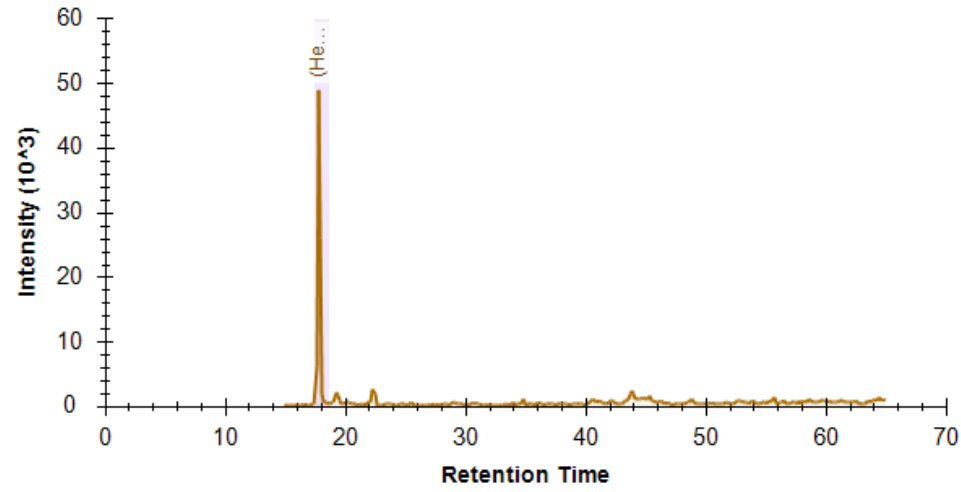


Spectral evidence for the reported OSCC tumour tissue *N*-glycans

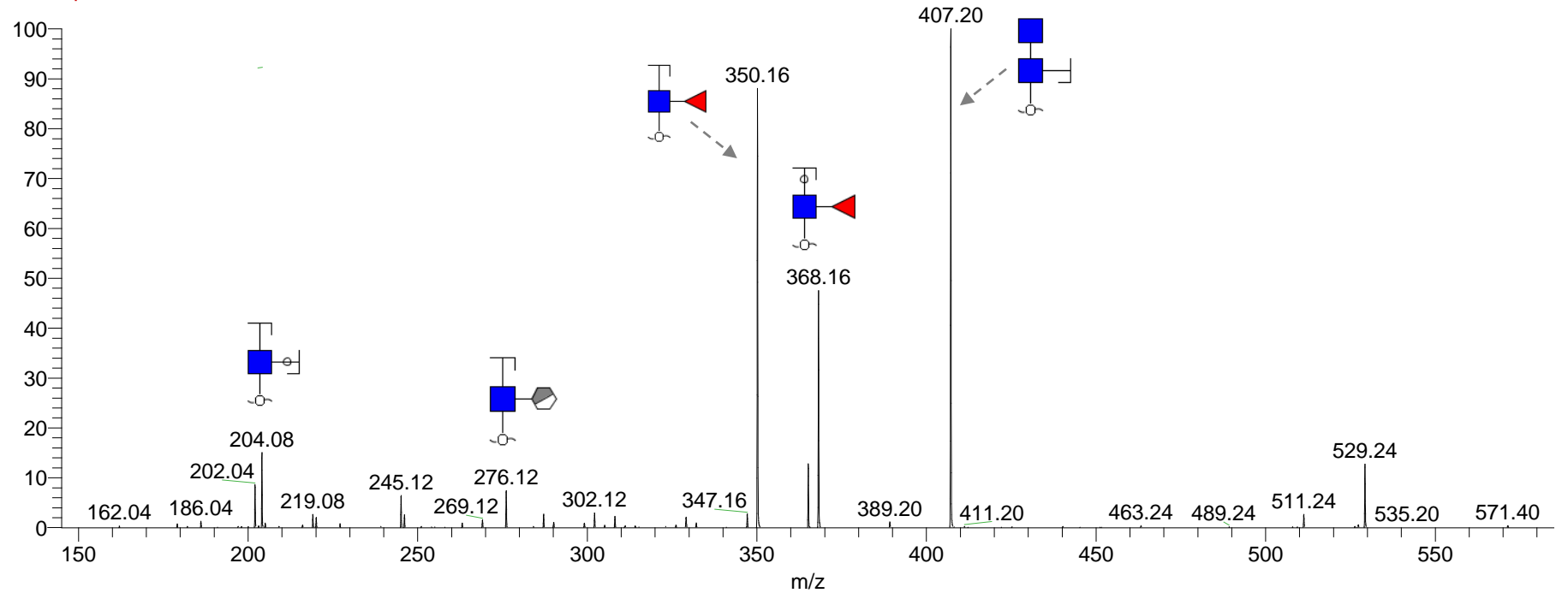
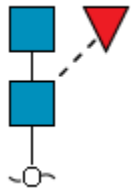
The *N*-glycans reported in this paper were characterised and quantified by:

- a. EIC (MS) of monoisotopic precursor ions and AUC integration (blue highlights in insert, from Skyline)
- b. PGC-LC retention time
- c. CID-MS/MS (-) manual annotation

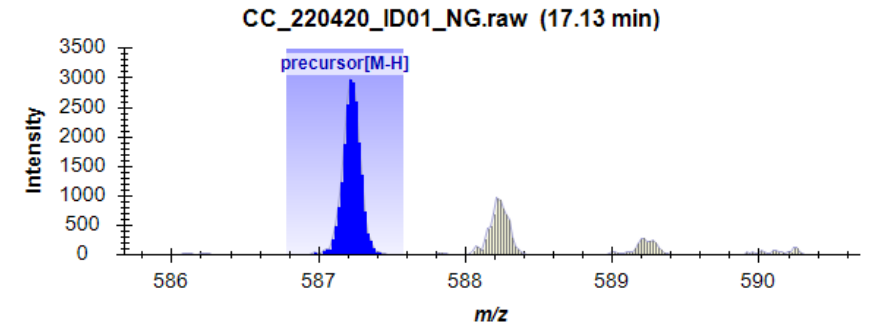
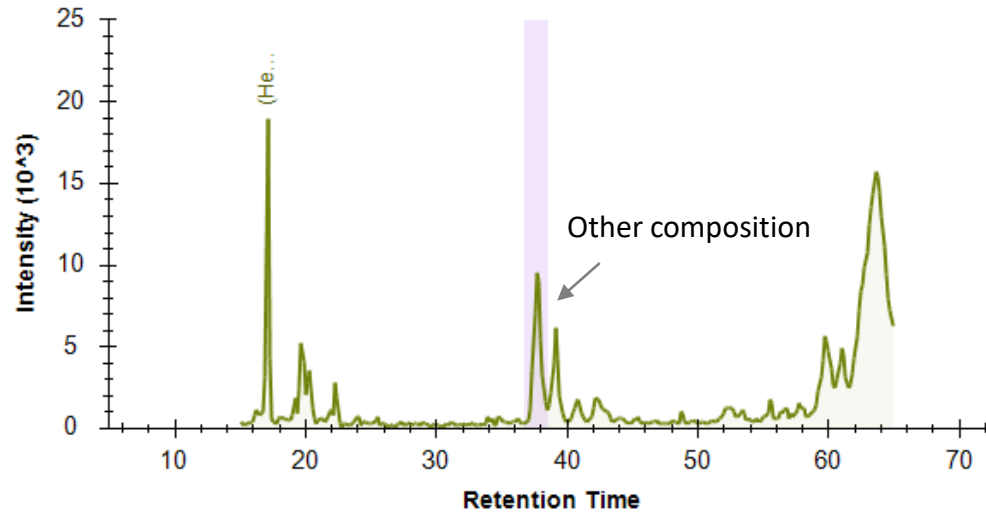
Glycan 1
(HexNAc)2(Deoxyhexose)1
 m/z 571.24 (1-)
 Retention time: 17.8 min
 Theo mass [M-H] = 571.24 Da



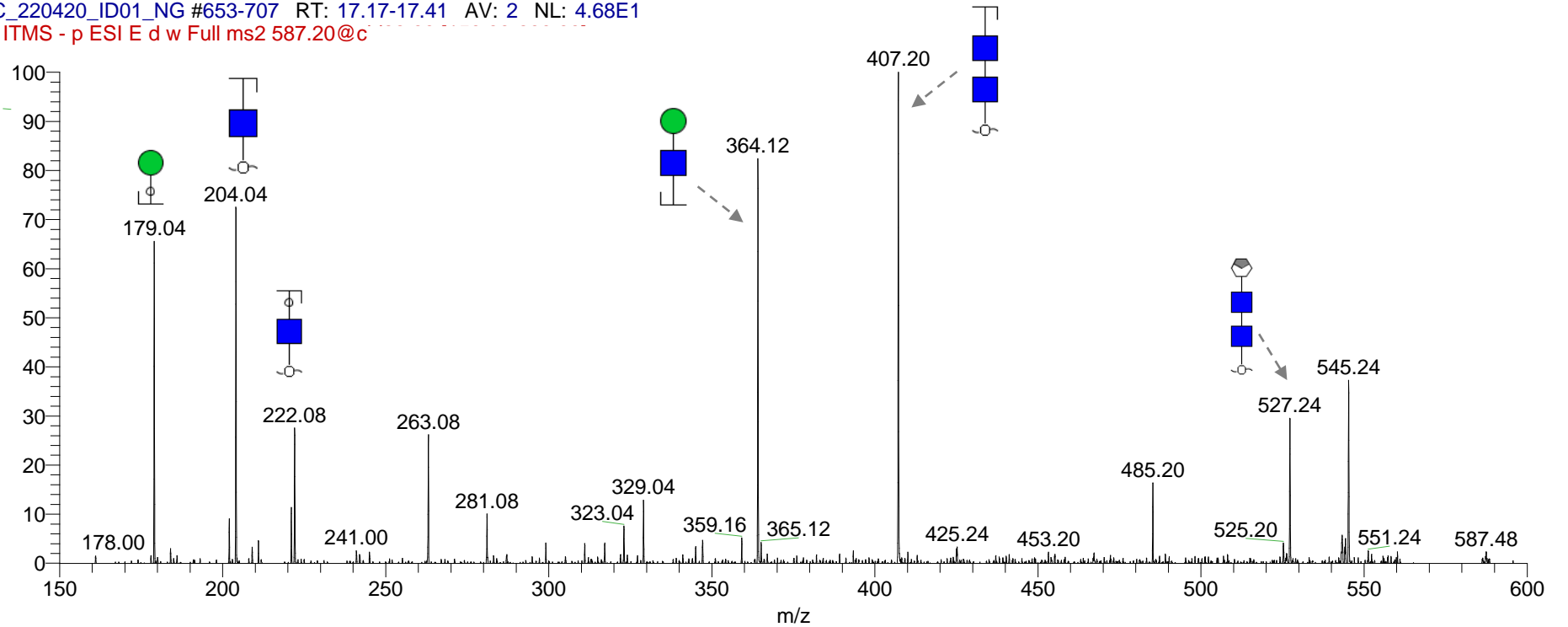
cc_220420_id01_ng #669-745 RT: 17.84-17.98 AV: 2 NL: 5.99E2
 F: ITMS - p ESI E d w Full ms2 571.26@c



Glycan 2
(Hex)1(HexNAc)2
 m/z 587.18 (1-)
 Retention time: 17.0 min
 Theo mass [M-H] = 587.18 Da

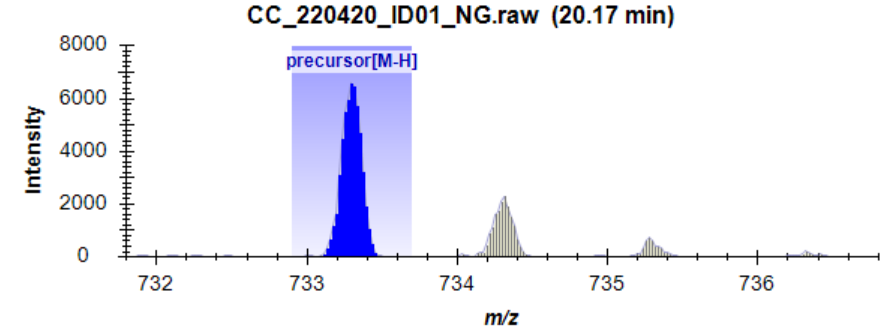
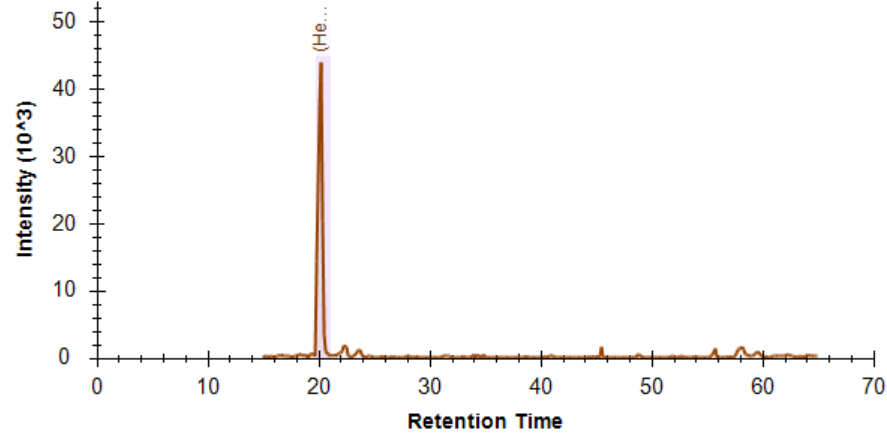


CC_220420_ID01_NG #653-707 RT: 17.17-17.41 AV: 2 NL: 4.68E1
 F: ITMS - p ESI E d w Full ms2 587.20@c

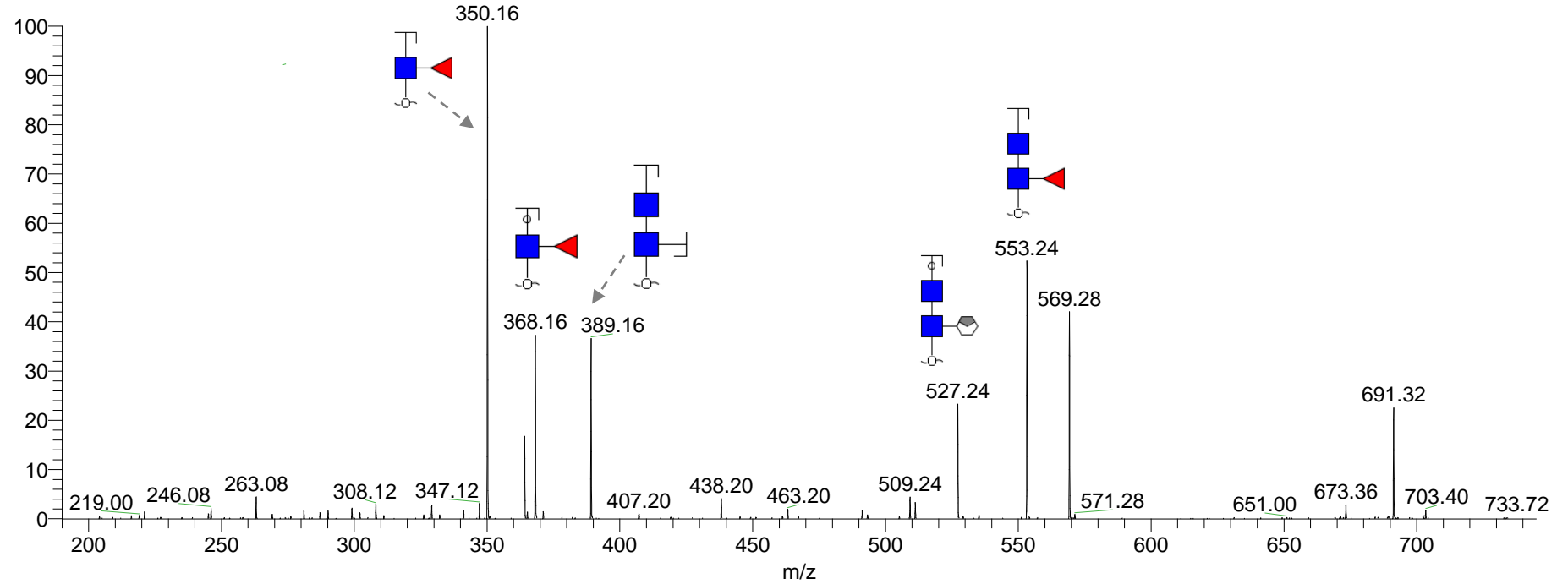
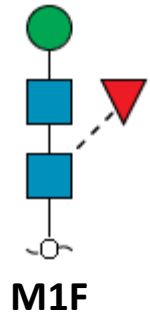


Glycan 3 (Hex)1(HexNAc)2(Deoxyhexose)1

m/z 733.30 (1-)
Retention time: 20 min
Theo mass [M-H] = 733.30 Da



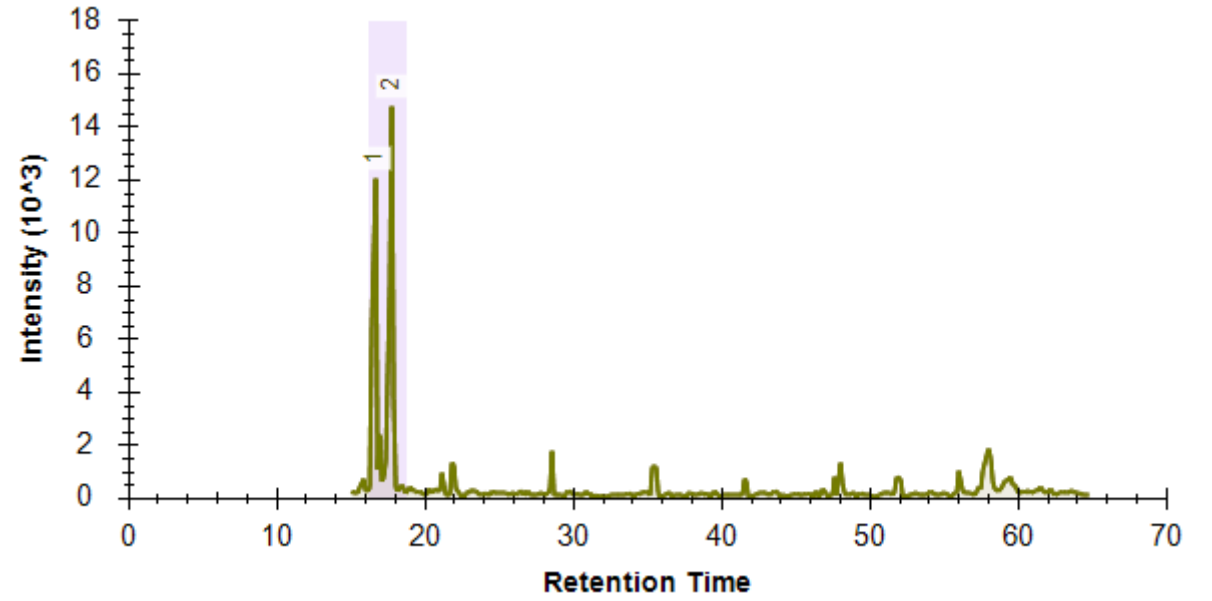
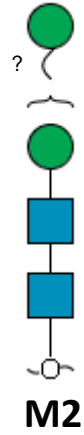
CC_220420_ID01_NG #752-829 RT: 20.03-20.58 AV: 4 NL: 1.92E2
F: ITMS - p ESI E d w Full ms2 733.30@c



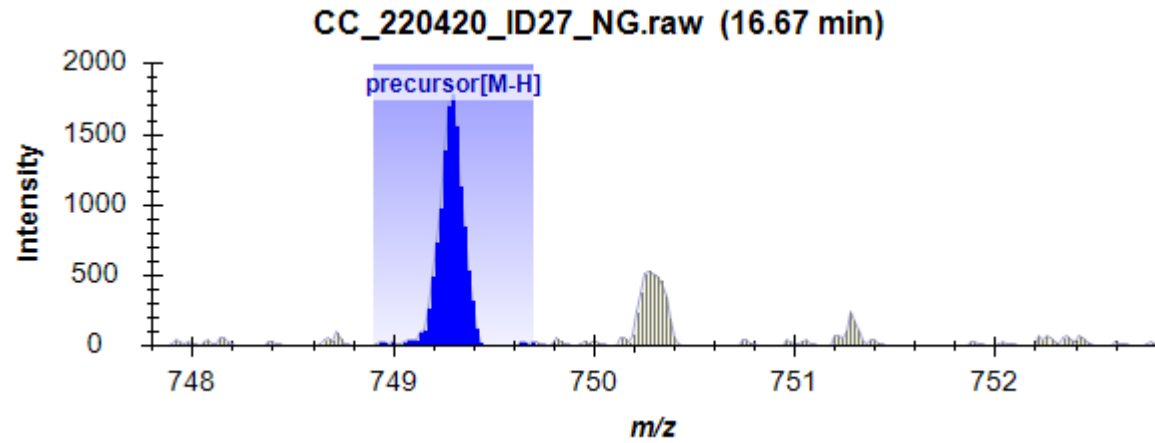
Glycan 4 (Hex)₂(HexNAc)₂

m/z 749.30 (1-)

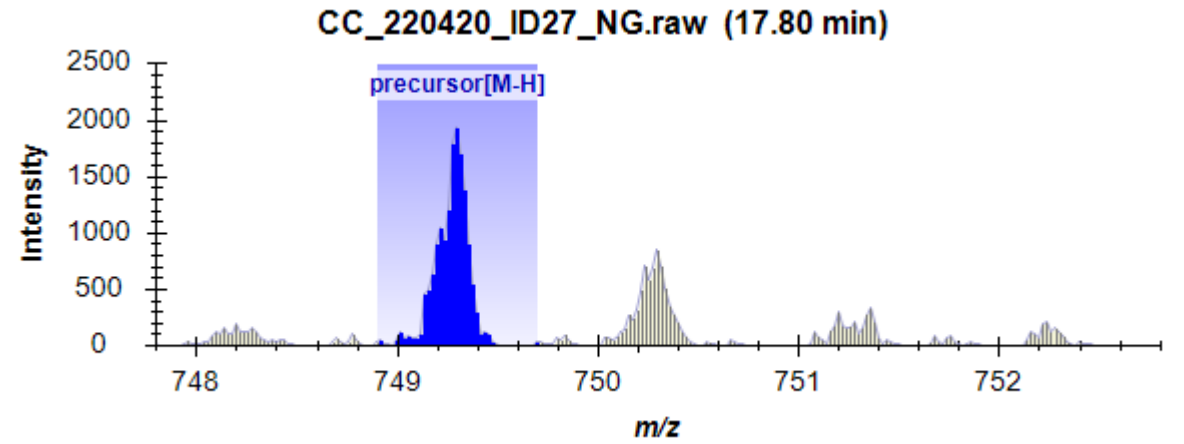
Theo mass [M-H] = 749.30 Da



6a



6b

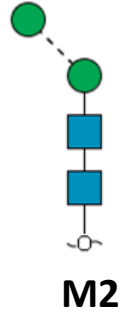


Glycan 4a

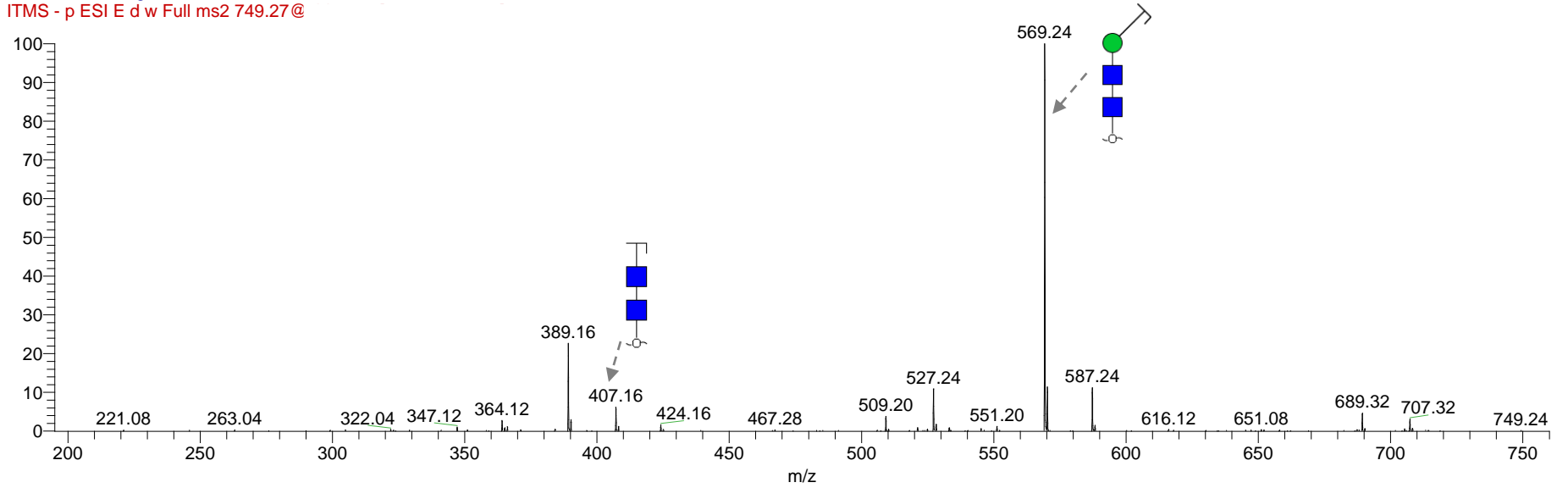
m/z 749.30 (1-)

Retention time: 16.6 min

Theo mass [M-H] = 749.30 Da



cc_220420_id27_ng #657-667 RT: 16.62-16.76 AV: 2 NL: 2.68E2
F: ITMS - p ESI E d w Full ms2 749.27@

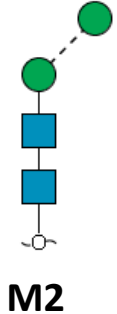


Glycan 4b

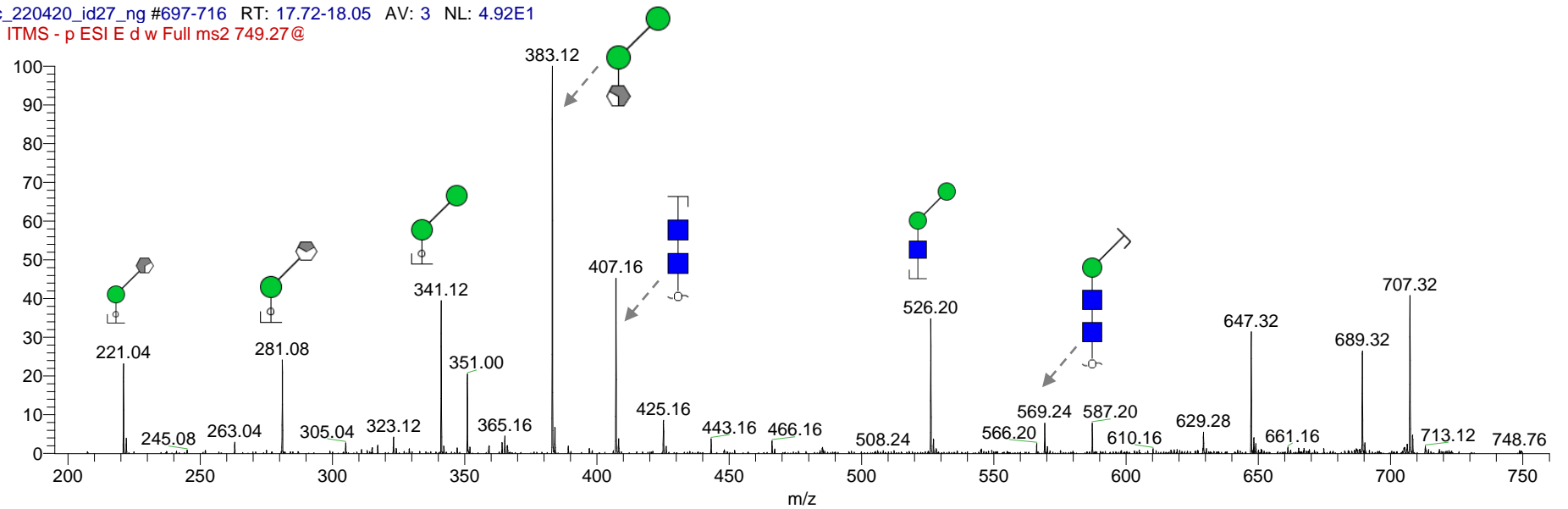
m/z 749.30 (1-)

Retention time: 18.1 min

Theo mass [M-H] = 749.30 Da



cc_220420_id27_ng #697-716 RT: 17.72-18.05 AV: 3 NL: 4.92E1
F: ITMS - p ESI E d w Full ms2 749.27@

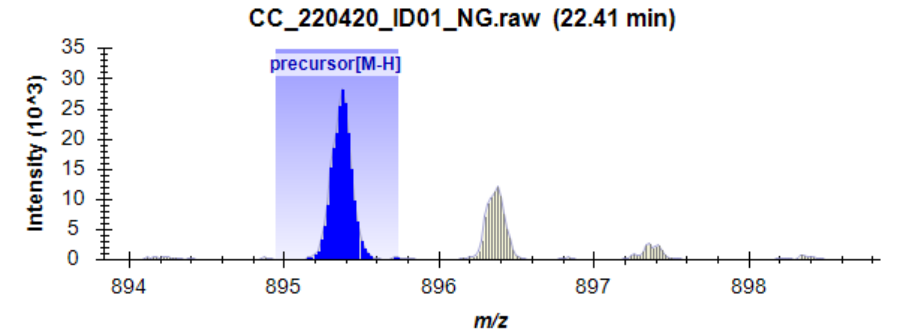
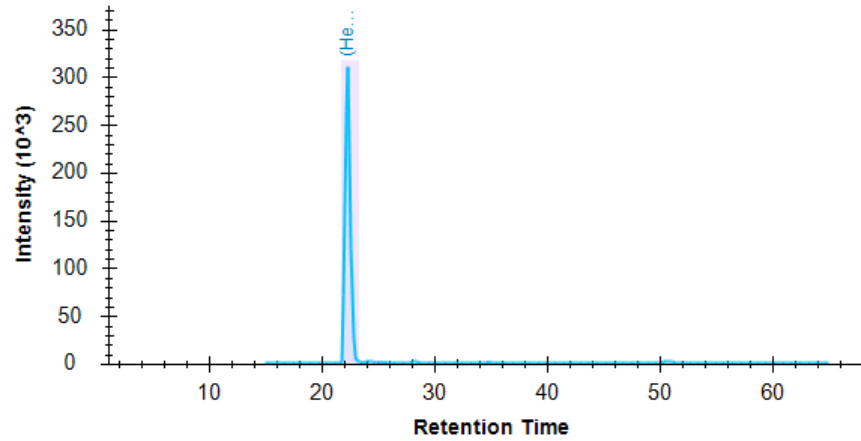


Glycan 5 (Hex)2(HexNAc)2(Deoxyhexose)1

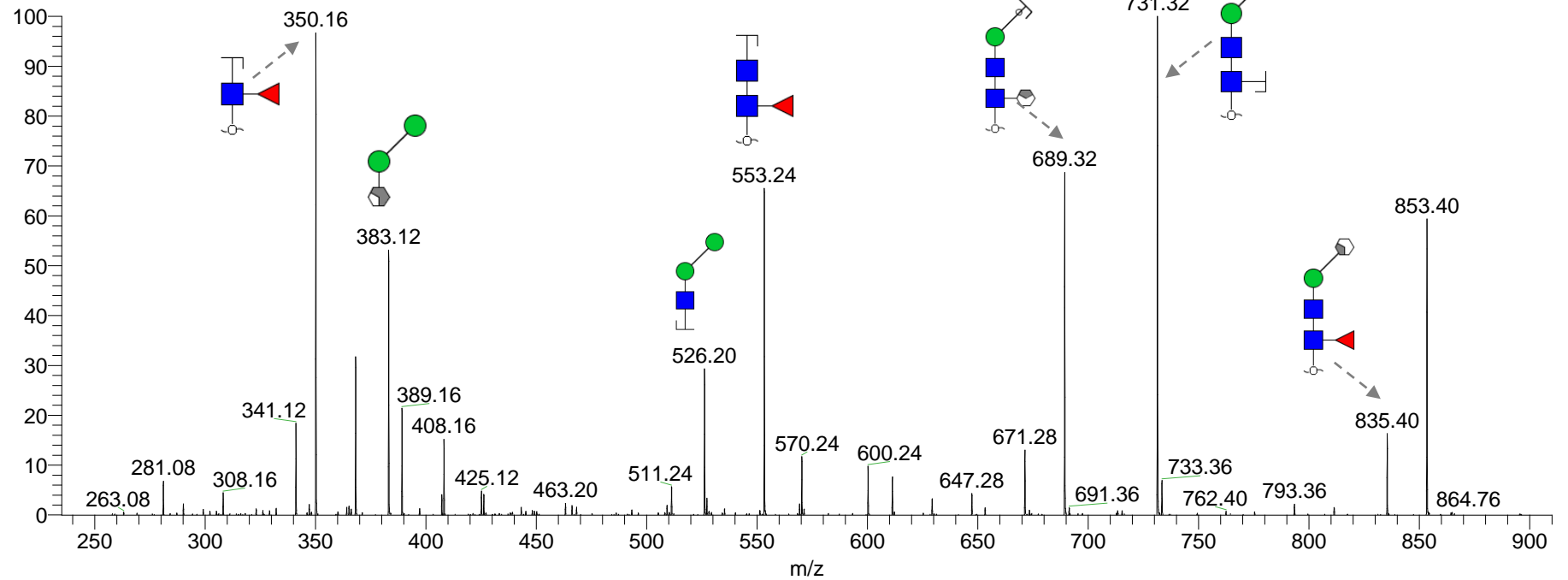
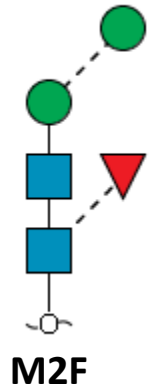
m/z 895.34 (1-)

Retention time: 22.0 min

Theo mass [M-H] = 895.34 Da



CC_220420_ID01_NG #822-920 RT: 22.06-23.16 AV: 8 NL: 3.02E2
F: ITMS - p ESI E d w Full ms2 895.36@c

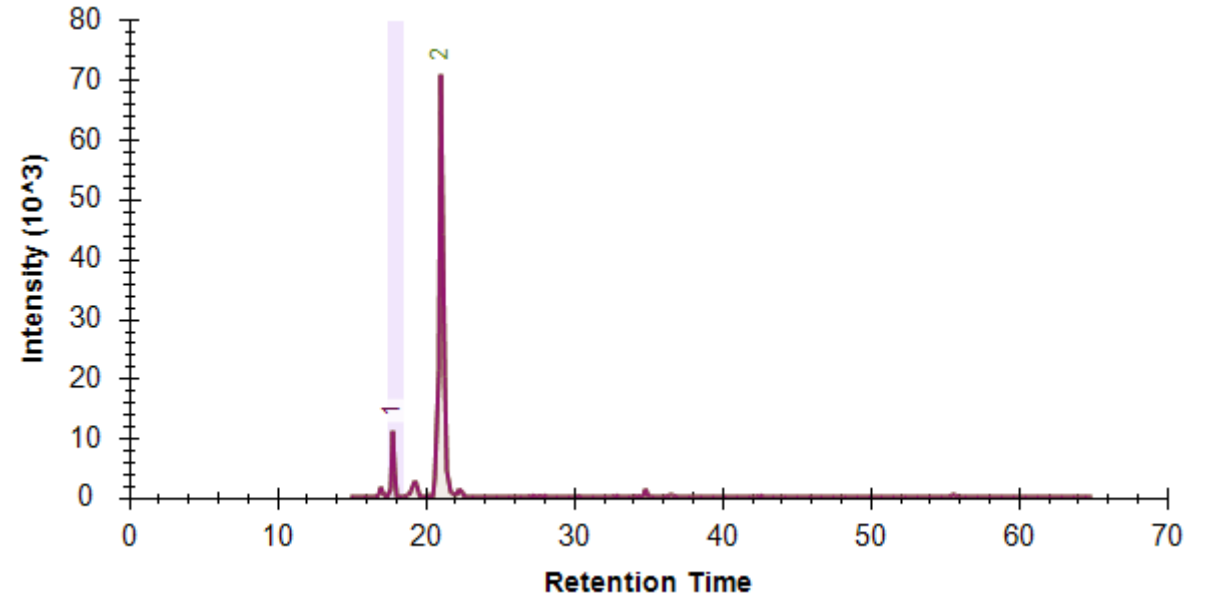
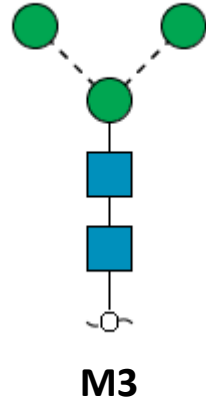


Note: No distinction intended between 3-arm/6-arm in glycan fragment scheme.

Glycan 6
(Hex)3(HexNAc)2

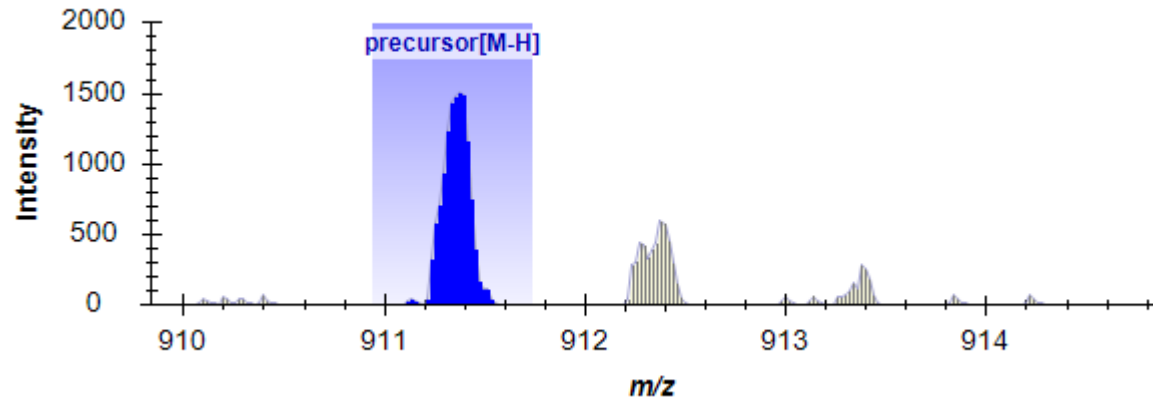
m/z 911.34 (1-)

Theo mass [M-H] = 911.34 Da



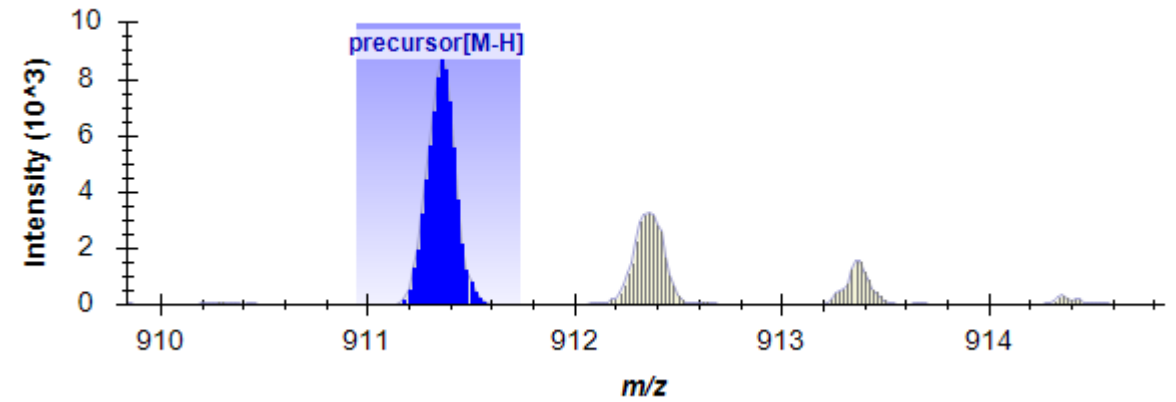
8a

CC_220420_ID01_NG.raw (17.78 min)



8b

CC_220420_ID01_NG.raw (21.04 min)

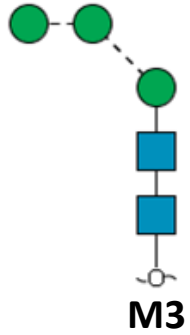


Glycan 6a

m/z 911.34 (1-)

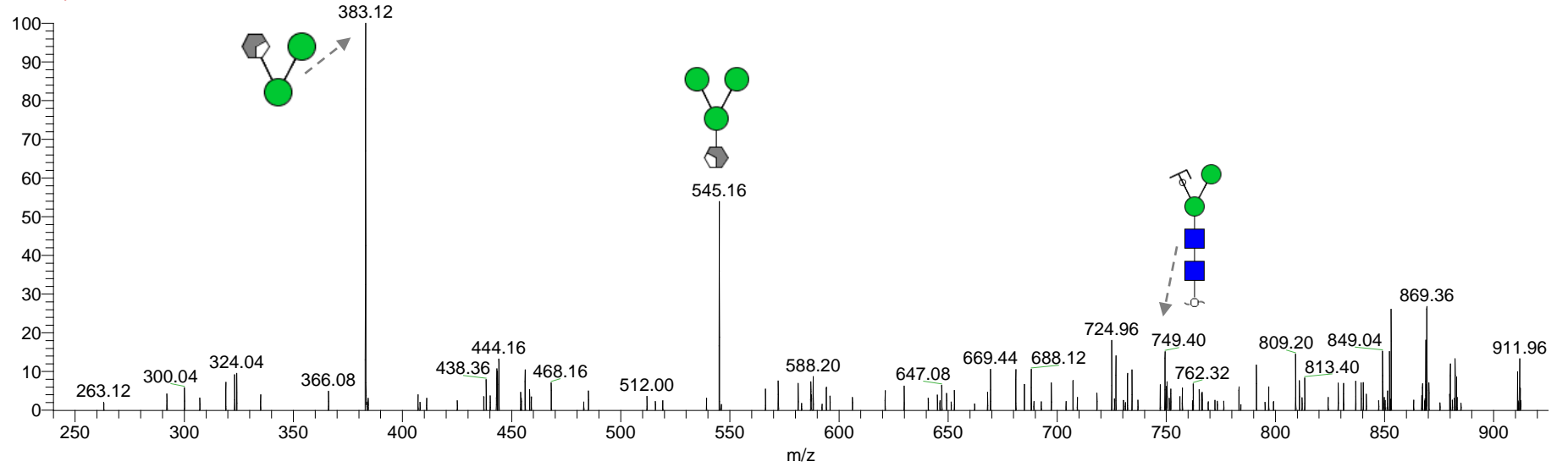
Retention time: 17.9 min

Theo mass [M-H] = 911.34 Da



cc_220420_id18_ng #702 RT: 18.18 AV: 1 NL: 5.88

F: ITMS - p ESI E d w Full ms2 911.34@

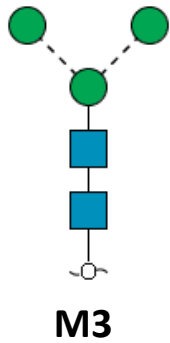


Glycan 6b

m/z 911.34 (1-)

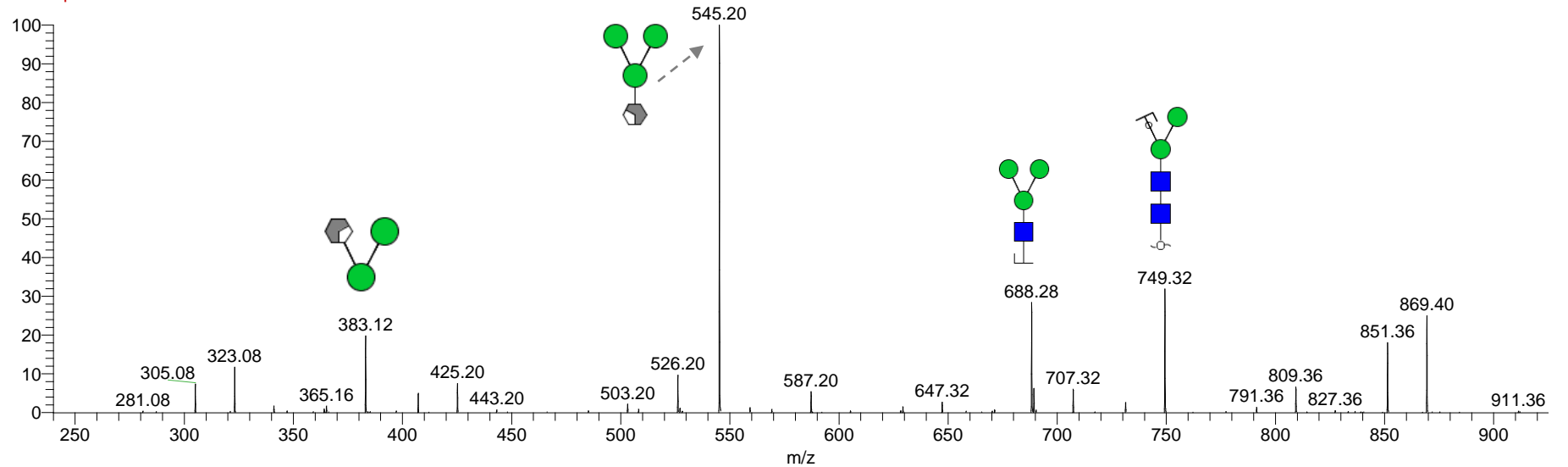
Retention time: 19.9 min

Theo mass [M-H] = 911.34 Da



CC_220420_ID01_NG #788-842 RT: 20.91-21.43 AV: 4 NL: 2.54E2

F: ITMS - p ESI E d w Full ms2 911.36@

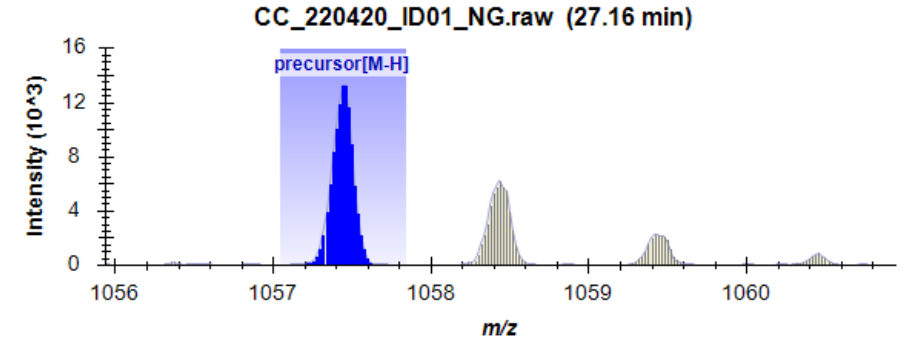
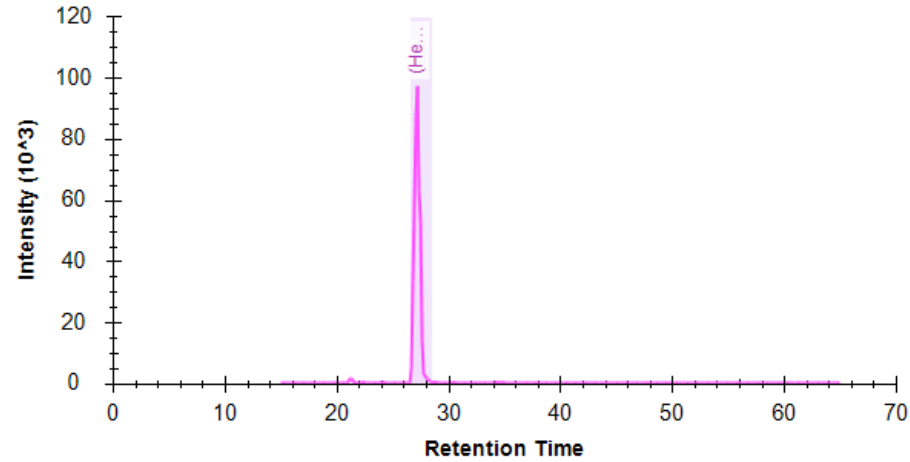


Glycan 7
(Hex)3(HexNAc)2(Deoxyhexose)1

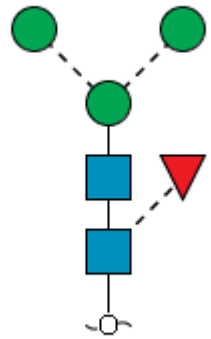
m/z 1057.44 (1-)

Retention time: 27.1 min

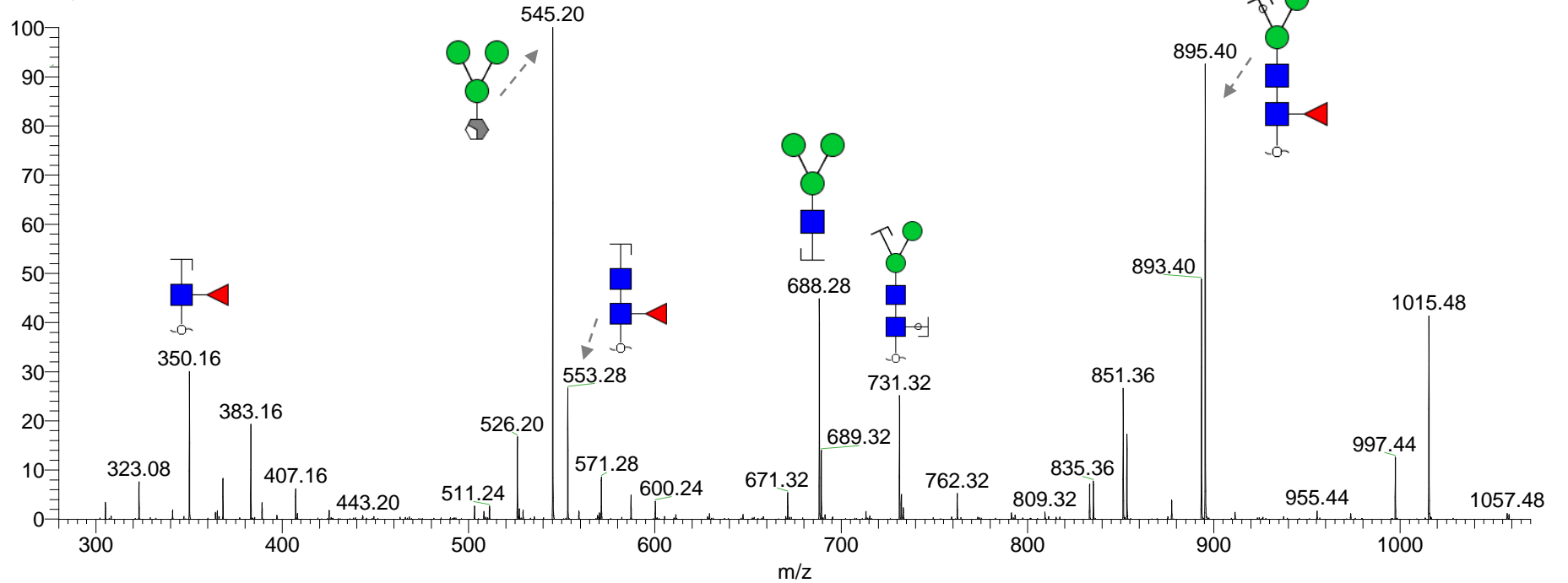
Theo mass [M-H] = 1057.44 Da



CC_220420_ID01_NG #993-1073 RT: 26.85-27.75 AV: 6 NL: 1.30E2
 F: ITMS - p ESI E d w Full ms2 1057.43@



M3F



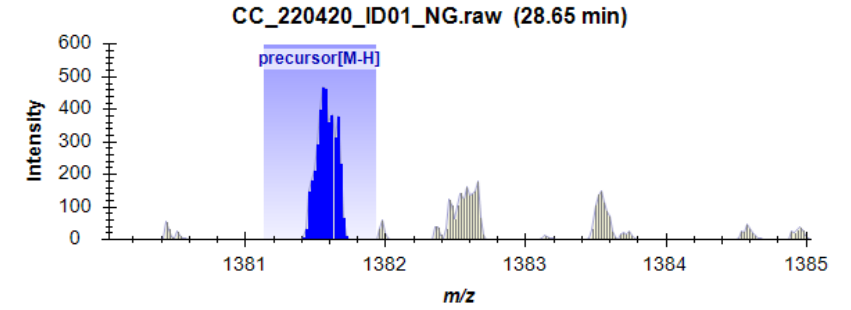
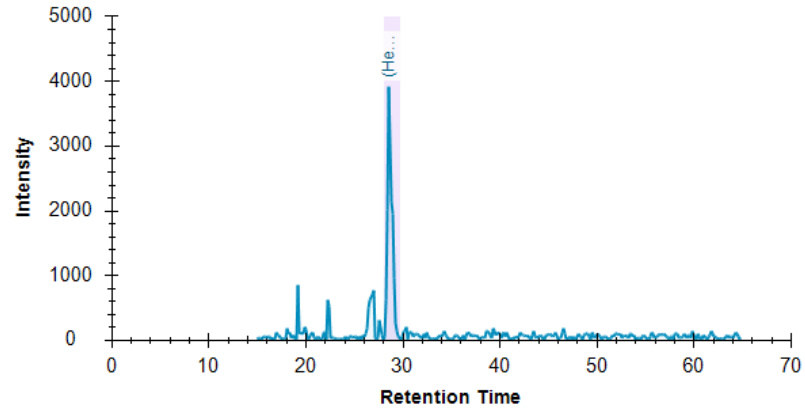
Note: No distinction intended between 3-arm/6-arm in glycan fragment scheme.

Glycan 8
(Hex)2(Deoxyhexose)1 + (Man)3(GlcNAc)2

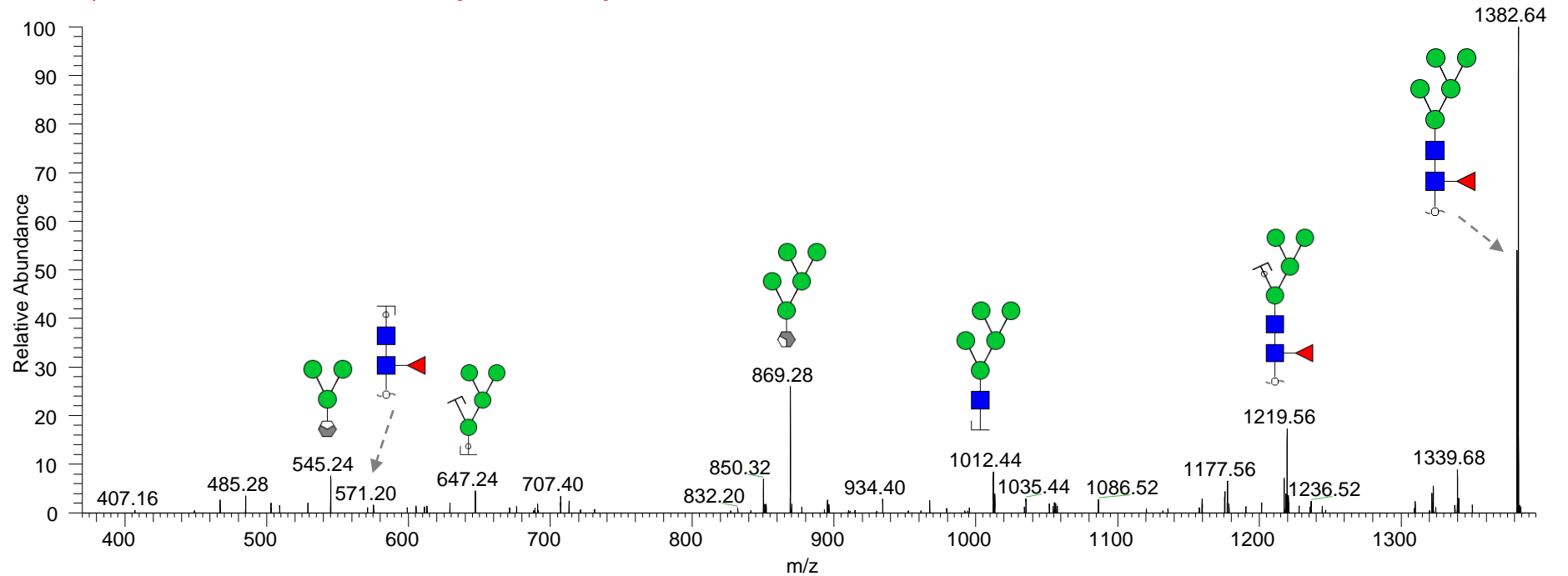
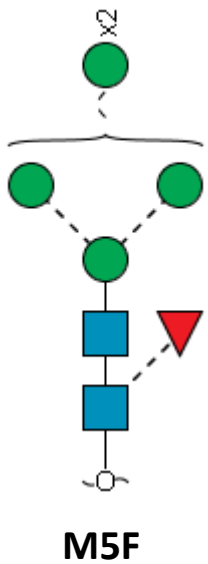
m/z 1381.53 (1-)

Retention time: 28.7 min

Theo mass [M-H] = 1381.53 Da



CC_220420_ID01_NG #1067 RT: 28.72 AV: 1 NL: 2.59E1
 F: ITMS - p ESI E d w Full ms2 1381.59@cid33.00 [370.00-1395.00]



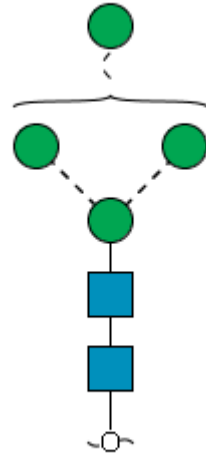
Note: No distinction intended between 3-arm/6-arm in glycan fragment scheme.

Glycan 9

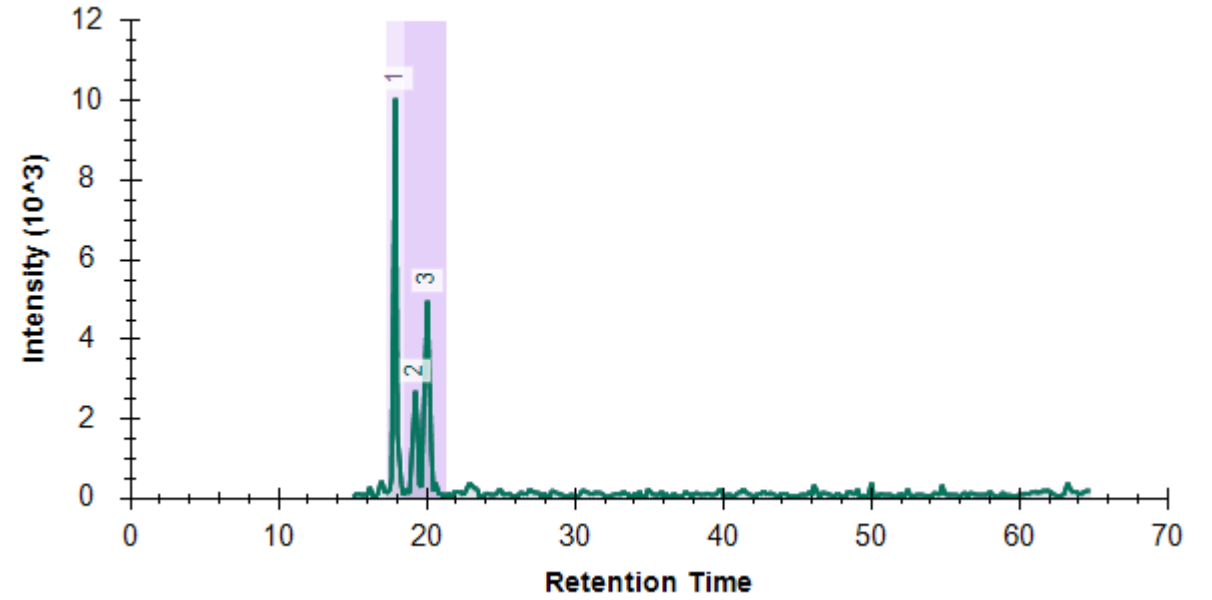
(Hex)4(HexNAc)2

m/z 1073.41 (1-)

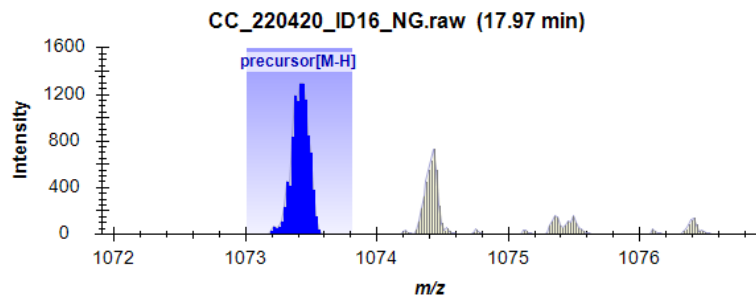
Theo mass [M-H] = 1073.41 Da



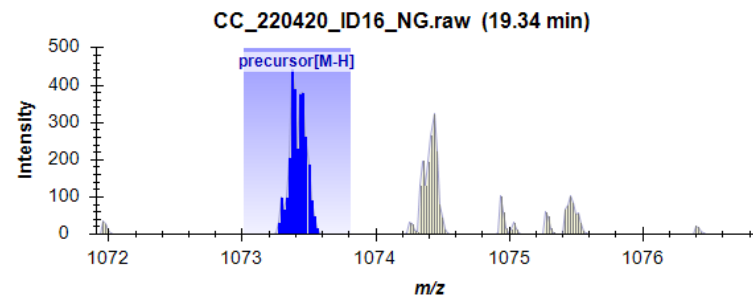
M4



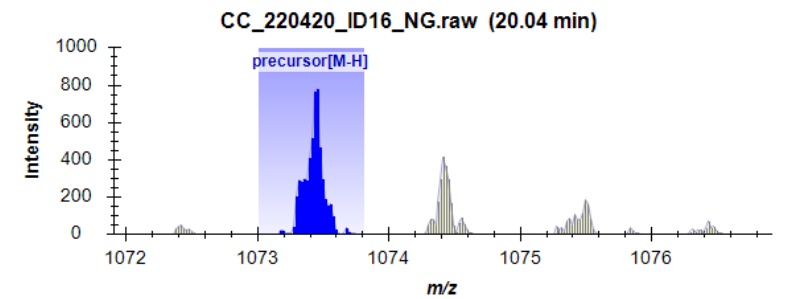
3a



3b



3c

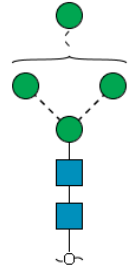


Glycan 9a

m/z 1073.41 (1-)

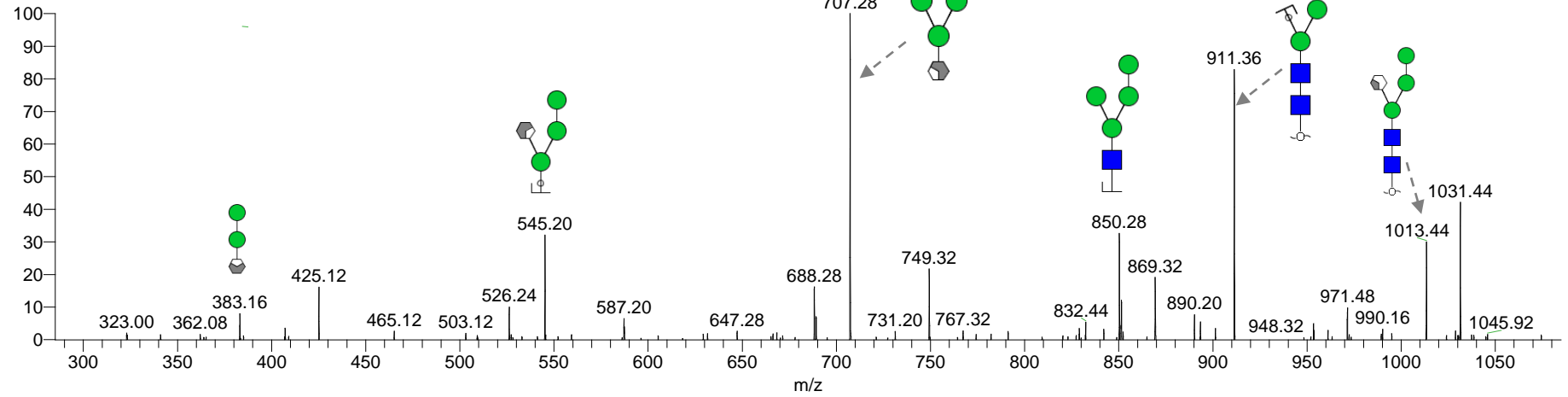
Retention time: 17.9 min

Theo mass [M-H] = 1073.41 Da



M4a

cc_220420_id16_ng #697 RT: 18.06 AV: 1 NL: 1.83E1
F: ITMS - p ESI E d w Full ms2 1073



Glycan 9b

m/z 1073.41 (1-)

Retention time: 19.1 min

Theo mass [M-H] = 1073.41 Da

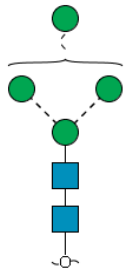
Structure not confirmed by MS/MS.

Glycan 9c

m/z 1073.41 (1-)

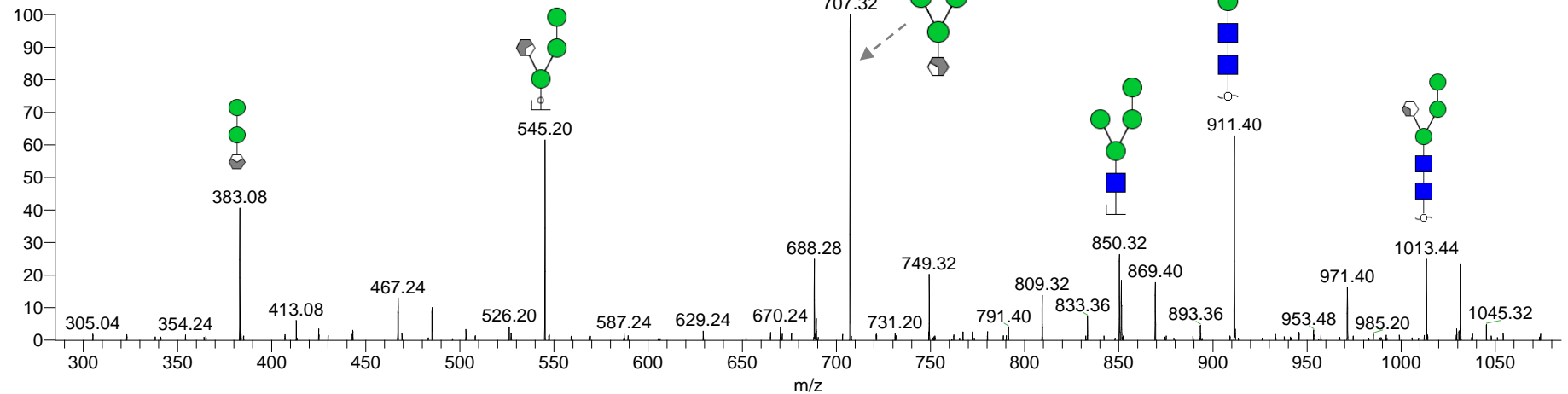
Retention time: 19.9 min

Theo mass [M-H] = 1073.41 Da



M4c

cc_220420_id16_ng #766 RT: 20.08 AV: 1 NL: 2.31E1
F: ITMS - p ESI E d w Full ms2 1073



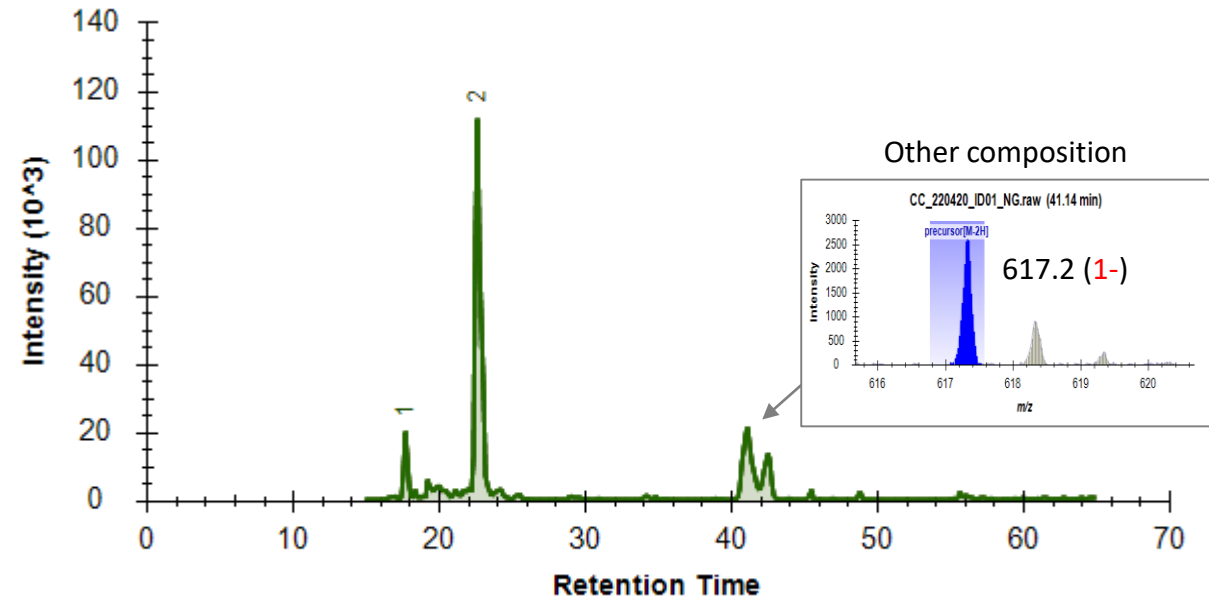
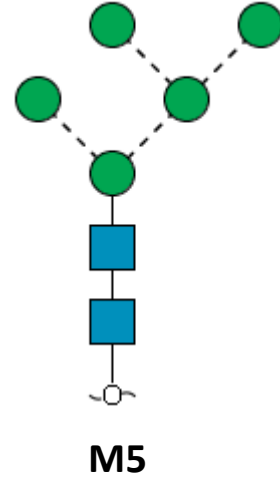
Note: No distinction intended between 3-arm/6-arm in glycan fragment scheme.

Glycan 10

(Hex)2 + (Man)3(GlcNAc)2

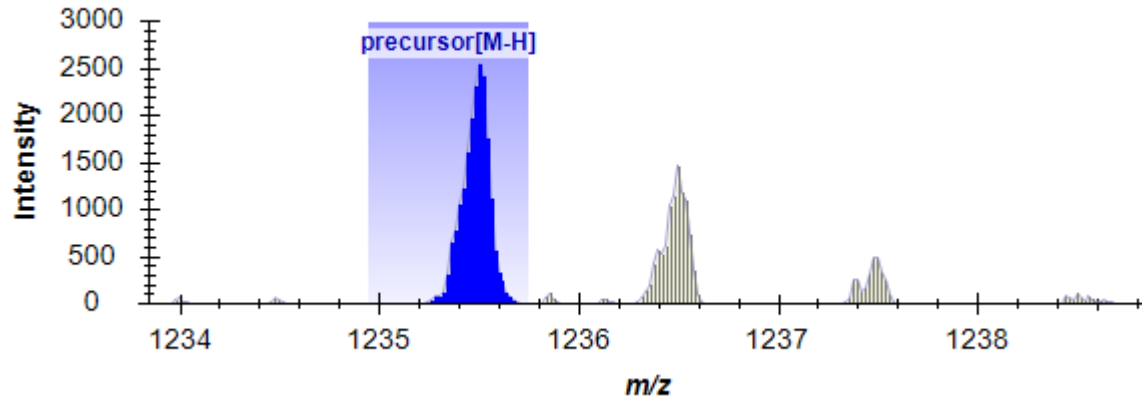
m/z 1235.44 (1-); 617.17 (2-)

Theo mass [M-H] = 1235.44 Da



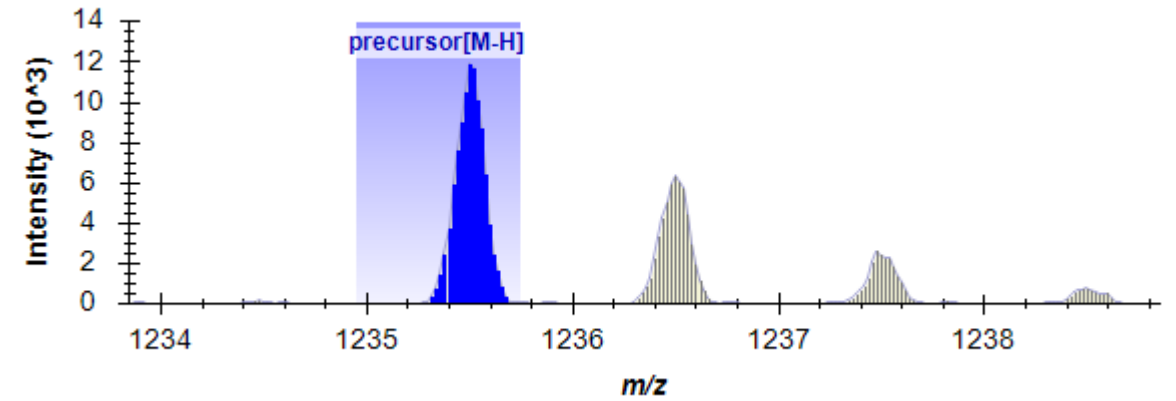
10a

CC_220420_ID01_NG.raw (17.78 min)



10b

CC_220420_ID01_NG.raw (22.71 min)

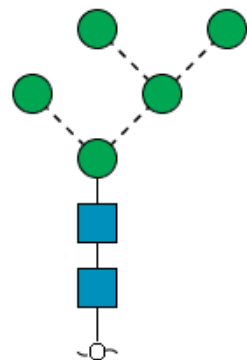


Glycan 10a

m/z 1235.44 (1-); 617.17 (2-)

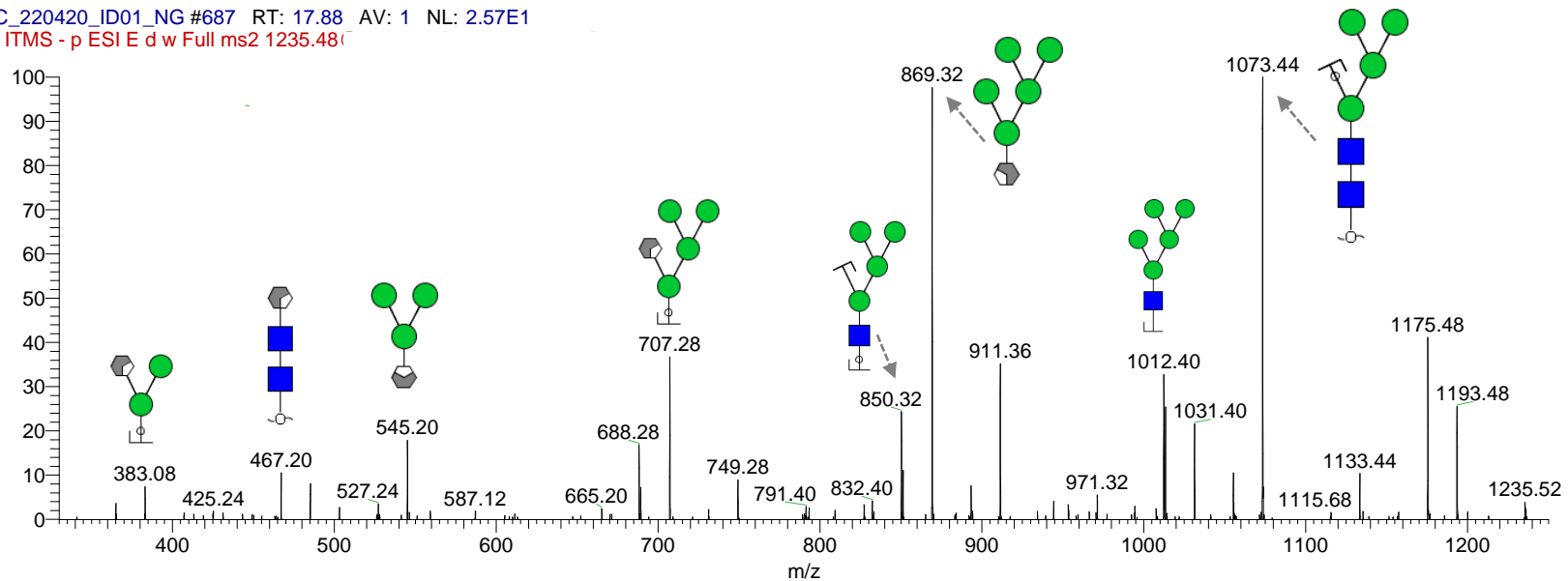
Retention time: 17.8 min

Theo mass [M-H] = 1235.44 Da



M5a

CC_220420_ID01_NG #687 RT: 17.88 AV: 1 NL: 2.57E1
F: ITMS - p ESI E d w Full ms2 1235.48

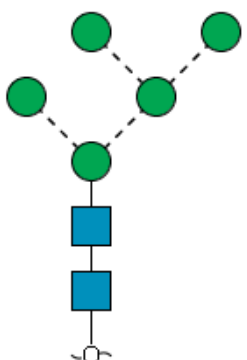


Glycan 10b

m/z 1235.44 (1-); 617.17 (2-)

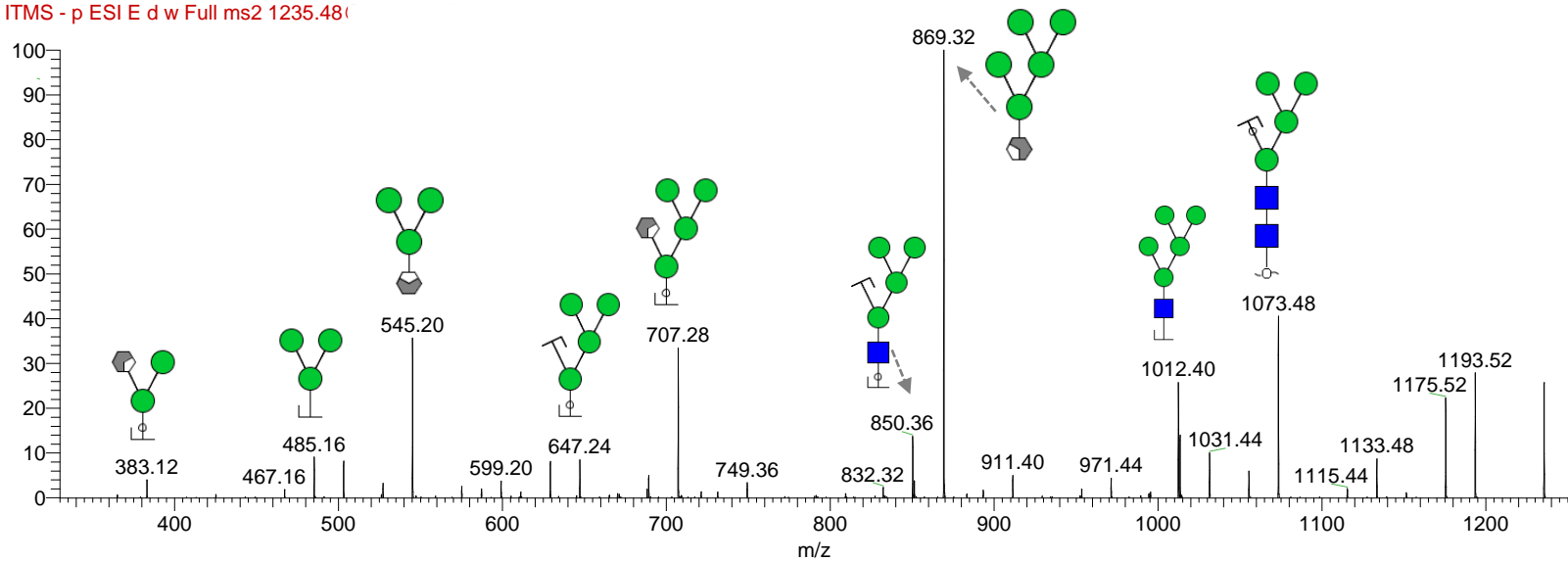
Retention time: 22.7 min

Theo mass [M-H] = 1235.44 Da



M5b

CC_220420_ID01_NG #844-912 RT: 22.61-23.38 AV: 5 NL: 1.83E2
F: ITMS - p ESI E d w Full ms2 1235.48

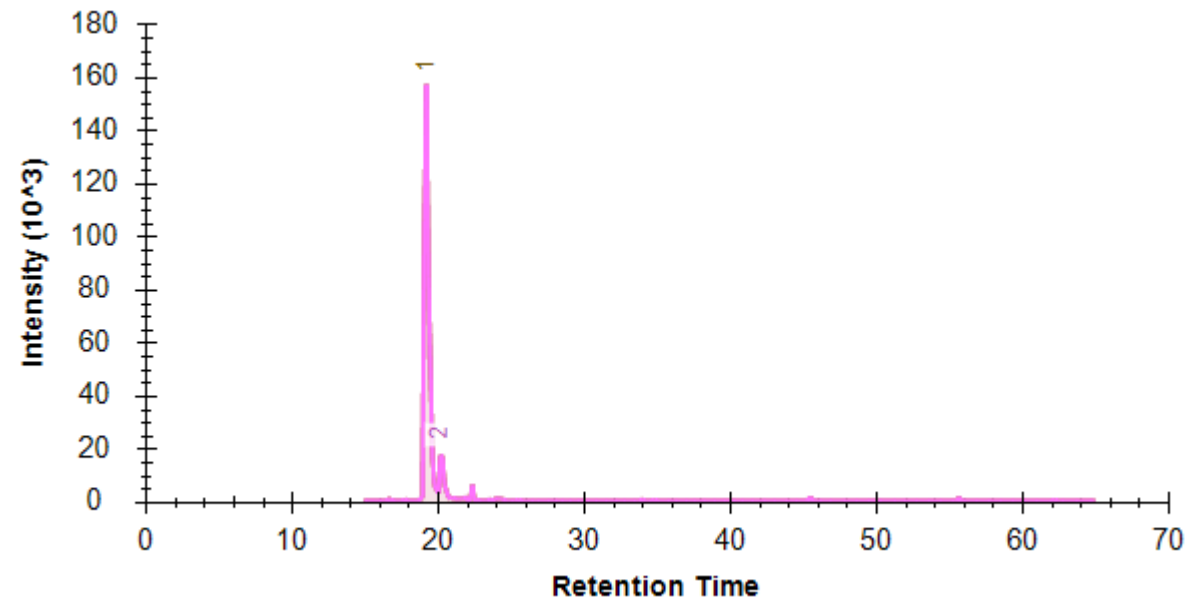
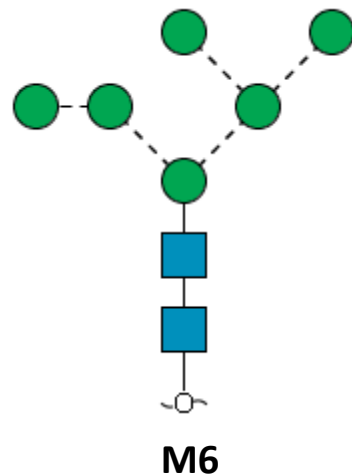


Glycan 11

(Hex)3 + (Man)3(GlcNAc)2

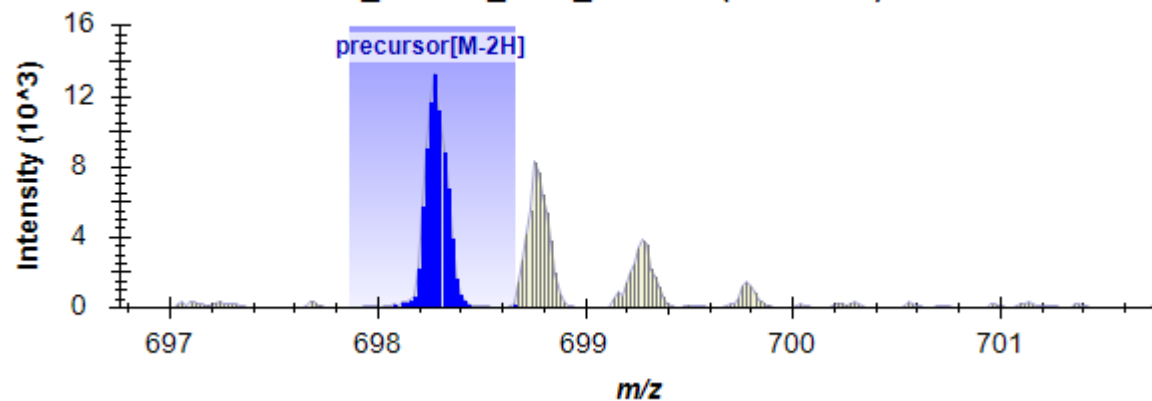
m/z 1397.53 (1-); 698.26 (2-)

Theo mass [M-H] = 1397.53 Da



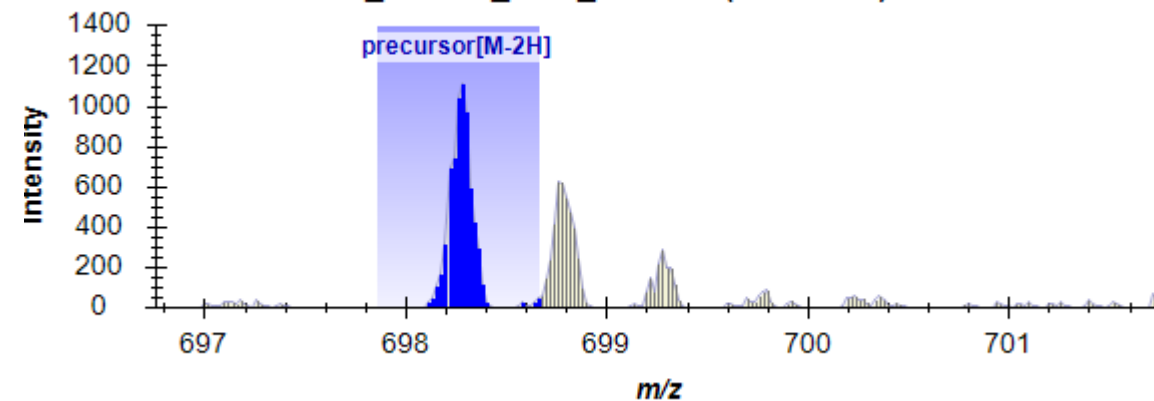
11a

CC_220420_ID01_NG.raw (19.27 min)



11b

CC_220420_ID01_NG.raw (20.34 min)

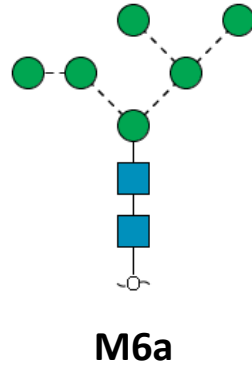


Glycan 11a

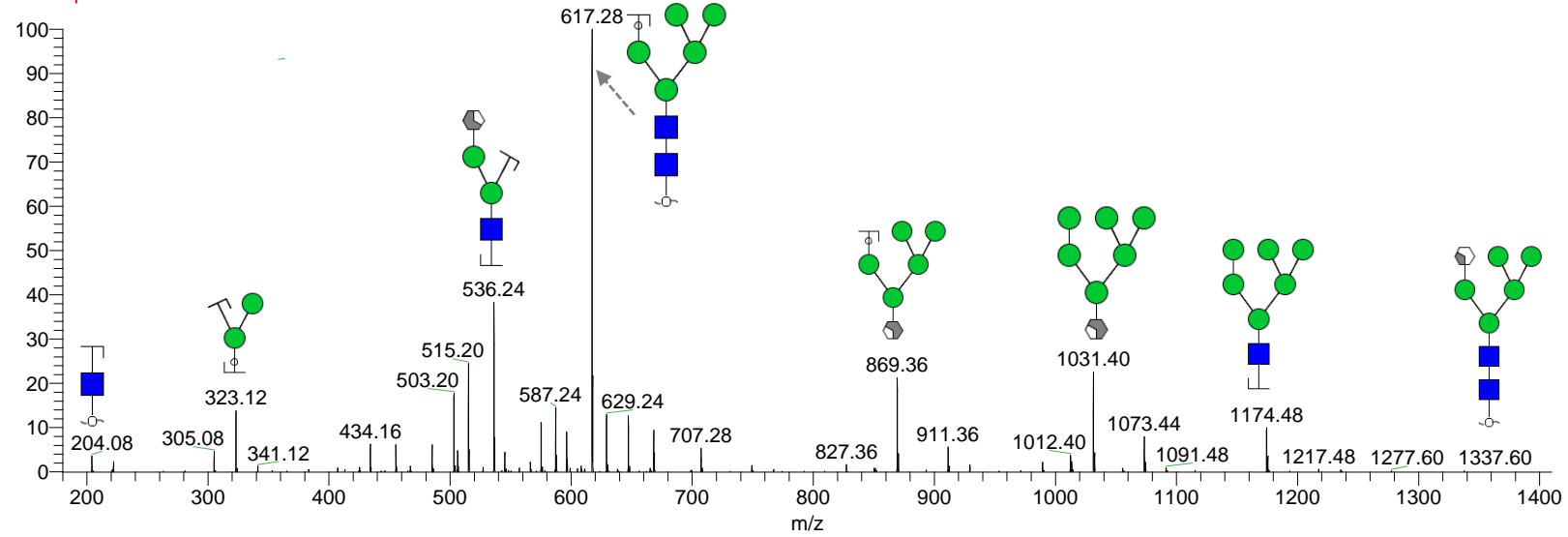
m/z 1397.53 (1-); 698.26 (2-)

Retention time: 20.2 min

Theo mass [M-H] = 1397.53 Da



CC_220420_ID01_NG #748-772 RT: 19.14-19.66 AV: 4 NL: 1.03E3
F: ITMS - p ESI E d w Full ms2 698.25@

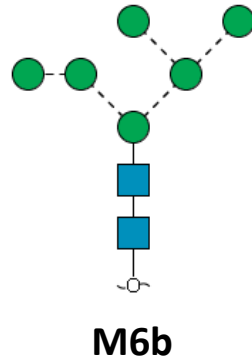


Glycan 11b

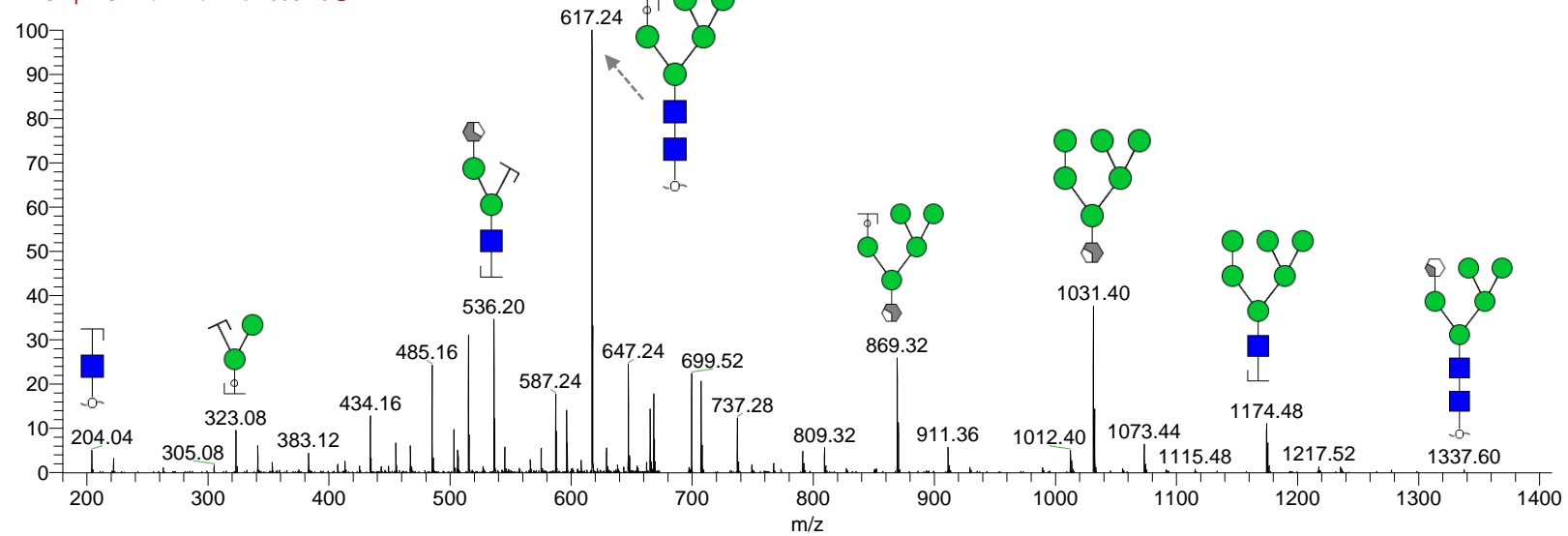
m/z 1397.53 (1-); 698.26 (2-)

Retention time: 19.3 min

Theo mass [M-H] = 1397.53 Da



CC_220420_ID01_NG #786-807 RT: 20.29-20.66 AV: 3 NL: 9.12E1
F: ITMS - p ESI E d w Full ms2 698.25@



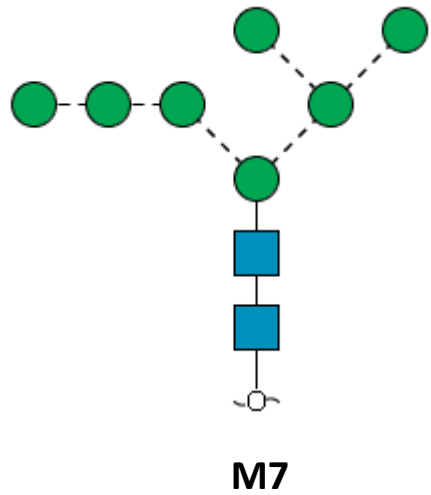
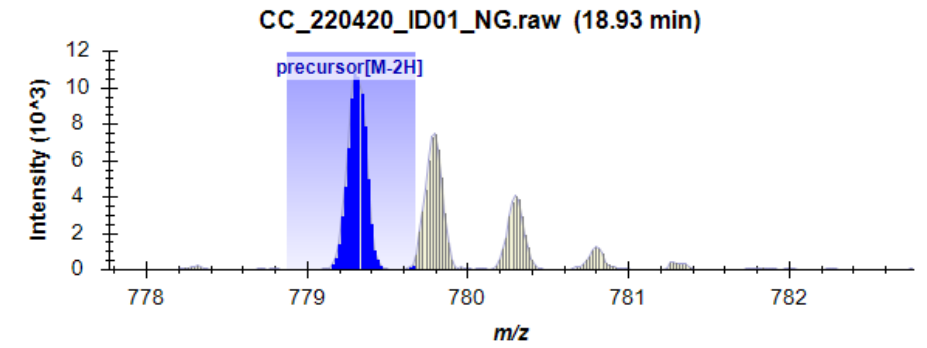
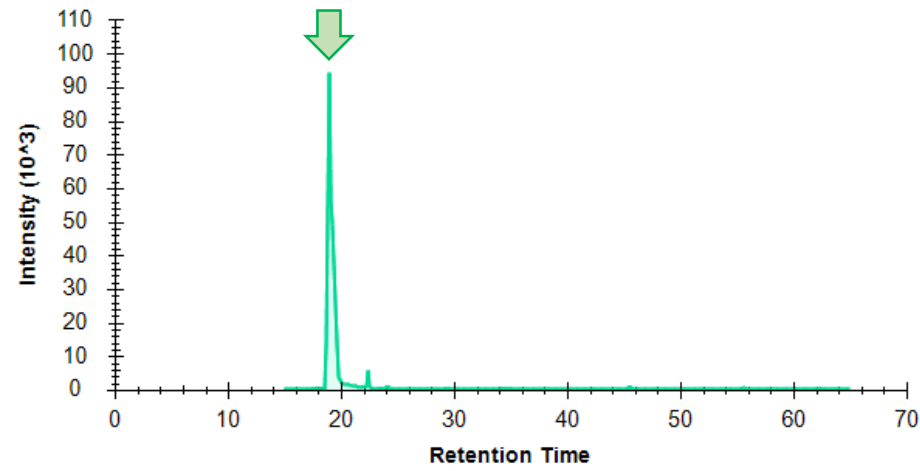
Glycan 12

(Hex)₄ + (Man)₃(GlcNAc)₂

m/z 1559.62 (1-); 779.27 (2-)

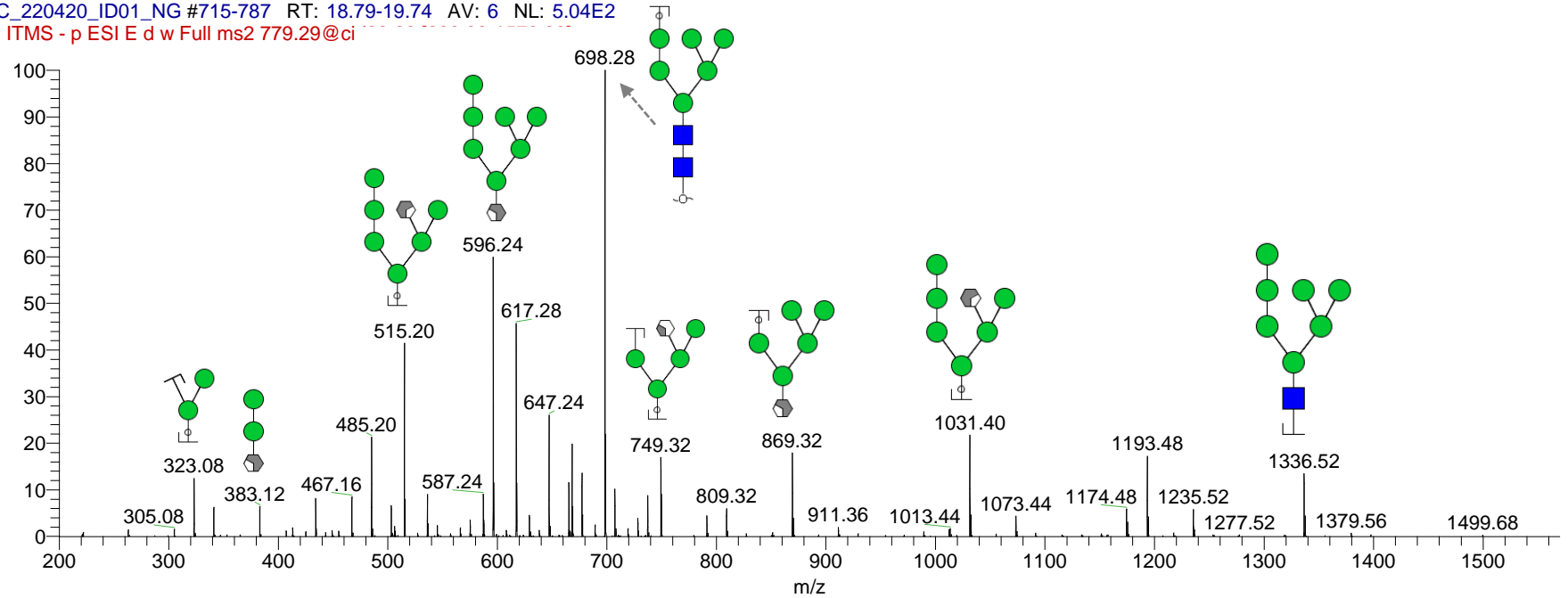
Retention time: 18.1 min

Theo mass [M-H] = 1559.62 Da



M7

CC_220420_ID01_NG #715-787 RT: 18.79-19.74 AV: 6 NL: 5.04E2
F: ITMS - p ESI E d w Full ms2 779.29@ci



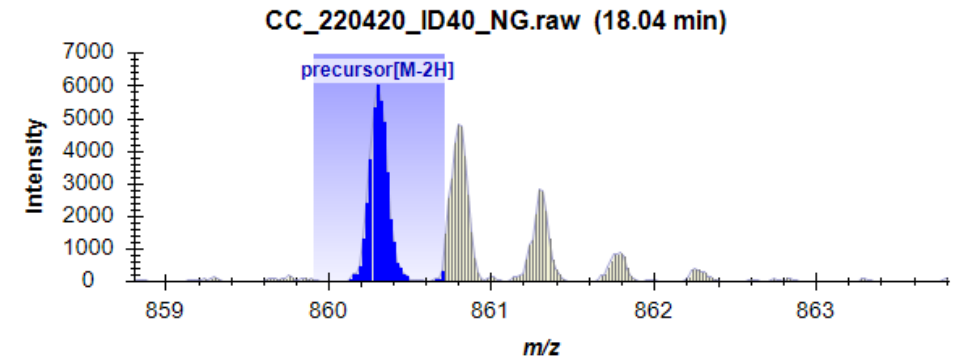
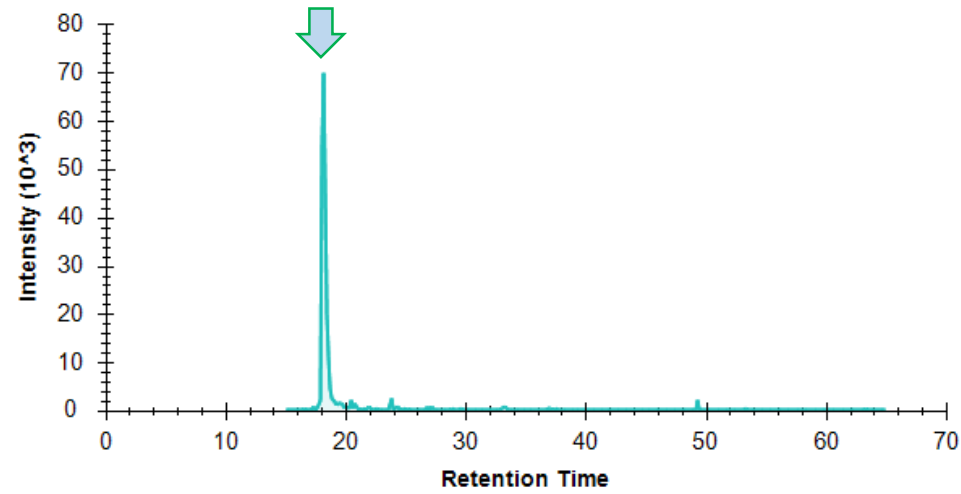
Glycan 13

(Hex)₅ + (Man)₃(GlcNAc)₂

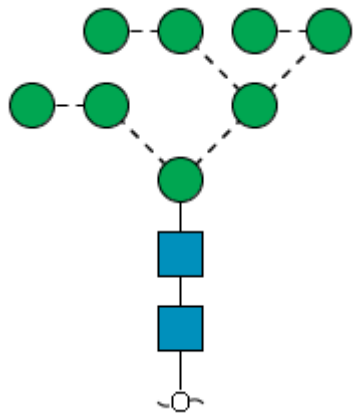
m/z 1721.64 (1-); 860.31 (2-)

Retention time: 18.2 min

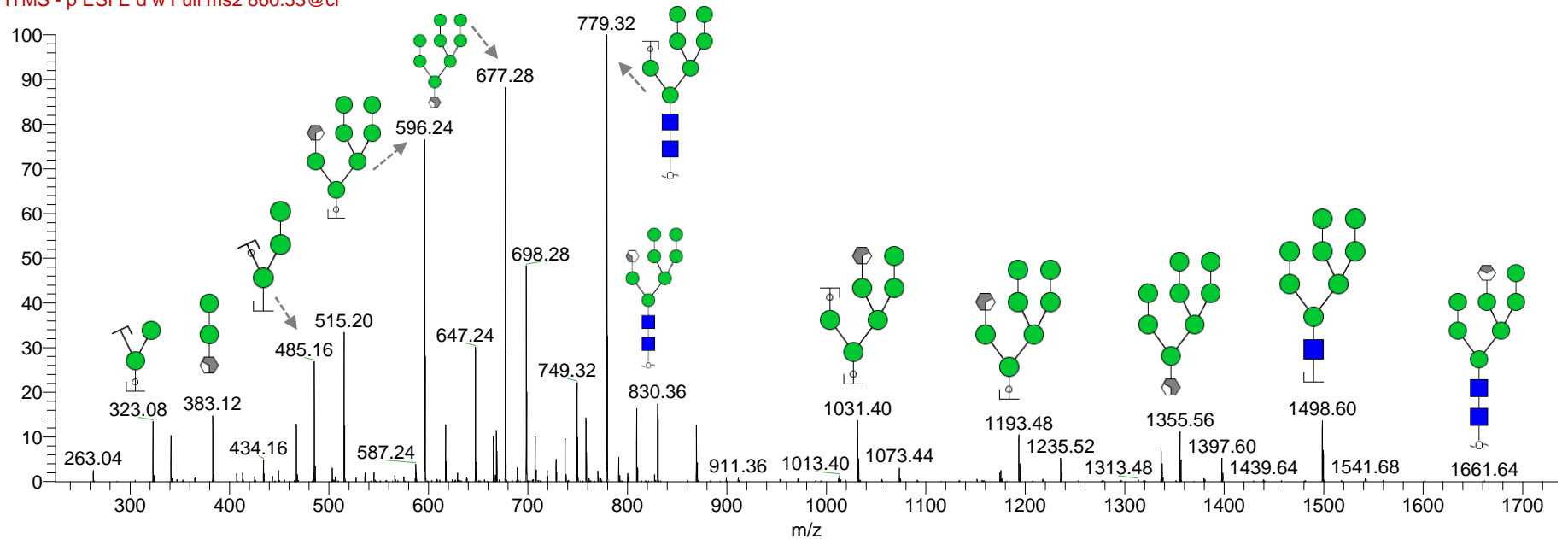
Theo mass [M-H] = 1721.64 Da



CC_220420_ID01_NG #727-777 RT: 18.85-19.22 AV: 3 NL: 6.66E2
F: ITMS - p ESI E d w Full ms2 860.33@ci



M8



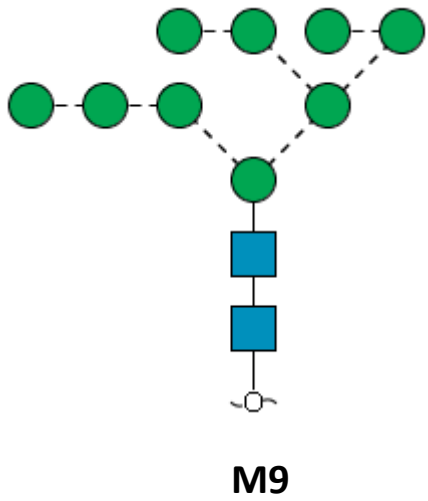
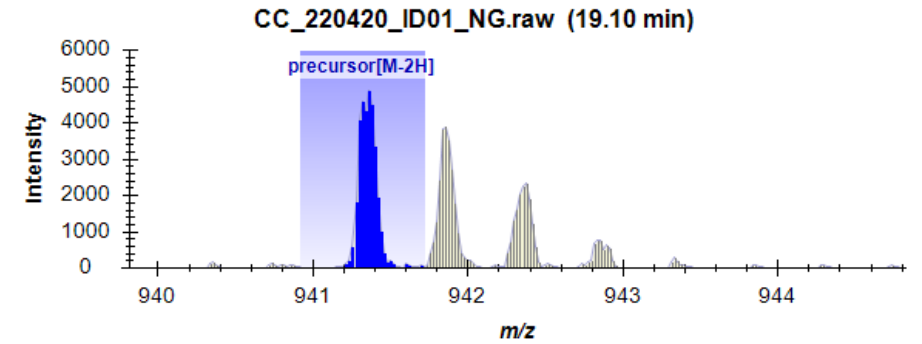
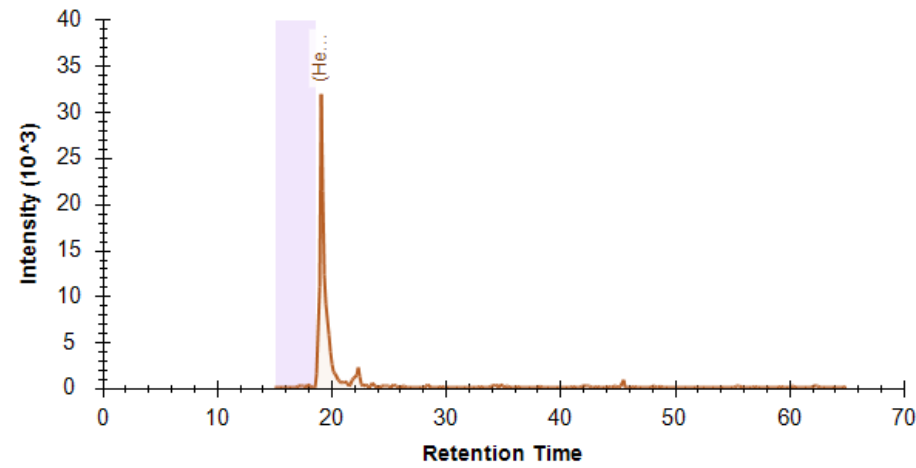
Glycan 14

(Hex)6 + (Man)3(GlcNAc)2

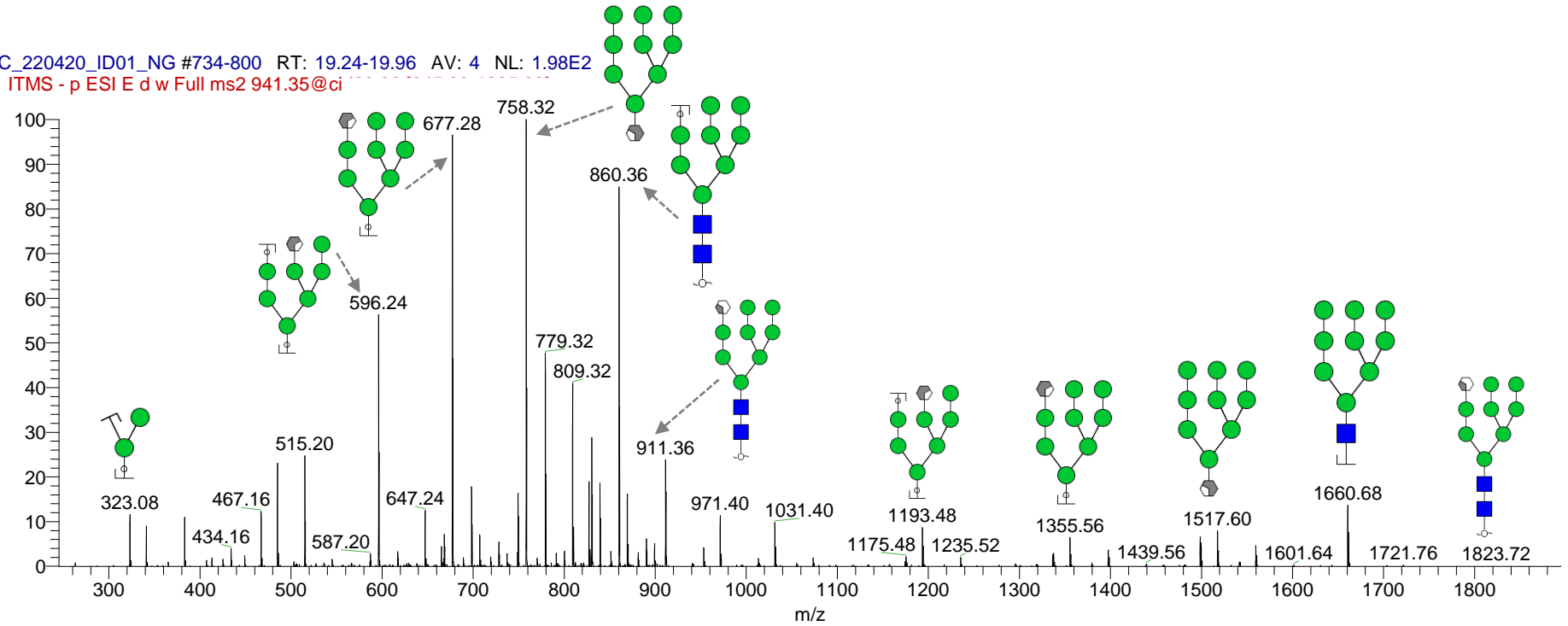
m/z 941.32 (2-)

Retention time: 18.4 min

Theo mass [M-H] = 1883.64 Da



CC_220420_ID01_NG #734-800 RT: 19.24-19.96 AV: 4 NL: 1.98E2
F: ITMS - p ESI E d w Full ms2 941.35@ci



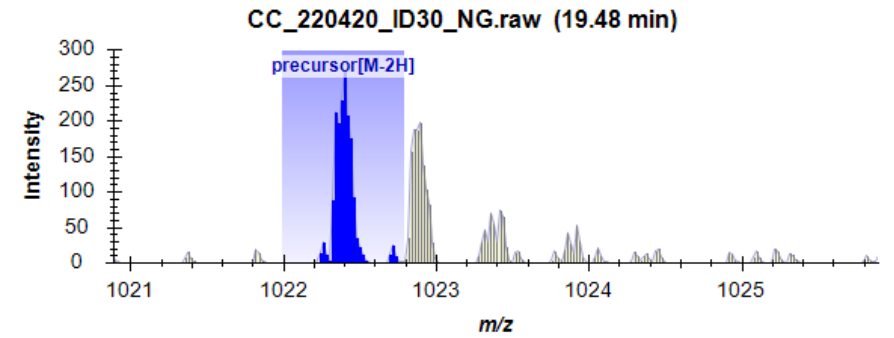
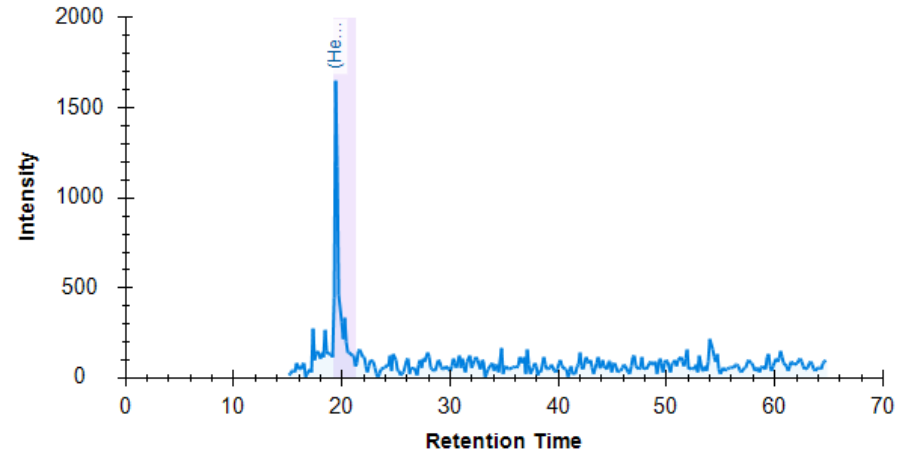
Glycan 15

(Hex)7 + (Man)3(GlcNAc)2

m/z 1022.39 (2-)

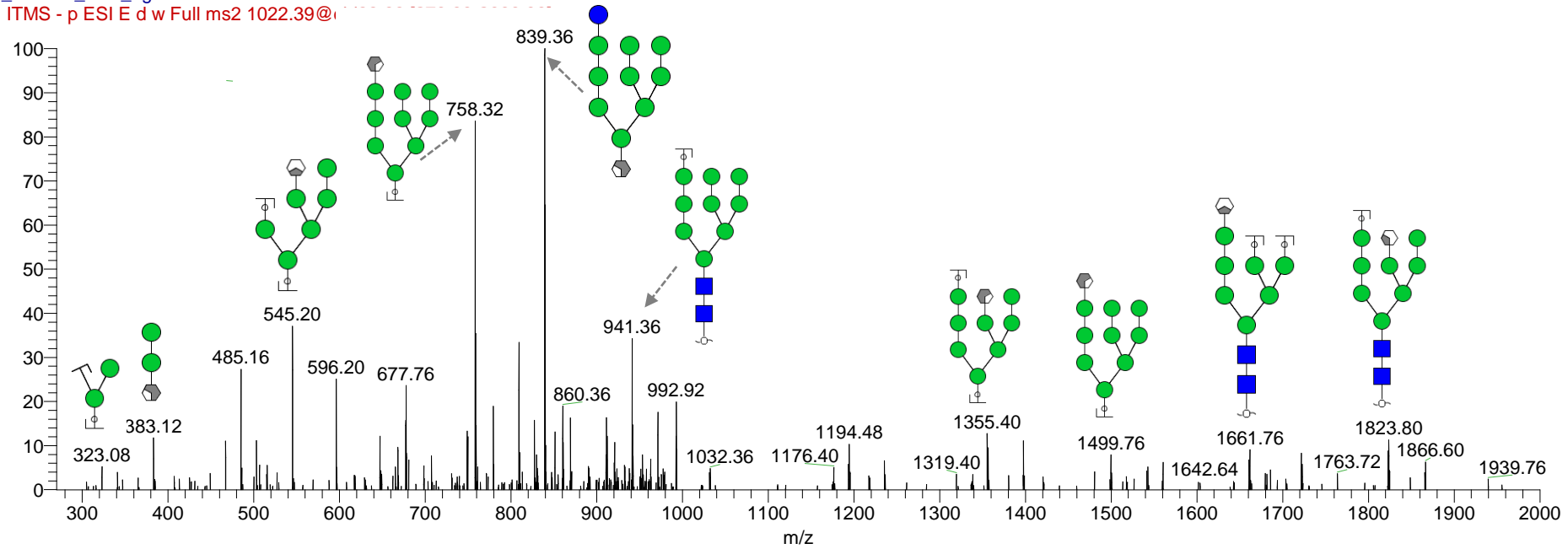
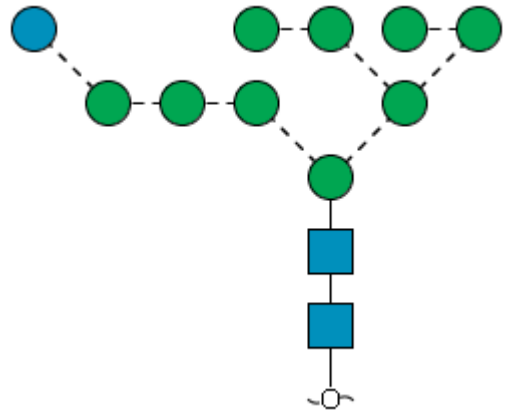
Retention time: 19.5 min

Theo mass [M-H] = 2045.78 Da



cc_220420_id30_ng #730 RT: 19.63 AV: 1 NL: 1.81E1

F: ITMS - p ESI E d w Full ms2 1022.39@



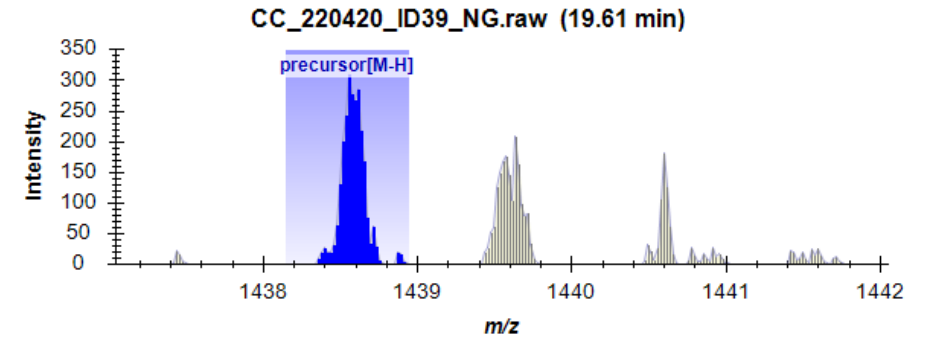
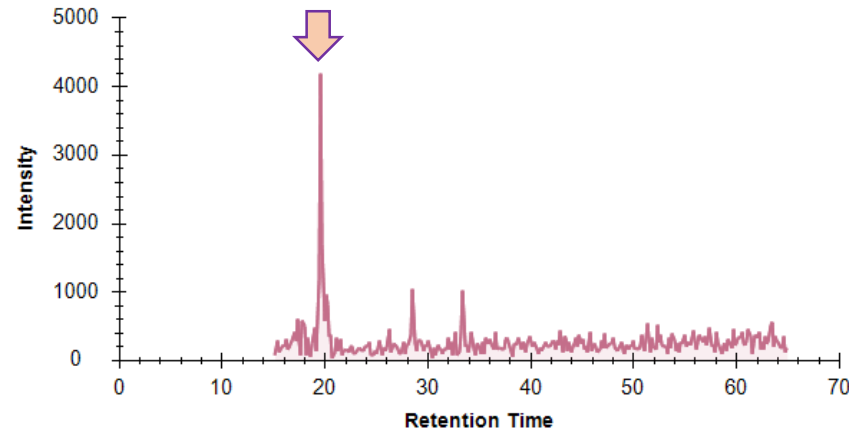
Glycan 16

(Hex)₂(HexNAc)₁ + (Man)₃(GlcNAc)₂

m/z 1438.58 (1-); 718.77 (2-)

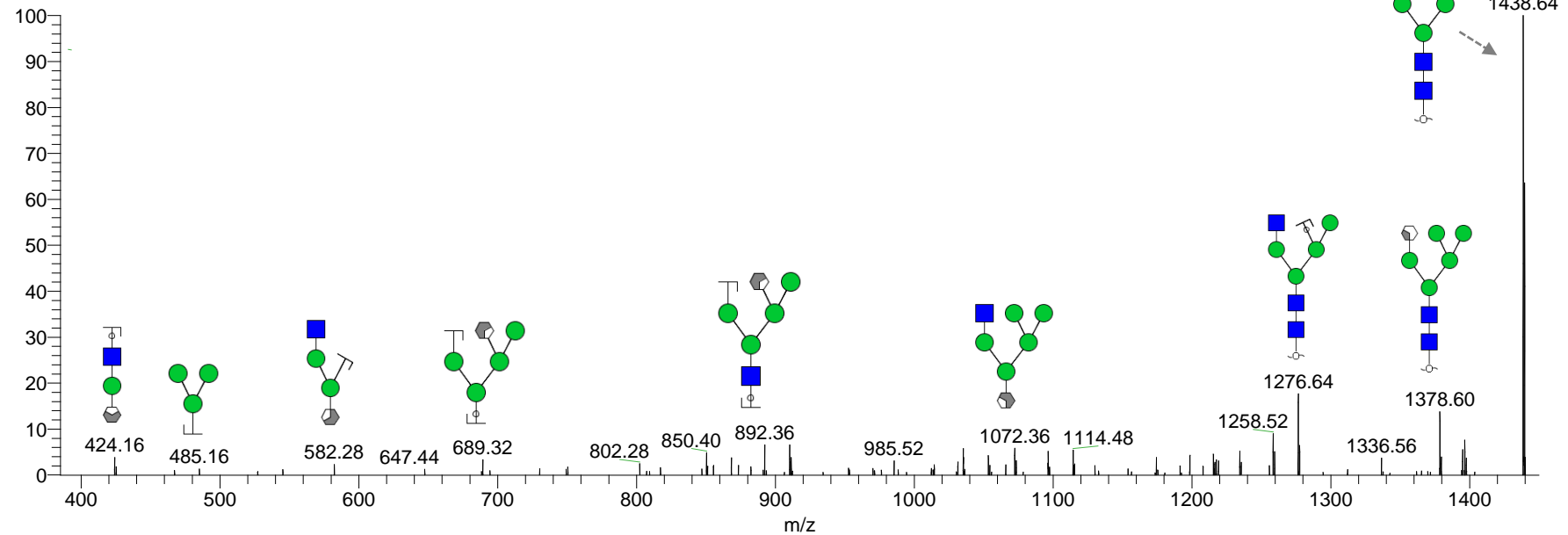
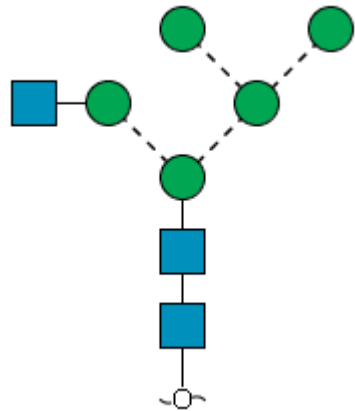
Retention time: 18.5 min

Theo mass [M-H] = 1438.58 Da



CC_220420_ID39_NG #740 RT: 19.76 AV: 1 NL: 2.26E1

F: ITMS - p ESI E d w Full ms2 1438.58@



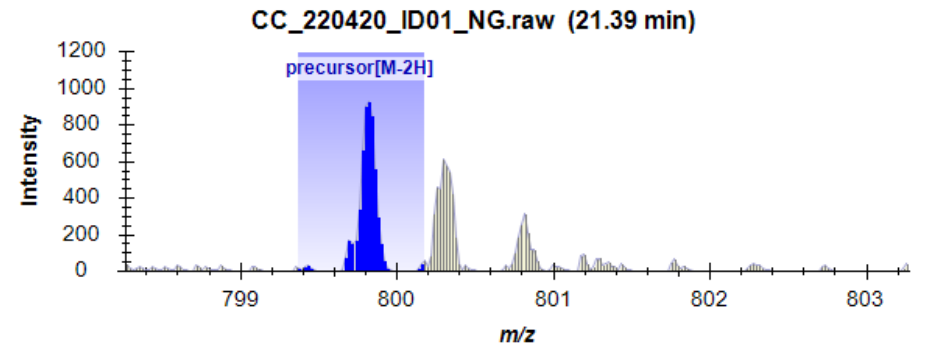
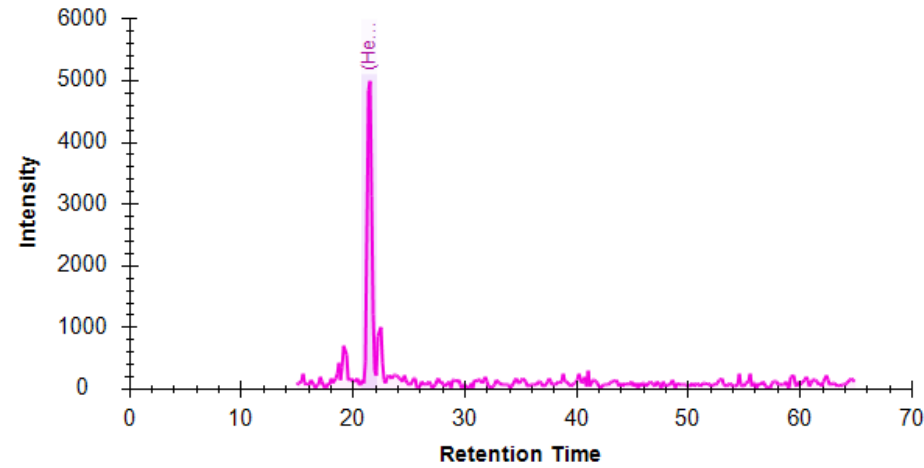
Glycan 17

(Hex)3(HexNAc)1 + (Man)3(GlcNAc)2

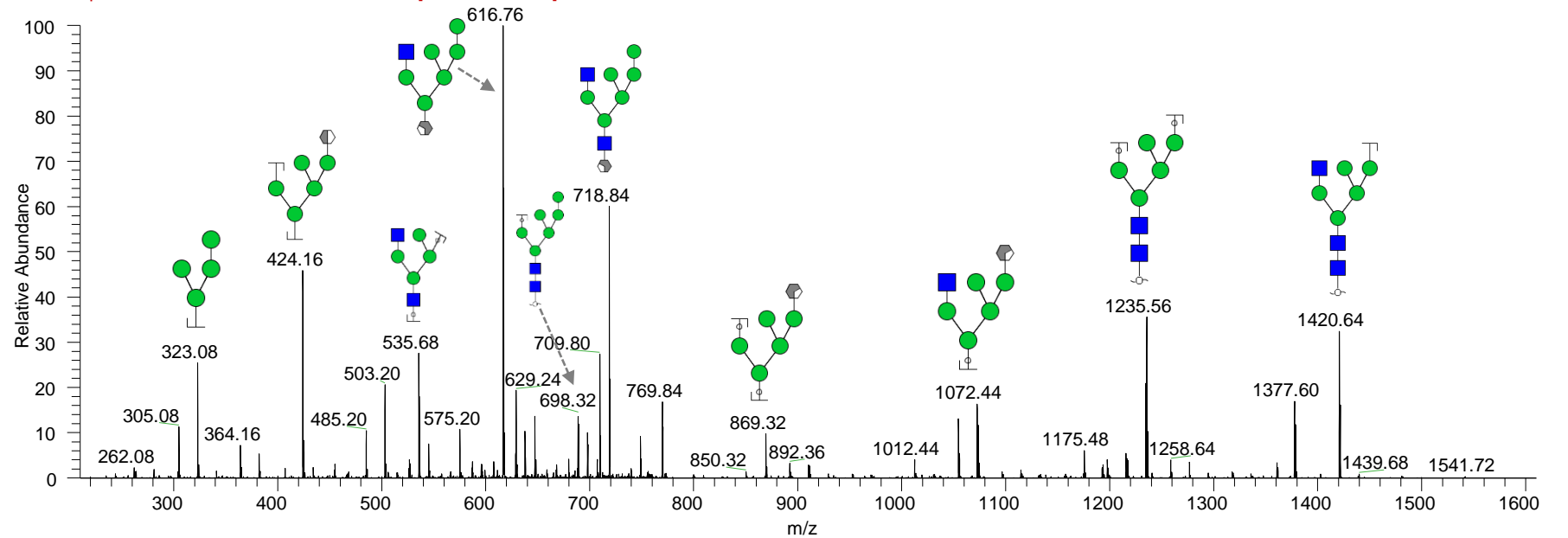
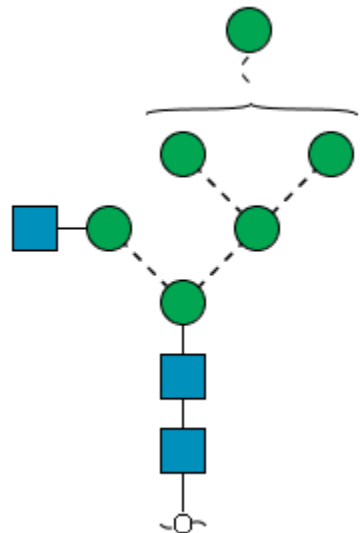
m/z 799.77 (2-)

Retention time: 22.1 min

Theo mass [M-H] = 1600.54 Da



CC_220420_ID01_NG #817-861 RT: 21.45-21.60 AV: 2 NL: 6.06E1
F: ITMS - p ESI E d w Full ms2 799.81@cid33.00 [210.00-1610.00]

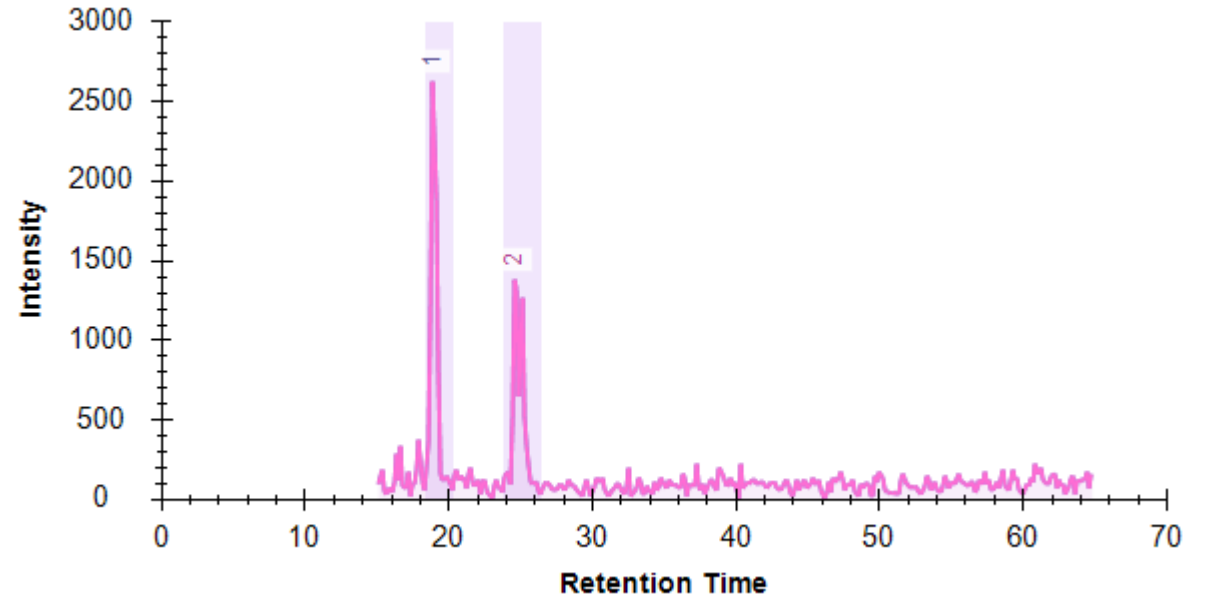
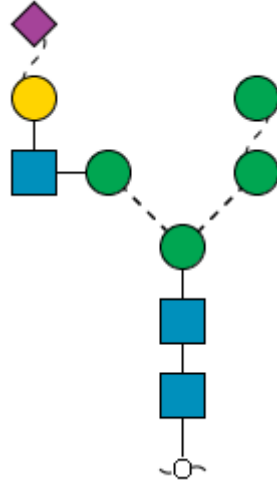


Glycan 18

(Hex)₂(HexNAc)₁(NeuAc)₁ + (Man)₃(GlcNAc)₂

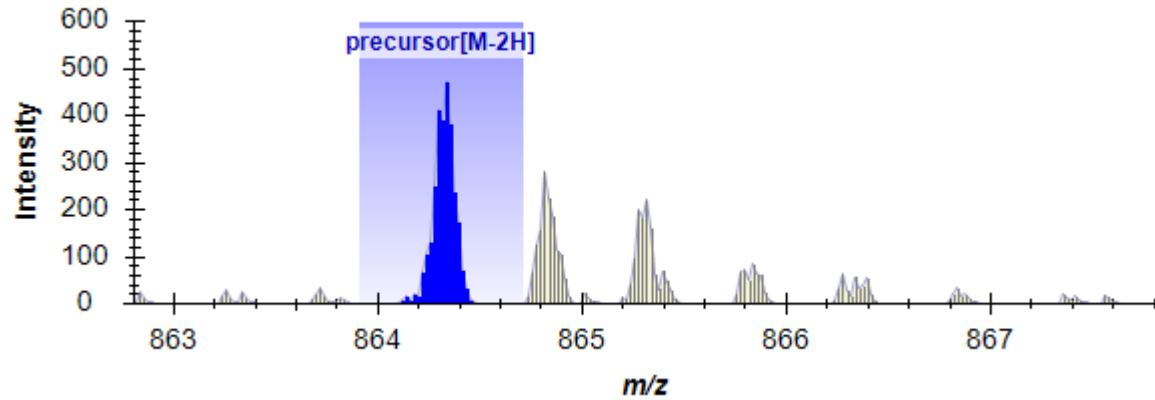
m/z 864.31 (2-)

Theo mass [M-H] = 1729.62 Da



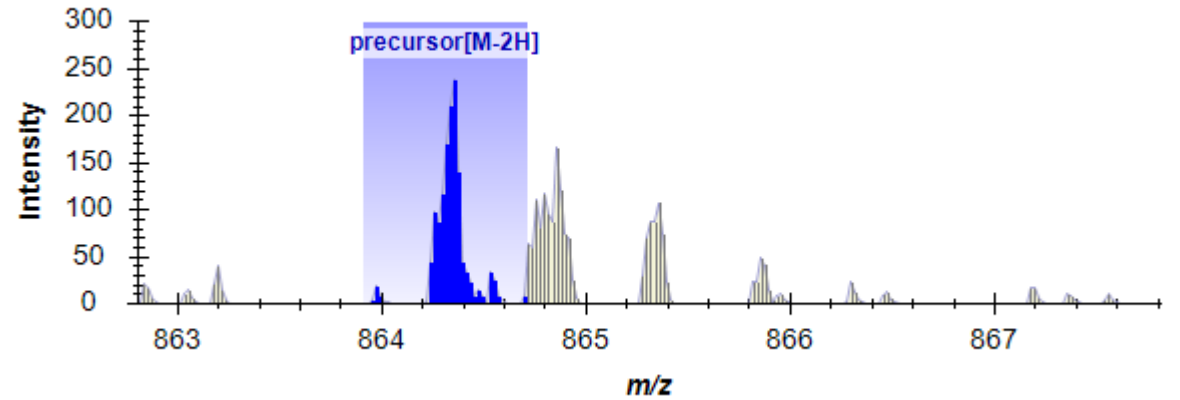
18a

CC_220420_ID23_NG.raw (18.95 min)



18b

CC_220420_ID23_NG.raw (24.61 min)

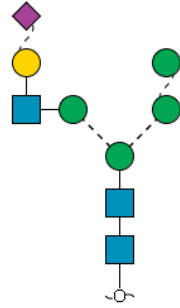


Glycan 18a

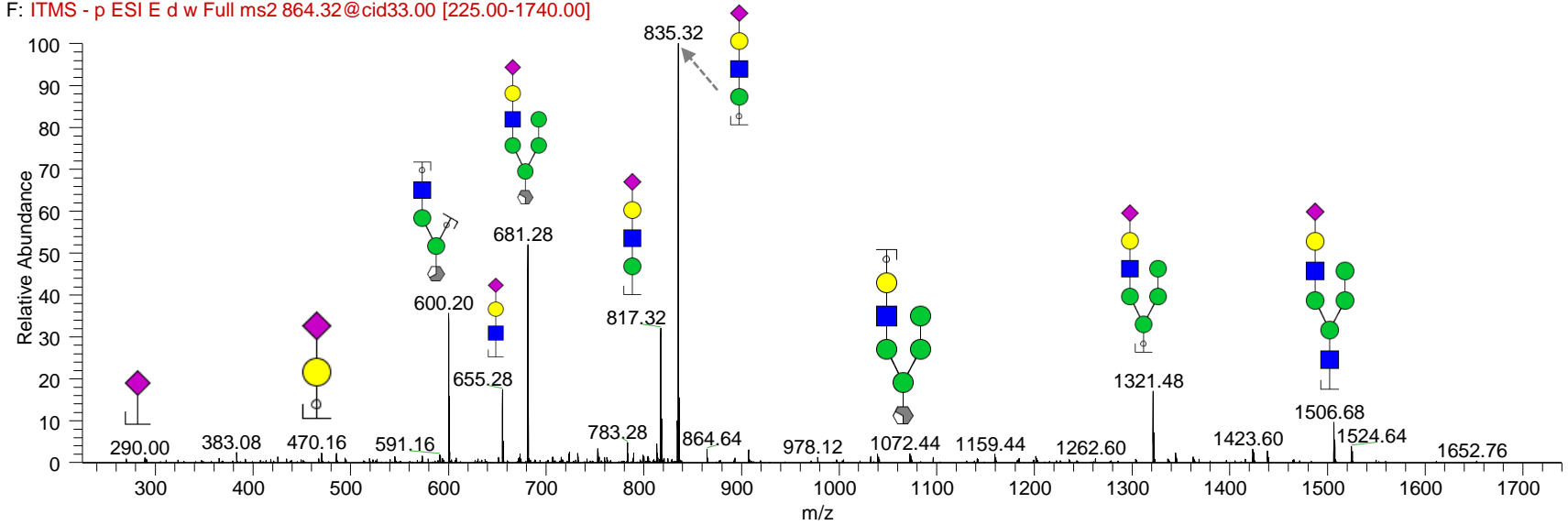
m/z 864.31 (2-)

Retention time: 18.9 min

Theo mass [M-H] = 1729.62 Da



cc_220420_id23_ng #715 RT: 19.02 AV: 1 NL: 7.20E1
F: ITMS - p ESI E d w Full ms2 864.32@cid33.00 [225.00-1740.00]

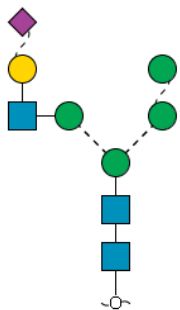


Glycan 18b

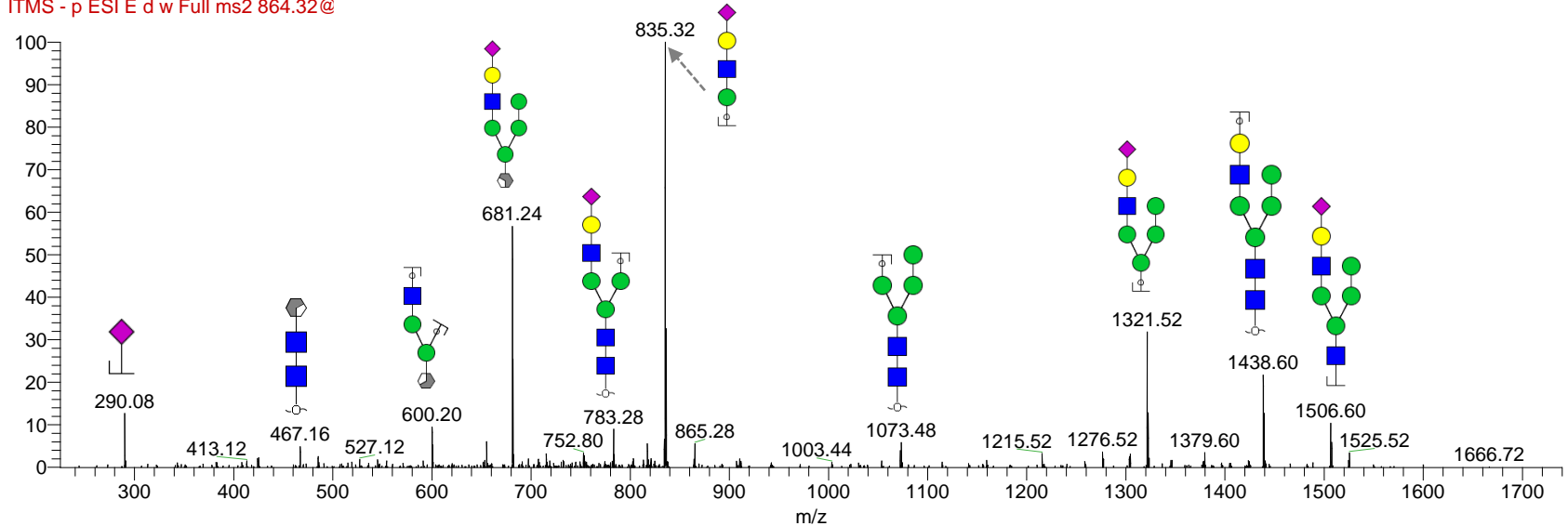
m/z 864.31 (2-)

Retention time: 24.6 min

Theo mass [M-H] = 1729.62 Da



cc_220420_id23_ng #919-974 RT: 24.75-24.91 AV: 2 NL: 3.59E1
F: ITMS - p ESI E d w Full ms2 864.32@



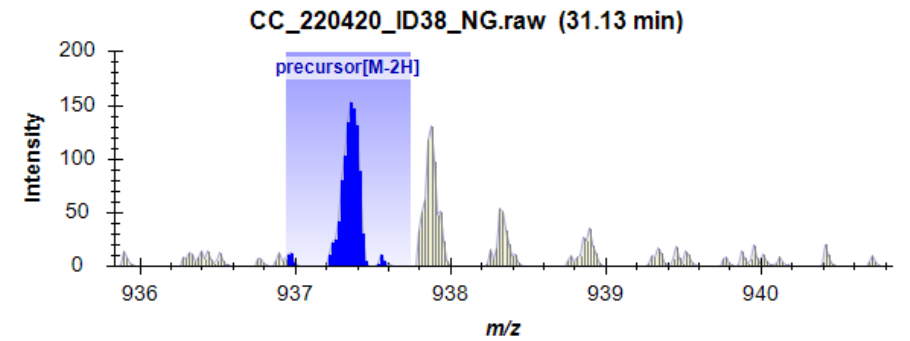
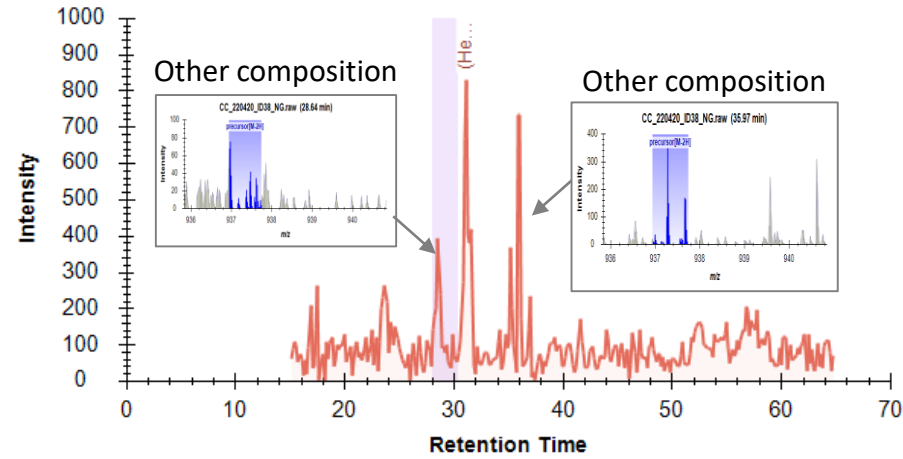
Glycan 19

(Hex)2(HexNAc)1(Deoxyhexose)1(NeuAc)1 + (Man)3(GlcNAc)2

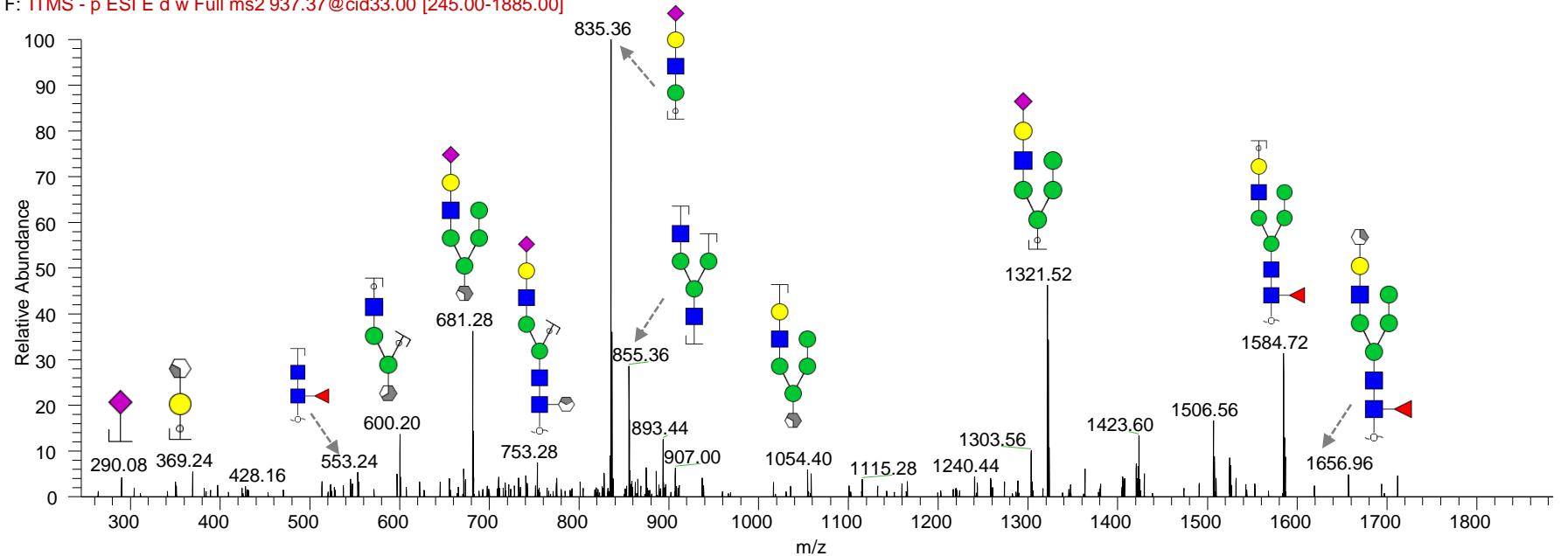
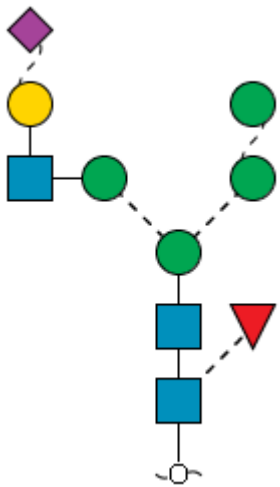
m/z 937.34 (2-)

Retention time: 29.5 min

Theo mass [M-H] = 1875.68 Da



cc_220420_id38_ng #1156 RT: 31.28 AV: 1 NL: 1.49E1
F: ITMS - p ESI E d w Full ms2 937.37@cid33.00 [245.00-1885.00]

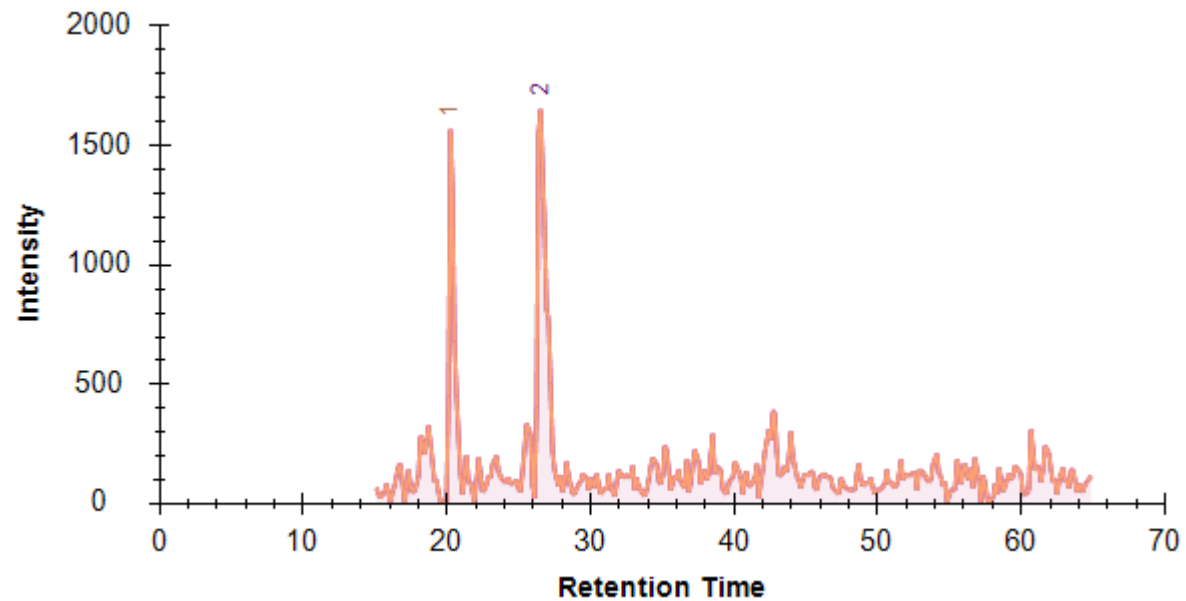
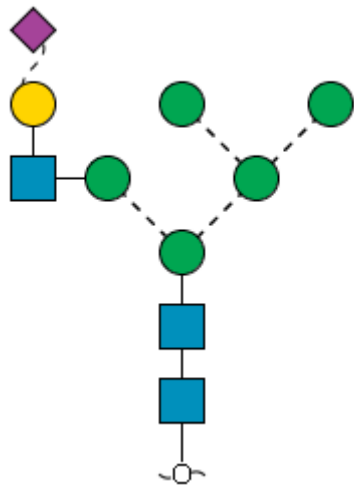


Glycan 20

(Hex)3(HexNAc)1(NeuAc)1 + (Man)3(GlcNAc)2

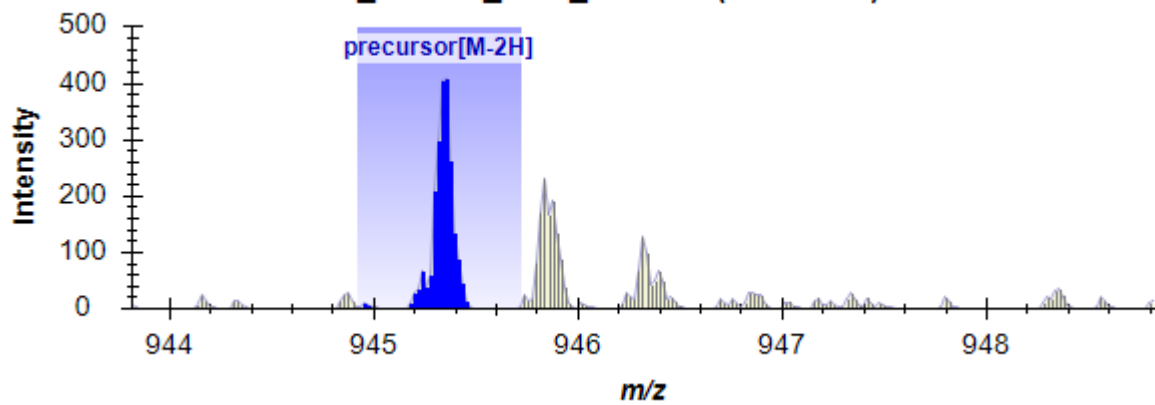
m/z 945.32 (2-)

Theo mass [M-H] = 1891.64 Da



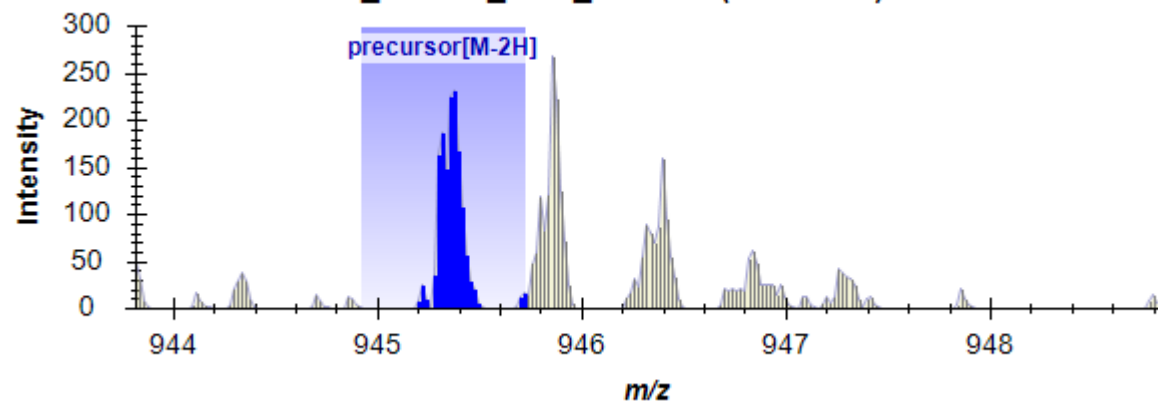
20a

CC_220420_ID37_NG.raw (20.37 min)



20b

CC_220420_ID37_NG.raw (26.72 min)

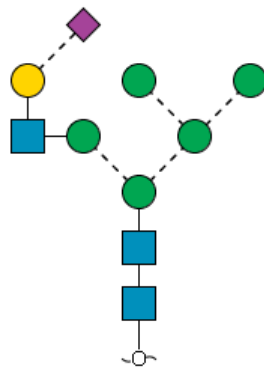


Glycan 20a

m/z 945.32 (2-)

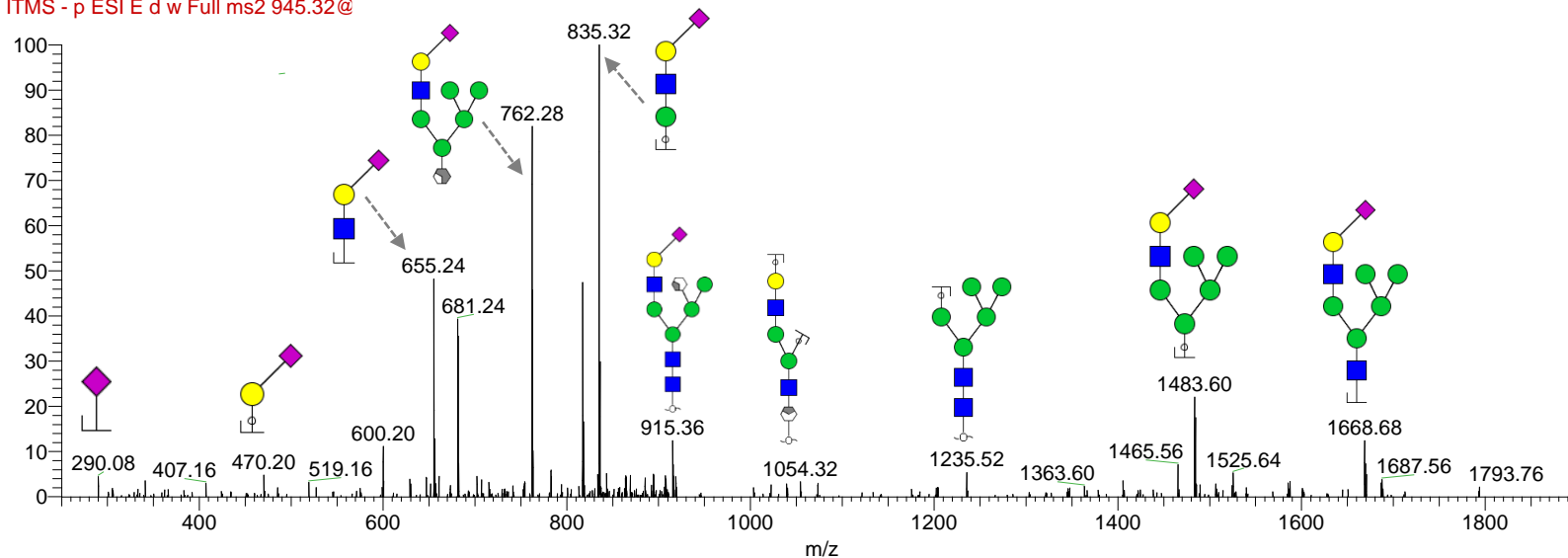
Retention time: 20.4 min

Theo mass [M-H] = 1891.64 Da



cc_220420_id37_ng #777 RT: 20.46 AV: 1 NL: 3.49E1

F: ITMS - p ESI E d w Full ms2 945.32@

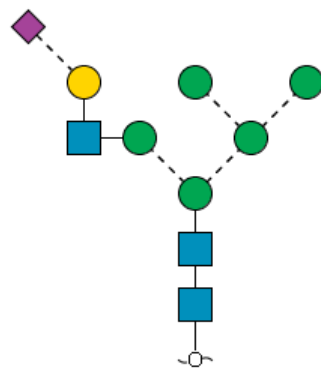


Glycan 20b

m/z 945.32 (2-)

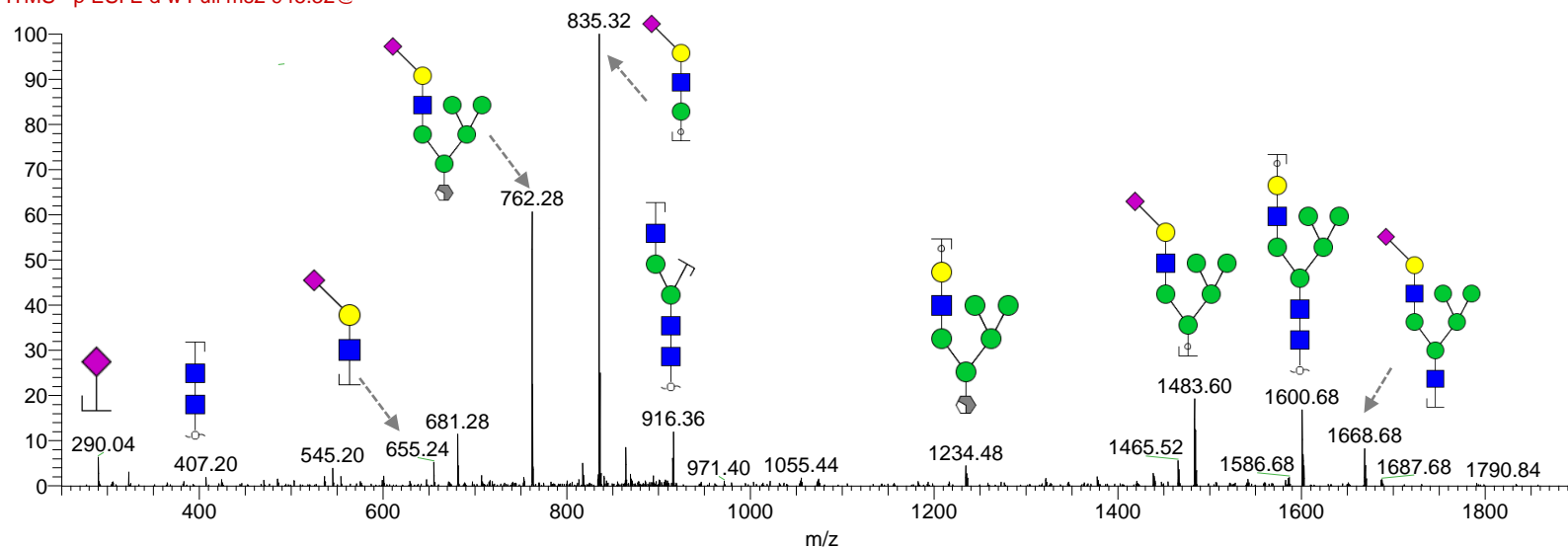
Retention time: 26.5 min

Theo mass [M-H] = 1891.64 Da



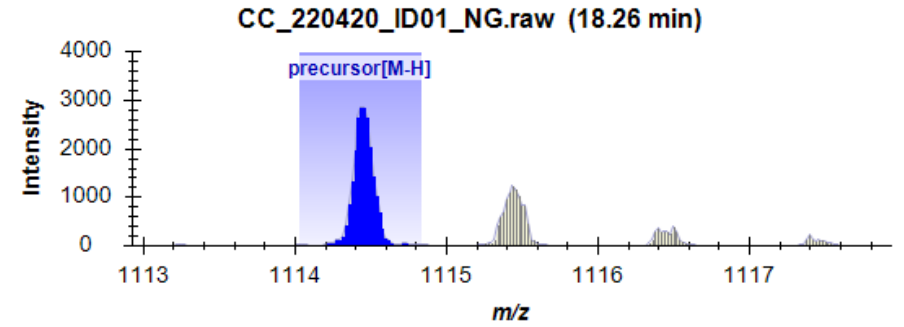
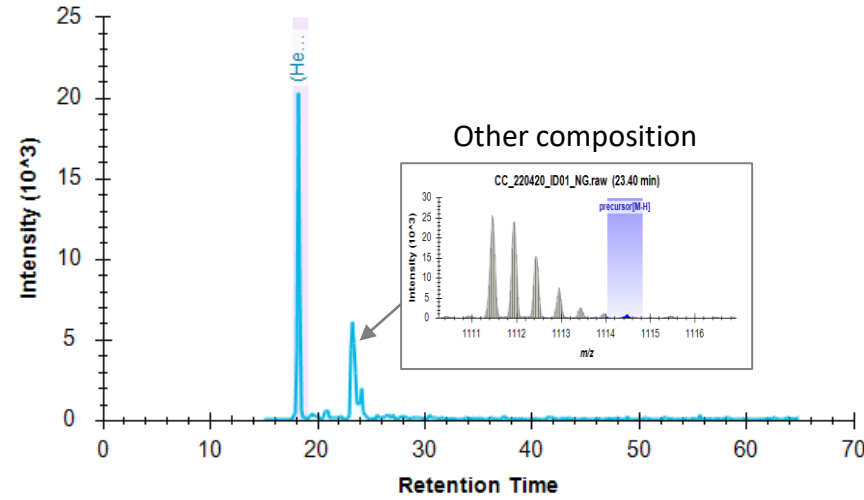
cc_220420_id37_ng #984-1058 RT: 26.66-27.24 AV: 2 NL: 5.57E1

F: ITMS - p ESI E d w Full ms2 945.32@

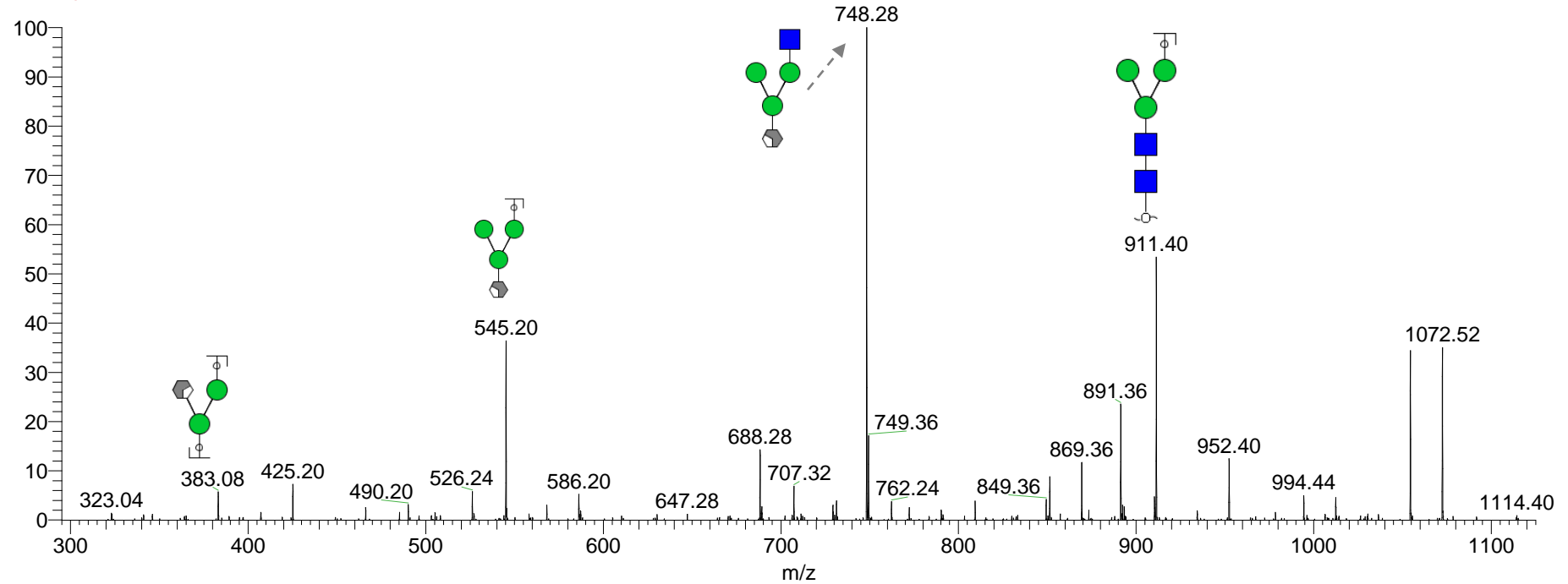
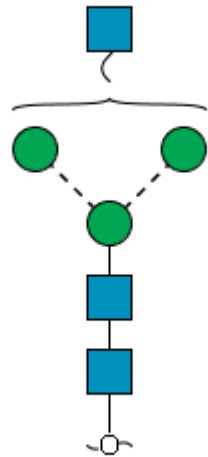


Note: This glycan has been annotated as $\alpha 2,6$ or $\alpha 2,3$ -sialyl isomer based on their elution time and 655/290 ions.

Glycan 21
(HexNAc)1 + (Man)3(GlcNAc)2
 m/z 1114.43 (1-)
 Retention time: 17.5 min
 Theo mass [M-H] = 1114.43 Da



CC_220420_ID01_NG #694-751 RT: 18.32-18.48 AV: 2 NL: 3.49E1
 F: ITMS - p ESI E d w Full ms2 1114.45@



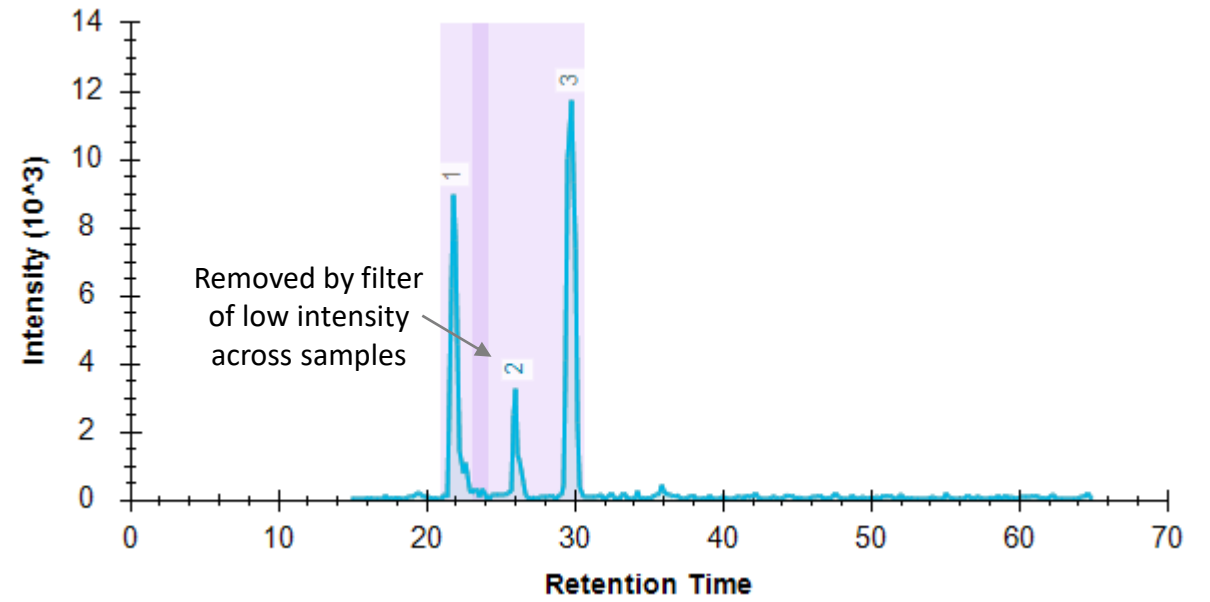
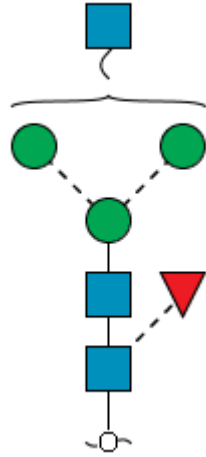
Note: No distinction intended between 3-arm/6-arm in glycan fragment scheme.

Glycan 22

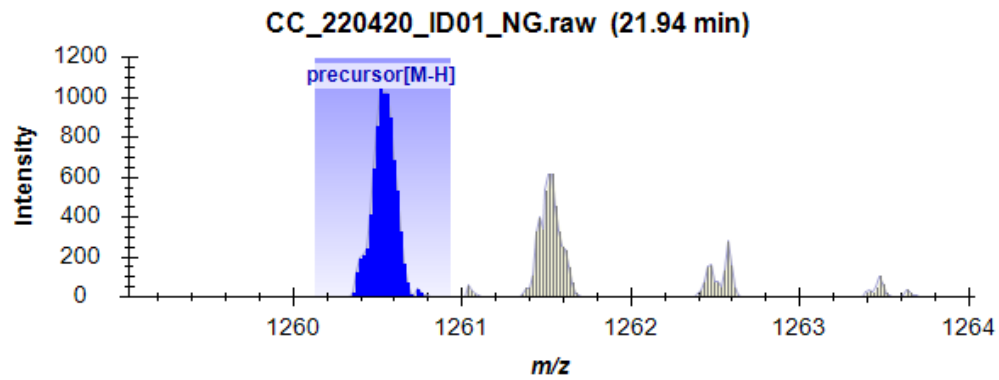
(HexNAc)1(Deoxyhexose)1 + (Man)3(GlcNAc)2

m/z 1260.53 (1-)

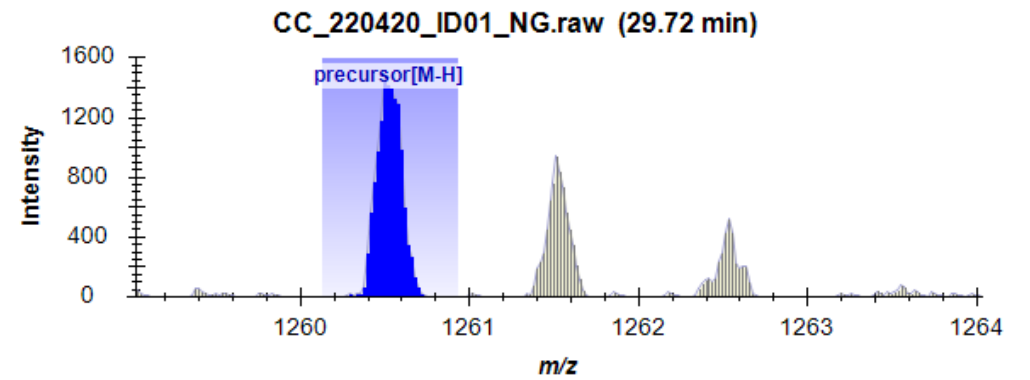
Theo mass [M-H] = 1260.53 Da



22a



22b

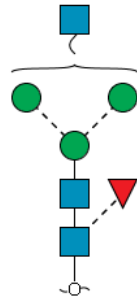


Glycan 22a

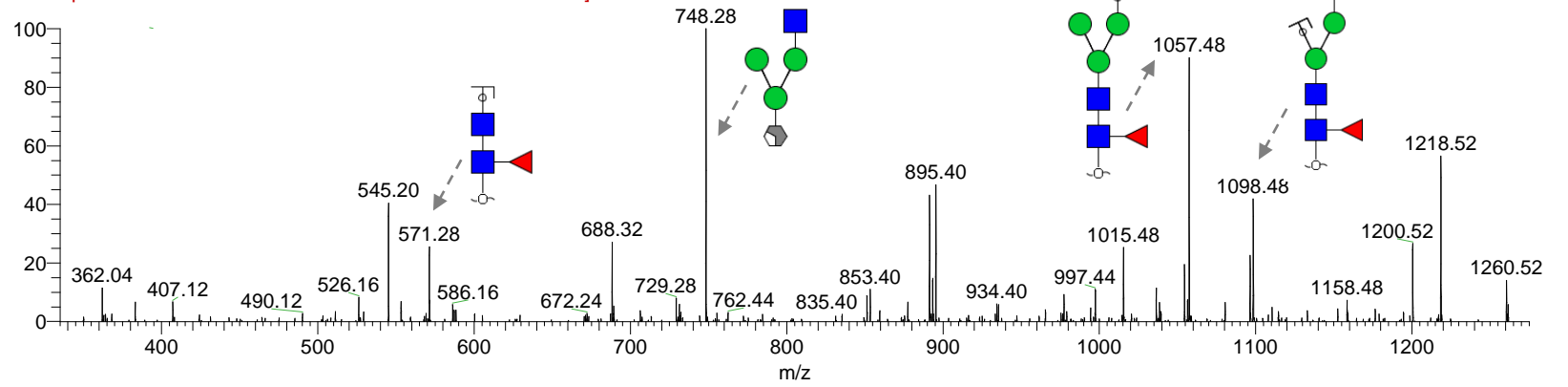
m/z 1260.53 (1-)

Retention time: 21.7 min

Theo mass [M-H] = 1260.53 Da



CC_220420_ID01_NG #811-885 RT: 21.82-22.21 AV: 3 NL: 1.06E1
F: ITMS - p ESI E d w Full ms2 1 275.00]

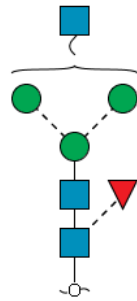


Glycan 22b

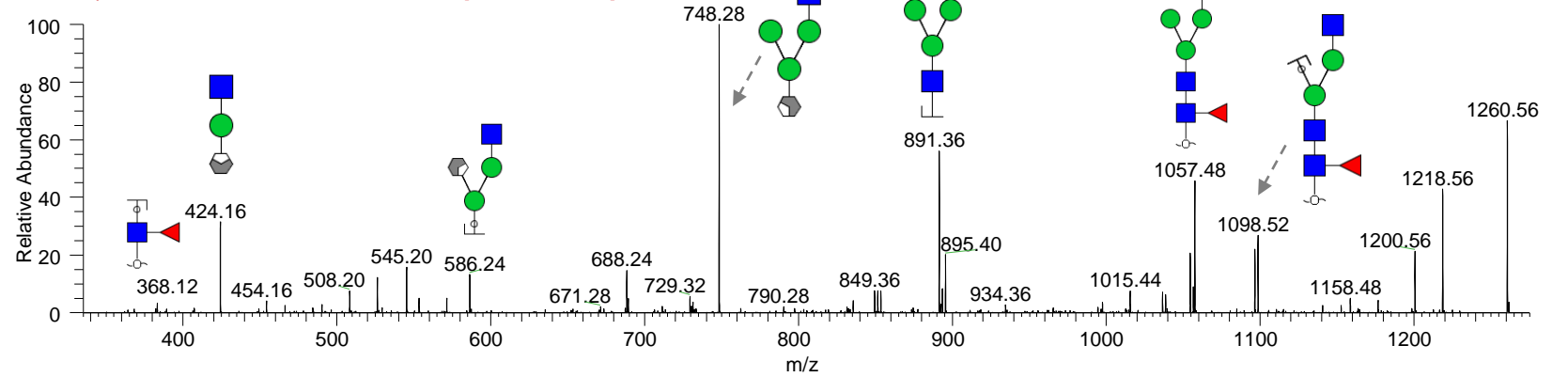
m/z 1260.53 (1-)

Retention time: 29.7 min

Theo mass [M-H] = 1260.53 Da



CC_220420_ID01_NG #1088-1135 RT: 29.60-30.13 AV: 4 NL: 2.01E1
F: ITMS - p ESI E d w Full ms2 1260.52@cid33.00 [335.00-1275.00]



Note: No distinction intended between 3-arm/6-arm in glycan fragment scheme.

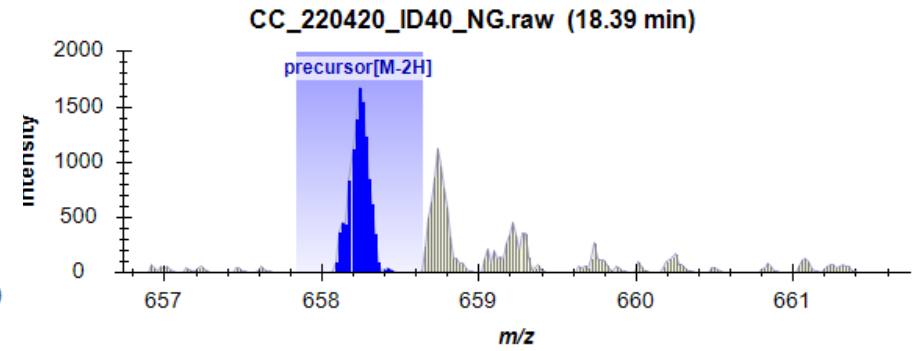
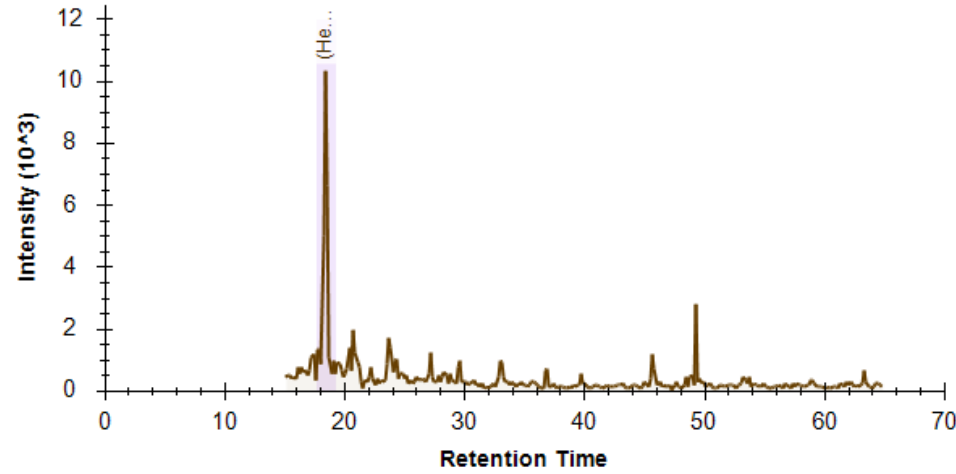
Glycan 23

(HexNAc)₂ + (Man)₃(GlcNAc)₂

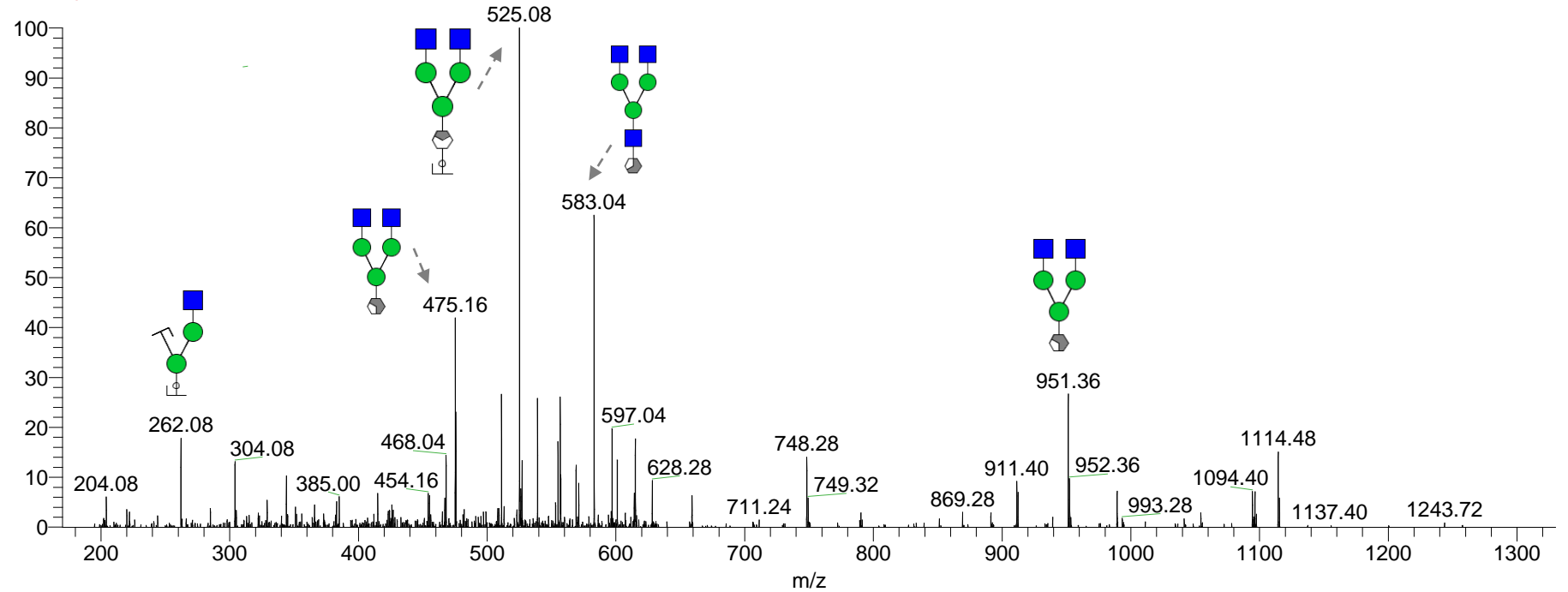
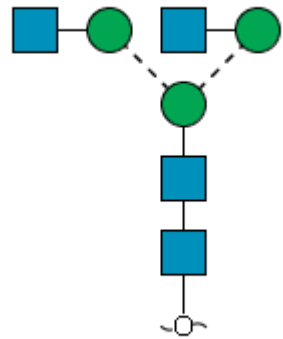
m/z 658.24 (2-)

Retention time: 18.4 min

Theo mass [M-2H] = 1317.48 Da



cc_220420_id40_ng #730 RT: 18.66 AV: 1 NL: 5.34E1
F: ITMS - p ESI E d w Full ms2 658.24@c



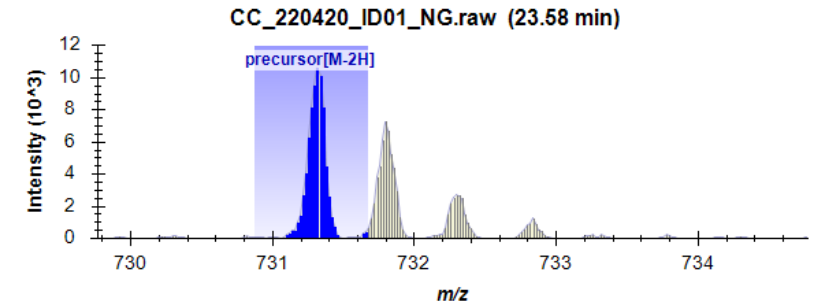
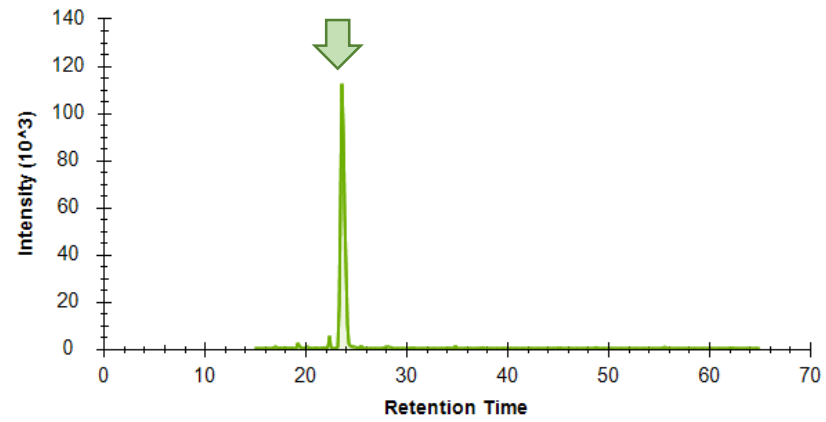
Glycan 24

(HexNAc)₂(Deoxyhexose)₁ + (Man)₃(GlcNAc)₂

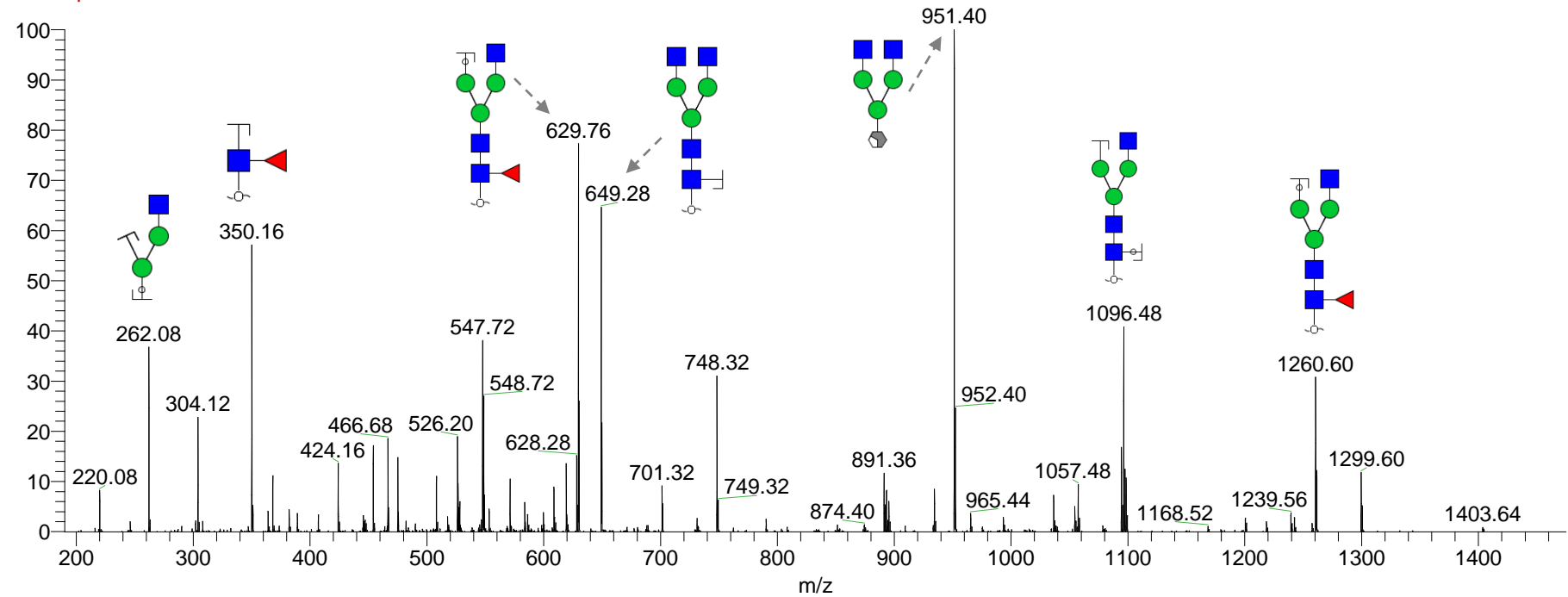
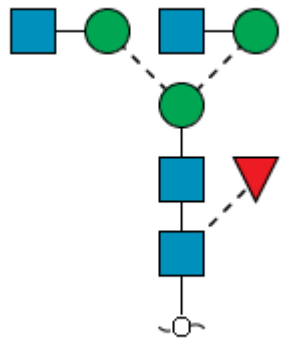
m/z 1463.63 (1-), 731.27 (2-)

Retention time: 23.6 min

Theo mass [M-H] = 1463.63 Da



CC_220420_ID01_NG #890-947 RT: 23.52-24.19 AV: 5 NL: 3.34E2
F: ITMS - p ESI E d w Full ms2 731.29@c



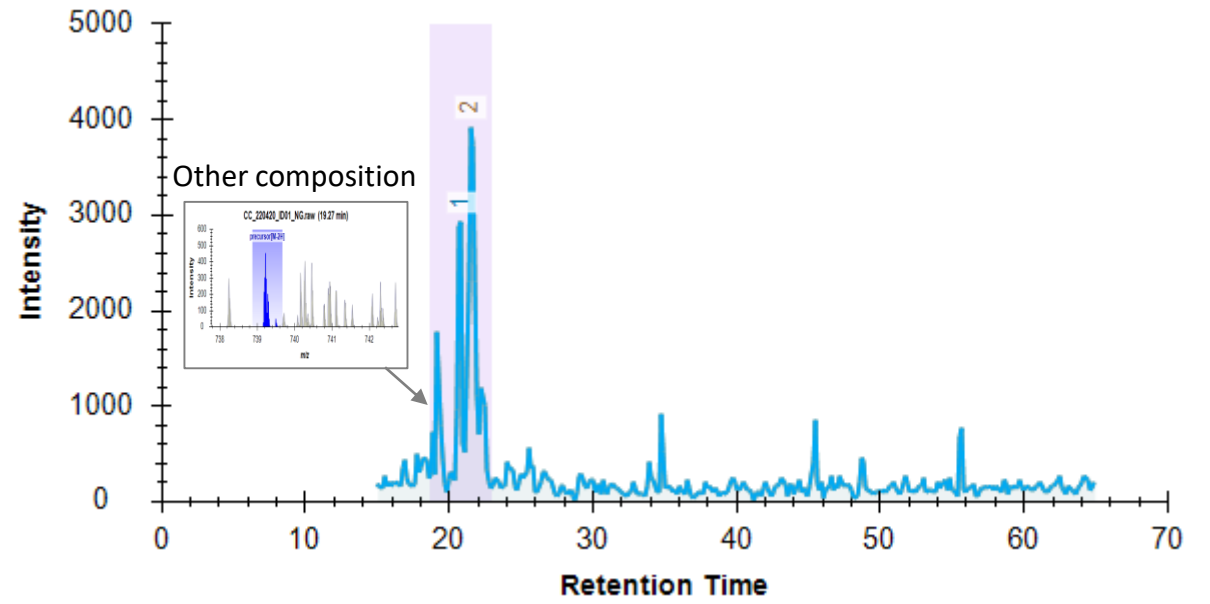
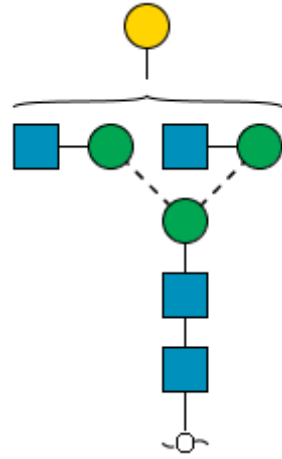
Note: No distinction intended between 3-arm/6-arm in glycan fragment scheme.

Glycan 25

(Hex)1(HexNAc)2 + (Man)3(GlcNAc)2

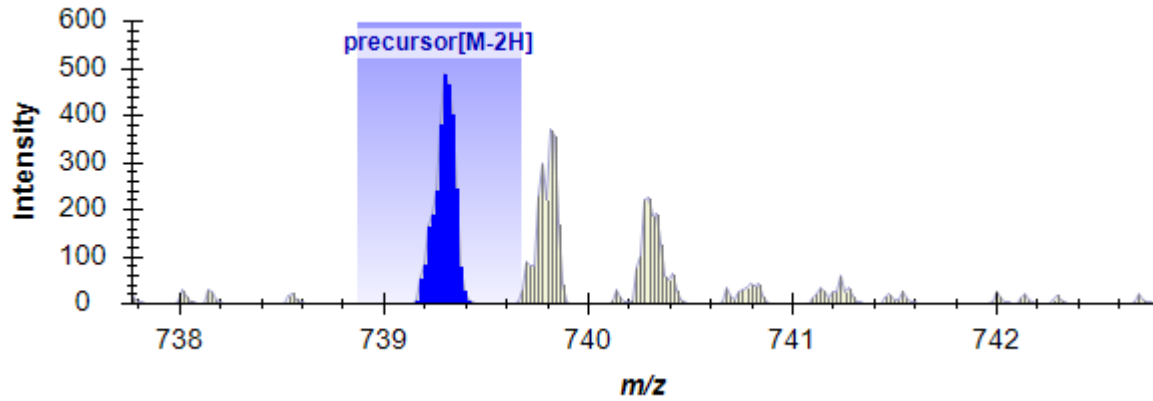
m/z 739.27 (2-)

Theo mass [M-H] = 1479.54 Da



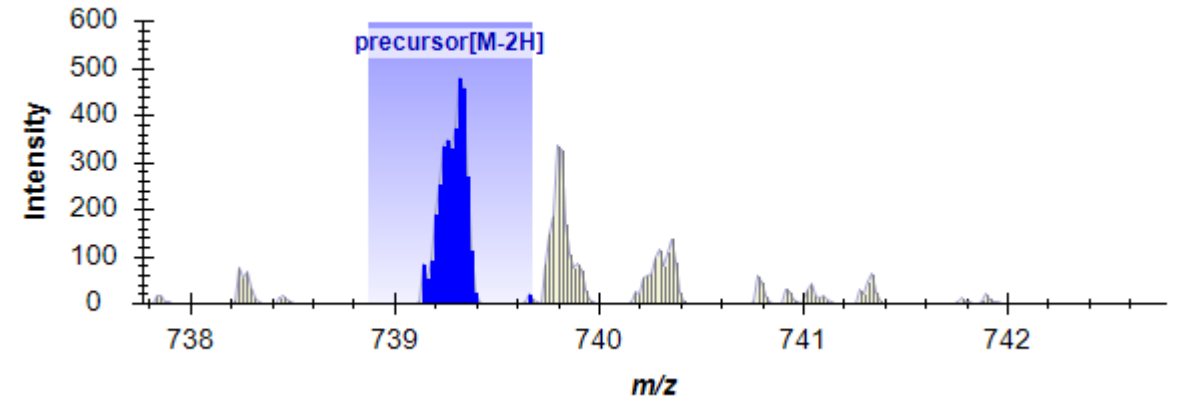
25a

CC_220420_ID01_NG.raw (20.68 min)



25b

CC_220420_ID01_NG.raw (21.75 min)

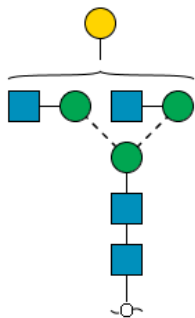


Glycan 25a

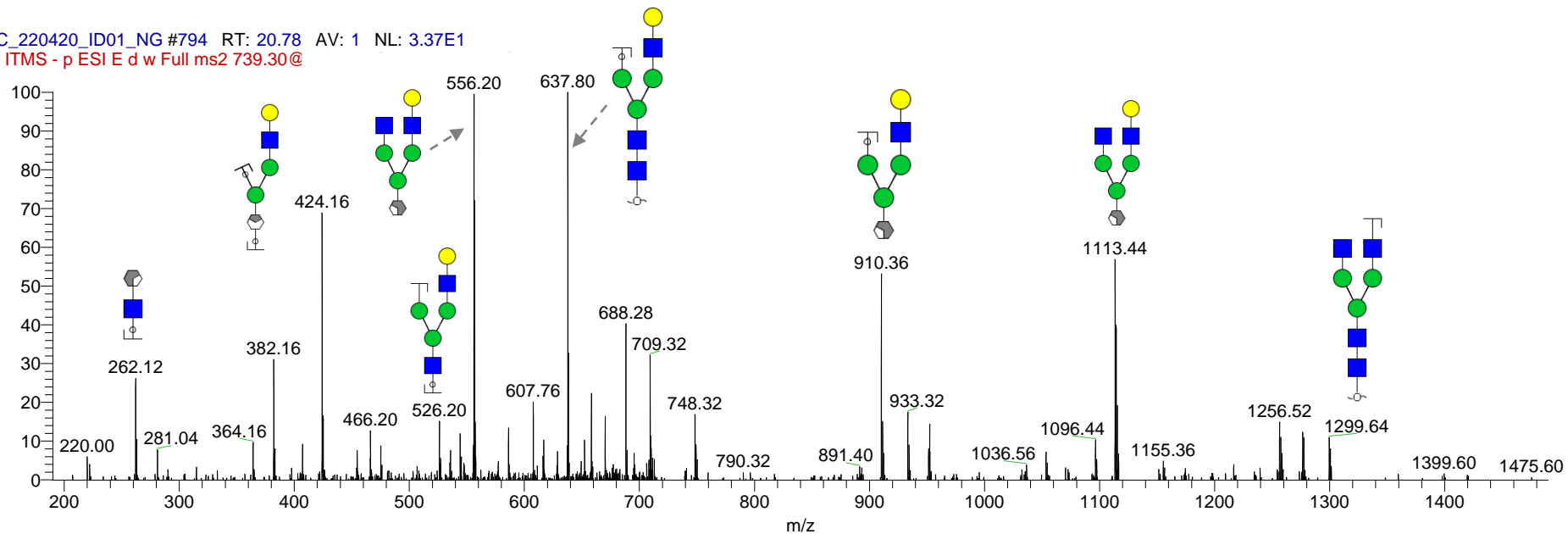
m/z 739.27 (2-)

Retention time: 19.6 min

Theo mass [M-H] = 1479.54 Da



CC_220420_ID01_NG #794 RT: 20.78 AV: 1 NL: 3.37E1
F: ITMS - p ESI E d w Full ms2 739.30@

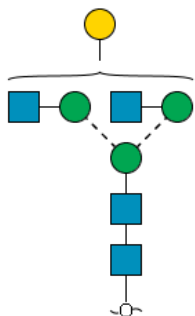


Glycan 25b

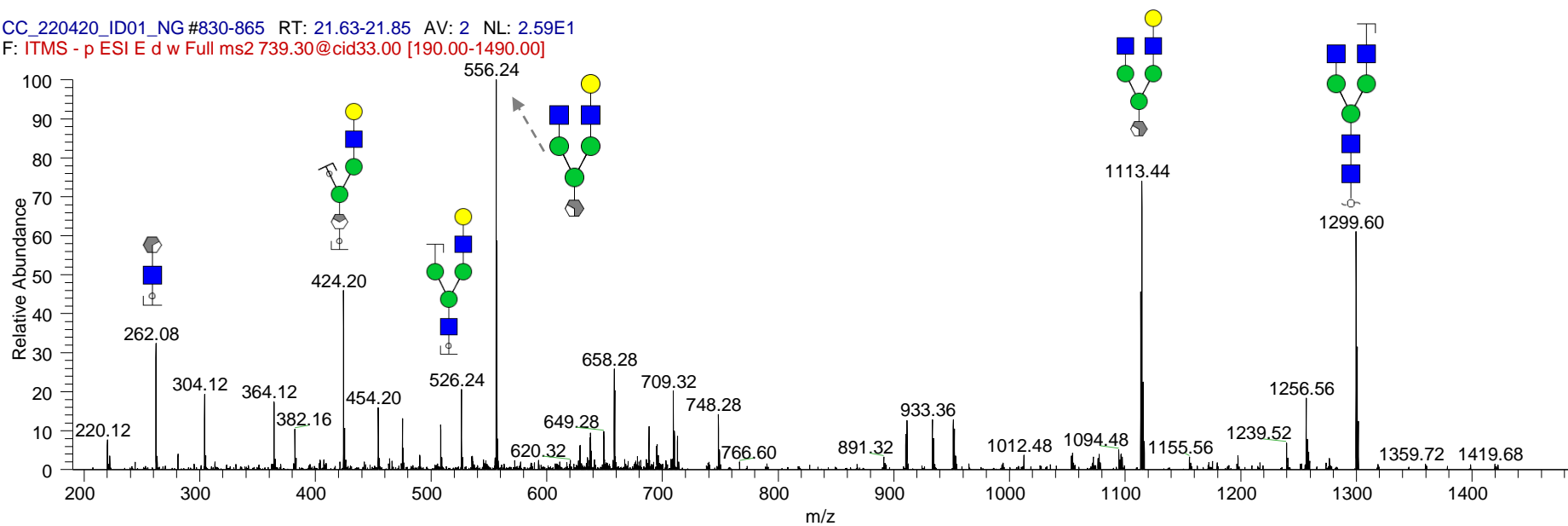
m/z 739.27 (2-)

Retention time: 20.3 min

Theo mass [M-H] = 1479.54 Da



CC_220420_ID01_NG #830-865 RT: 21.63-21.85 AV: 2 NL: 2.59E1
F: ITMS - p ESI E d w Full ms2 739.30@cid33.00 [190.00-1490.00]



Note: No distinction intended between 3-arm/6-arm in glycan fragment scheme.

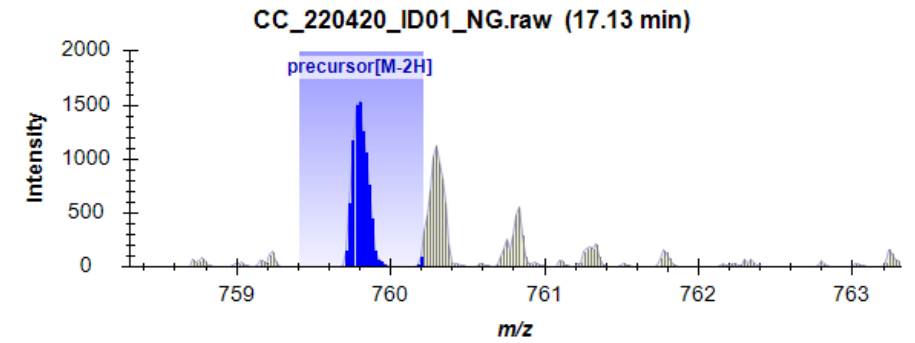
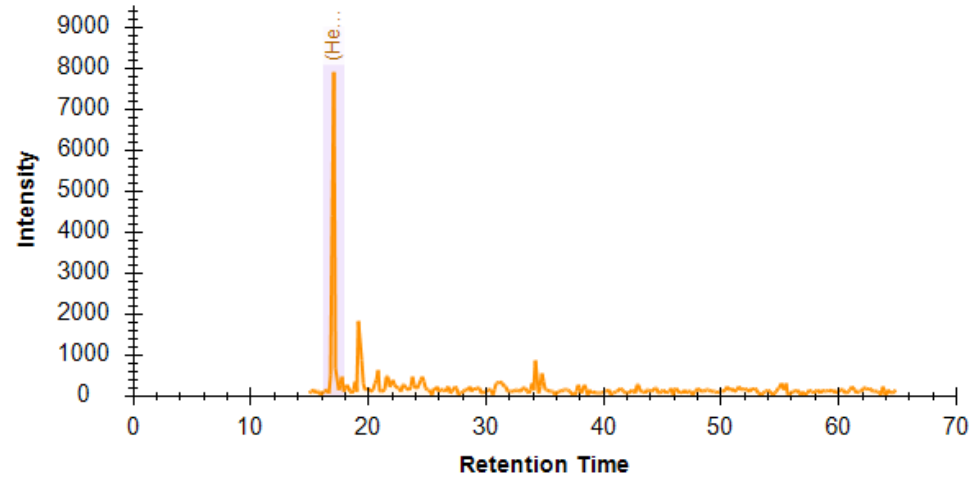
Glycan 26

(HexNAc)₃ + (Man)₃(GlcNAc)₂

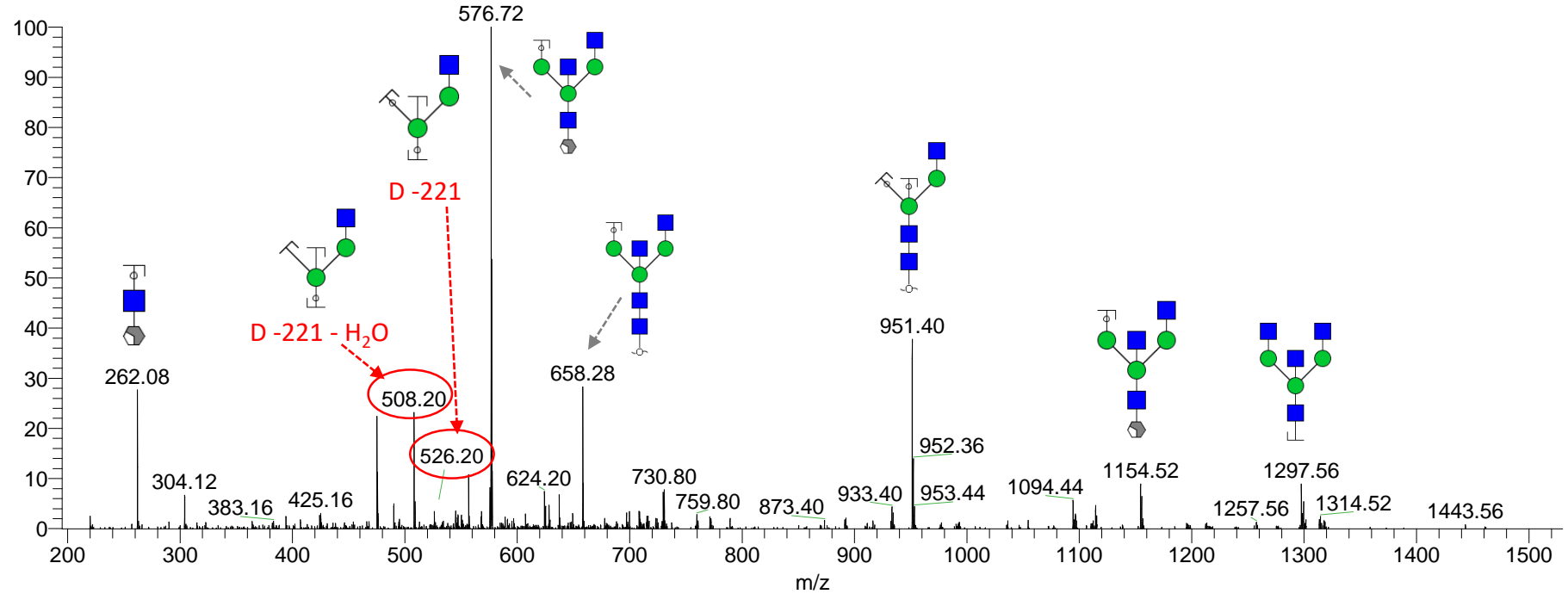
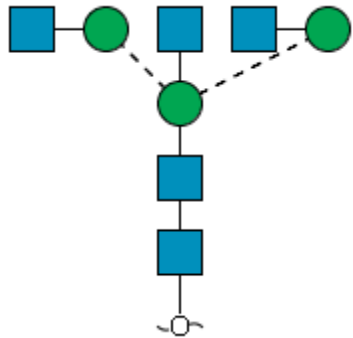
m/z 759.81 (2-)

Retention time: 17.2 min

Theo mass [M-H] = 1520.6 Da



CC_220420_ID01_NG #668 RT: 17.20 AV: 1 NL: 7.56E1
F: ITMS - p ESI E d w Full ms2 759.81@c



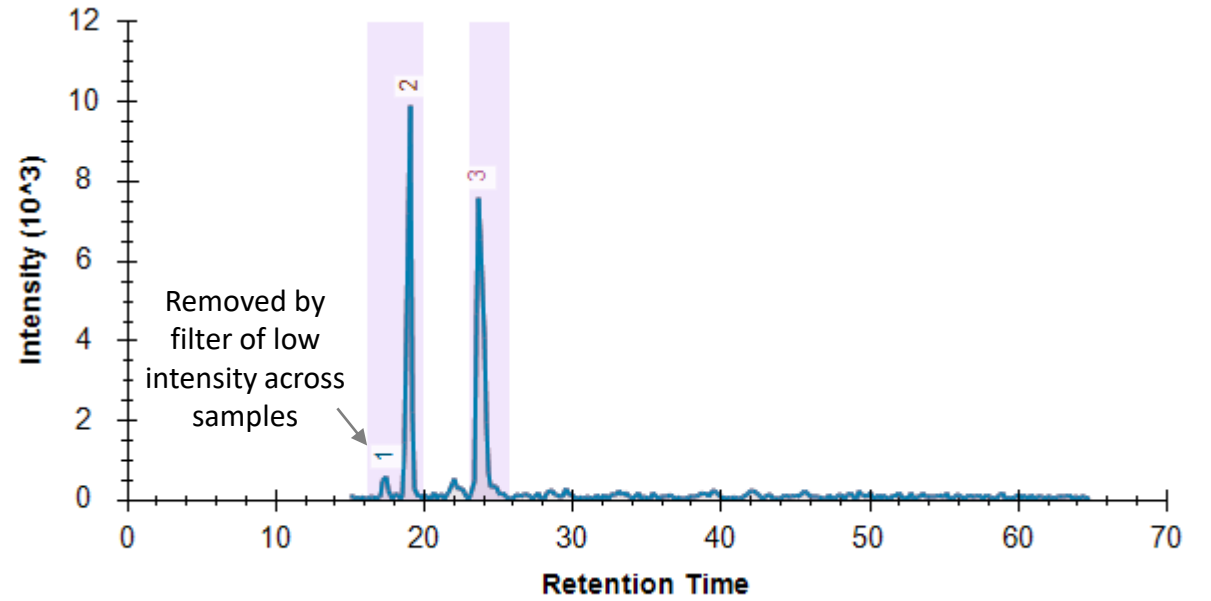
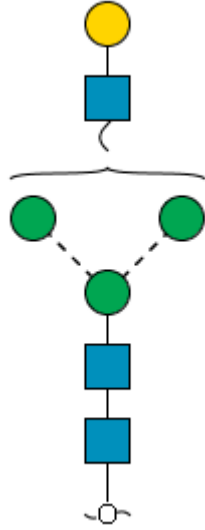
Note: No distinction intended between 3-arm/6-arm in glycan fragment scheme.

Glycan 27

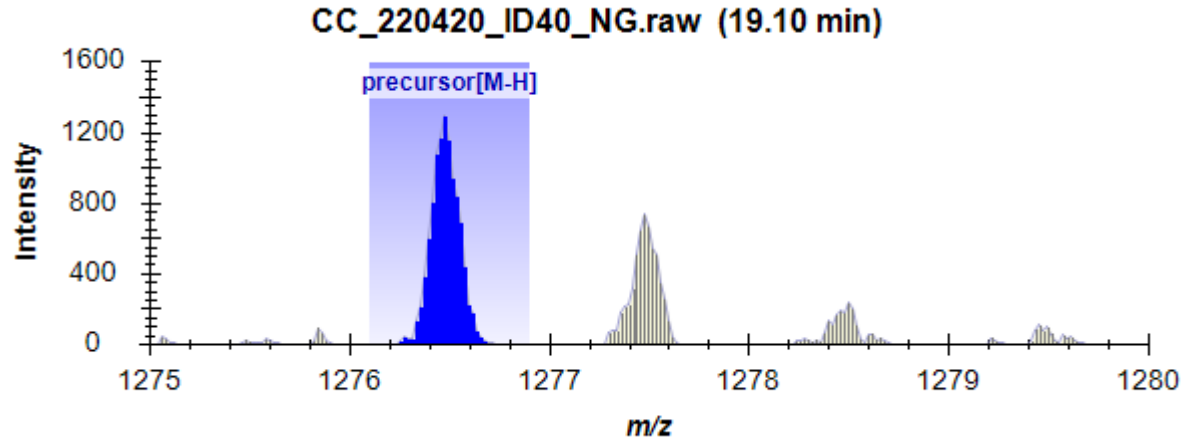
(Hex)1(HexNAc)1 + (Man)3(GlcNAc)2

m/z 1276.50 (1-)

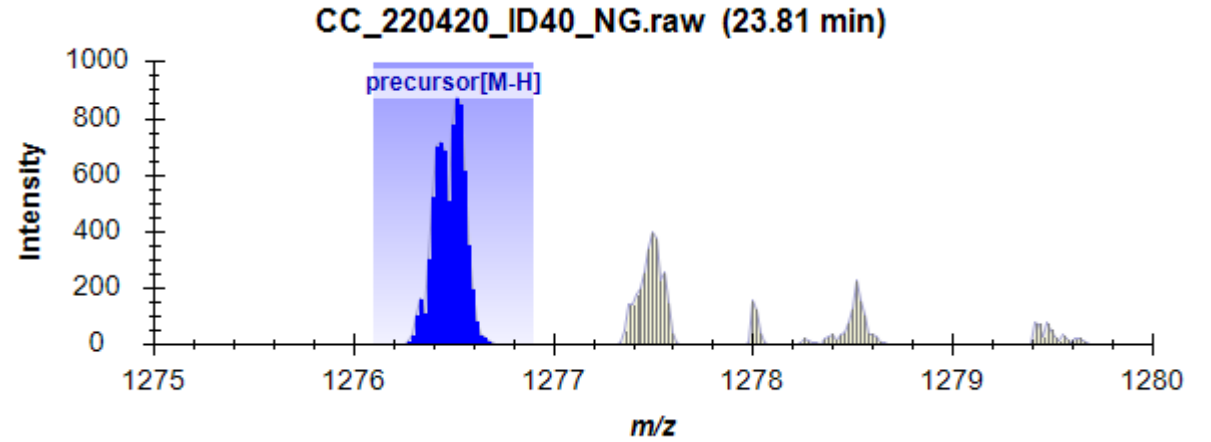
Theo mass [M-H] = 1276.50 Da



27a



27b

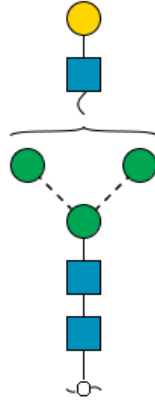


Glycan 27a

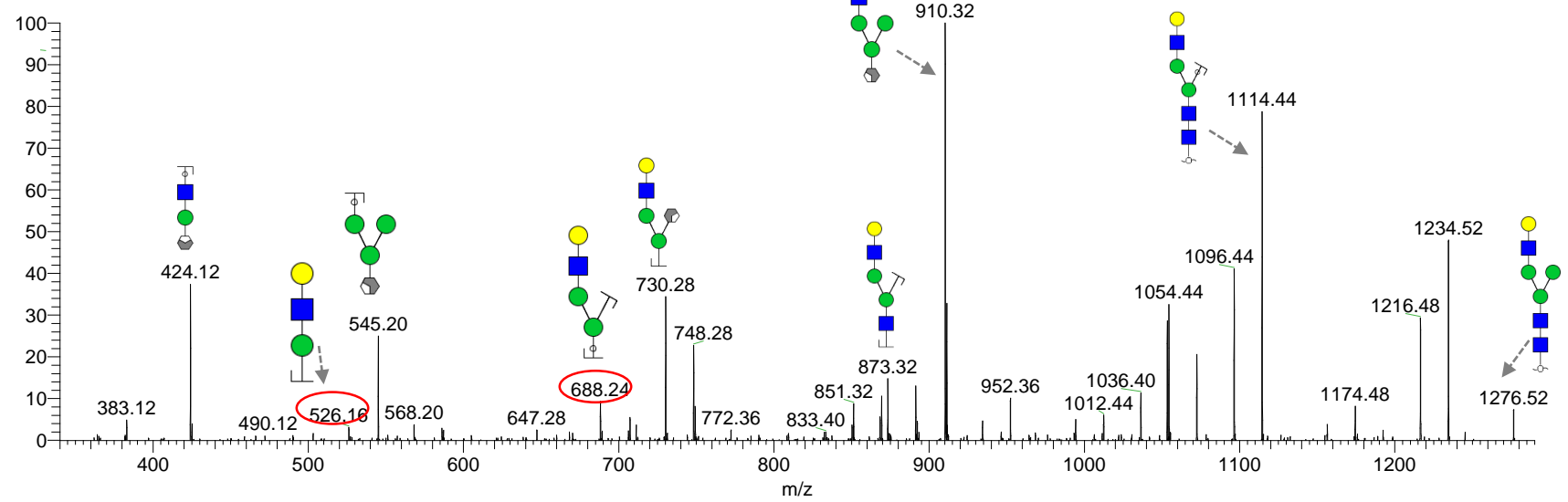
m/z 1276.50 (1-)

Retention time: 19.1 min

Theo mass [M-H] = 1276.50 Da



cc_220420_id40_ng #741-781 RT: 18.96-19.14 AV: 2 NL: 2.96E1
F: ITMS - p ESI E d w Full ms2 1276.48

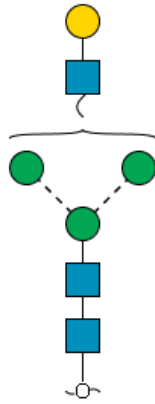


Glycan 27b

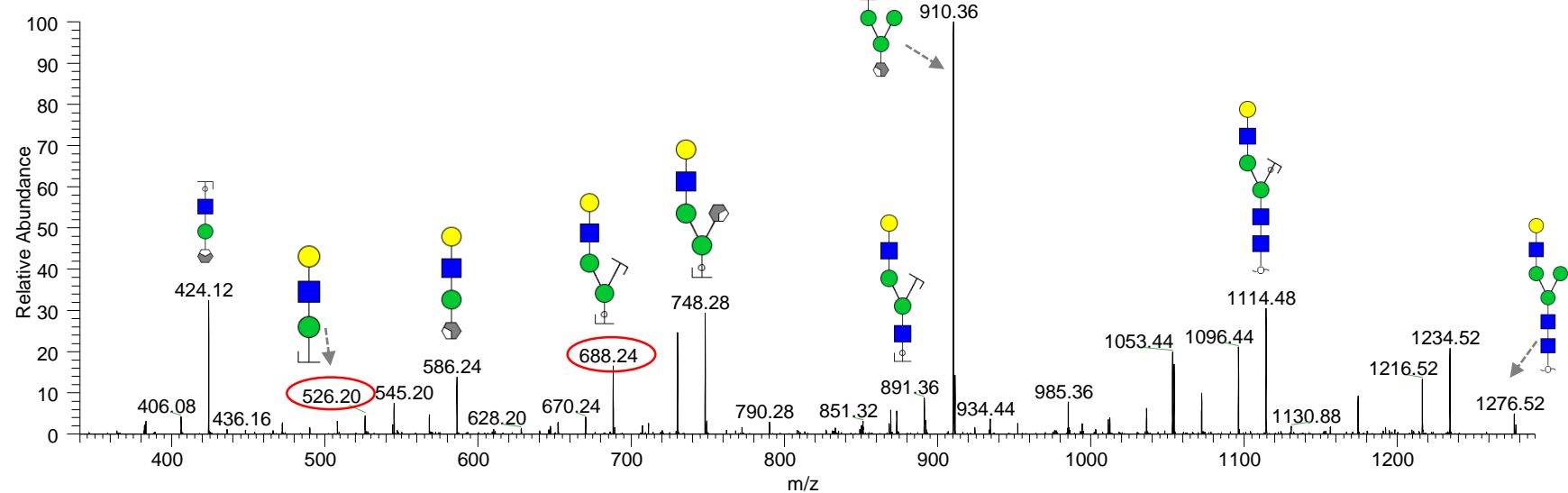
m/z 1276.50 (1-)

Retention time: 23.6 min

Theo mass [M-H] = 1276.50 Da



cc_220420_id40_ng #912-956 RT: 23.68-24.27 AV: 4 NL: 2.32E1
F: ITMS - p ESI E d w Full ms2 1276.48@cid33.00 [340.00-1290.00]



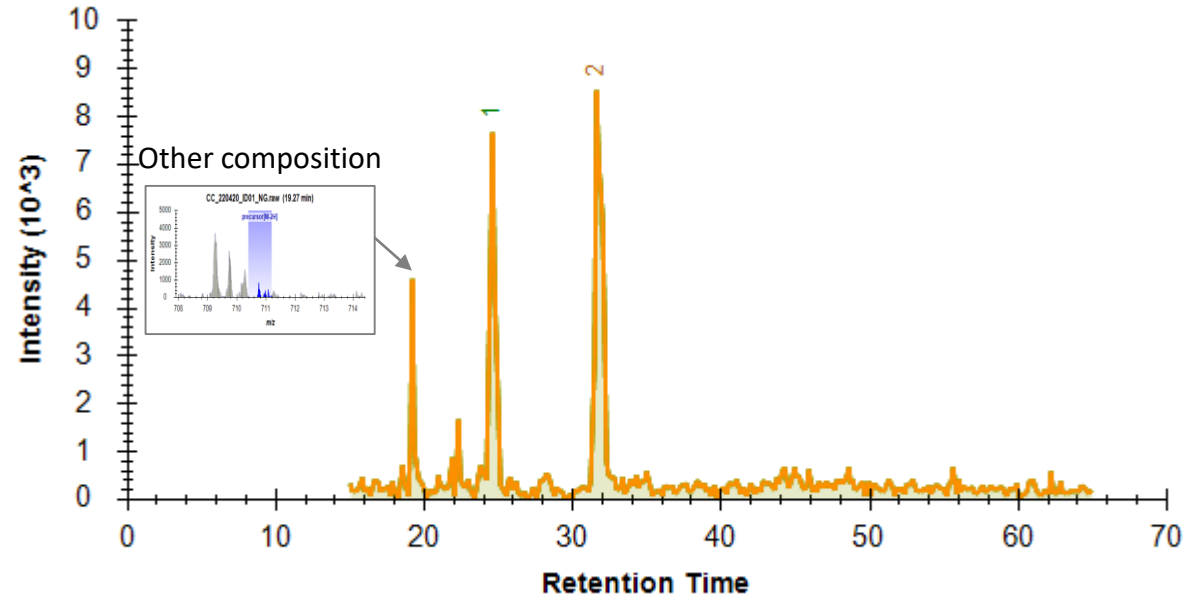
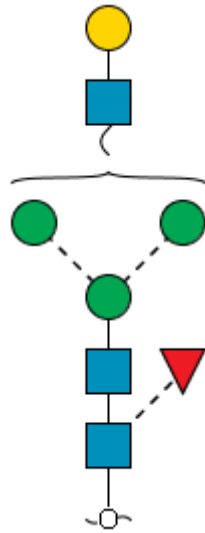
Note: No distinction intended between 3-arm/6-arm in glycan fragment scheme.

Glycan 28

(Hex)1(HexNAc)1(Deoxyhexose)1 + (Man)3(GlcNAc)2

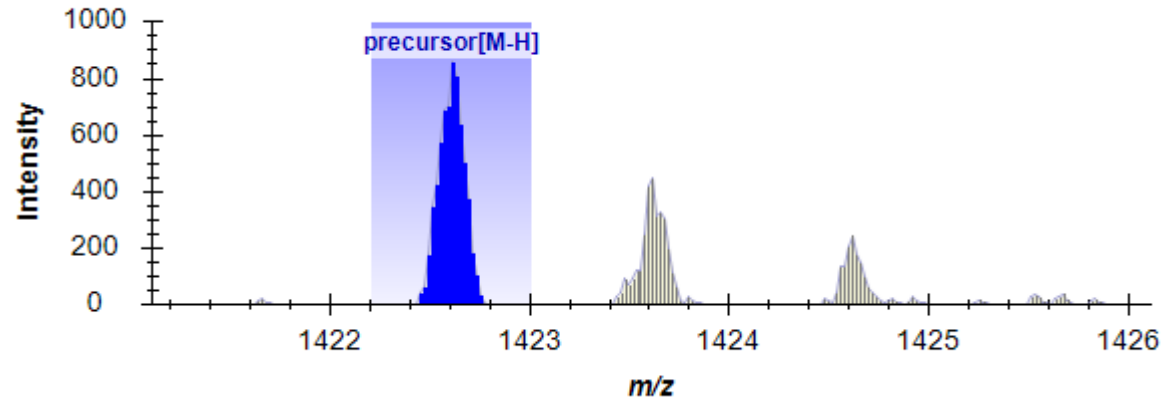
m/z 1422.61 (1-); 710.82 (2-)

Theo mass [M-H] = 1422.61 Da



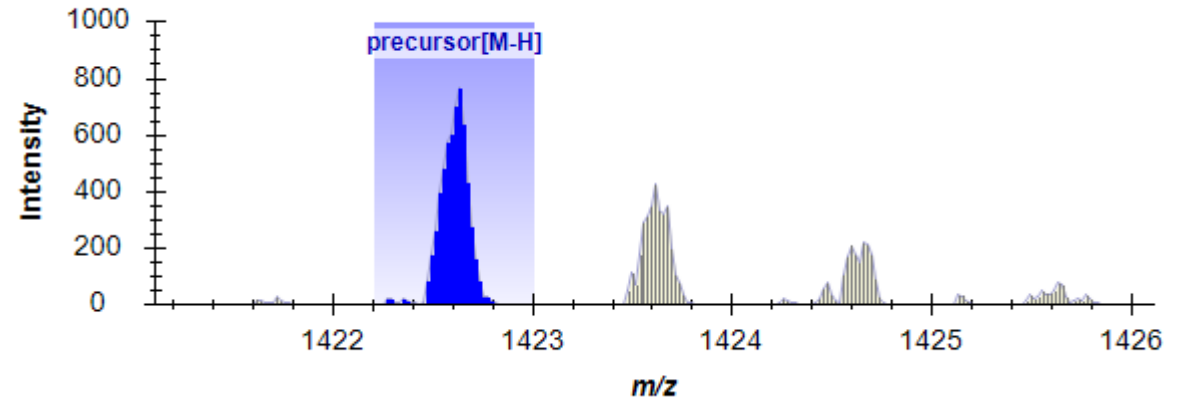
28a

CC_220420_ID01_NG.raw (24.65 min)



28b

CC_220420_ID01_NG.raw (31.66 min)

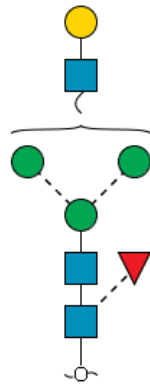


Glycan 28a

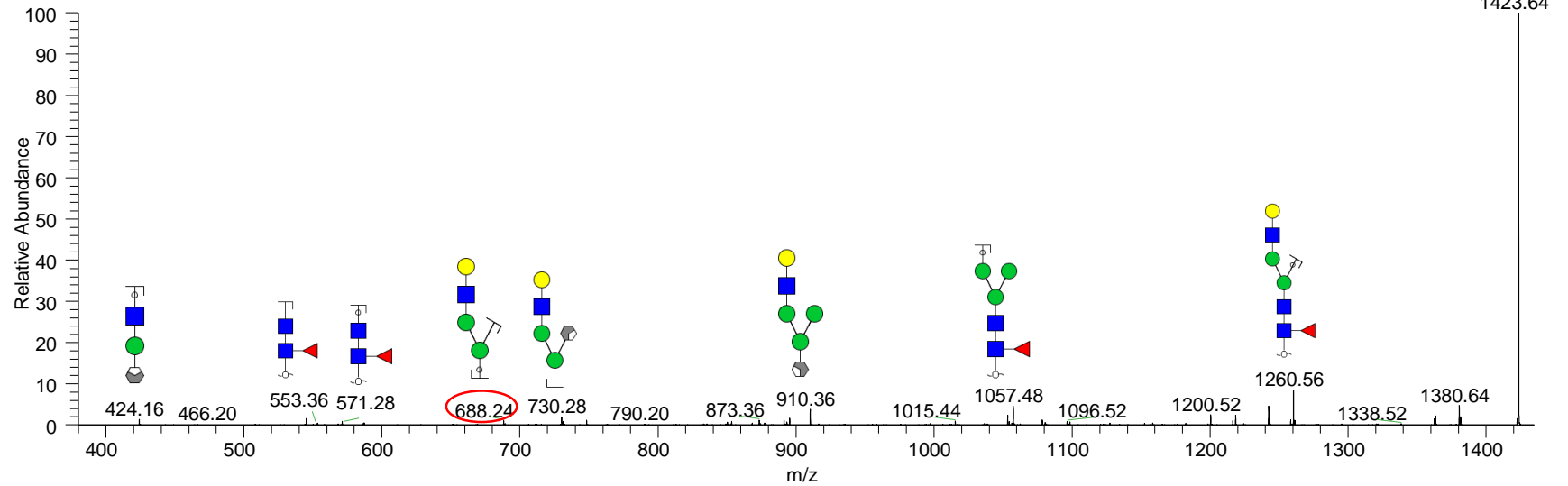
m/z 1422.61 (1-); 710.82 (2-)

Retention time: 24.6 min

Theo mass [M-H] = 1422.61 Da



CC_220420_ID01_NG#918-966 RT: 24.55-24.94 AV: 3 NL: 1.27E2
F: ITMS - p ESI E d w Full ms2 1422.60@cid33.00 [380.00-1435.00]

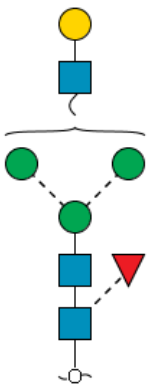


Glycan 28b

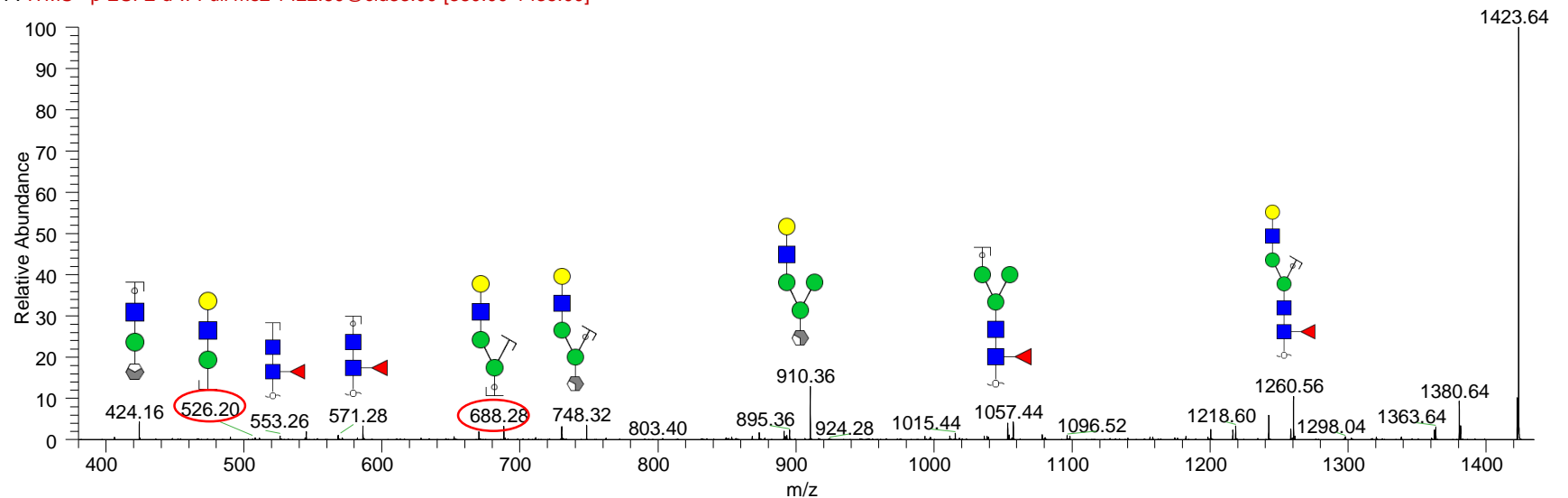
m/z 1422.61 (1-); 710.82 (2-)

Retention time: 31.6 min

Theo mass [M-H] = 1422.61 Da



CC_220420_ID01_NG#1148-1215 RT: 31.64-32.07 AV: 4 NL: 6.95E1
F: ITMS - p ESI E d w Full ms2 1422.60@cid33.00 [380.00-1435.00]



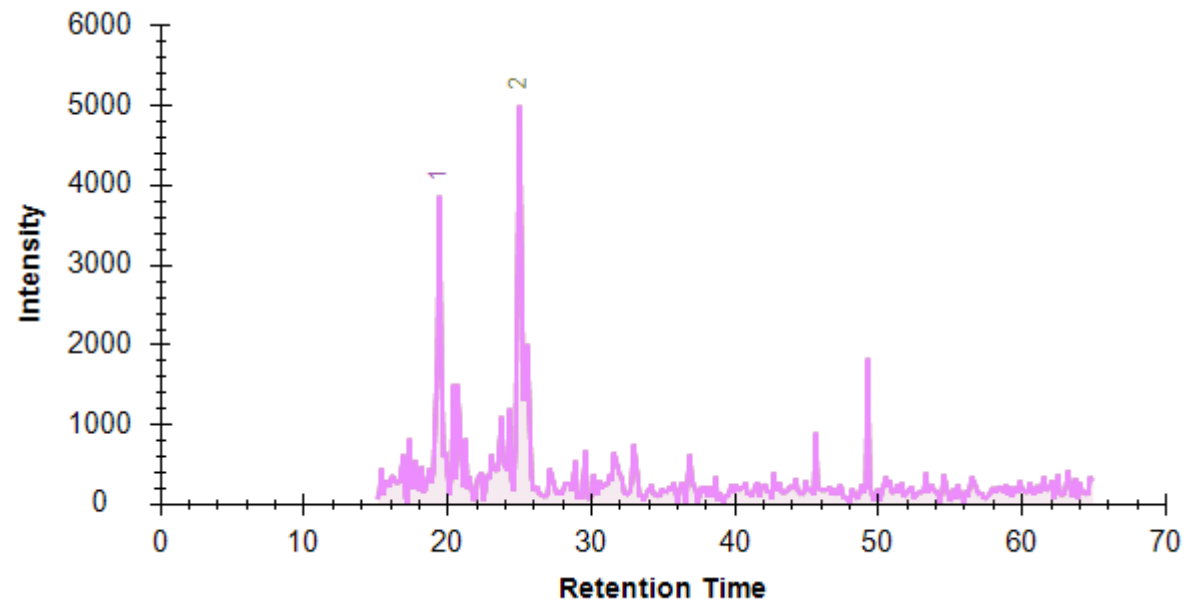
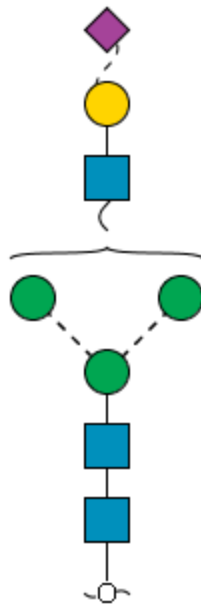
Note: No distinction intended between 3-arm/6-arm in glycan fragment scheme.

Glycan 29

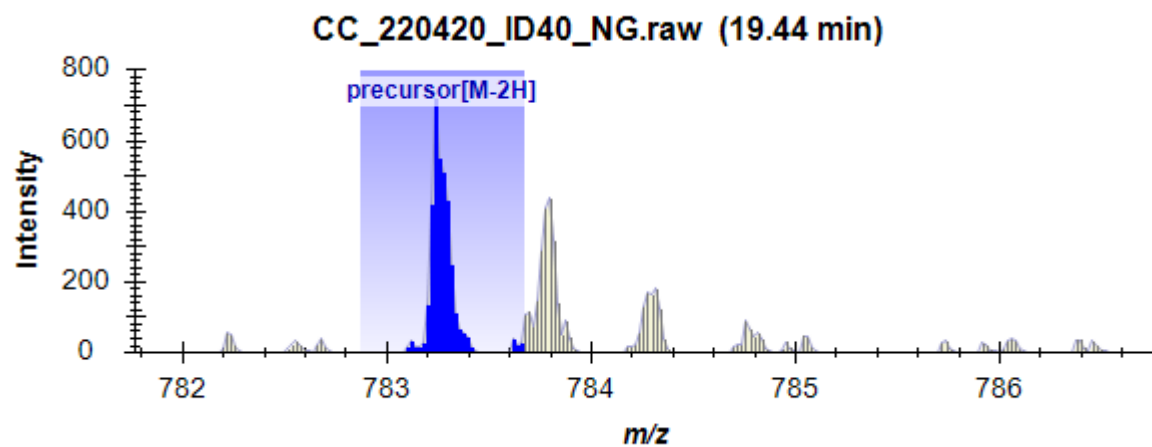
(Hex)1(HexNAc)1(NeuAc)1 + (Man)3(GlcNAc)2

m/z 1567.67 (1-), 783.27 (2-)

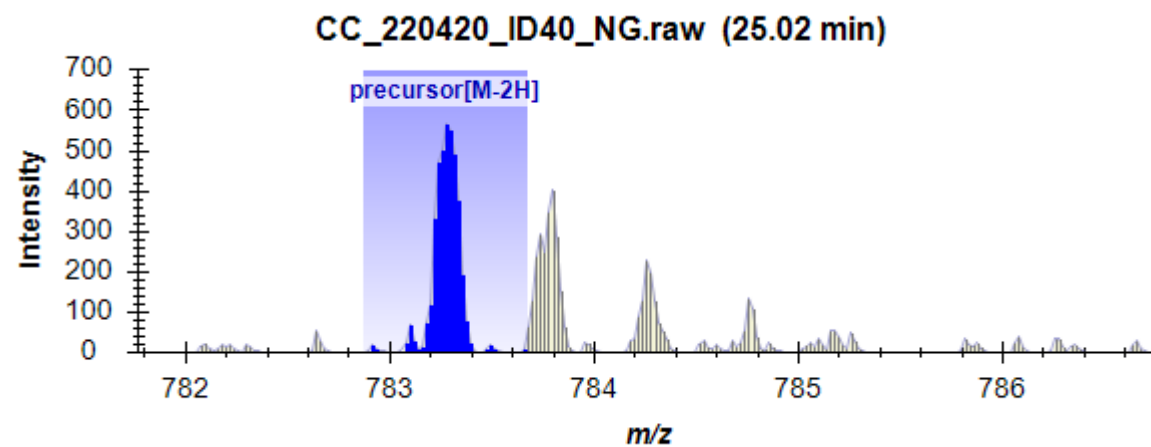
Theo mass [M-H] = 1567.54 Da



29a



29b

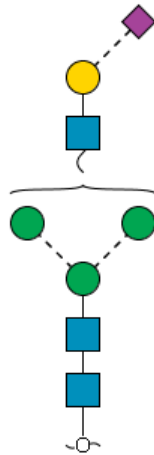


Glycan 29a

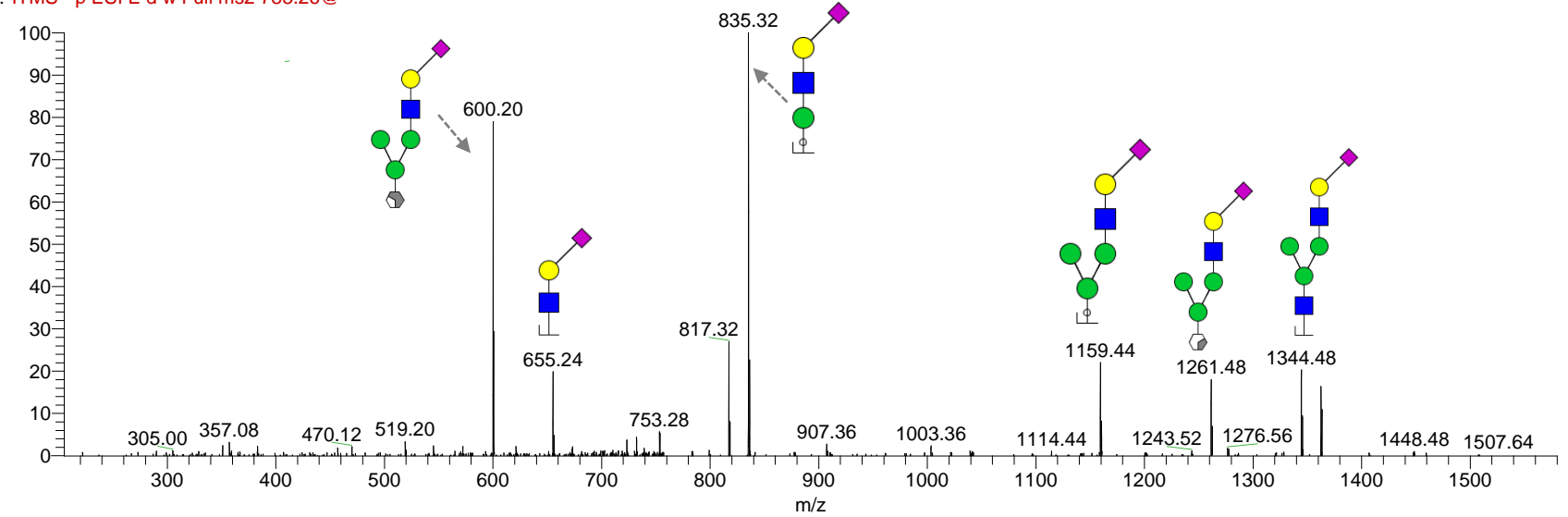
m/z 1567.67 (1-), 783.27 (2-)

Retention time: 19.8 min

Theo mass [M-H] = 1567.54 Da



CC_220420_ID40_NG #757 RT: 19.48 AV: 1 NL: 7.48E1
F: ITMS - p ESI E d w Full ms2 783.26@

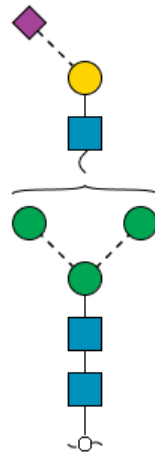


Glycan 29b

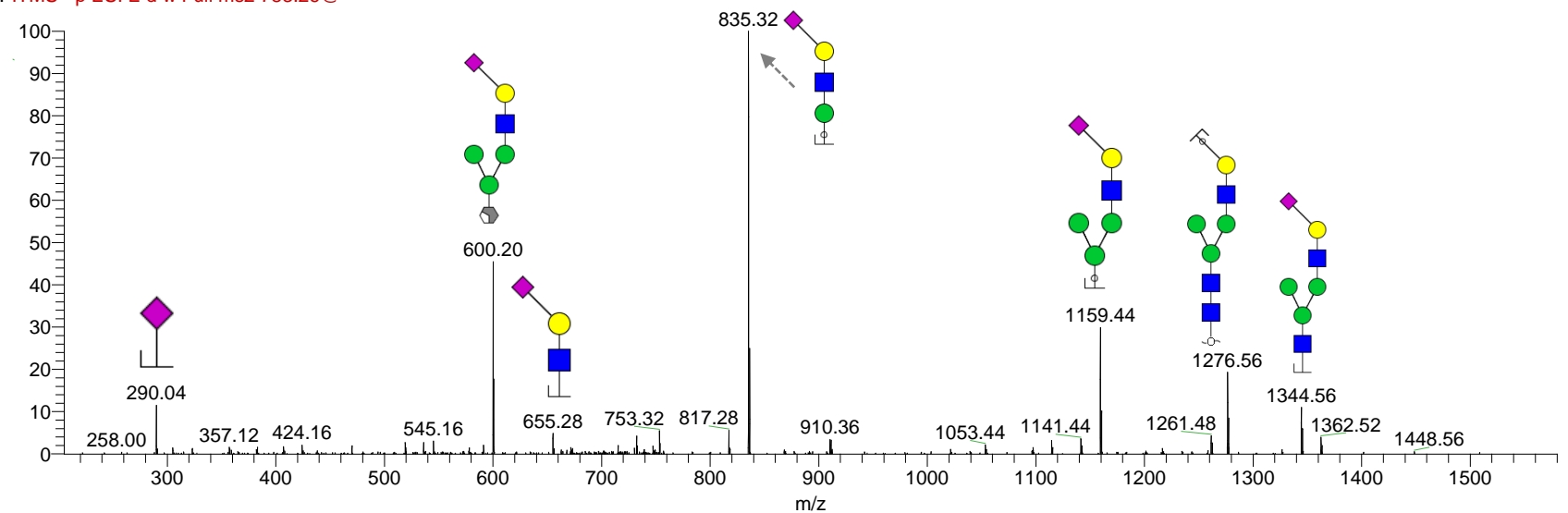
m/z 1567.67 (1-), 783.27 (2-)

Retention time: 25.6 min

Theo mass [M-H] = 1567.54 Da



CC_220420_ID40_NG #952-992 RT: 25.15-25.32 AV: 2 NL: 7.45E1
F: ITMS - p ESI E d w Full ms2 783.26@



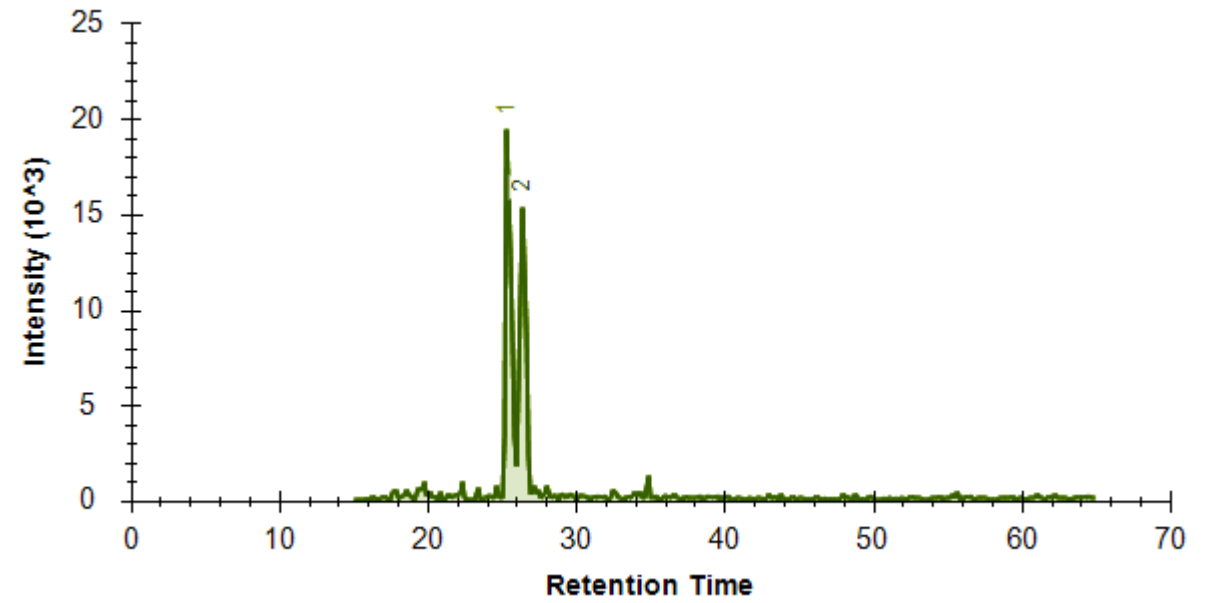
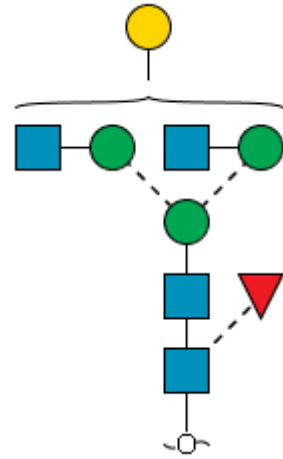
Notes: No distinction intended between 3-arm/6-arm in glycan fragment scheme. This glycan has been annotated as α 2,6 or α 2,3-sialyl isomer based on their elution time.

Glycan 30

(Hex)1(HexNAc)2(Deoxyhexose)1 + (Man)3(GlcNAc)2

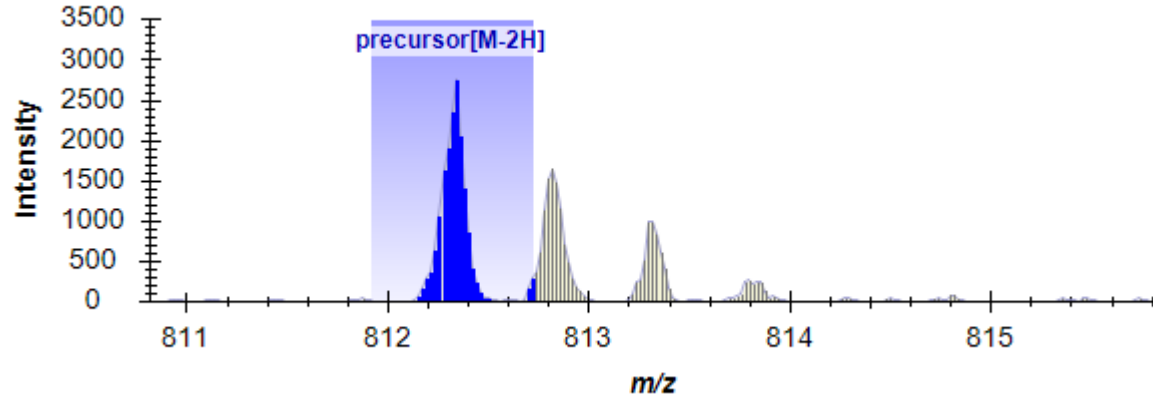
m/z 1625.7 (1-), 812.32 (2-)

Theo mass [M-H] = 1625.64 Da



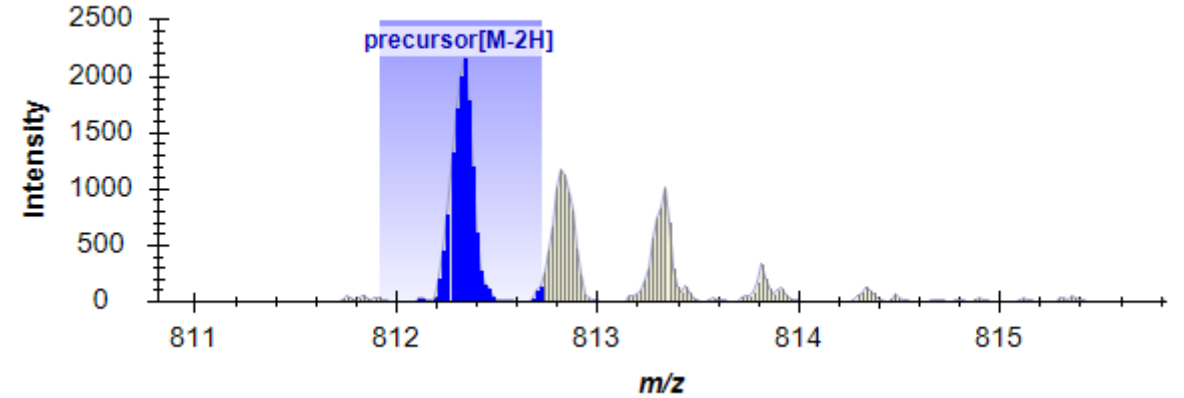
30a

CC_220420_ID01_NG.raw (25.38 min)



30b

CC_220420_ID01_NG.raw (26.42 min)

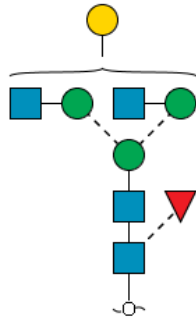


Glycan 30a

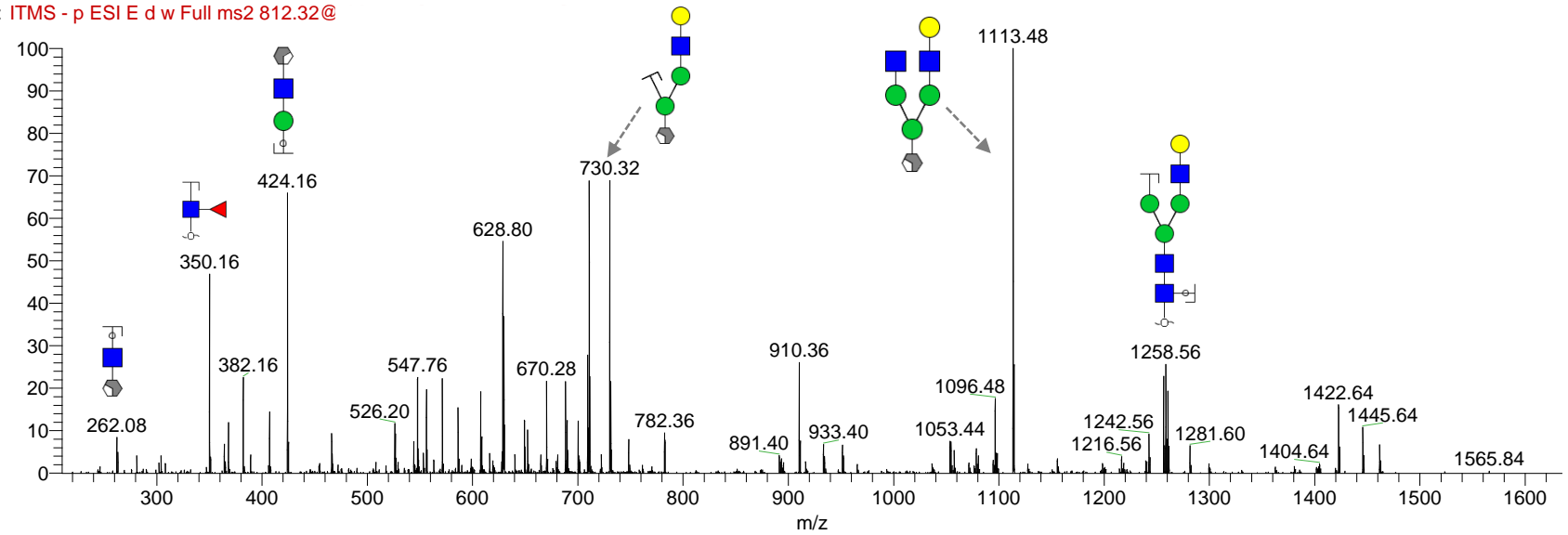
m/z 1625.7 (1-), 812.32 (2-)

Retention time: 25.4 min

Theo mass [M-H] = 1625.64 Da



CC_220420_ID01_NG #959-982 RT: 25.33-25.80 AV: 4 NL: 7.66E1
F: ITMS - p ESI E d w Full ms2 812.32@

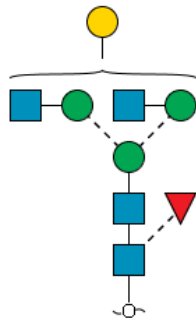


Glycan 30b

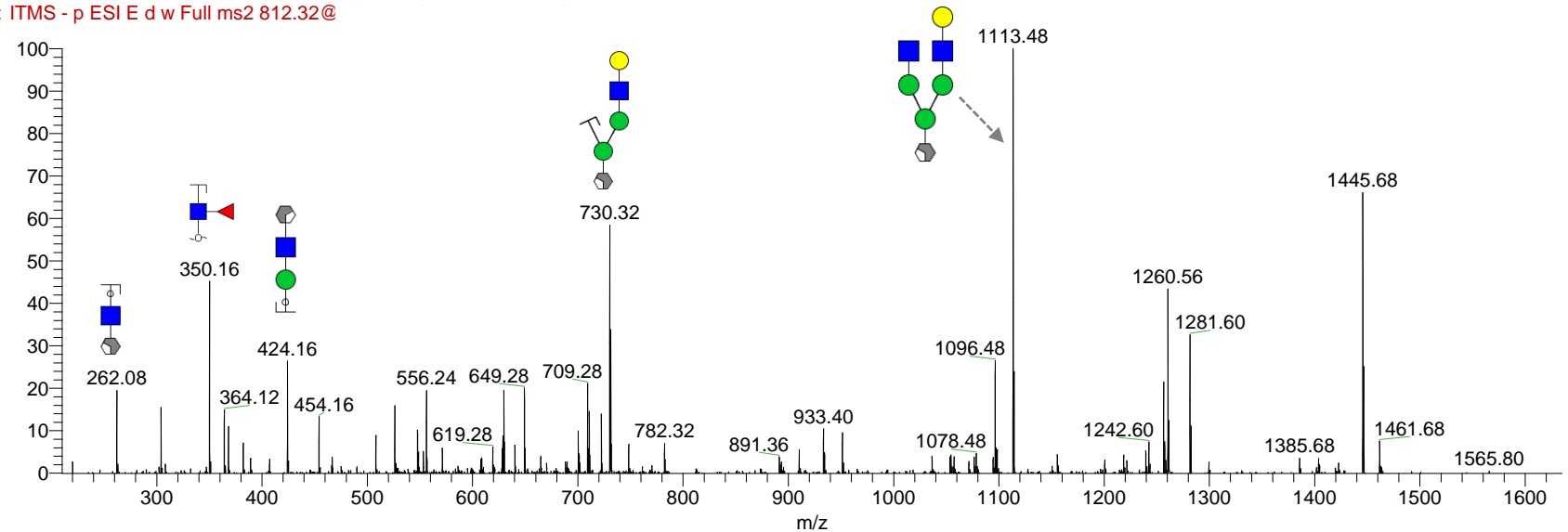
m/z 1625.7 (1-), 812.32 (2-)

Retention time: 26.4 min

Theo mass [M-H] = 1625.64 Da



CC_220420_ID01_NG #992-1020 RT: 26.22-26.72 AV: 4 NL: 6.76E1
F: ITMS - p ESI E d w Full ms2 812.32@



Note: No distinction intended between 3-arm/6-arm in glycan fragment scheme.

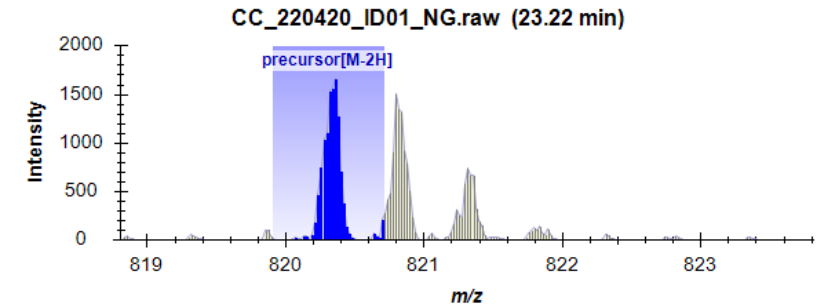
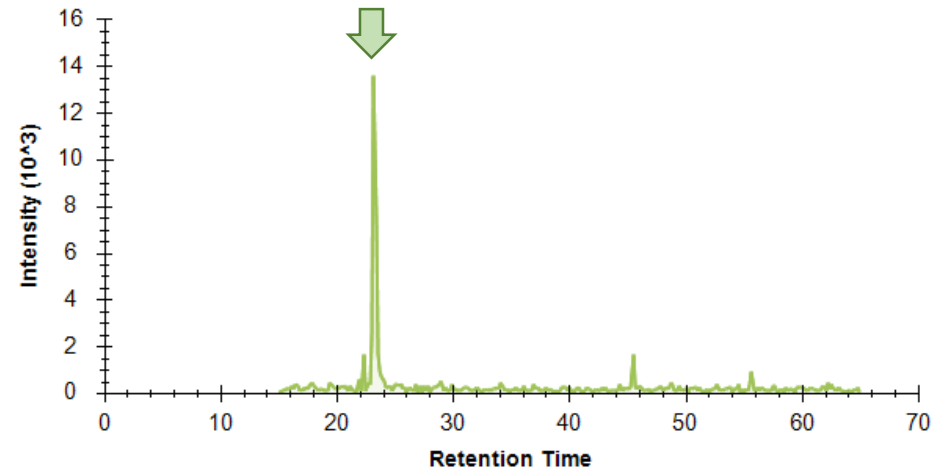
Glycan 31

(Hex)₂(HexNAc)₂ + (Man)₃(GlcNAc)₂

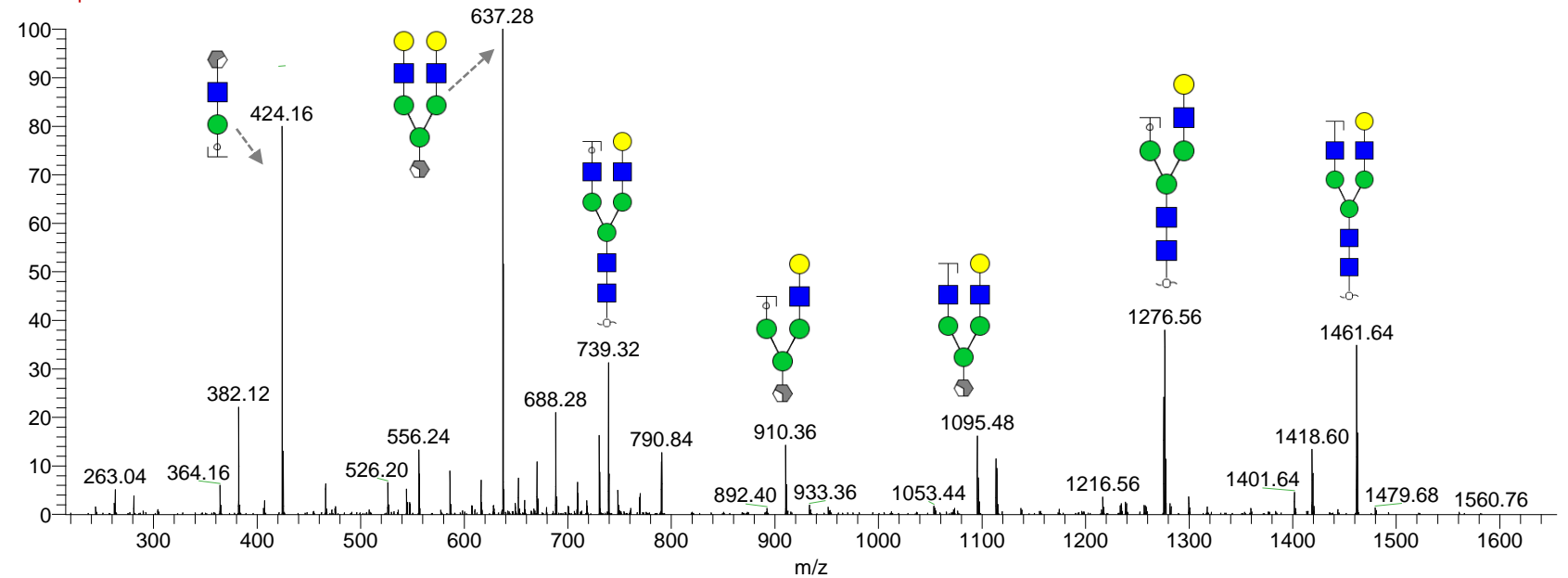
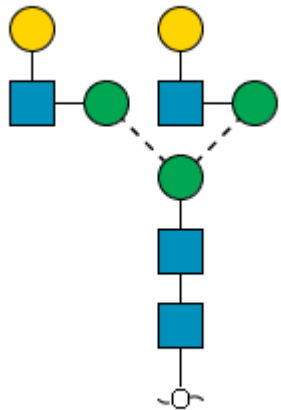
m/z 1641.71 (-1), 820.31 (2-)

Retention time: 21.8 min

Theo mass [M-H] = 1641.62 Da



CC_220420_ID01_NG #869 RT: 23.32 AV: 1 NL: 1.32E2
F: ITMS - p ESI E d w Full ms2 820.33@ci



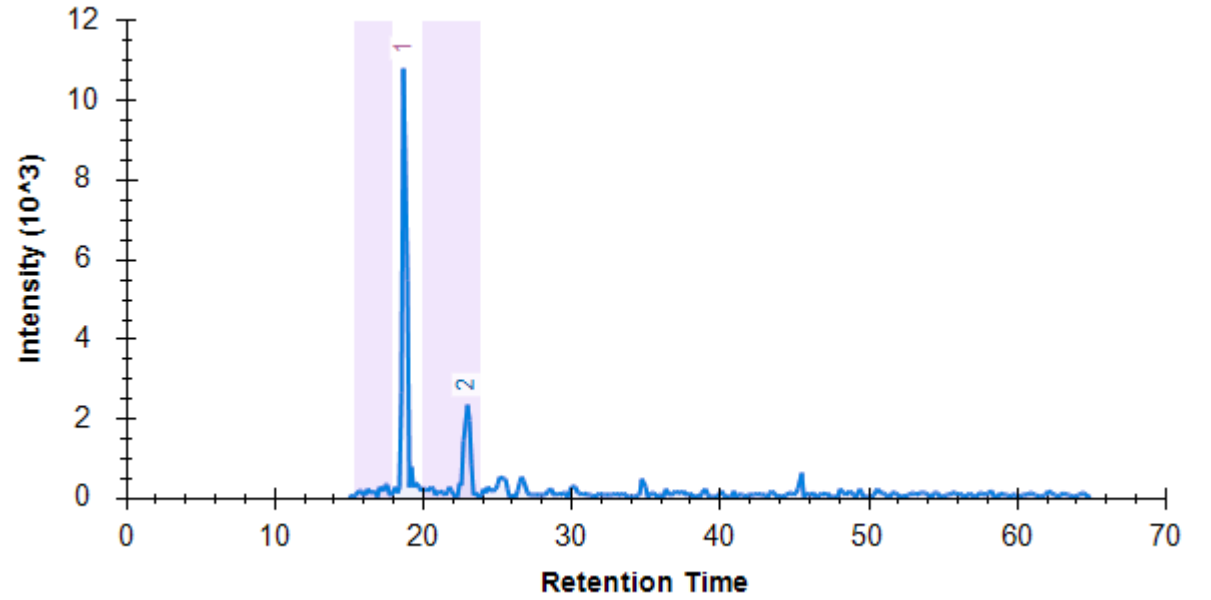
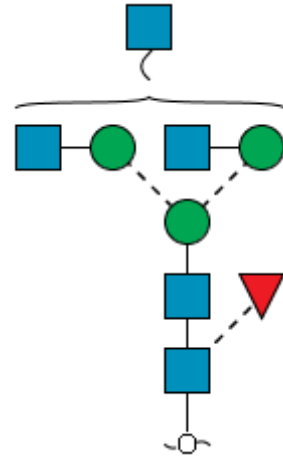
Note: No distinction intended between 3-arm/6-arm in glycan fragment scheme.

Glycan 32

(HexNAc)₃(Deoxyhexose)₁ + (Man)₃(GlcNAc)₂

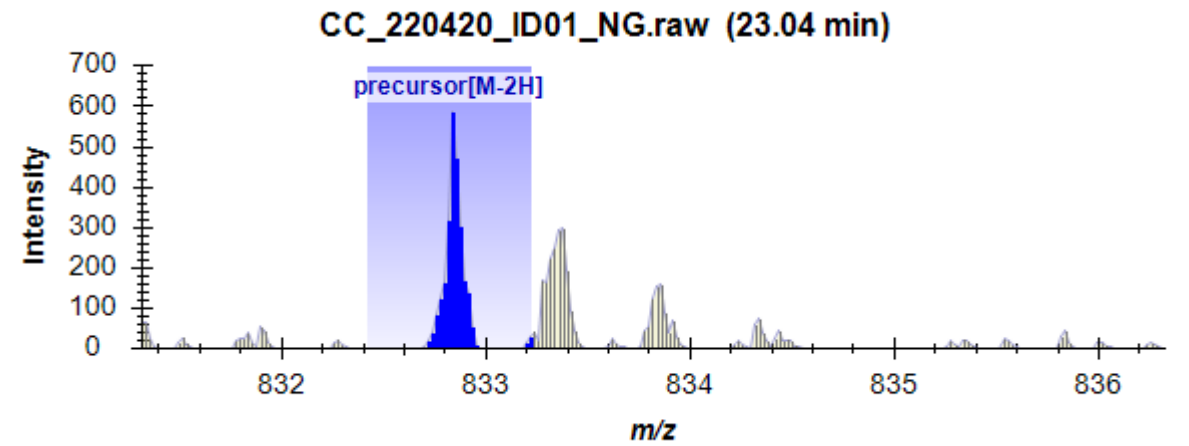
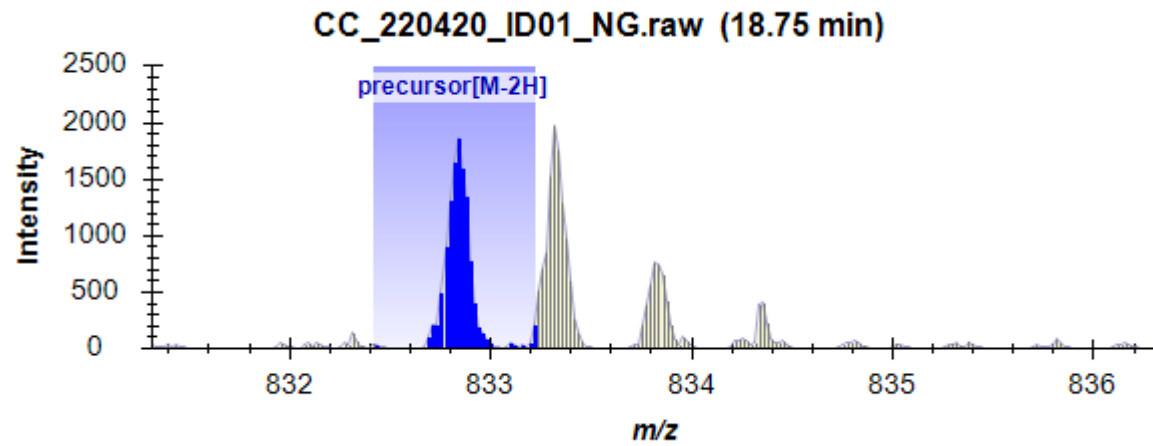
m/z 832.82 (2-)

Theo mass [M-H] = 1666.64 Da



32a

32b

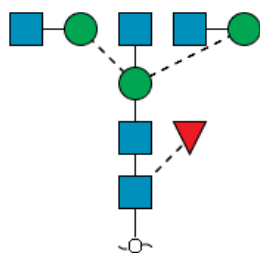


Glycan 32a

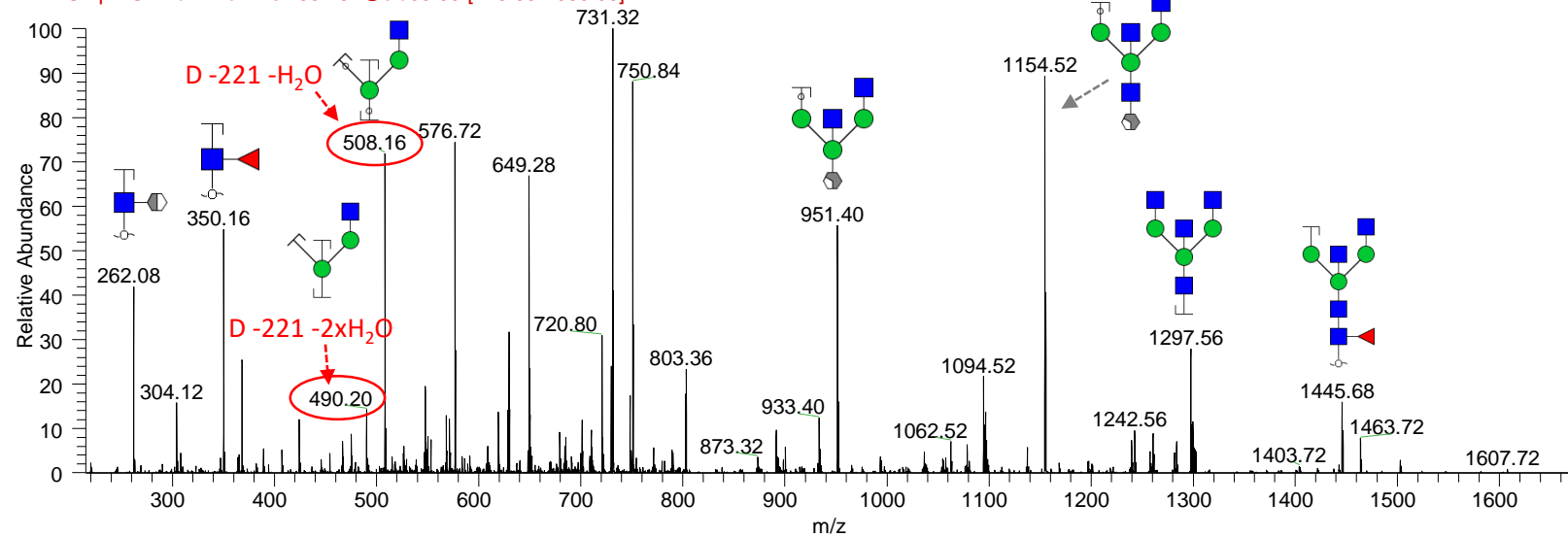
m/z 832.82 (2-)

Retention time: 17.9 min

Theo mass [M-H] = 1666.64 Da



CC_220420_ID01_NG#733 RT: 18.82 AV: 1 NL: 7.71E1
F: ITMS - p ESI E d w Full ms2 832.84@cid33.00 [215.00-1680.00]

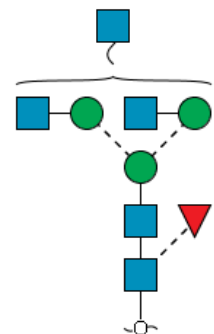


Glycan 32b

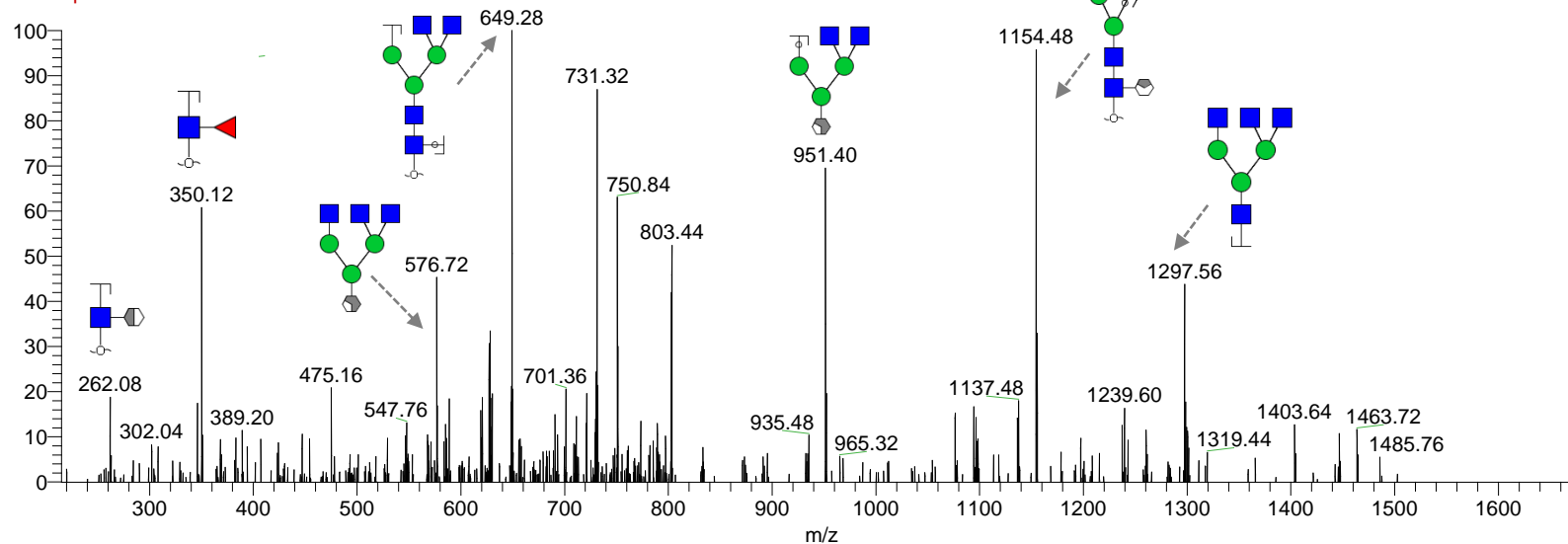
m/z 832.82 (2-)

Retention time: 23.7 min

Theo mass [M-H] = 1666.64 Da



cc_220420_id21_ng #893 RT: 23.78 AV: 1 NL: 1.05E1
F: ITMS - p ESI E d w Full ms2 832.84@



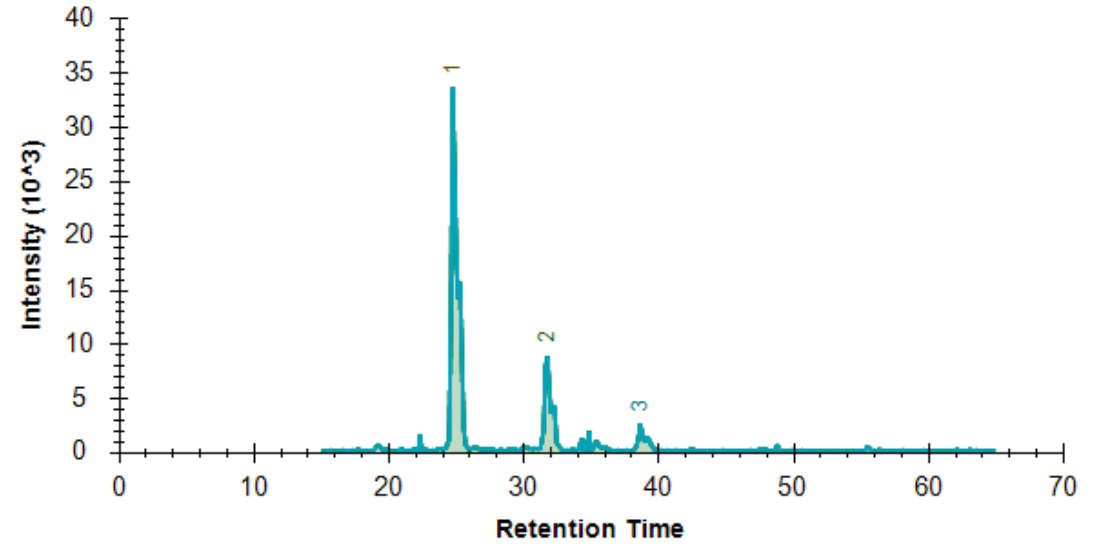
Note: No distinction intended between 3-arm/6-arm in glycan fragment scheme.

Glycan 33

(Hex)1(HexNAc)1(Deoxyhexose)1(NeuAc)1 + (Man)3(GlcNAc)2

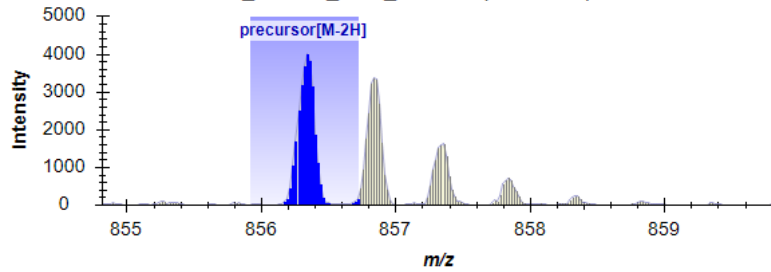
m/z 1713.73 (1-), 856.32 (2-)

Theo mass [M-H] = 1713.64 Da



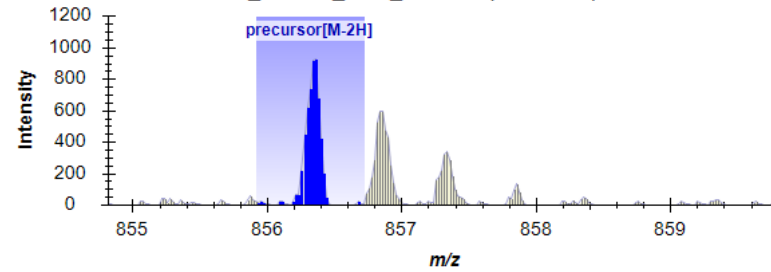
33a

CC_220420_ID01_NG.raw (24.84 min)



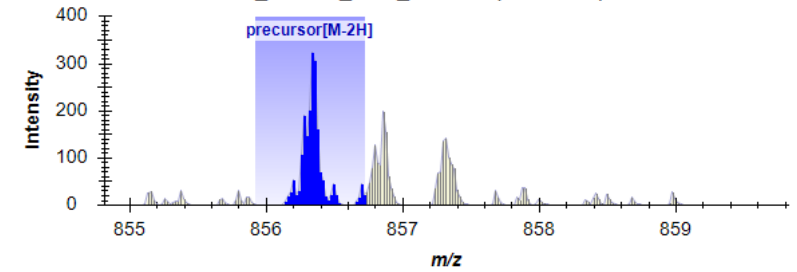
33b

CC_220420_ID01_NG.raw (31.66 min)



33c

CC_220420_ID01_NG.raw (38.72 min)

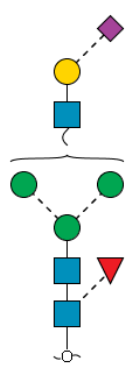


Glycan 33a

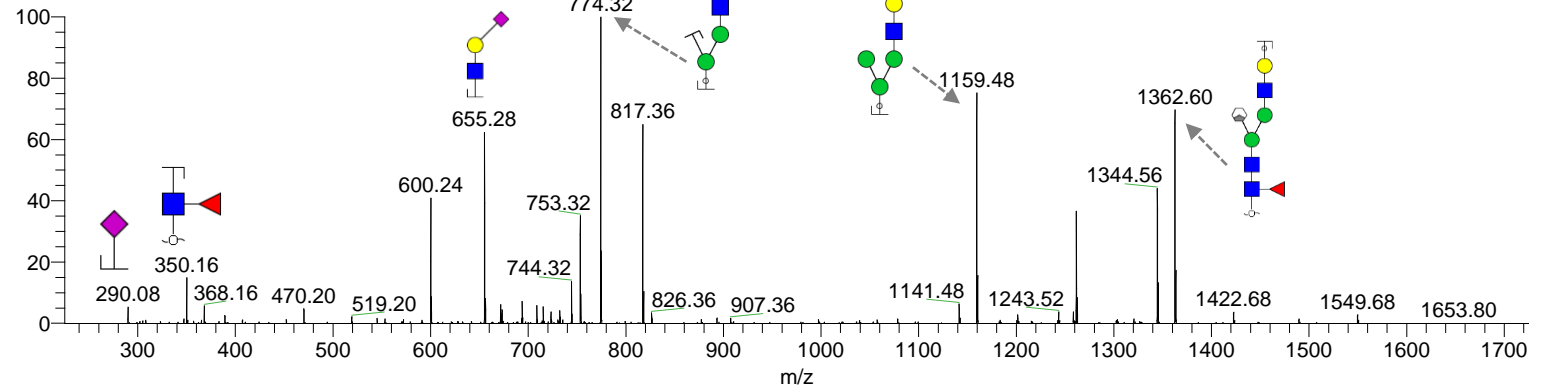
m/z 1713.73 (1-), 856.32 (2-)

Retention time: 24.9 min

Theo mass [M-H] = 1713.64 Da



CC_220420_ID01_NG #933-989 RT: 24.69-25.45 AV: 5 NL: 2.13E2
F: ITMS - p ESI E d w Full ms2 ξ [25.00]

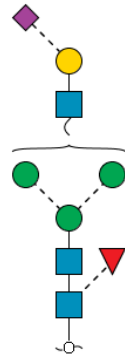


Glycan 33b

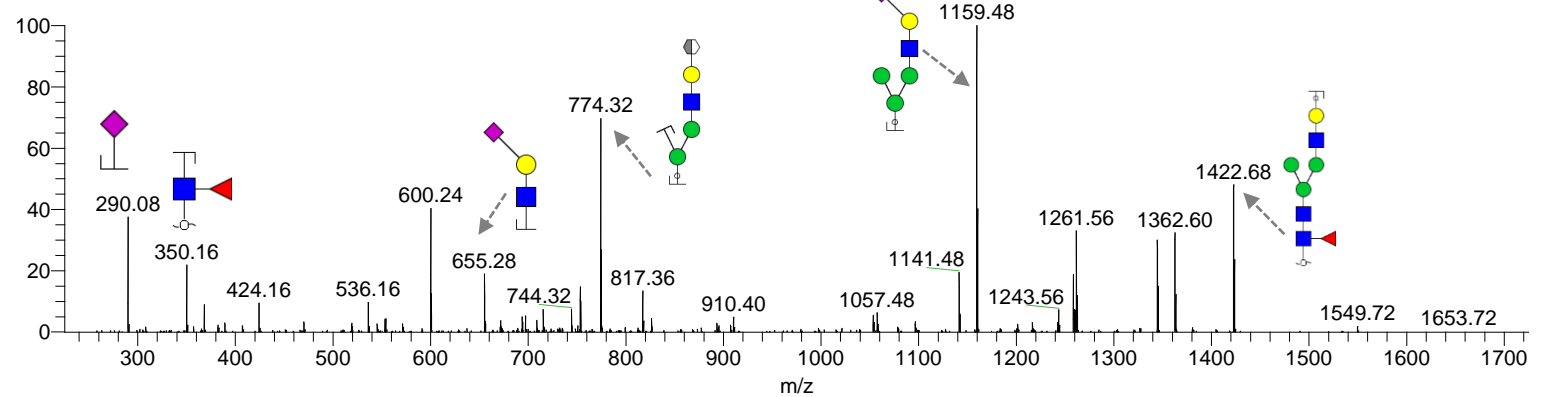
m/z 1713.73 (1-), 856.32 (2-)

Retention time: 31,7 min

Theo mass [M-H] = 1713.64 Da



CC_220420_ID01_NG #1150-1233 RT: 31.78-32.48 AV: 5 NL: 5.48E1
F: ITMS - p ESI E d w Full ms2 ξ [25.00]

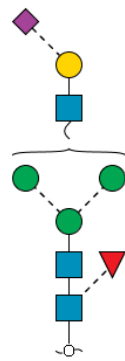


Glycan 33c

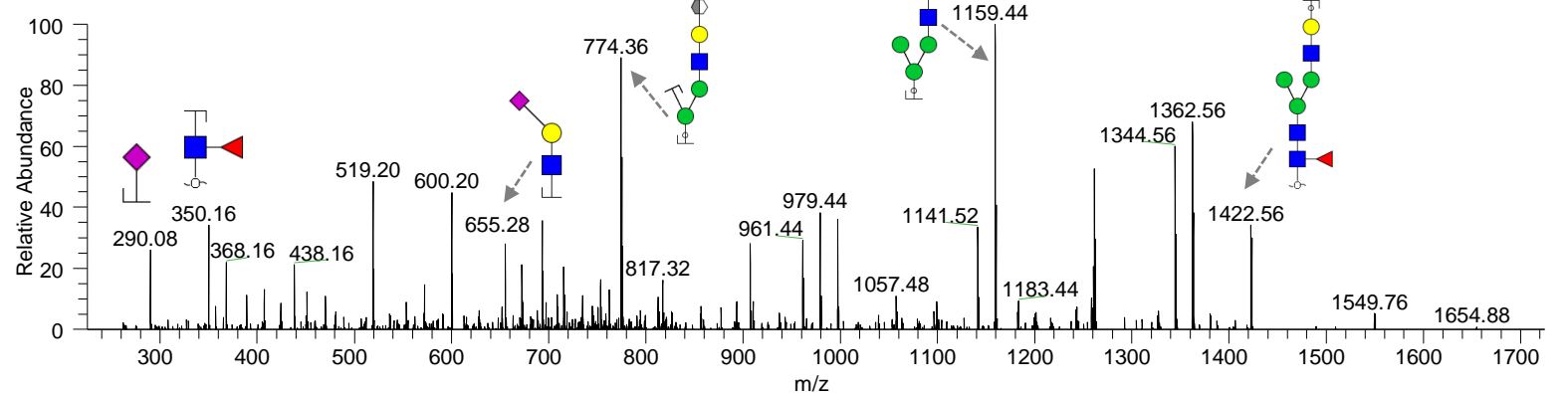
m/z 1713.73 (1-), 856.32 (2-)

Retention time: 38,7 min

Theo mass [M-H] = 1713.64 Da



CC_220420_ID01_NG #1396-1457 RT: 38.81-39.33 AV: 2 NL: 1.11E1
F: ITMS - p ESI E d w Full ms2 856.32@cid33.00 [225.00-1725.00]



Notes: No distinction intended between 3-arm/6-arm in glycan fragment scheme. This glycan has been annotated as α2,6 or α2,3-sialyl isomer based on their elution time and 655/290 ions.

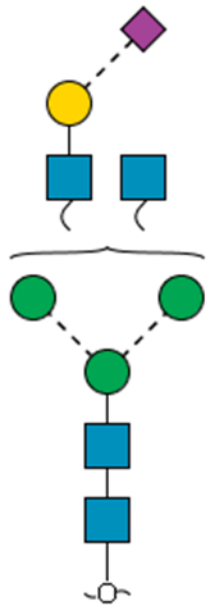
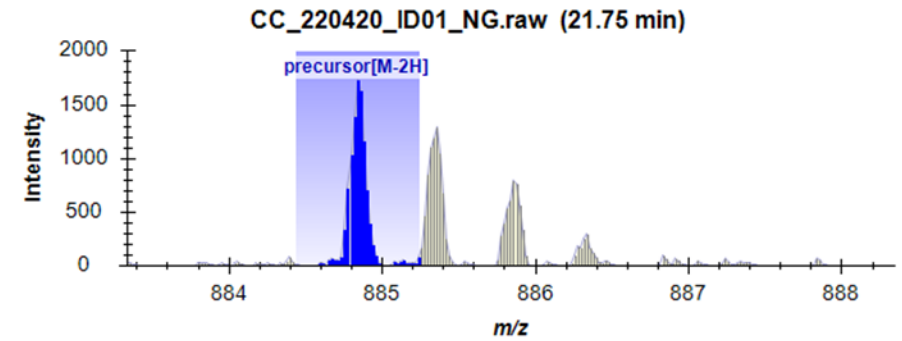
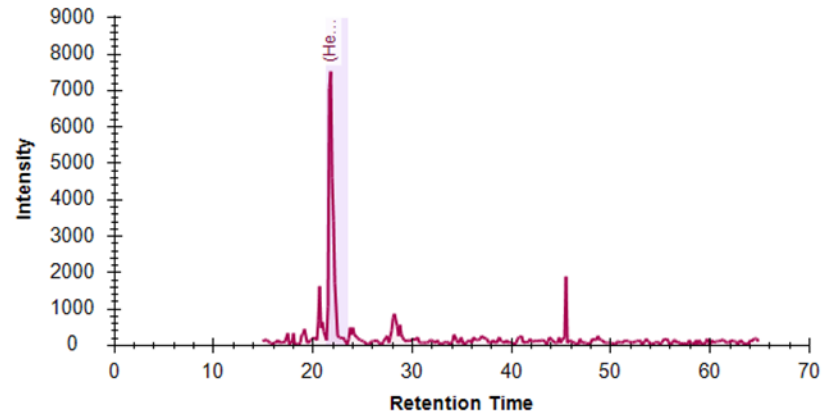
Glycan 34

(Hex)1(HexNAc)2(NeuAc)1 + (Man)3(GlcNAc)2

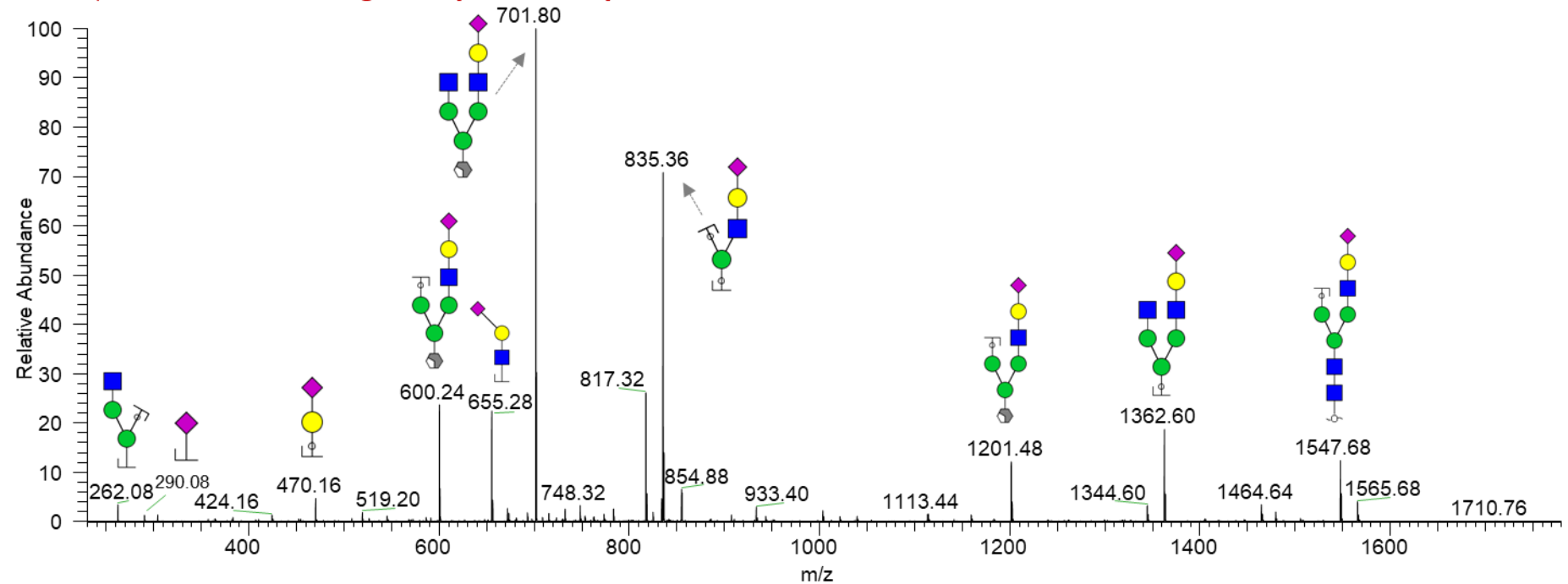
m/z 884.84 (2-)

Retention time: 21.7 min

Theo mass [M-H] = 1770.68 Da



CC_220420_ID01_NG #824-877 RT: 21.79-22.23 AV: 3 NL: 1.84E2
F: ITMS - p ESI E d w Full ms2 884.84@cid33.00 [230.00-1780.00]



Note: No distinction intended between 3-arm/6-arm in glycan fragment scheme.

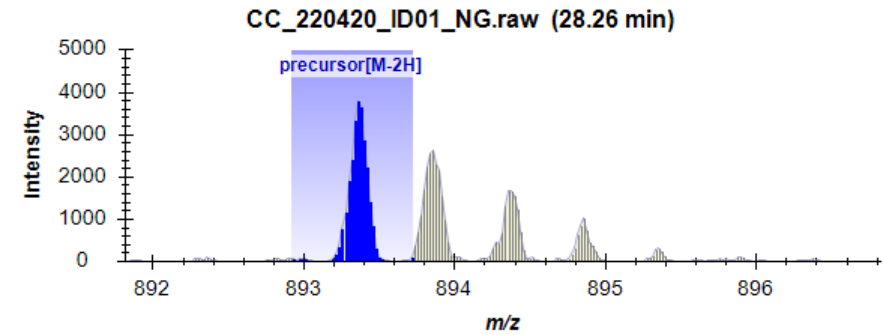
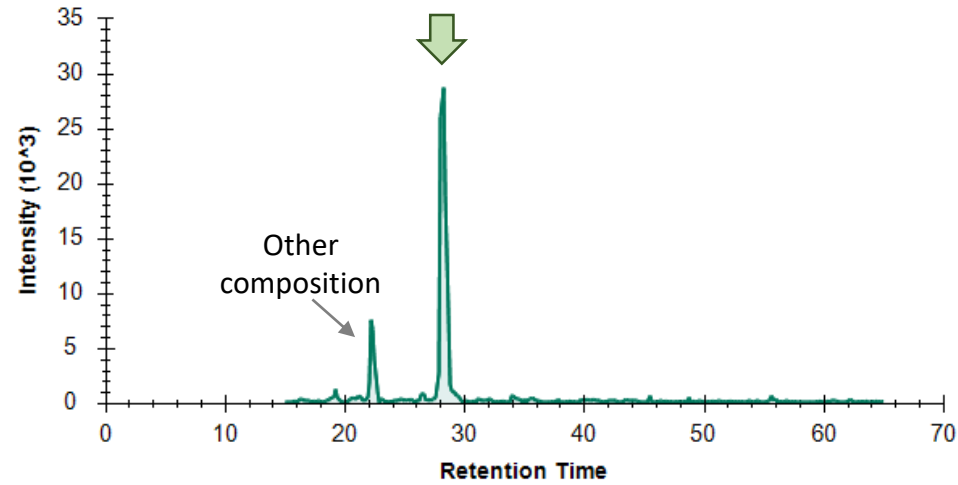
Glycan 35

(Hex)2(HexNAc)2(Deoxyhexose)1 + (Man)3(GlcNAc)2

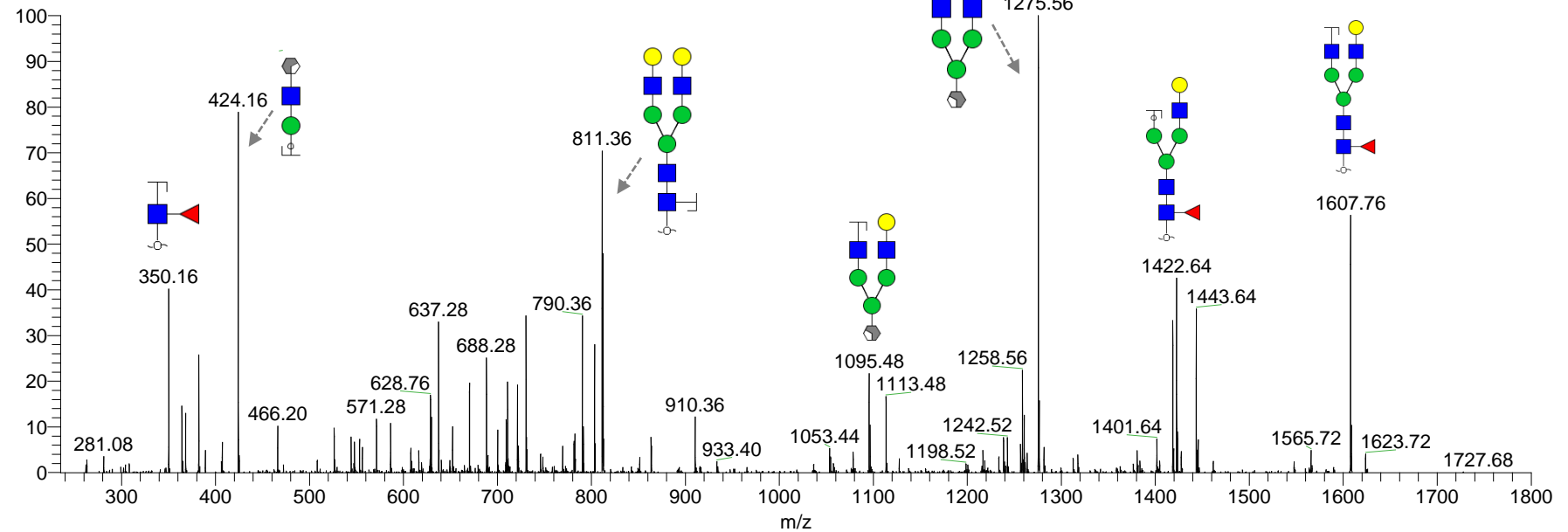
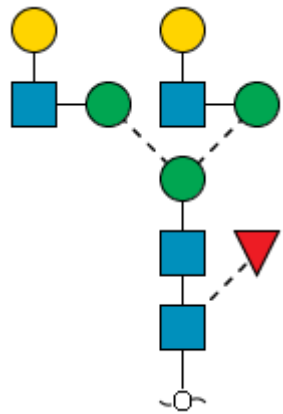
m/z 1787.73 (1-), 893.32 (2-)

Retention time: 28.2 min

Theo mass [M-H] = 1787.64 Da



CC_220420_ID01_NG #1046-1101 RT: 28.10-28.69 AV: 4 NL: 9.87E1
F: ITMS - p ESI E d w Full ms2 893.35@ci



Note: No distinction intended between 3-arm/6-arm in glycan fragment scheme.

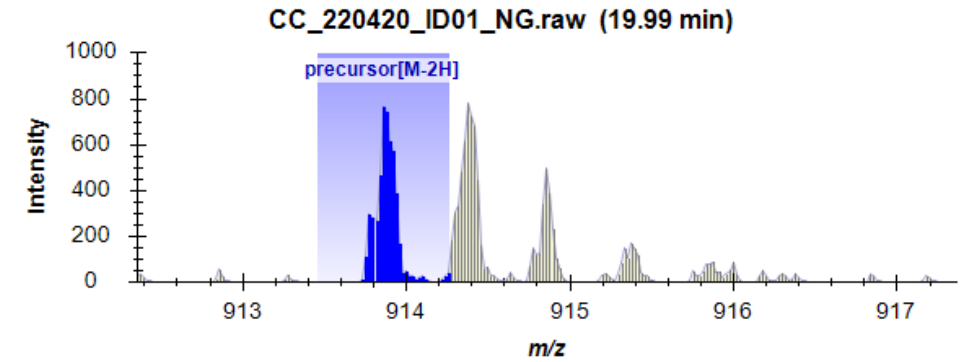
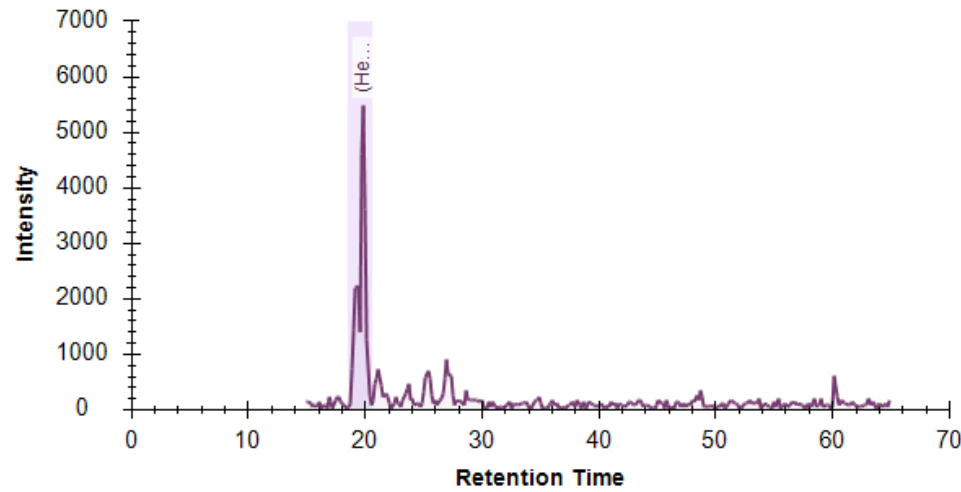
Glycan 36

(Hex)1(HexNAc)3(Deoxyhexose)1 + (Man)3(GlcNAc)2

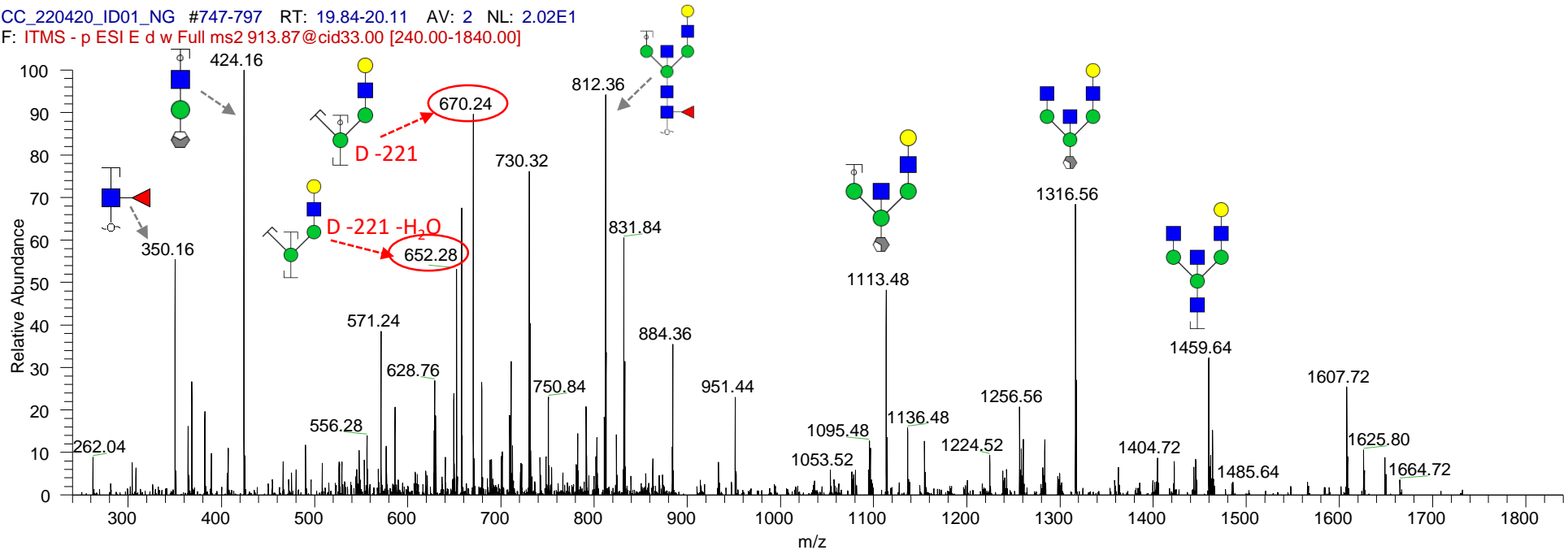
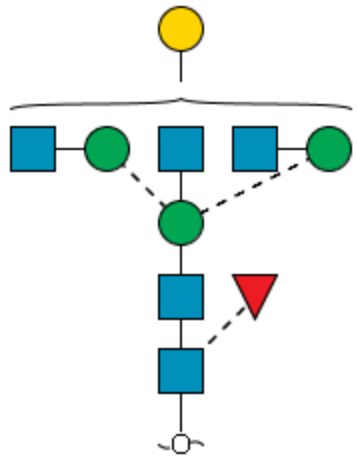
m/z 913.86 (2-)

Retention time: 19.2 min

Theo mass [M-H] = 1828.72 Da



CC_220420_ID01_NG #747-797 RT: 19.84-20.11 AV: 2 NL: 2.02E1
F: ITMS - p ESI E d w Full ms2 913.87@cid33.00 [240.00-1840.00]



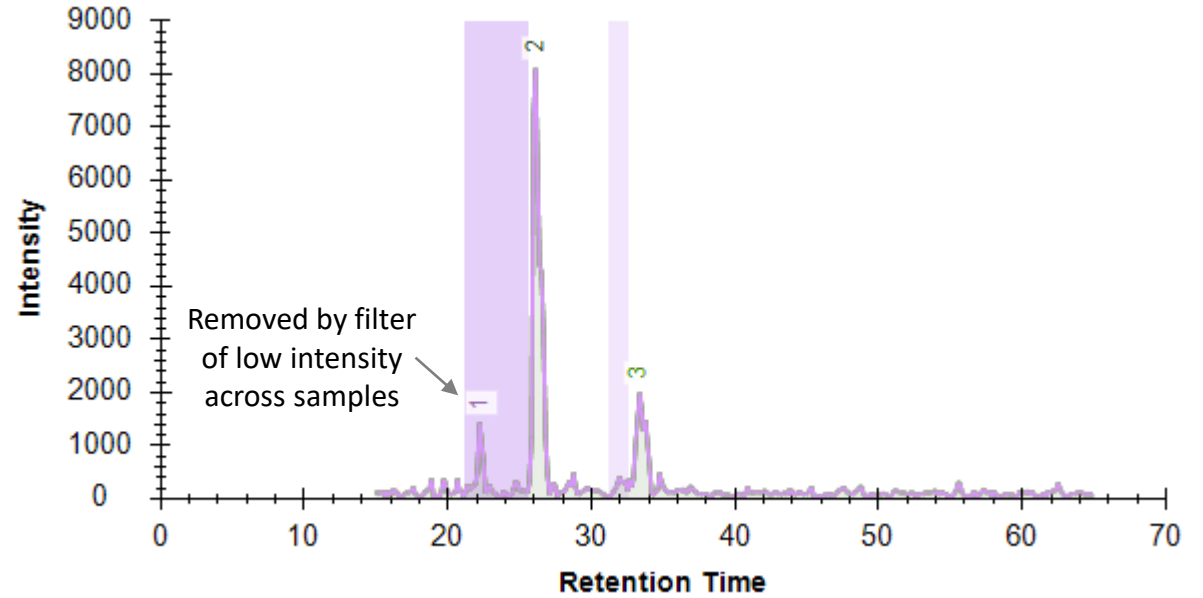
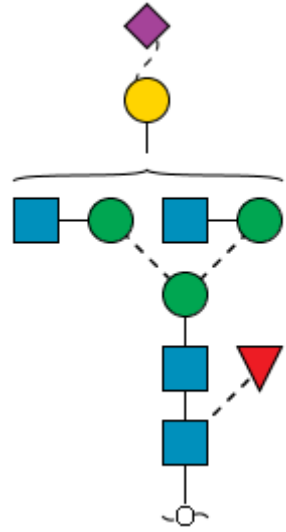
Note: No distinction intended between 3-arm/6-arm in glycan fragment scheme.

Glycan 37

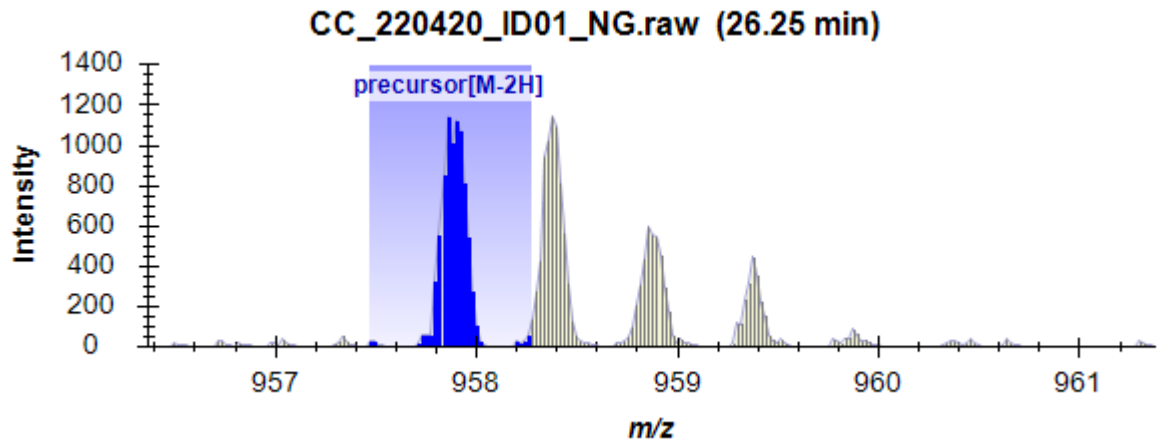
(Hex)1(HexNAc)2(Deoxyhexose)1(NeuAc)1 + (Man)3(GlcNAc)2

m/z 957.87 (2-)

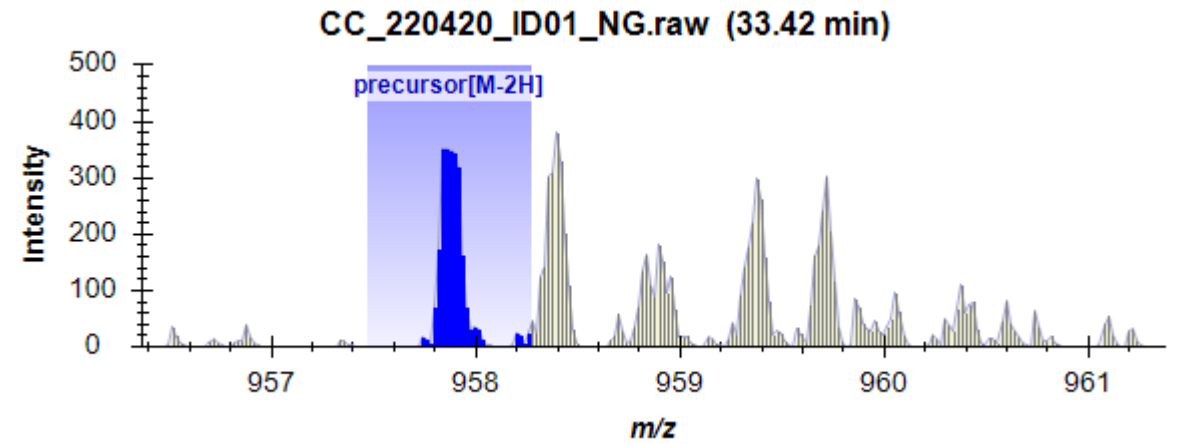
Theo mass [M-H] = 1916.74 Da



37a



37b

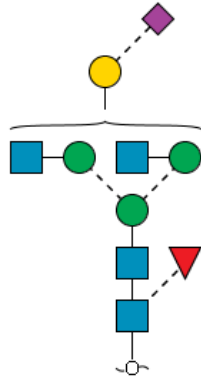


Glycan 37a

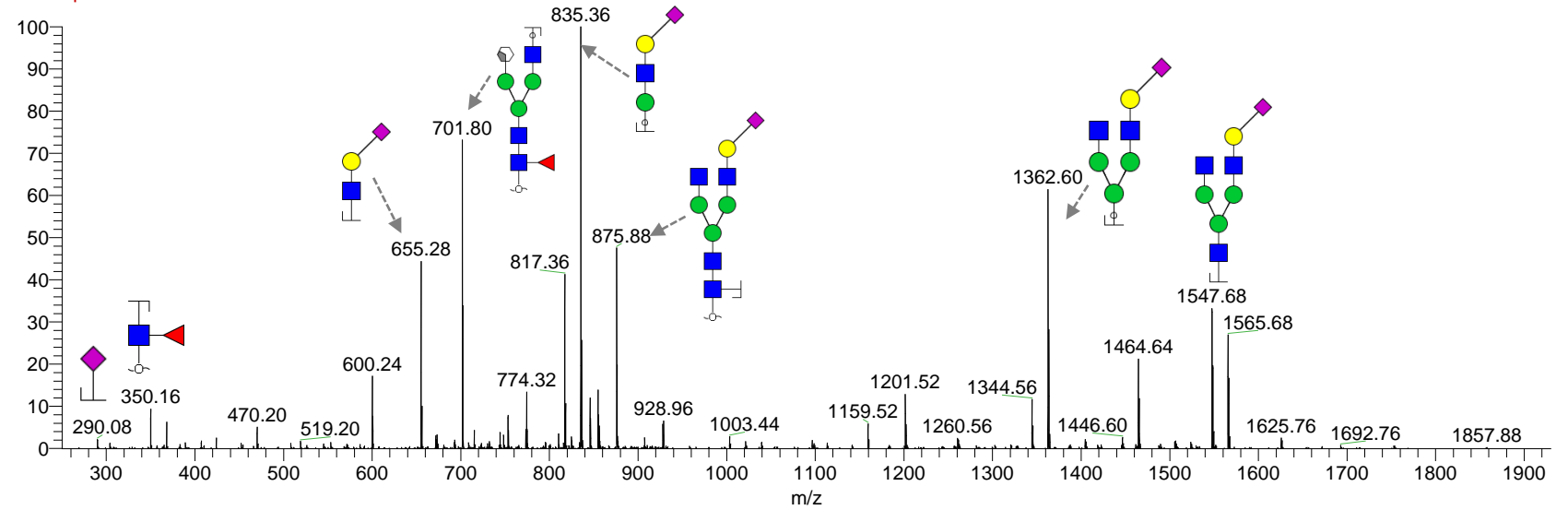
m/z 957.87 (2-)

Retention time: 24.9 min

Theo mass [M-H] = 1916.74 Da



CC_220420_ID01_NG #979-1021 RT: 26.13-26.78 AV: 4 NL: 1.11E2
F: ITMS - p ESI E d w Full ms2 957.88@

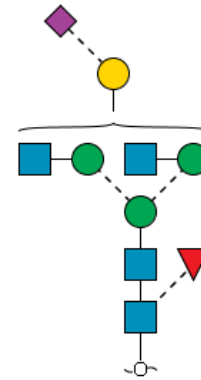


Glycan 37b

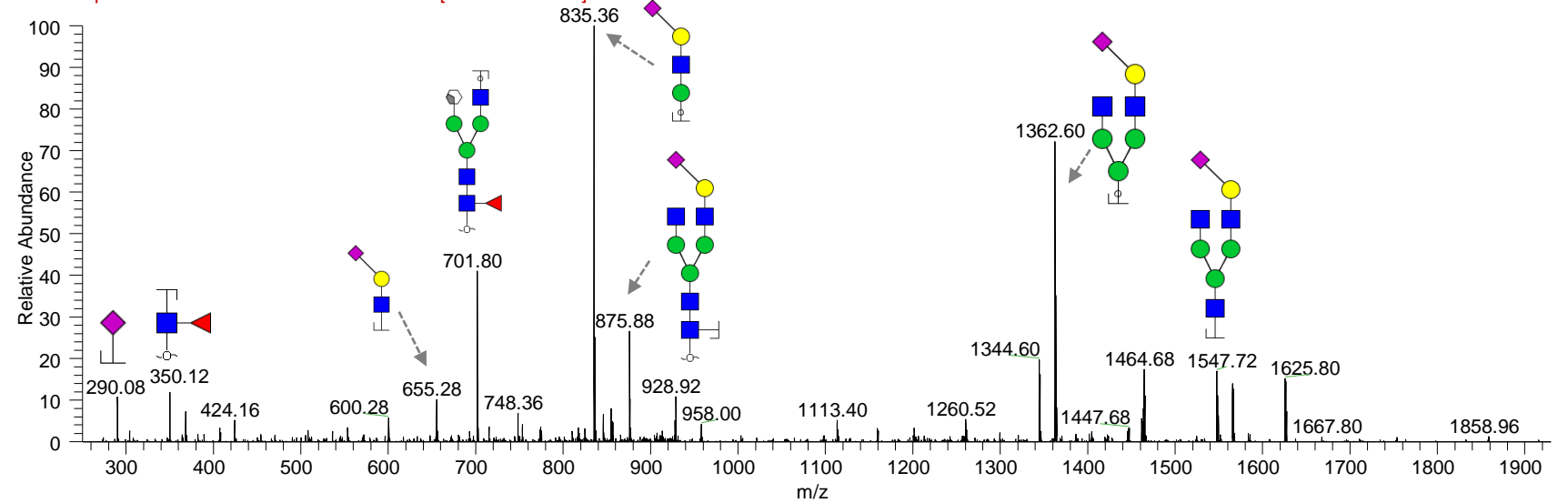
m/z 957.87 (2-)

Retention time: 32.2 min

Theo mass [M-H] = 1916.74 Da



CC_220420_ID01_NG #1213-1269 RT: 33.57-33.88 AV: 2 NL: 3.85E1
F: ITMS - p ESI E d w Full ms2 957.88@cid33.00 [250.00-1930.00]



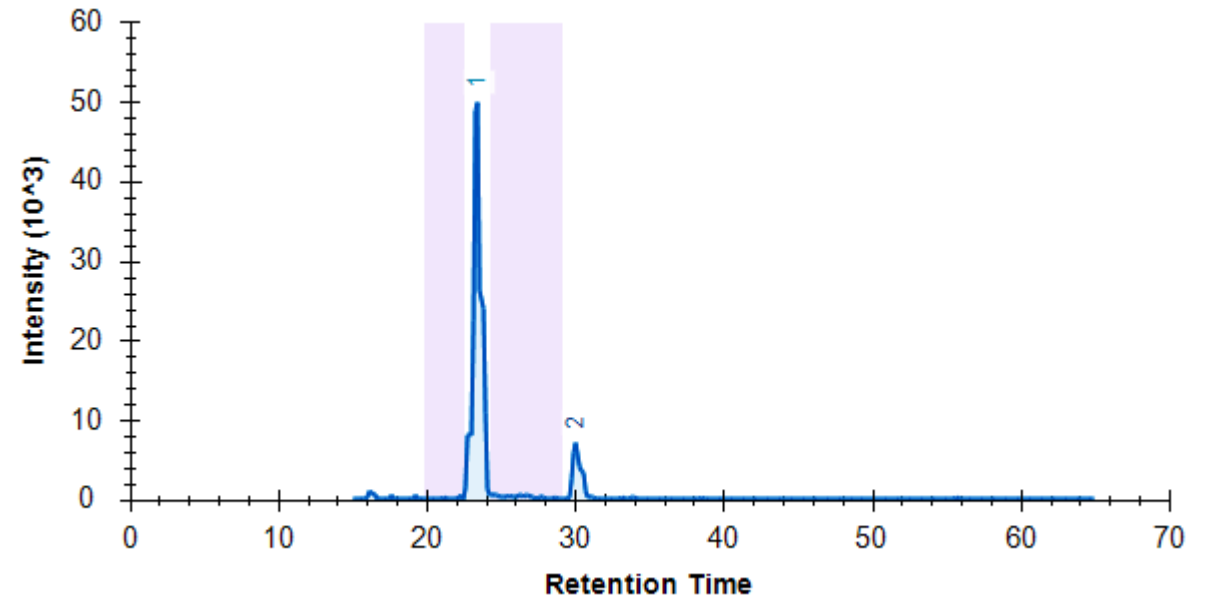
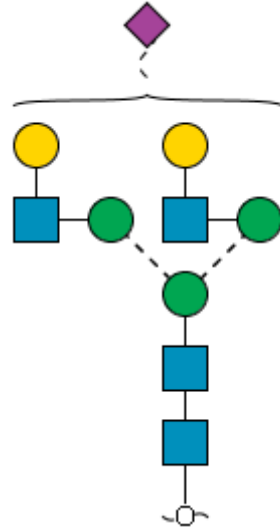
Notes: No distinction intended between 3-arm/6-arm in glycan fragment scheme. This glycan has been annotated as α 2,6 or α 2,3-sialyl isomer based on their elution time and 655/290 ions.

Glycan 38

(Hex)2(HexNAc)2(NeuAc)1 + (Man)3(GlcNAc)2

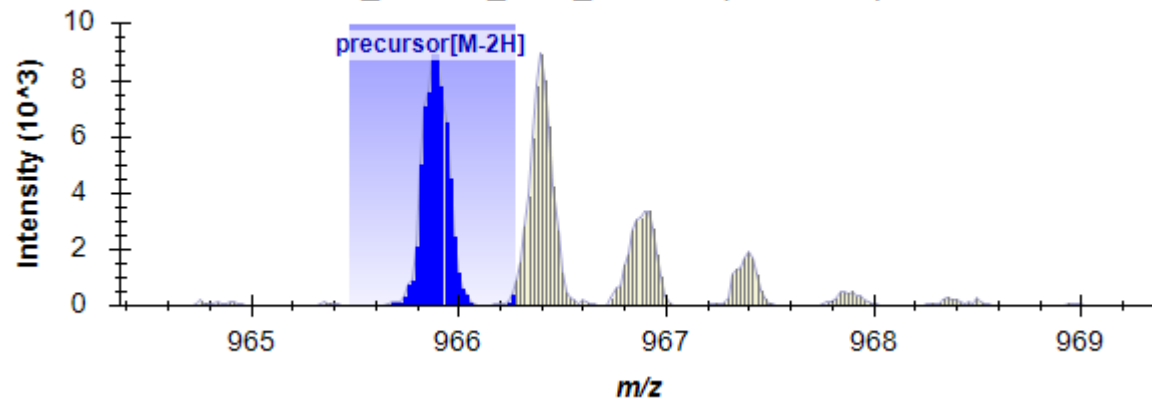
m/z 965.87 (2-)

Theo mass [M-H] = 1932.74 Da



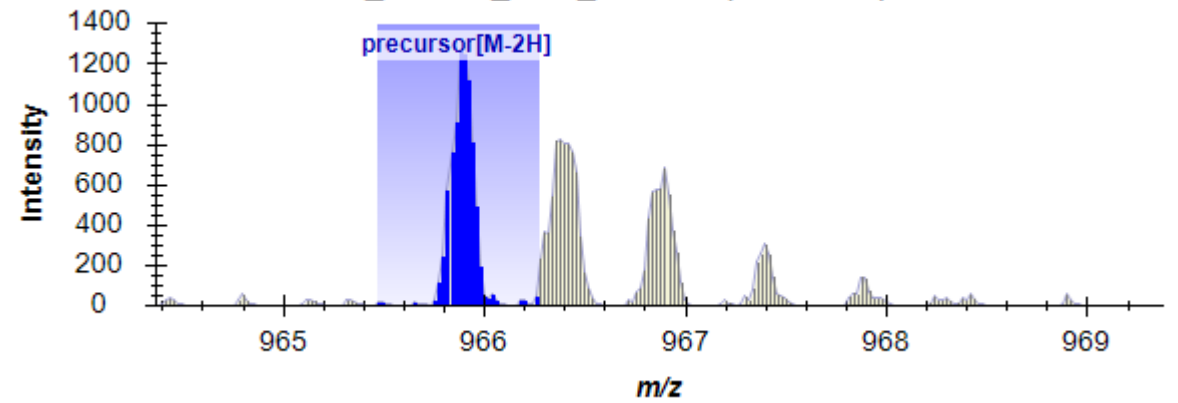
38a

CC_220420_ID01_NG.raw (23.40 min)



38b

CC_220420_ID01_NG.raw (30.07 min)

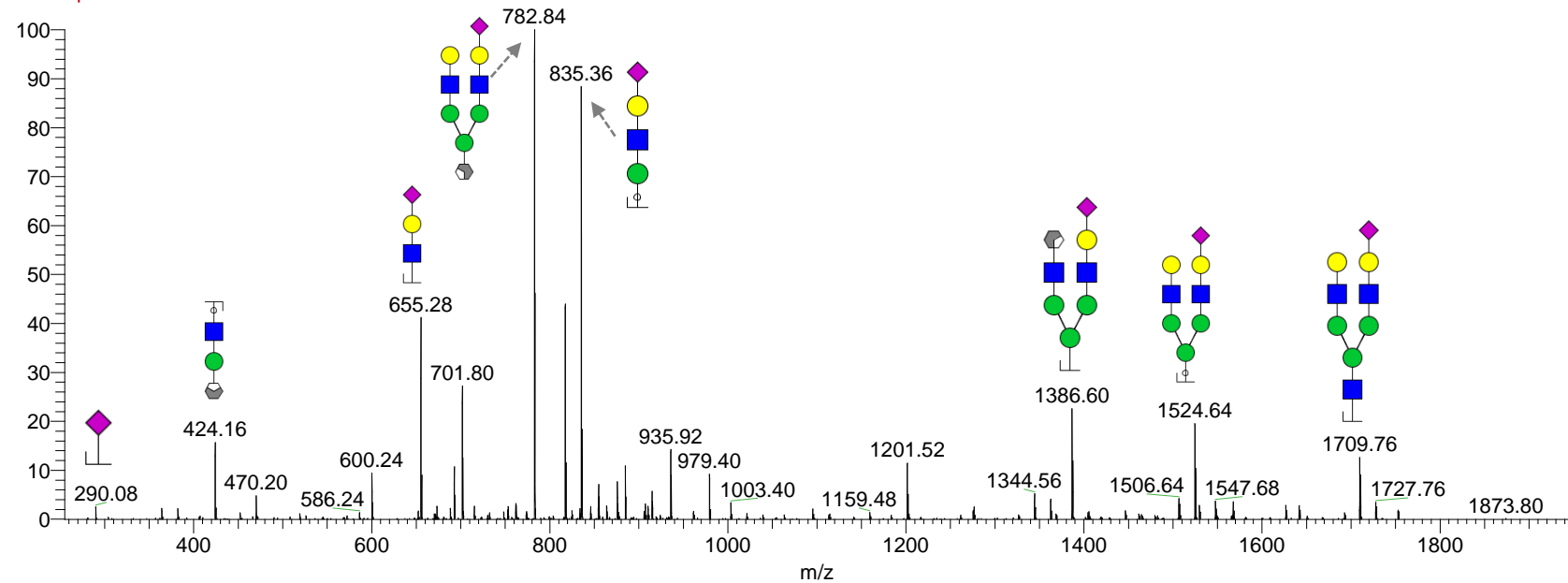
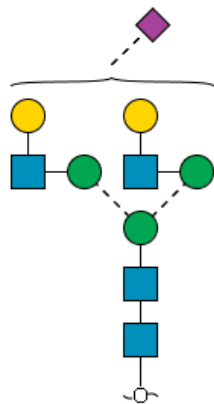


Glycan 38a

m/z 965.87 (2-)

Retention time: 21.9 min

Theo mass [M-H] = 1932.74 Da

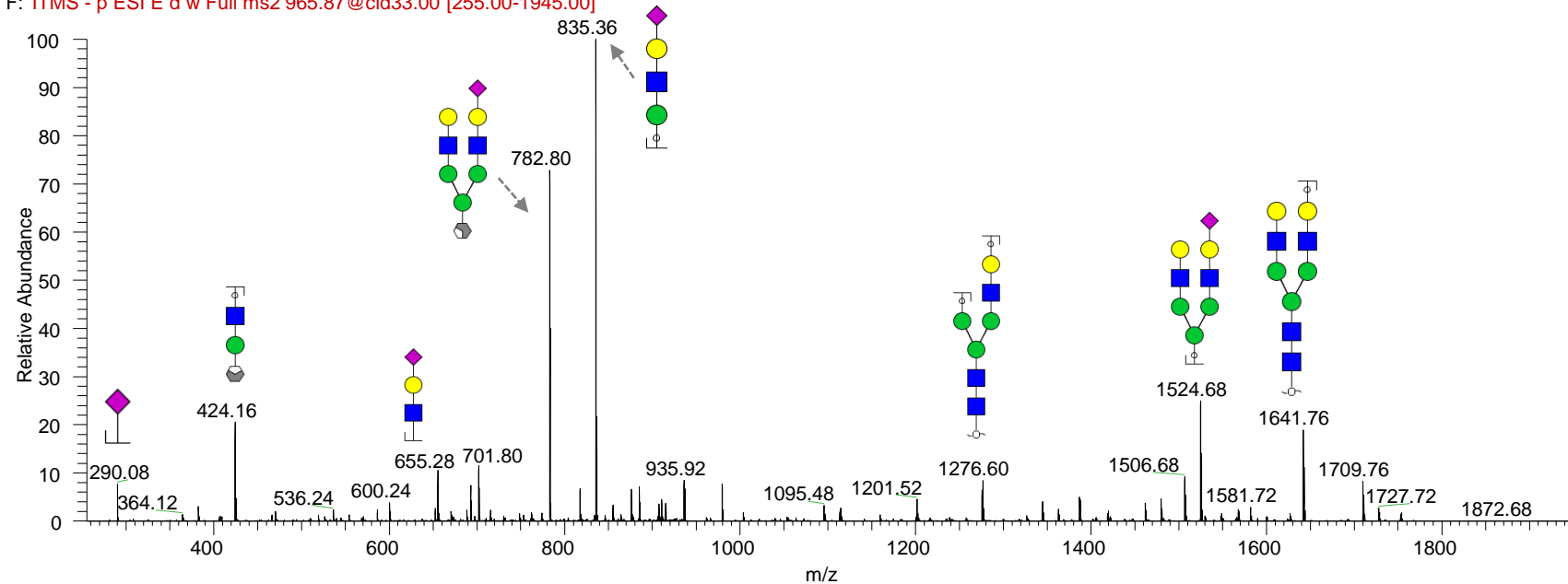
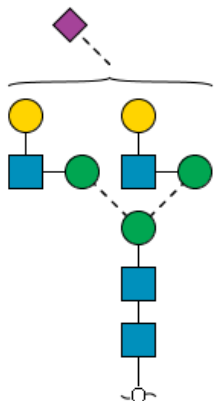


Glycan 38b

m/z 965.87 (2-)

Retention time: 28.8 min

Theo mass [M-H] = 1932.74 Da



Note: No distinction intended between 3-arm/6-arm in glycan fragment scheme. This glycan has been annotated as α 2,6 or α 2,3-sialyl isomer based on their elution time and 655/290 ions.

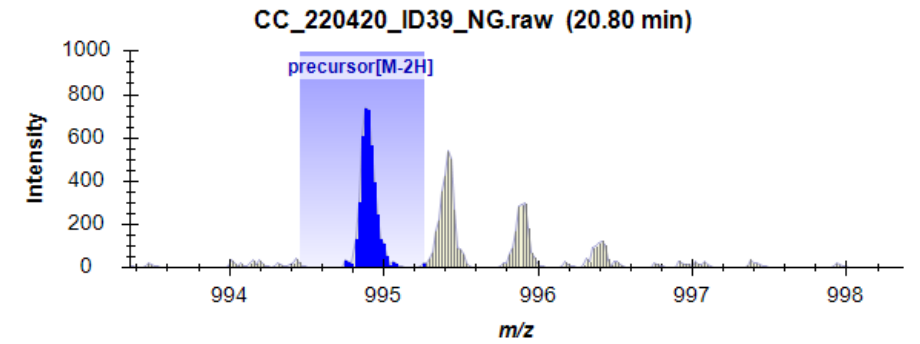
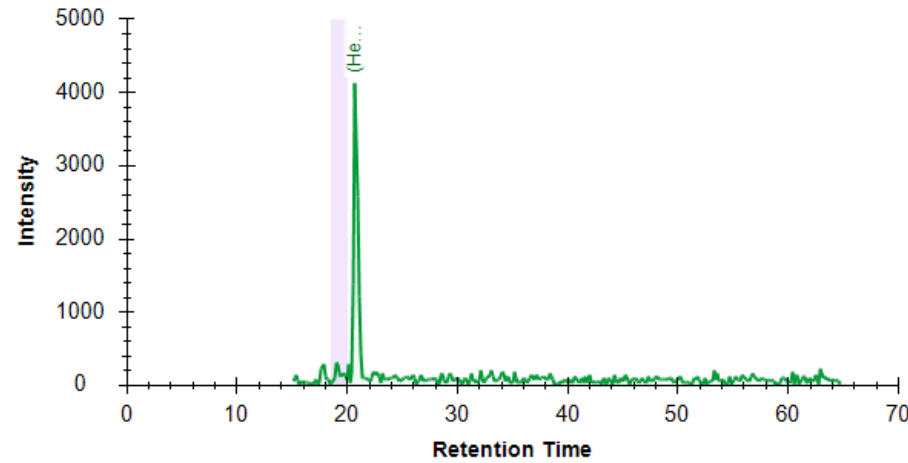
Glycan 39

(Hex)₂(HexNAc)₃(Deoxyhexose)₁ + (Man)₃(GlcNAc)₂

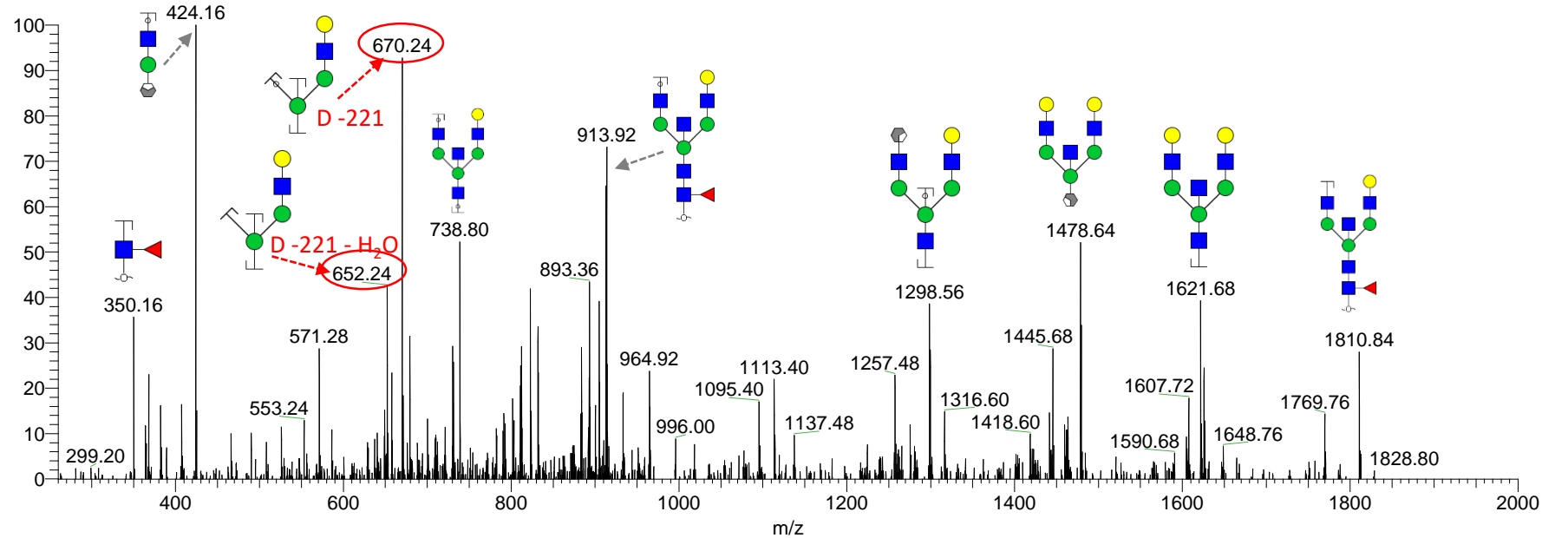
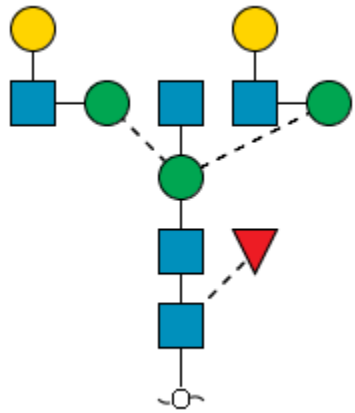
m/z 994.86 (2-)

Retention time: 19.5 min

Theo mass [M-H] = 1990.72 Da



cc_220420_id39_ng #777-832 RT: 20.84-21.09 AV: 2 NL: 1.03E1
F: ITMS - p ESI E d w Full ms2 994.90@ci



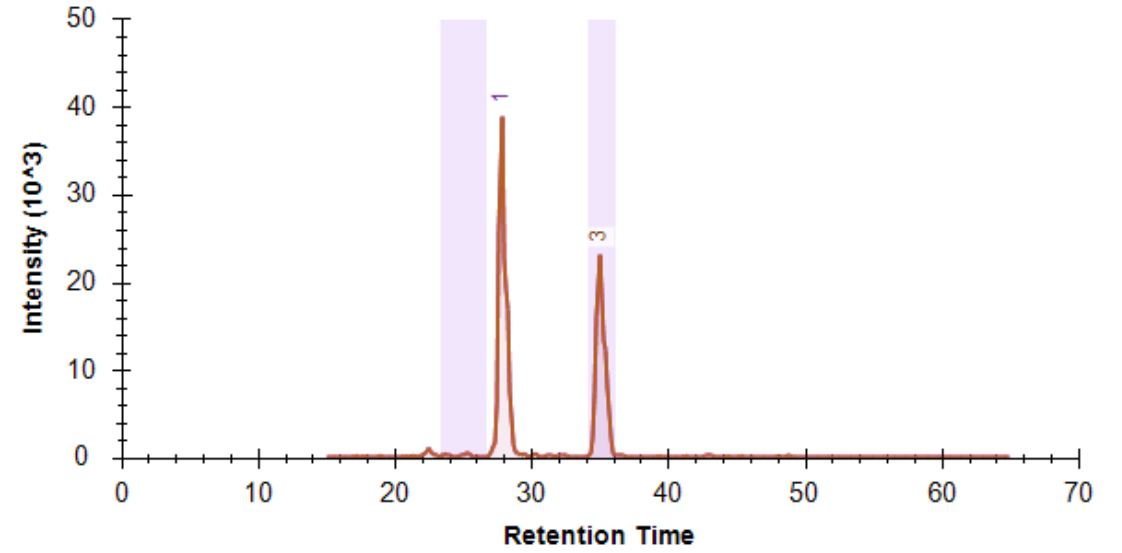
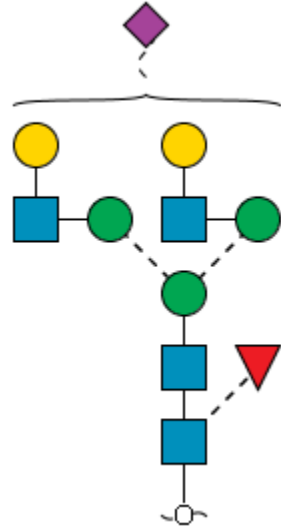
Note: No distinction intended between 3-arm/6-arm in glycan fragment scheme.

Glycan 40

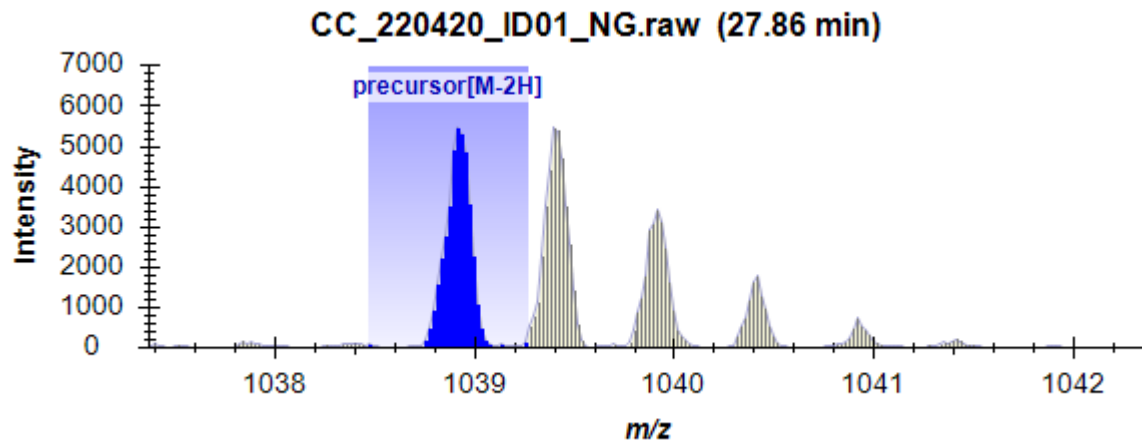
(Hex)2(HexNAc)2(Deoxyhexose)1(NeuAc)1 + (Man)3(GlcNAc)2

m/z 1038.87 (2-)

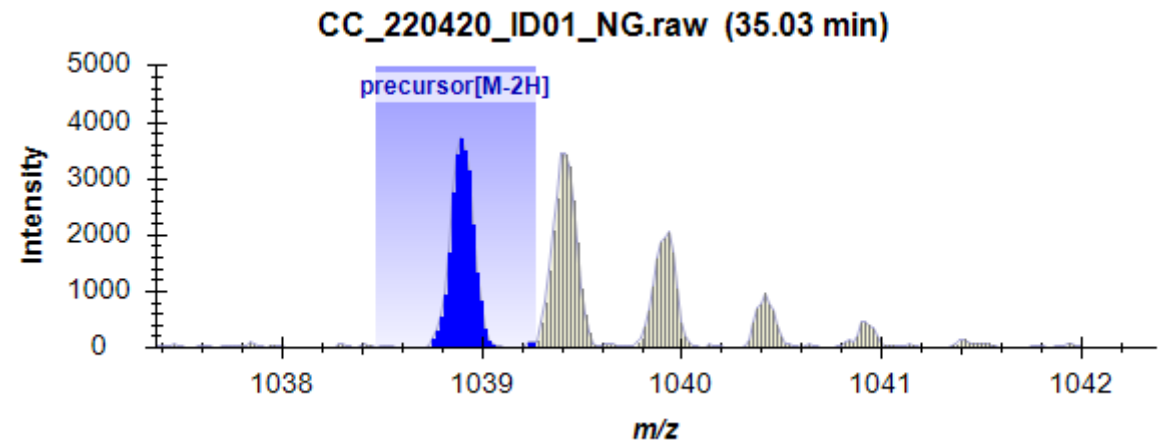
Theo mass [M-H] = 2078.74 Da



40a

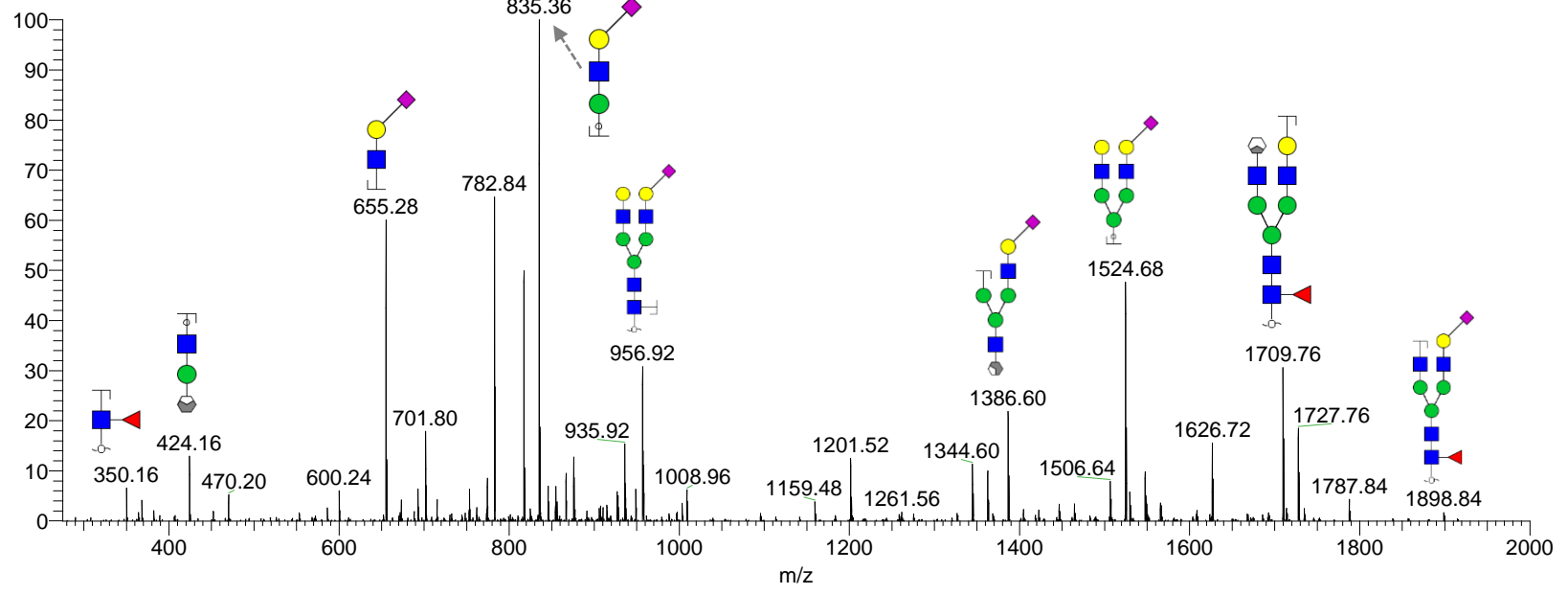
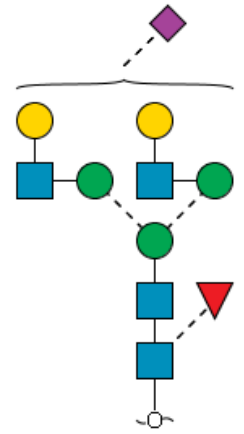


40b



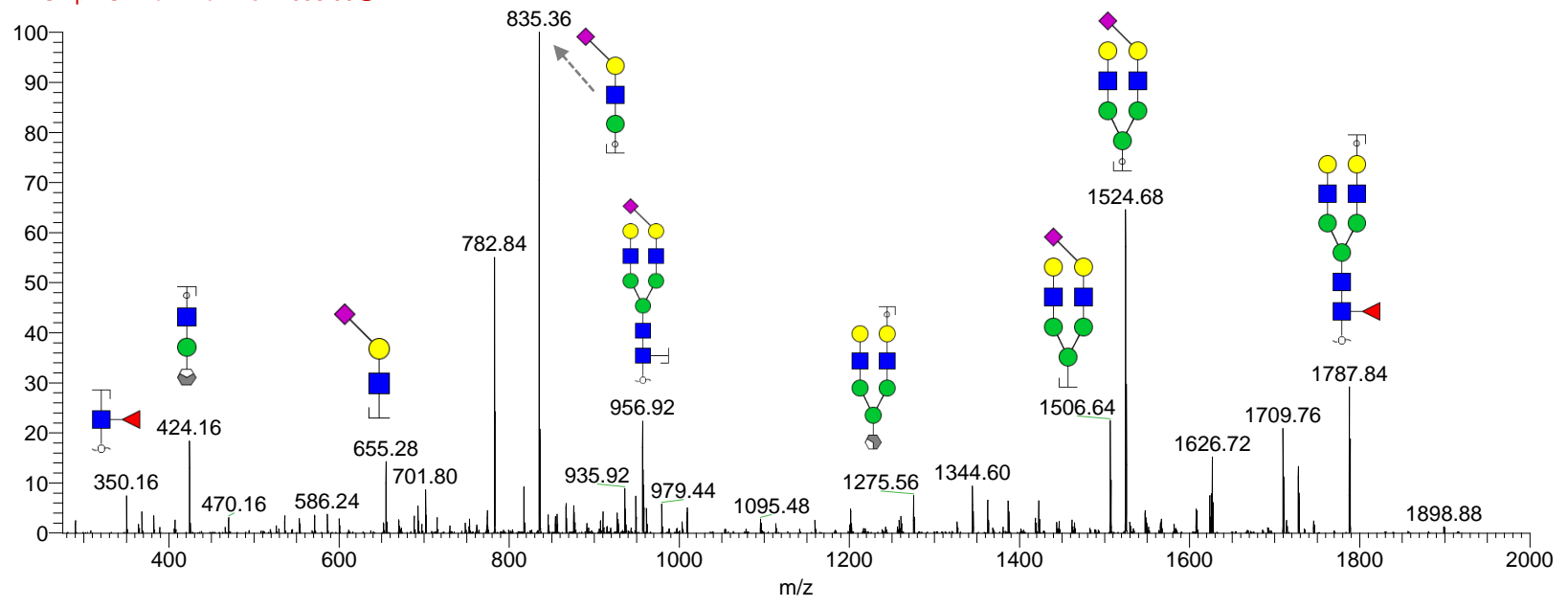
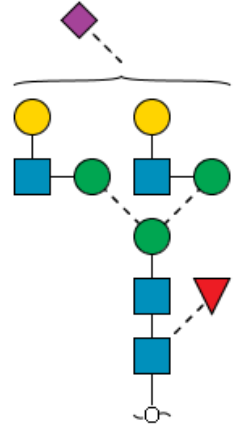
Glycan 40a

m/z 1038.87 (2-)
 Retention time: 26.3 min
 Theo mass [M-H] = 2078.74 Da



Glycan 40b

m/z 1038.87 (2-)
 Retention time: 33.4 min
 Theo mass [M-H] = 2078.74 Da



Notes: No distinction intended between 3-arm/6-arm in glycan fragment scheme. This glycan has been annotated as $\alpha 2,6$ or $\alpha 2,3$ -sialyl isomer based on their elution time and 655/290 ions.

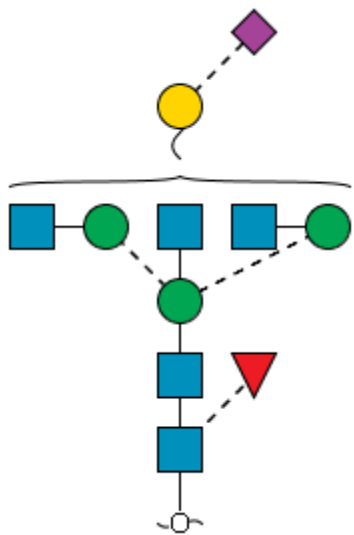
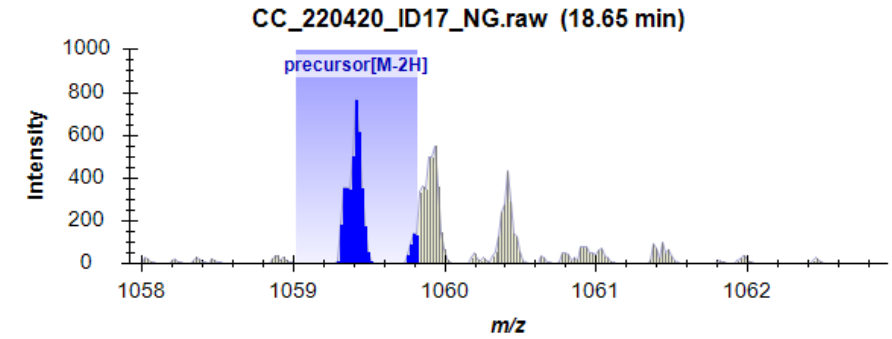
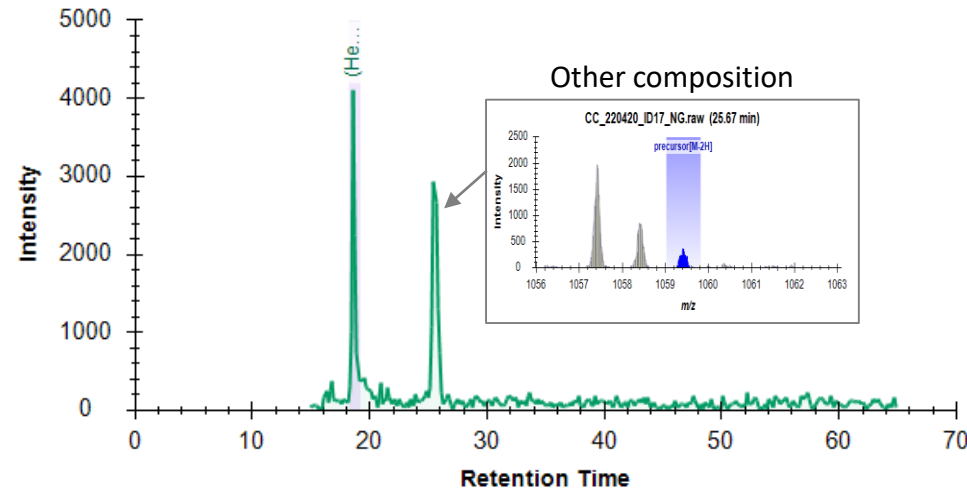
Glycan 41

(Hex)1(HexNAc)3(Deoxyhexose)1(NeuAc)1 + (Man)3(GlcNAc)2

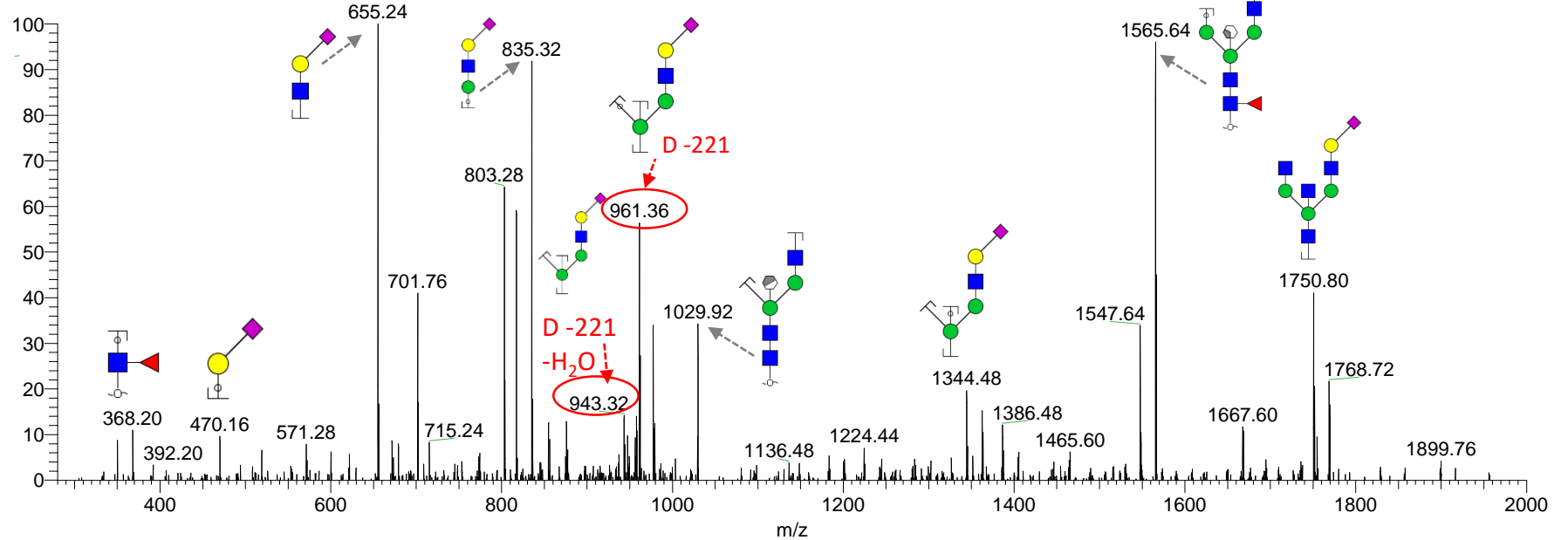
m/z 1059.42 (2-)

Retention time: 18.6 min

Theo mass [M-H] = 2119.84 Da



cc_220420_id17_ng #704 RT: 18.72 AV: 1 NL: 3.19E1
F: ITMS - p ESI E d w Full ms2 1059.42@



Note: No distinction intended between 3-arm/6-arm in glycan fragment scheme. This glycan has been annotated as α 2,6-sialyl isomer based on 655/290 ions.

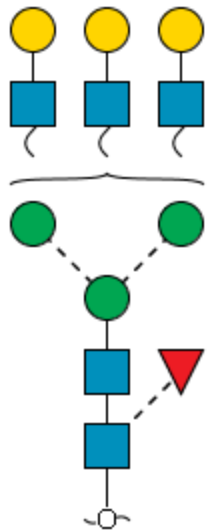
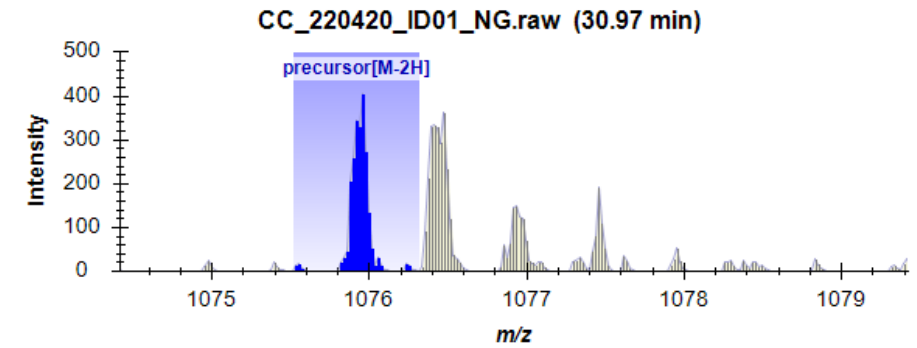
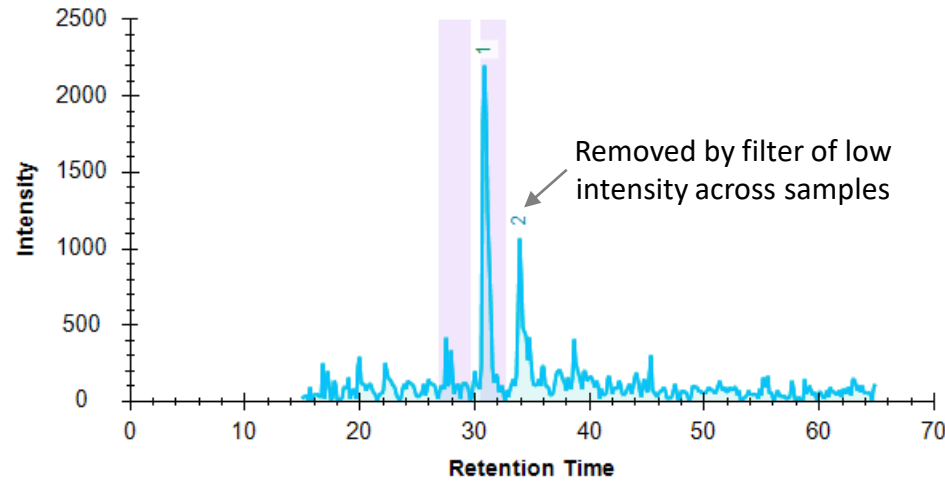
Glycan 42

(Hex)₃(HexNAc)₃(Deoxyhexose)₁ + (Man)₃(GlcNAc)₂

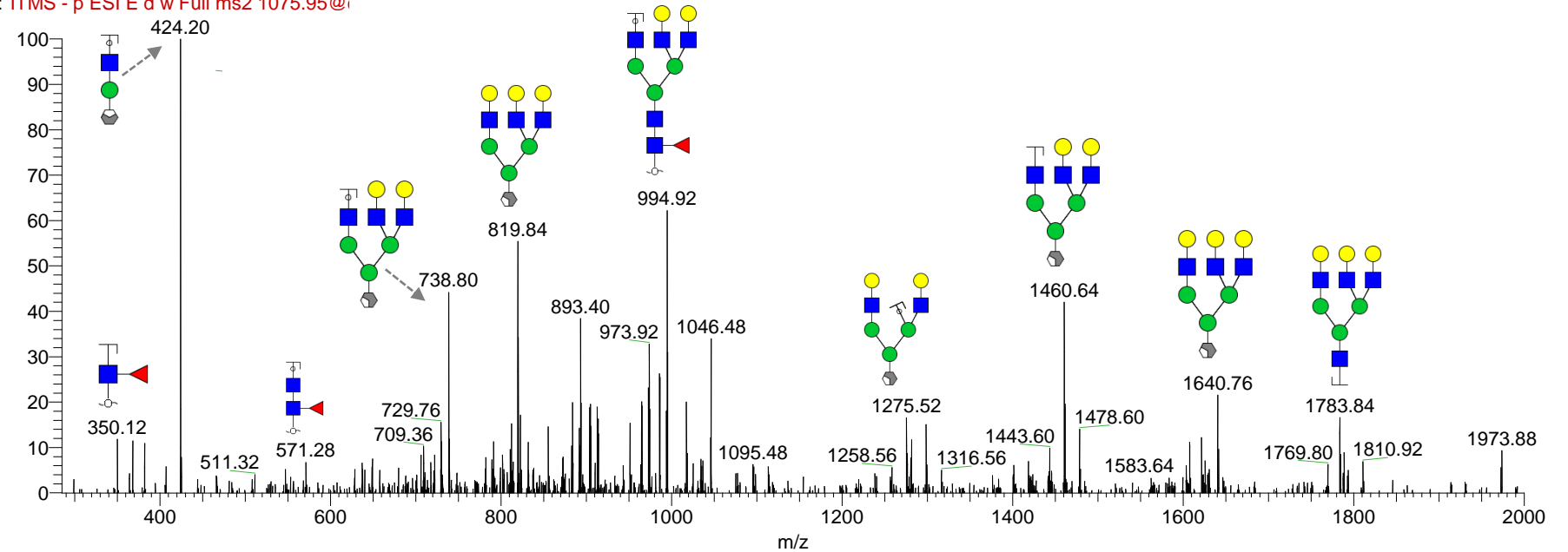
m/z 1075.92 (2-)

Retention time: 29.3 min

Theo mass [M-H] = 2152.84 Da



CC_220420_ID01_NG #1122-1198 RT: 30.93-31.29 AV: 2 NL: 1.39E1
F: ITMS - p ESI E d w Full ms2 1075.95@:



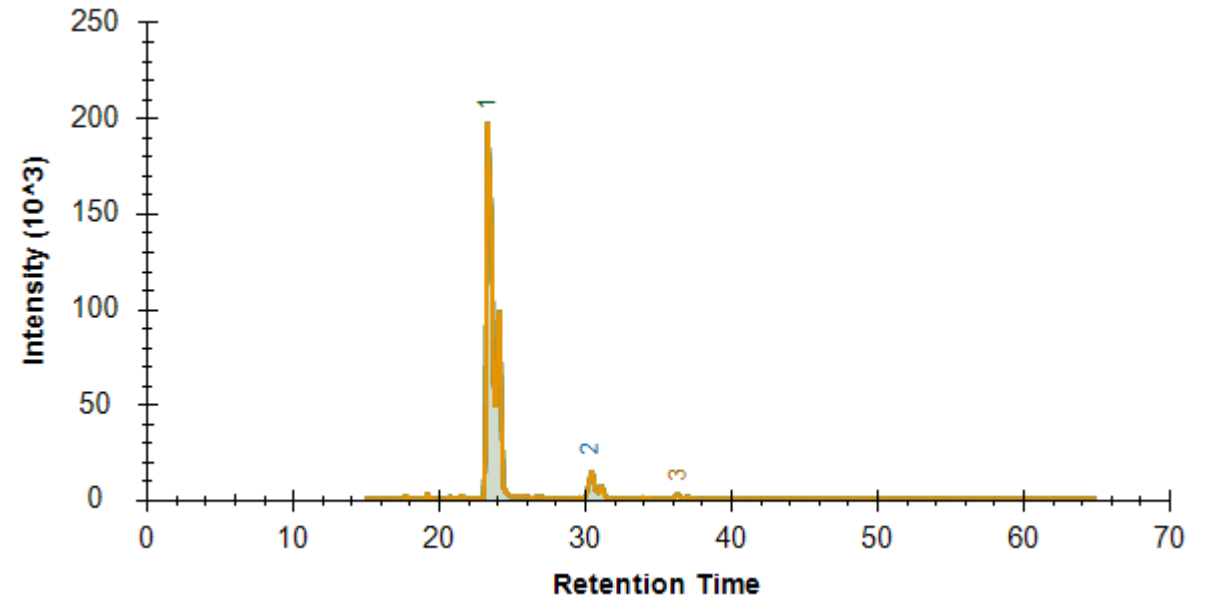
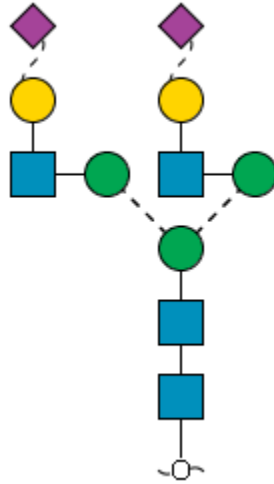
Note: No distinction intended between 3-arm/6-arm in glycan fragment scheme.

Glycan 43

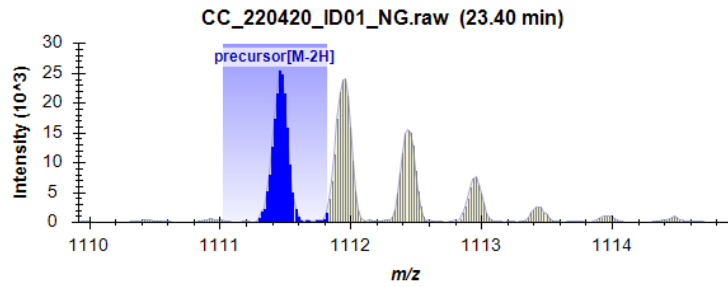
(Hex)₂(HexNAc)₂(NeuAc)₂ + (Man)₃(GlcNAc)₂

m/z 1111.42 (1-); 740.61 (2-)

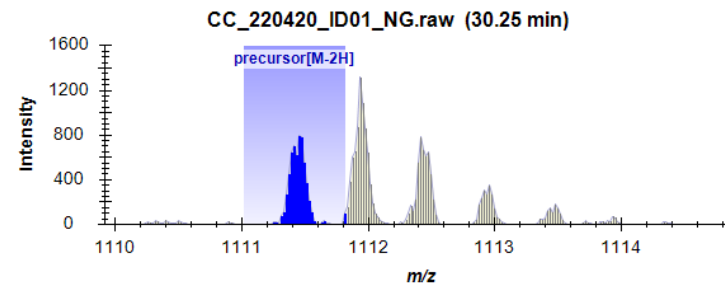
Theo mass [M-H] = 2223.83 Da



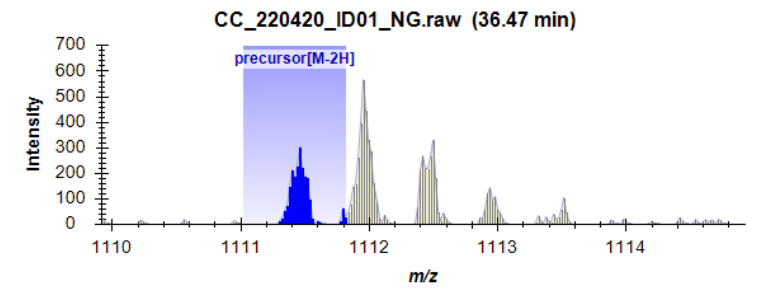
41a



41b



41c

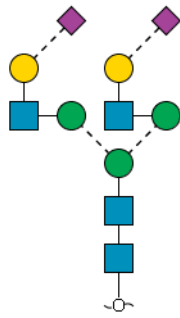


Glycan 43a

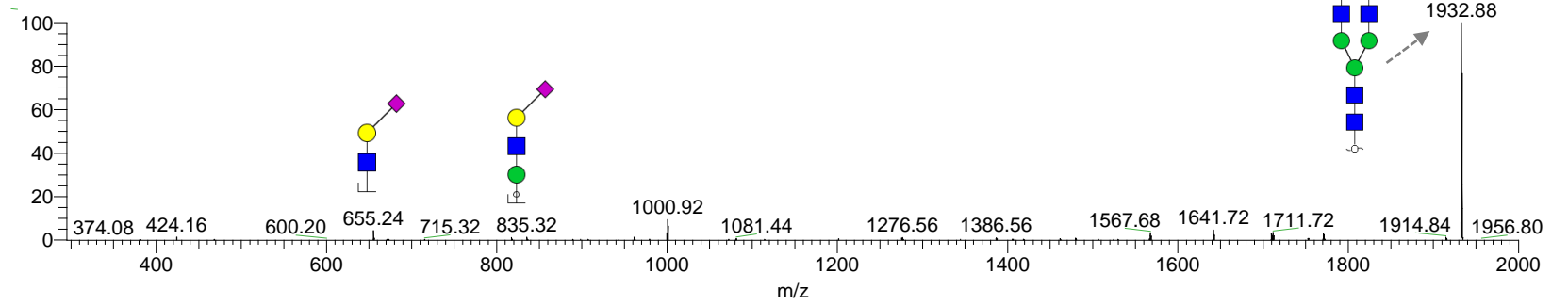
m/z 1111.42 (1-); 740.61 (2-)

Retention time: 23.3 min

Theo mass [M-H] = 2223.83 Da



cc_220420_id41_ng #871-957 RT: 23.08-24.12 AV: 5 NL: 1.33E3
F: [ITMS - p ESI E d w Full m]0-2000.00]

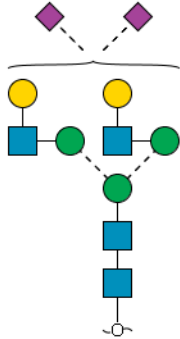


Glycan 43b

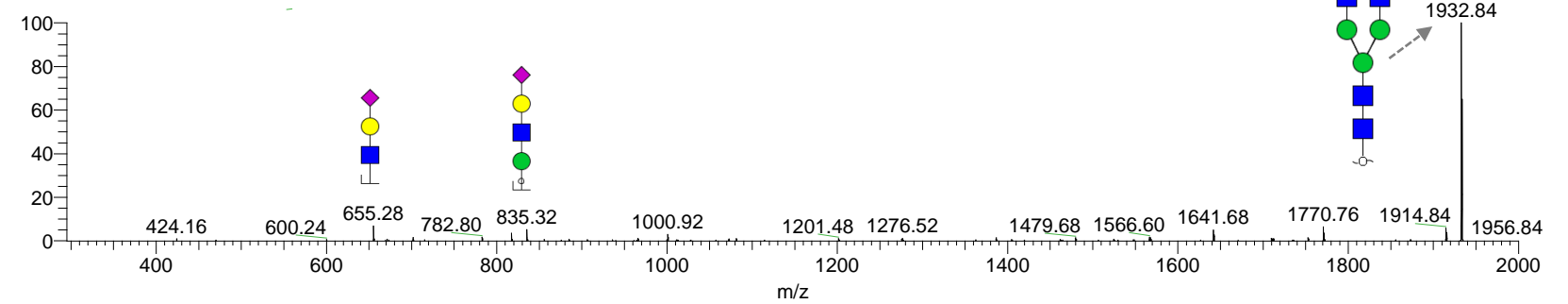
m/z 1111.42 (1-); 740.61 (2-)

Retention time: 36.3 min

Theo mass [M-H] = 2223.83 Da



cc_220420_id41_ng #1100-1195 RT: 30.30-31.34 AV: 7 NL: 1.65E2
F: [ITMS - p ESI E d w Full m]0-2000.00]

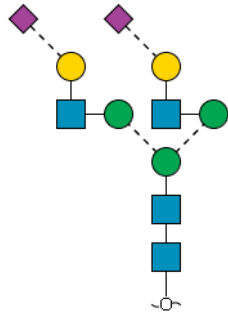


Glycan 43c

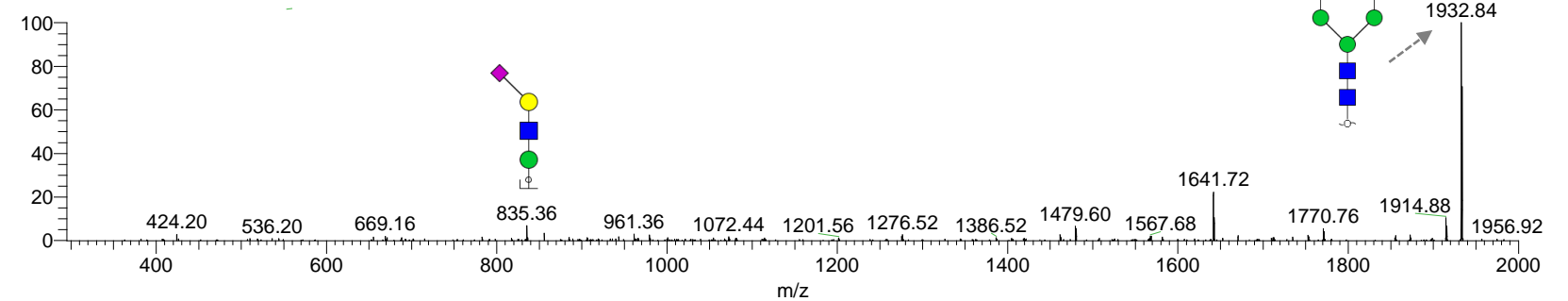
m/z 1111.42 (1-); 740.61 (2-)

Retention time: 36.3 min

Theo mass [M-H] = 2223.83 Da



cc_220420_id41_ng #1313-1411 RT: 36.39-37.14 AV: 3 NL: 5.21E1
F: [ITMS - p ESI E d w Full m]0-2000.00]



Notes: No distinction intended between 3-arm/6-arm in glycan fragment scheme. This glycan has been annotated as α 2,6 or α 2,3-sialyl isomer based on their elution time.

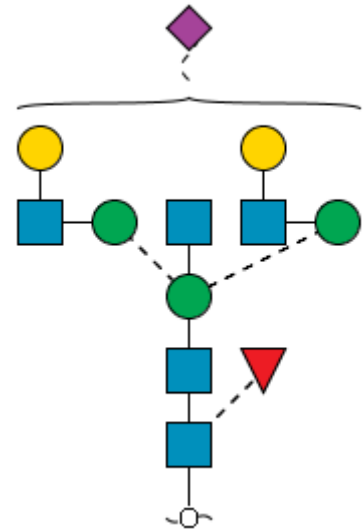
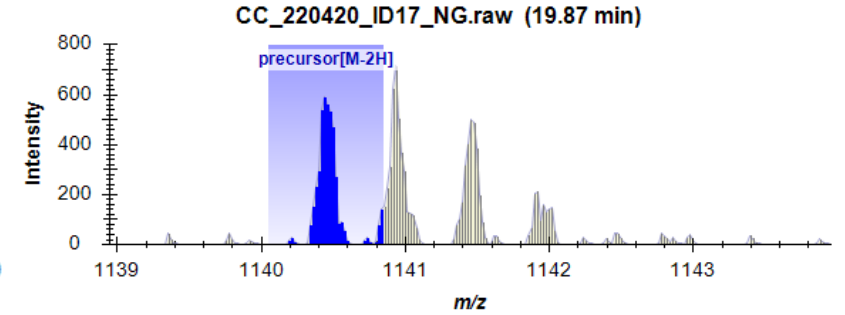
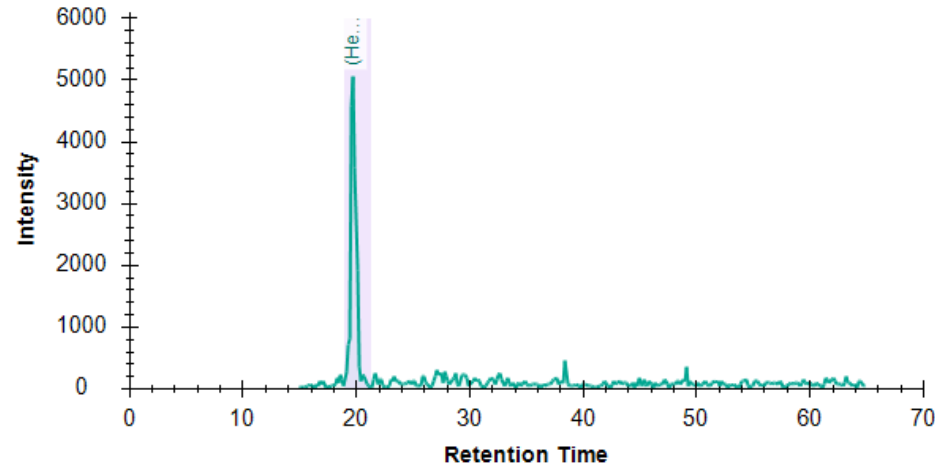
Glycan 44

(Hex)2(HexNAc)3(Deoxyhexose)1(NeuAc)1 + (Man)3(GlcNAc)2

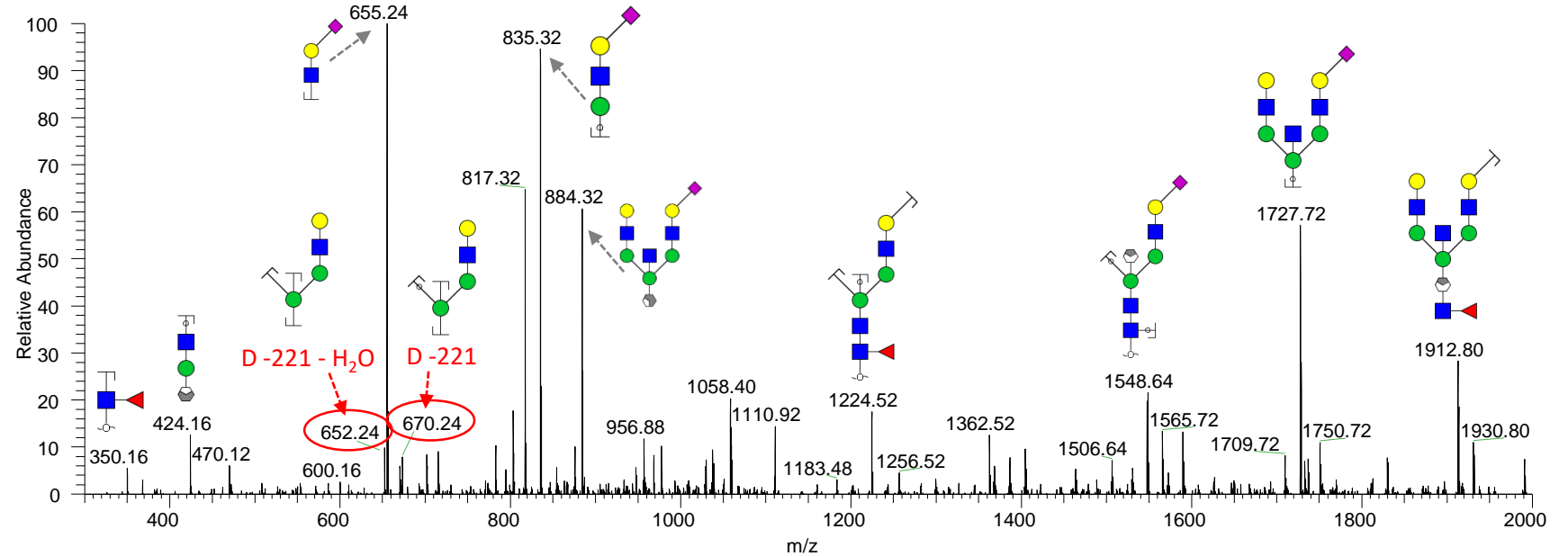
m/z 1140.45 (2-)

Retention time: 19.7 min

Theo mass [M-H] = 2281.92 Da



CC_220420_ID17_NG #757 RT: 20.02 AV: 1 NL: 4.89E1
F: ITMS - p ESI E d w Full ms2 1140.45@cid33.00 [300.00-2000.00]



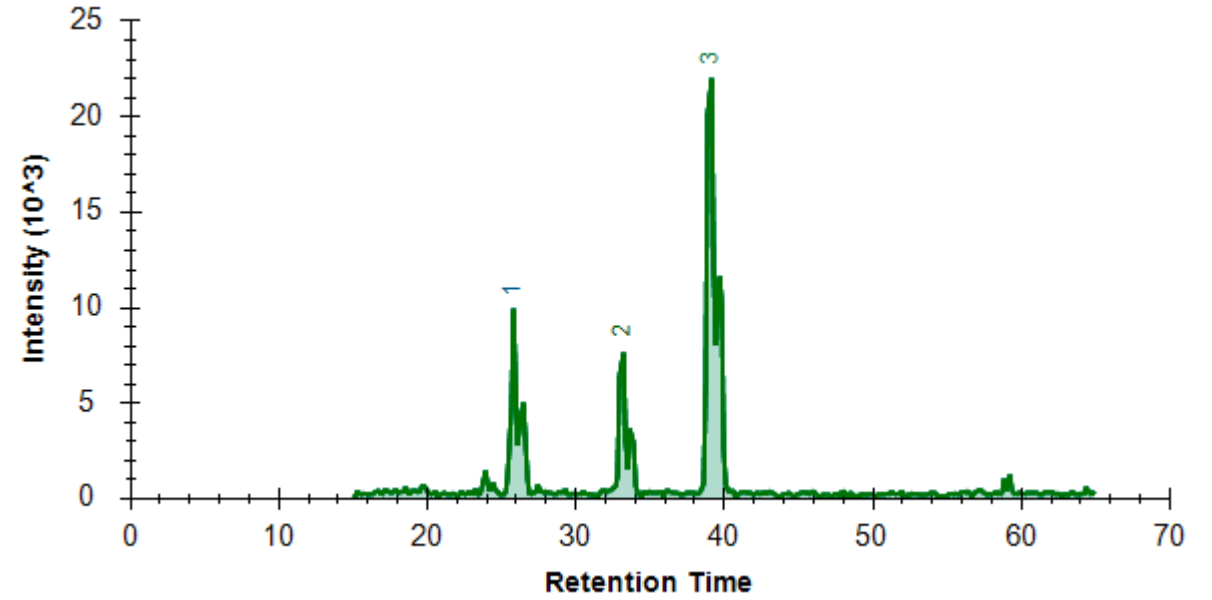
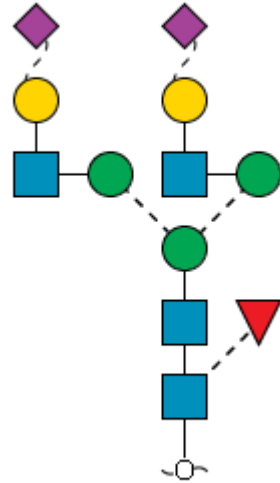
Notes: No distinction intended between 3-arm/6-arm in glycan fragment scheme. This glycan has been annotated as α 2,6-sialyl isomer based on 655/290 ions.

Glycan 45

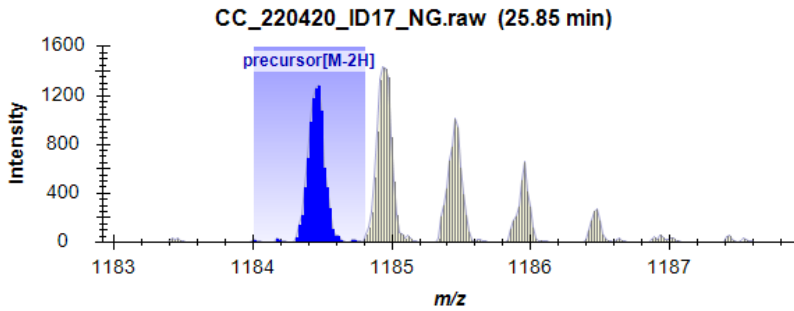
(Hex)₂(HexNAc)₂(Deoxyhexose)₁(NeuAc)₂ + (Man)₃(GlcNAc)₂

m/z 1184.42 (2-); 789.27 (-3)

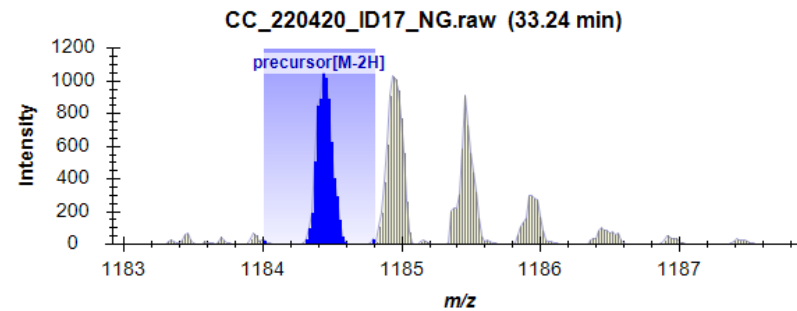
Theo mass [M-H] = 2369.84 Da



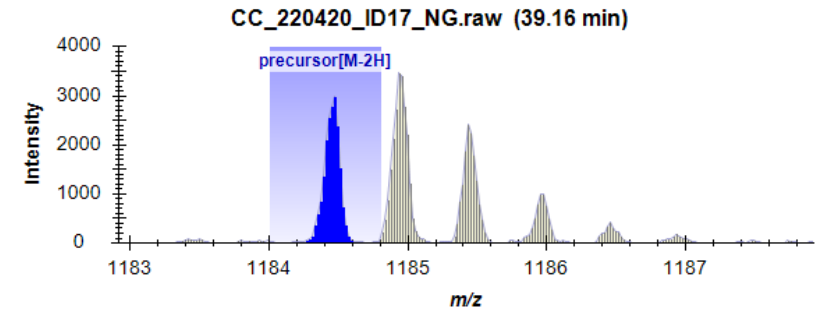
45a



45b



45c

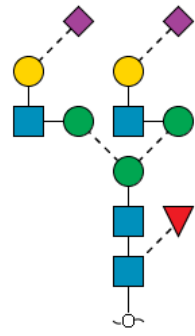


Glycan 45a

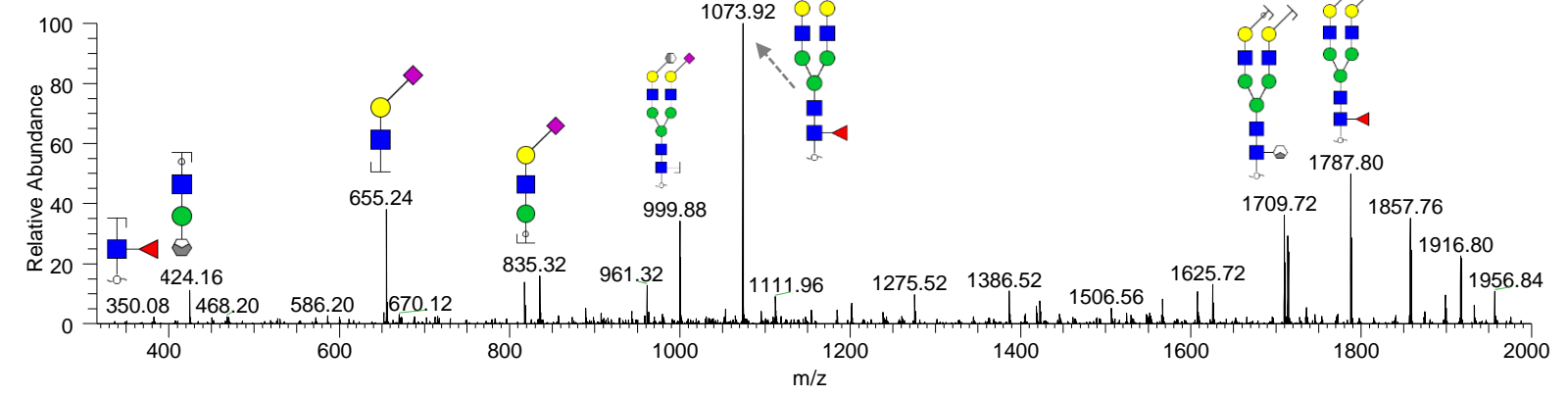
m/z 1184.42 (2-); 789.27 (-3)

Retention time: 26 min

Theo mass [M-H] = 2369.84 Da



CC_220420_ID17_NG #943-1017 RT: 25.76-26.69 AV: 3 NL: 1.72E1
F: ITMS - p ESI E d w Full ms2 1184.44@cid33.00 [315.00-2000.00]

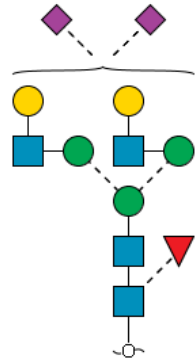


Glycan 45b

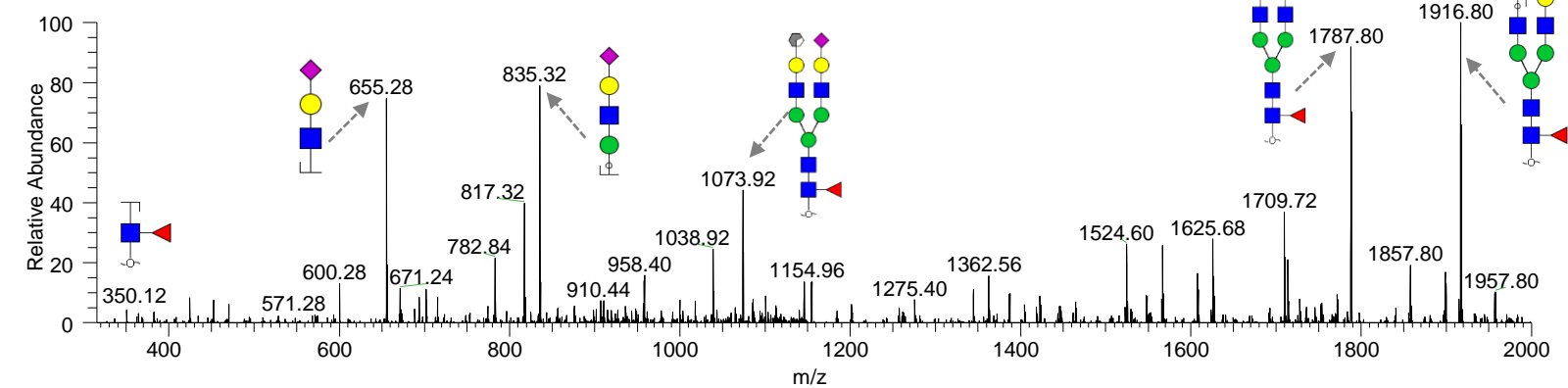
m/z 1184.42 (2-); 789.27 (-3)

Retention time: 33 min

Theo mass [M-H] = 2369.84 Da



CC_220420_ID17_NG #1205-1269 RT: 33.12-33.85 AV: 4 NL: 8.21
F: ITMS - p ESI E d w Full ms2 1184.44@cid33.00 [315.00-2000.00]

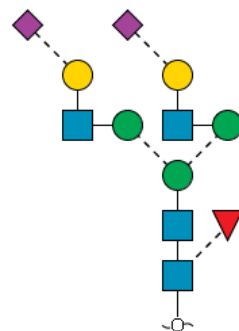


Glycan 45c

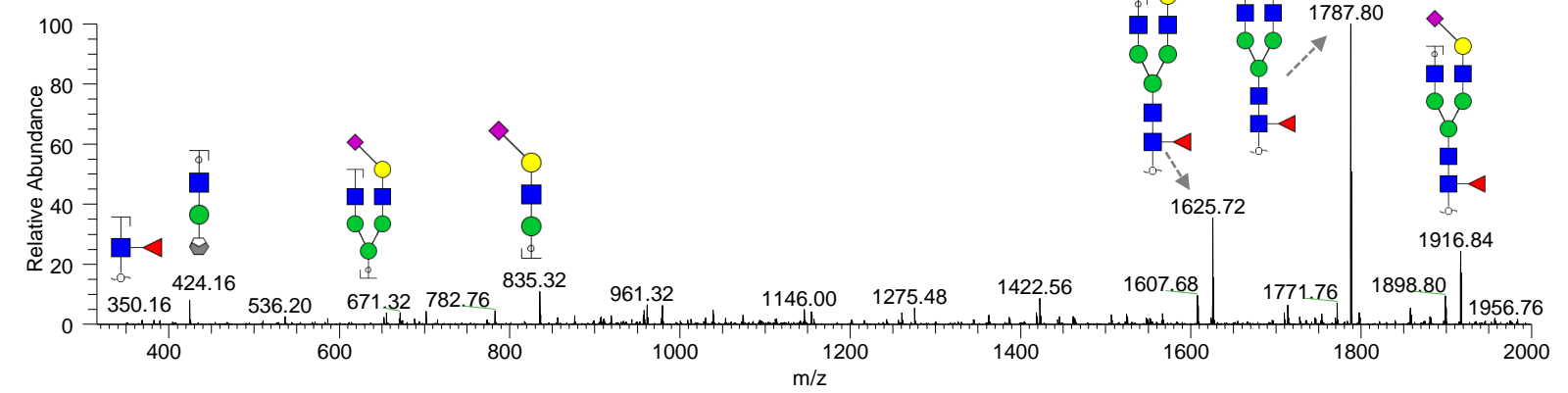
m/z 1184.42 (2-); 789.27 (-3)

Retention time: 39.2 min

Theo mass [M-H] = 2369.84 Da



CC_220420_ID17_NG #1433-1511 RT: 39.75-40.13 AV: 3 NL: 3.74E1
F: ITMS - p ESI E d w Full ms2 1184.44@cid33.00 [315.00-2000.00]



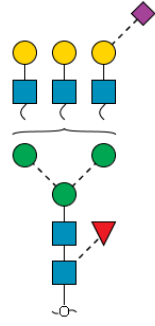
Notes: No distinction intended between 3-arm/6-arm in glycan fragment scheme. This glycan has been annotated as α 2,6 or α 2,3-sialyl isomer based on their elution time and 655/290 ions.

Glycan 46a

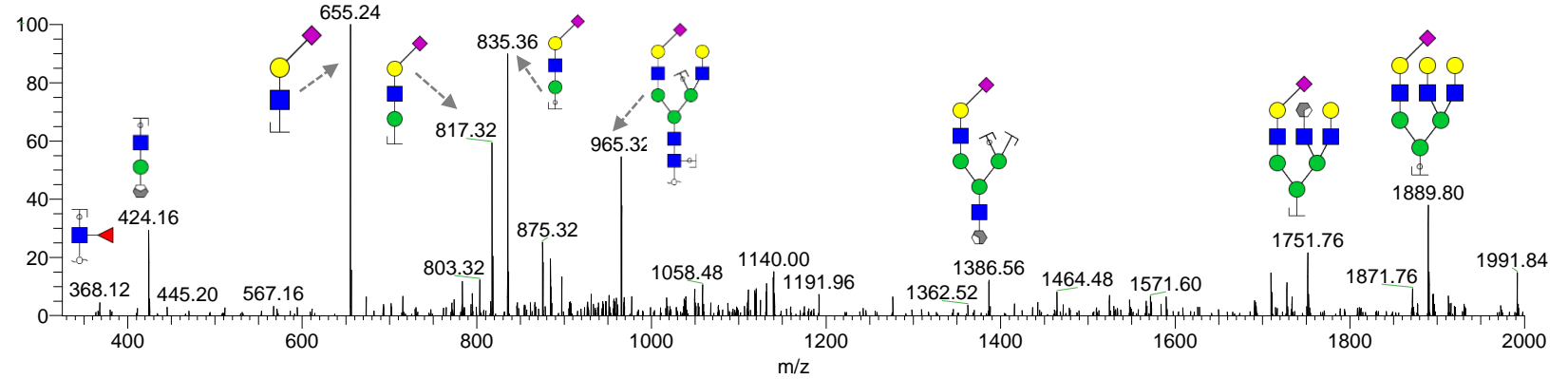
m/z 1221.47 (2-)

Retention time: 28.7 min

Theo mass [M-H] = 2443.94 Da



cc_220420_id24_ng #1036 RT: 28.68 AV: 1 NL: 1.88E1
F: ITMS - p ESI E d w Full ms2 1

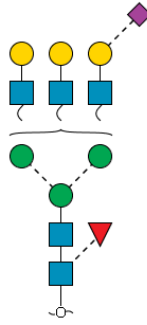


Glycan 46b

m/z 1221.47 (2-)

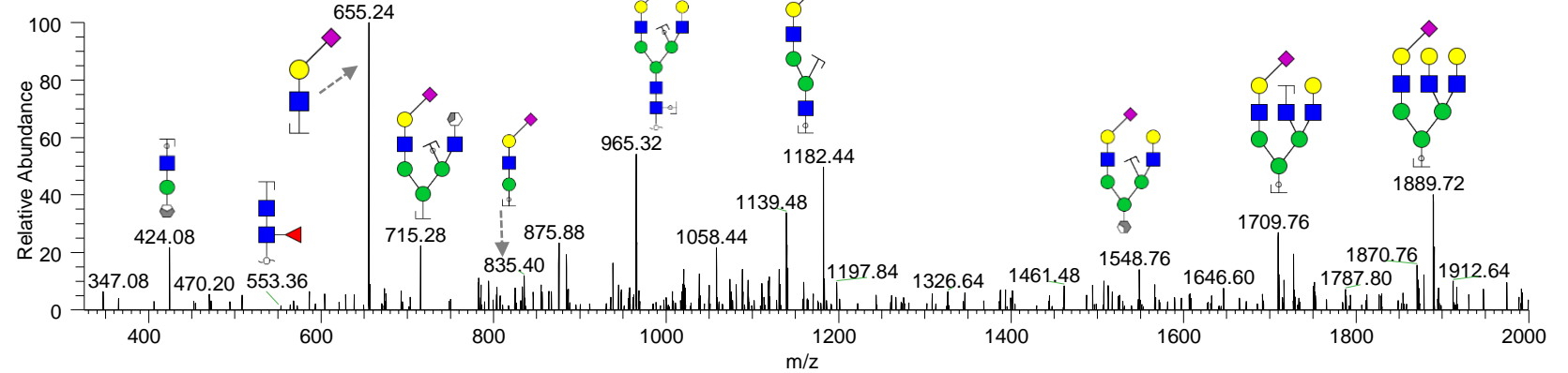
Retention time: 31.9 min

Theo mass [M-H] = 2443.94 Da



cc_220420_id40_ng #1174 RT: 31.44 AV: 1 NL: 8.56

F: ITMS - p ESI E d w Full ms2 1221.43@cid33.00 [325.00-2000.00]

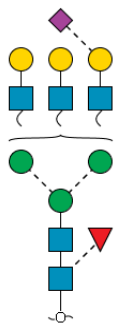


Glycan 46c

m/z 1221.47 (2-)

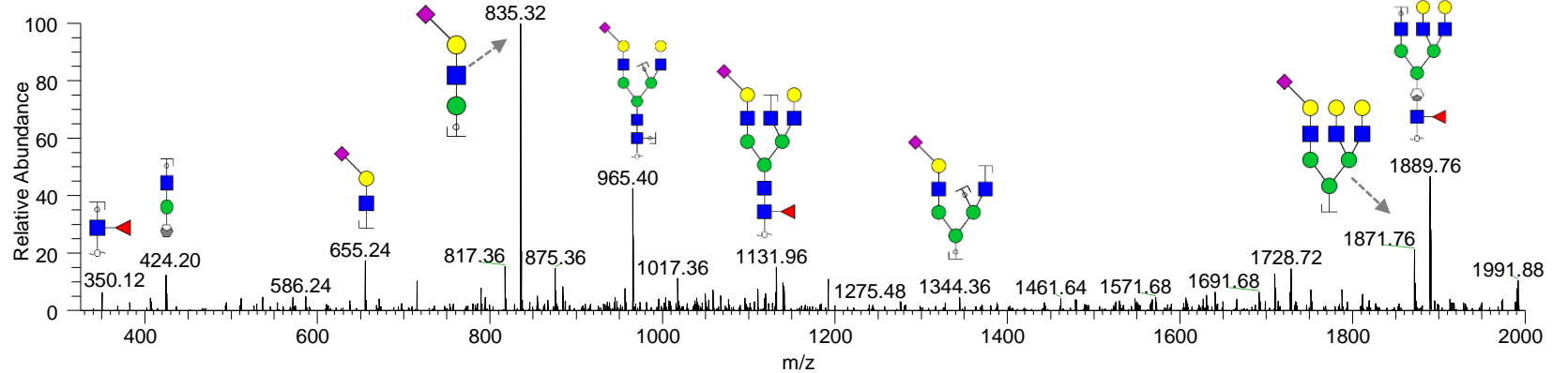
Retention time: 34.9 min

Theo mass [M-H] = 2443.94 Da



cc_220420_id24_ng #1250 RT: 34.90 AV: 1 NL: 2.62E1

F: ITMS - p ESI E d w Full ms2 1221.47@cid33.00 [325.00-2000.00]



Notes: No distinction intended between 3-arm/6-arm in glycan fragment scheme. This glycan has been annotated as α 2,6 or α 2,3-sialyl isomer based on their elution time and 655/290 ions.

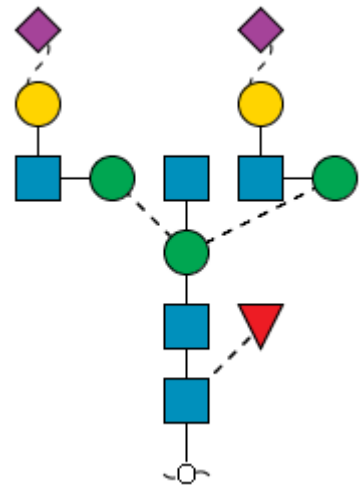
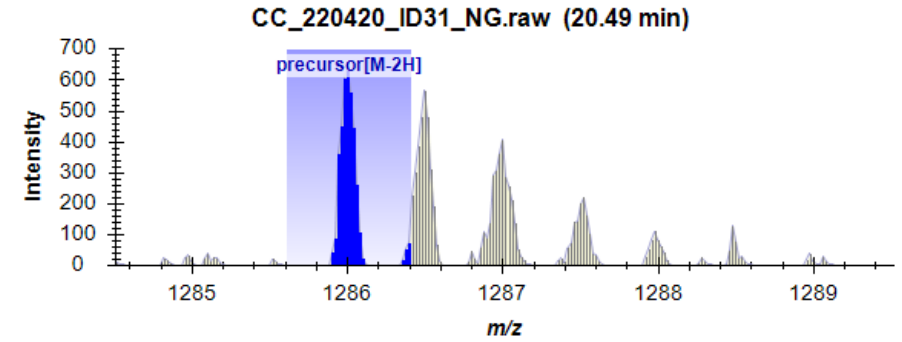
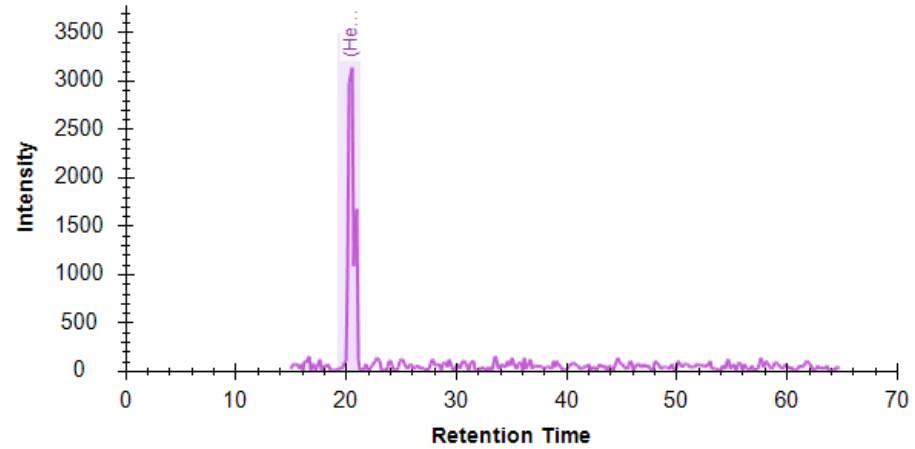
Glycan 47

(Hex)₂(HexNAc)₃(Deoxyhexose)₁(NeuAc)₂ + (Man)₃(GlcNAc)₂

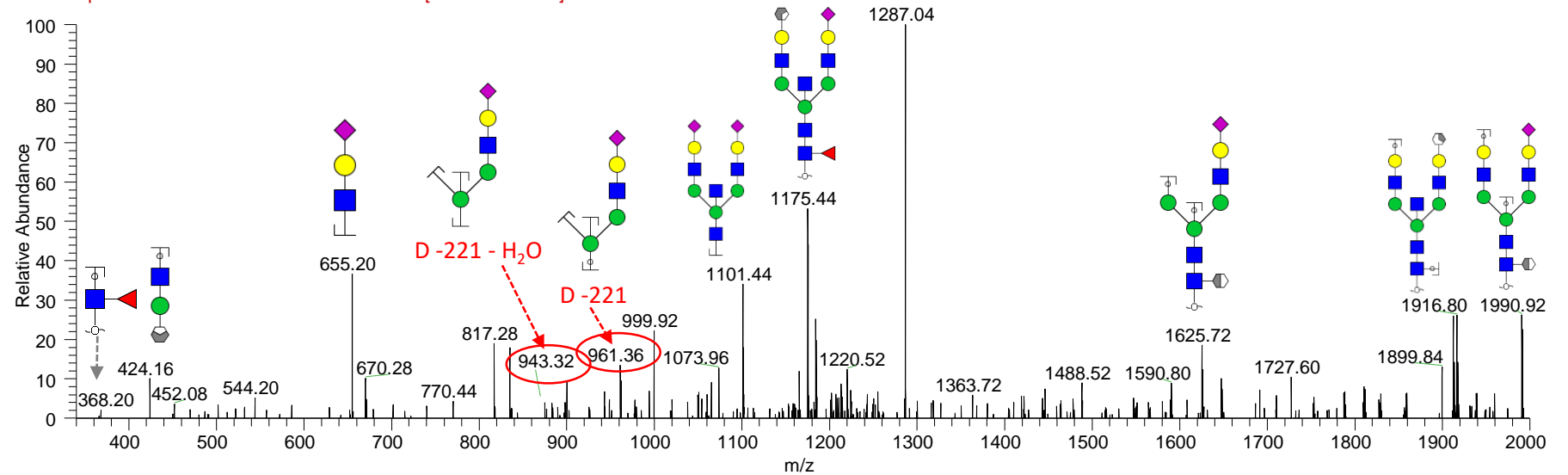
m/z 1286.01 (2-)

Retention time: 19.9 min

Theo mass [M-H] = 2573.02 Da



cc_220420_id31_ng #774-850 RT: 20.58-21.15 AV: 2 NL: 5.67
F: ITMS - p ESI E d w Full ms2 1286.02@cid33.00 [340.00-2000.00]



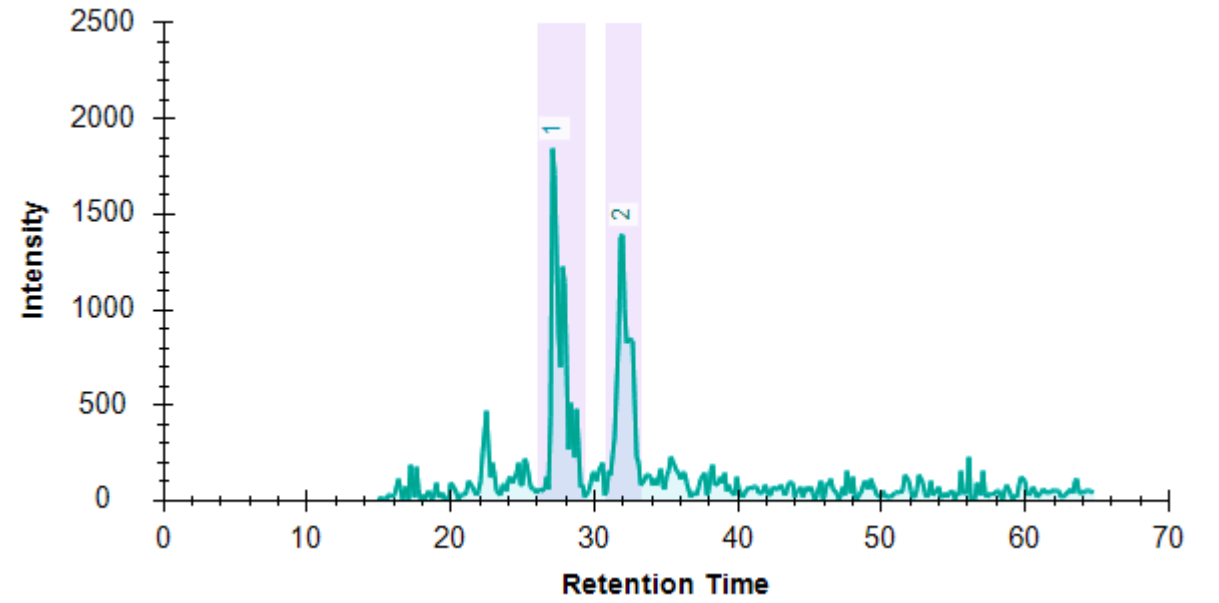
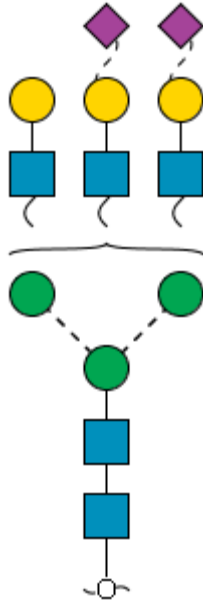
Note: No distinction intended between 3-arm/6-arm in glycan fragment scheme.

Glycan 48

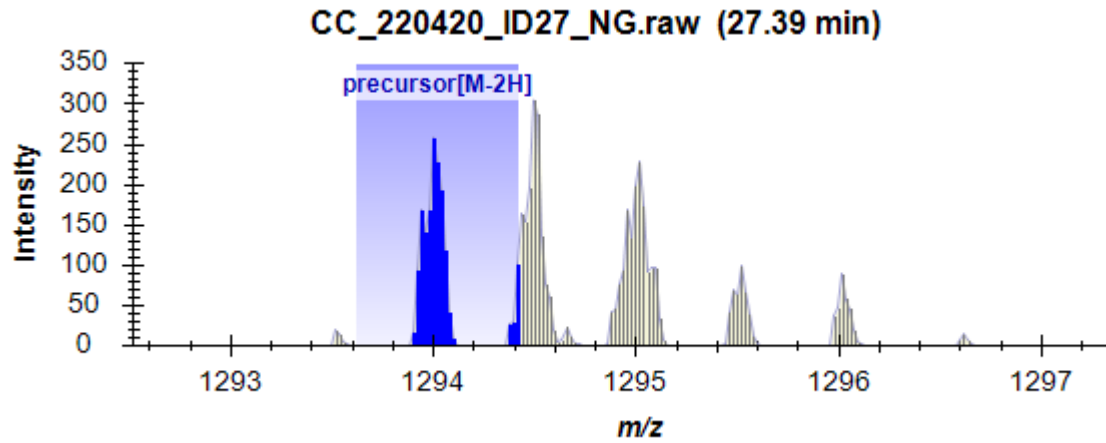
(Hex)₃(HexNAc)₃(NeuAc)₂ + (Man)₃(GlcNAc)₂

m/z 1294.02 (2-)

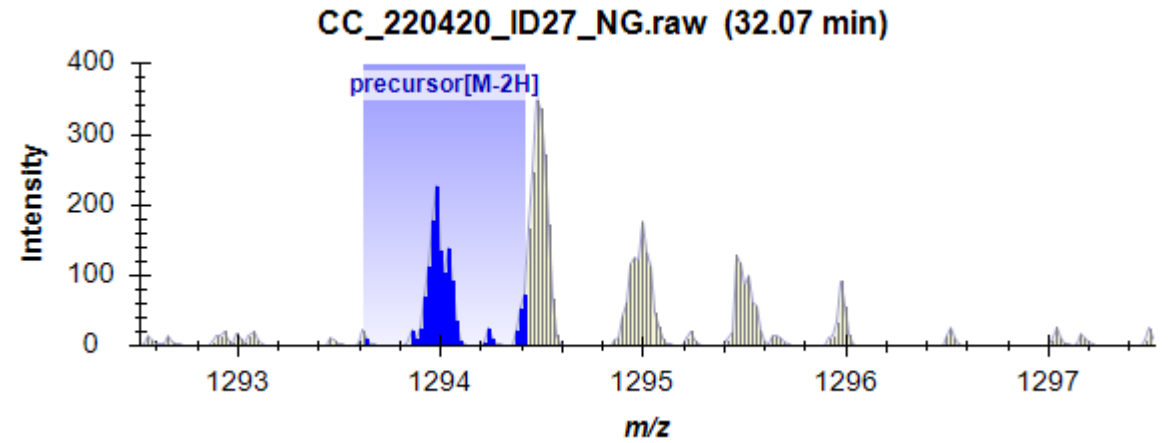
Theo mass [M-H] = 2589.04 Da



48a



48b

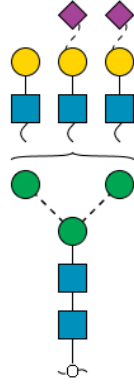


Glycan 48a

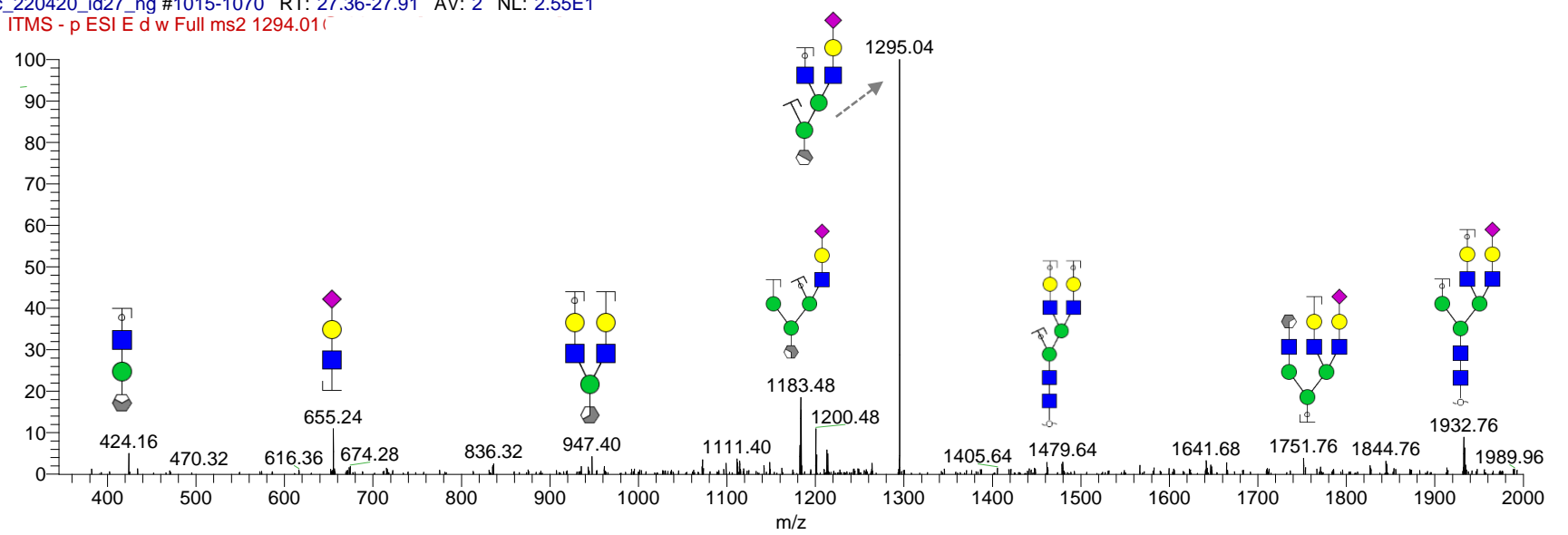
m/z 1294.02 (2-)

Retention time: 27.2 min

Theo mass [M-H] = 2589.04 Da



cc_220420_id27_ng #1015-1070 RT: 27.36-27.91 AV: 2 NL: 2.55E1
F: ITMS - p ESI E d w Full ms2 1294.01



Glycan 48b

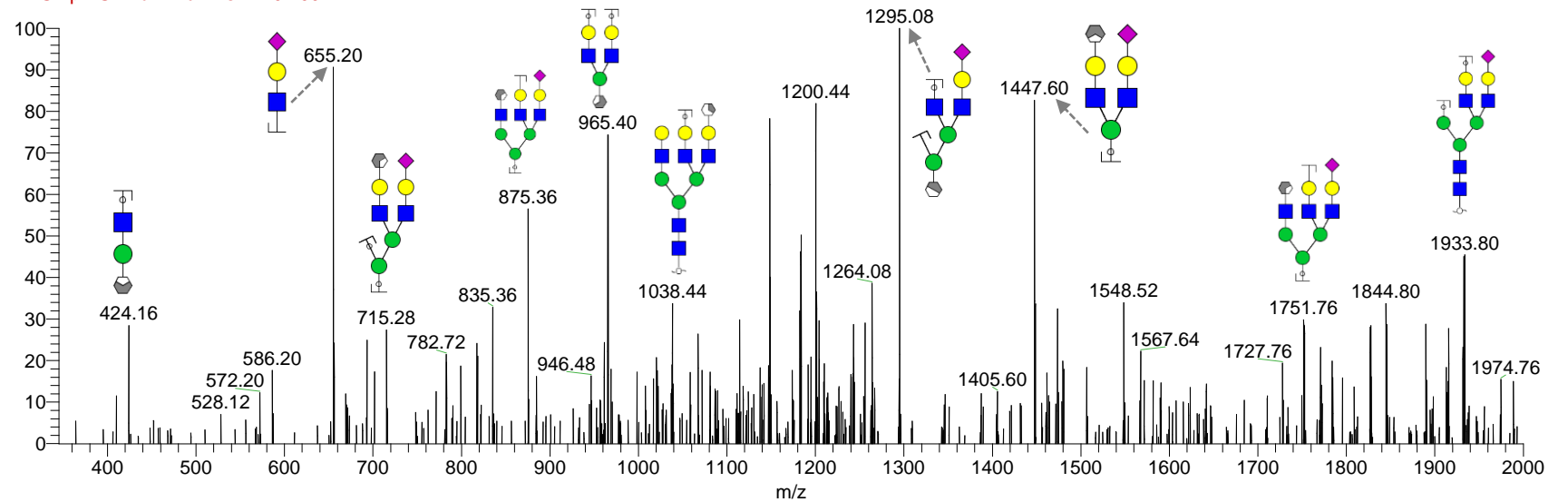
m/z 1294.02 (2-)

Retention time: 32 min

Theo mass [M-H] = 2589.04 Da



cc_220420_id41_ng #1199-1267 RT: 32.86-33.05 AV: 2 NL: 2.80
F: ITMS - p ESI E d w Full ms2 1294.00



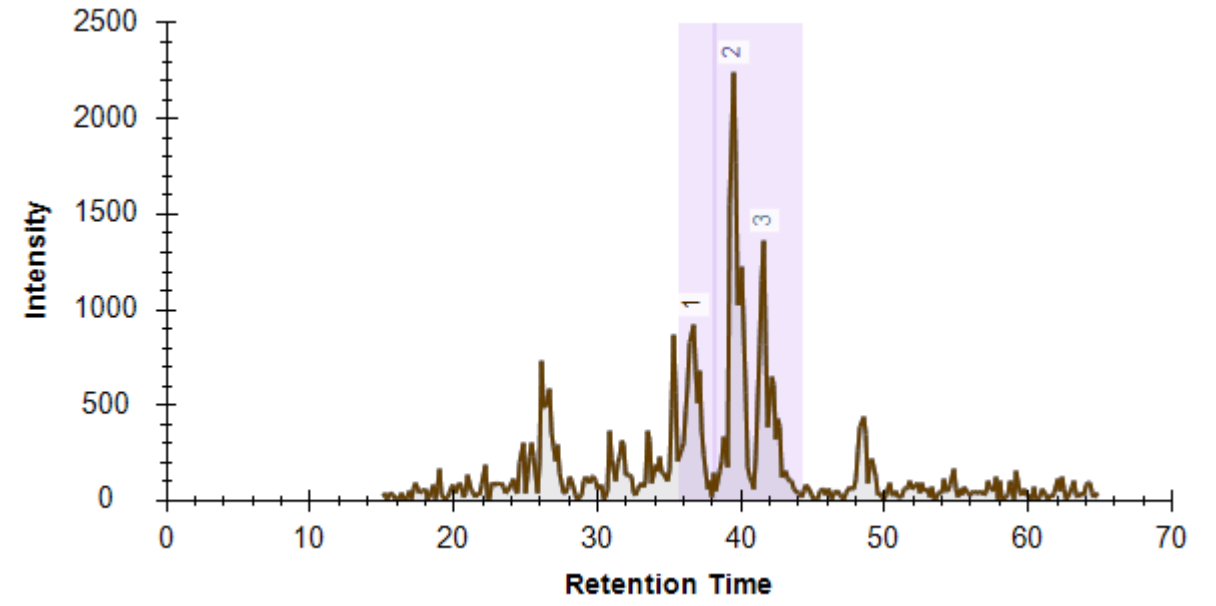
Note: No distinction intended between 3-arm/6-arm in glycan fragment scheme.

Glycan 49

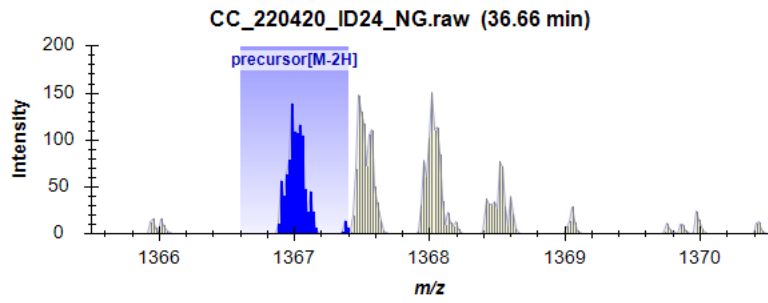
(Hex)3(HexNAc)3(Deoxyhexose)1(NeuAc)2 + (Man)3(GlcNAc)2

m/z 1367.02 (2-)

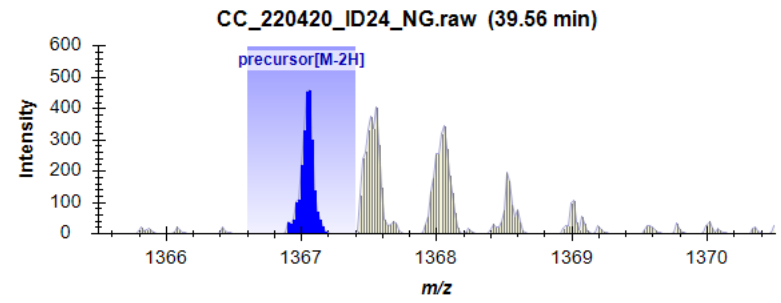
Theo mass [M-H] = 2735.04 Da



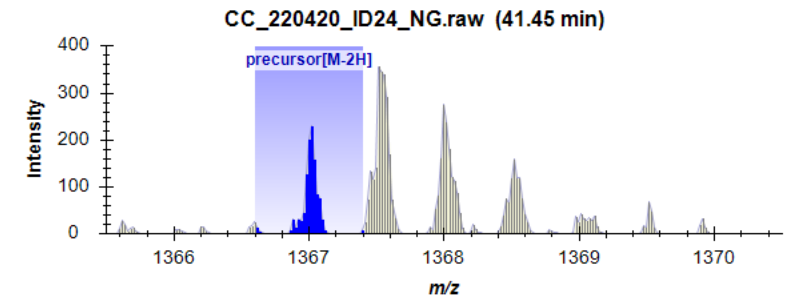
49a



49b



49c

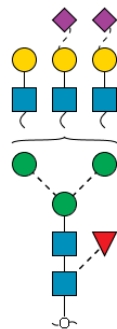


Glycan 49a

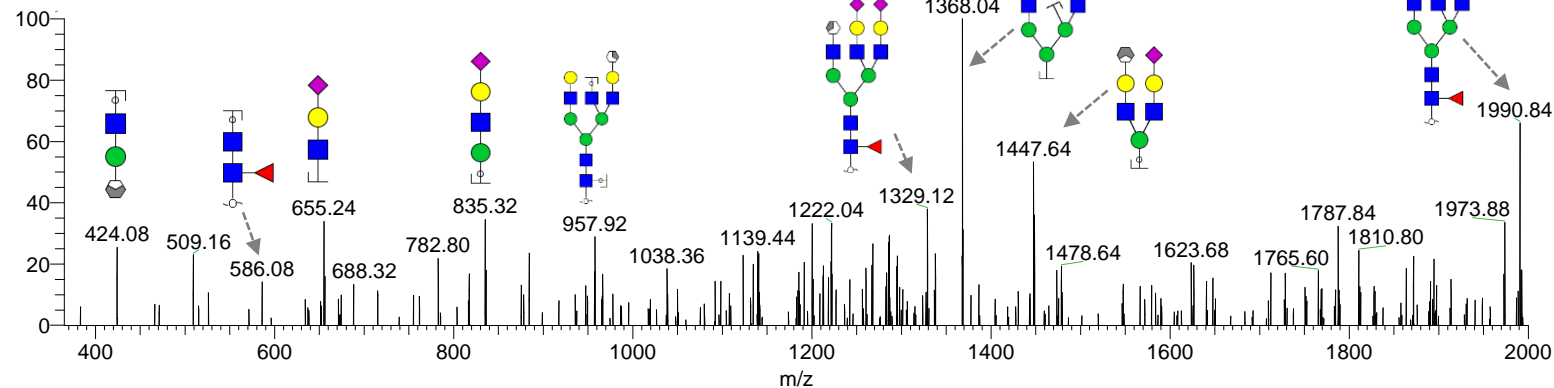
m/z 1367.02 (2-)

Retention time: 36 min

Theo mass [M-H] = 2735.04 Da



cc_220420_id24_ng #1321-1370 RT: 36.77-36.97 AV: 2 NL: 2.20
F: ITMS - p ESI E d w Full ms2 1 [000.00]

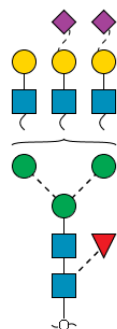


Glycan 49b

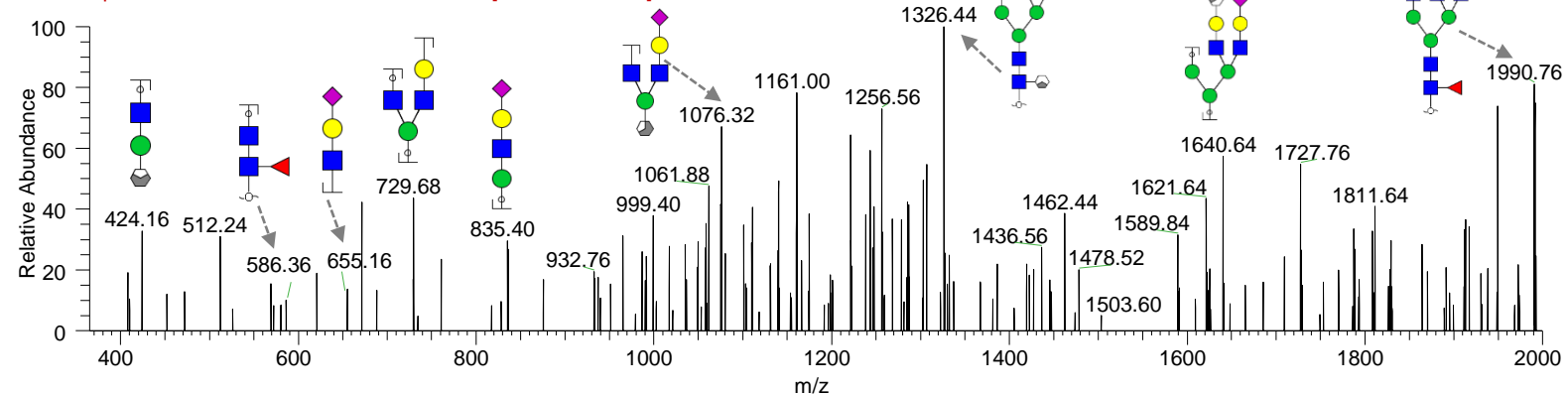
m/z 1367.02 (2-)

Retention time: 39.6 min

Theo mass [M-H] = 2735.04 Da



CC_220420_ID40_NG #1462 RT: 39.57 AV: 1 NL: 1.69
F: ITMS - p ESI E d w Full ms2 1367.03@cid33.00 [365.00-2000.00]

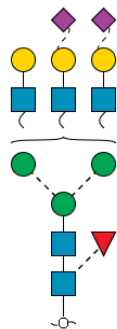


Glycan 49c

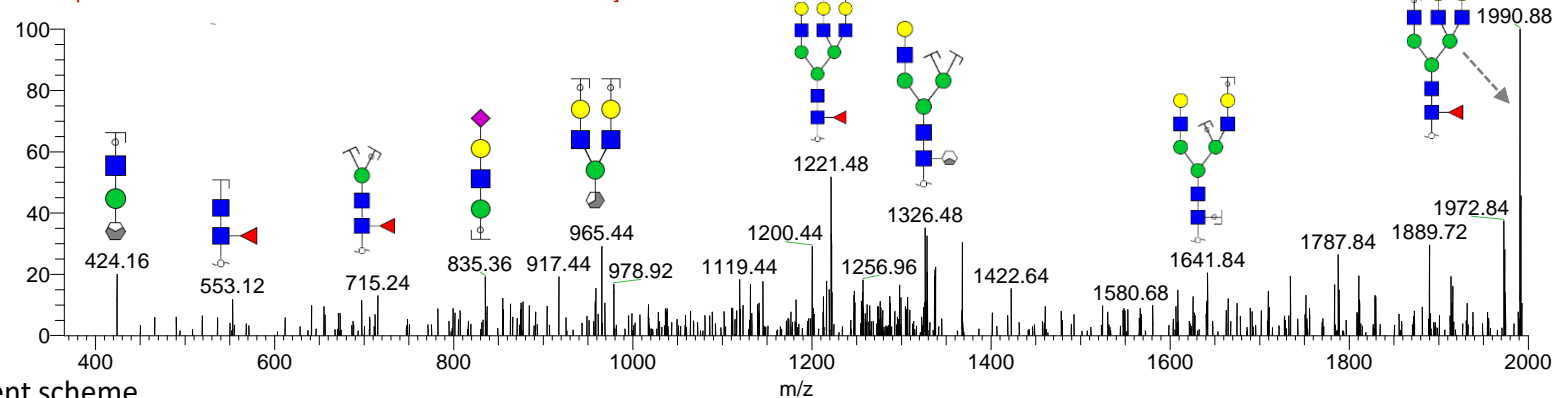
m/z 1367.02 (2-)

Retention time: 41.4 min

Theo mass [M-H] = 2735.04 Da



cc_220420_id24_ng #1496-1547 RT: 41.59-41.95 AV: 3 NL: 2.46
F: ITMS - p ESI E d w Full ms2 1 [000.00]



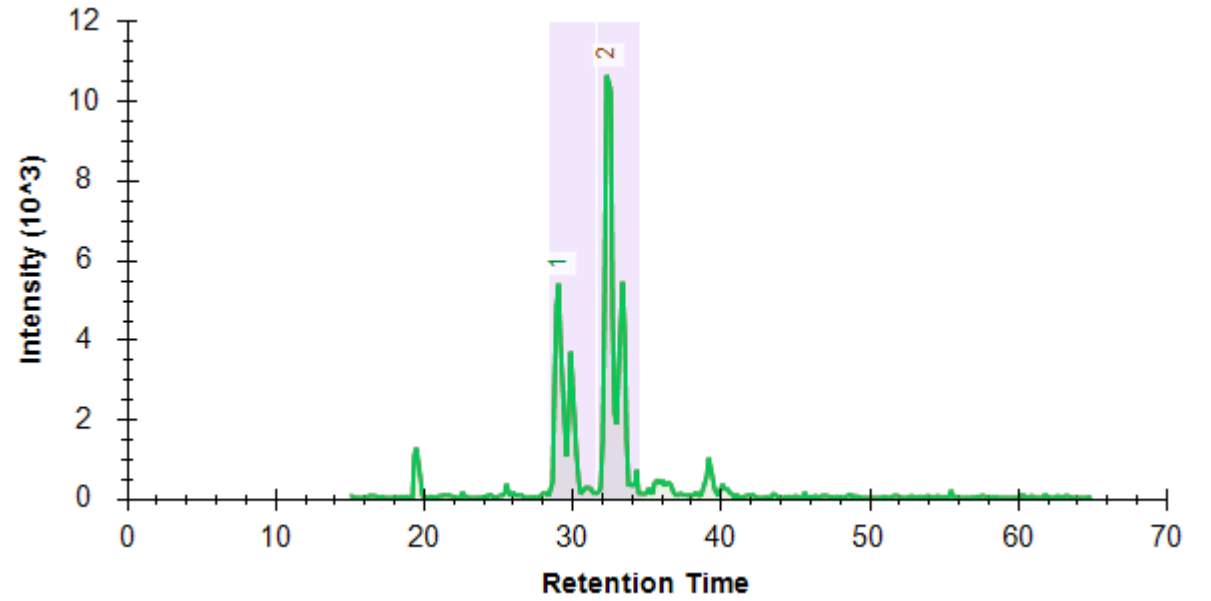
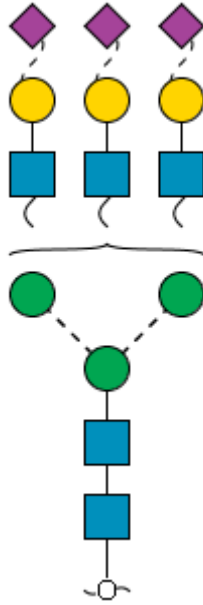
Note: No distinction intended between 3-arm/6-arm in glycan fragment scheme.

Glycan 50

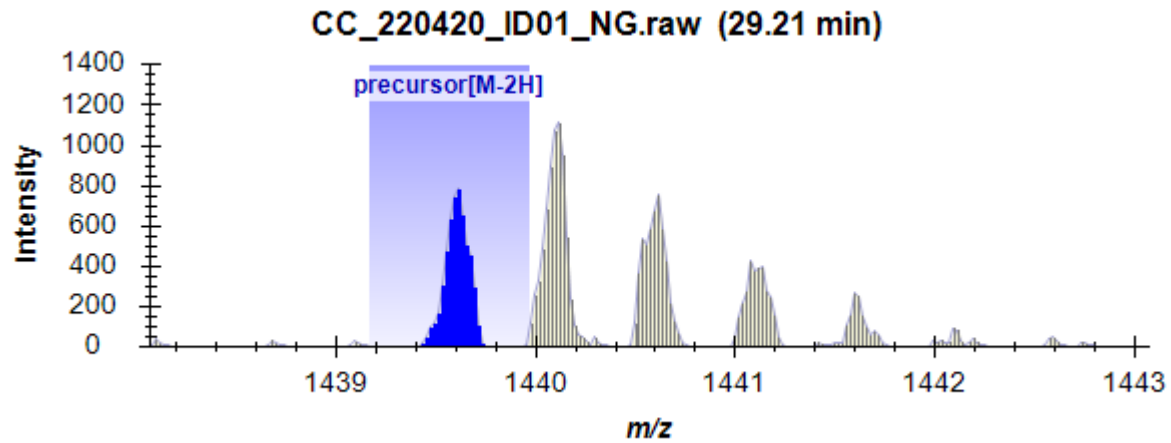
(Hex)₃(HexNAc)₃(NeuAc)₃ + (Man)₃(GlcNAc)₂

m/z 1439.57 (2-)

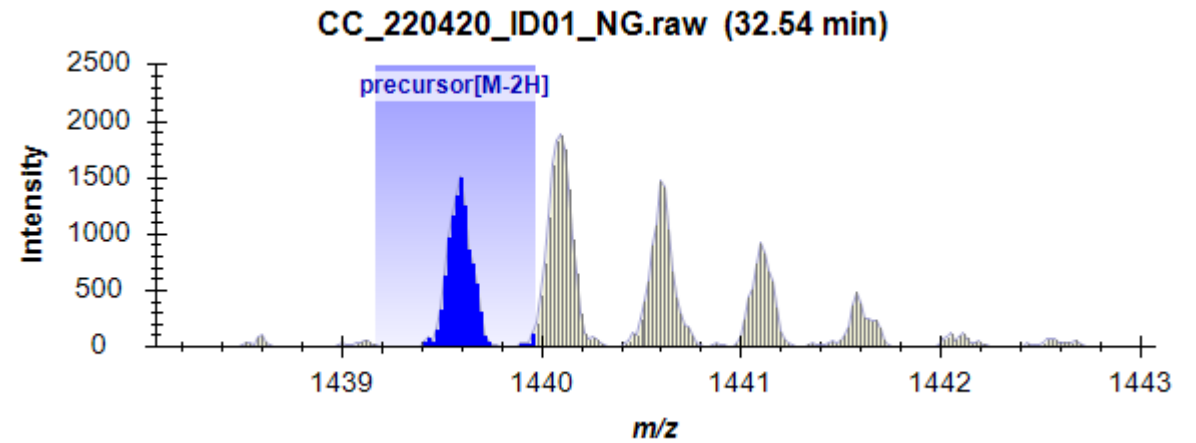
Theo mass [M-H] = 2880.14 Da



50a



50b

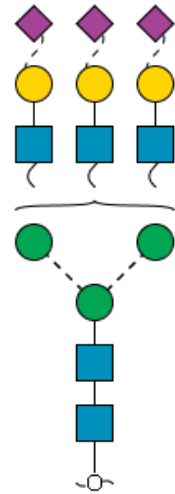


Glycan 50a

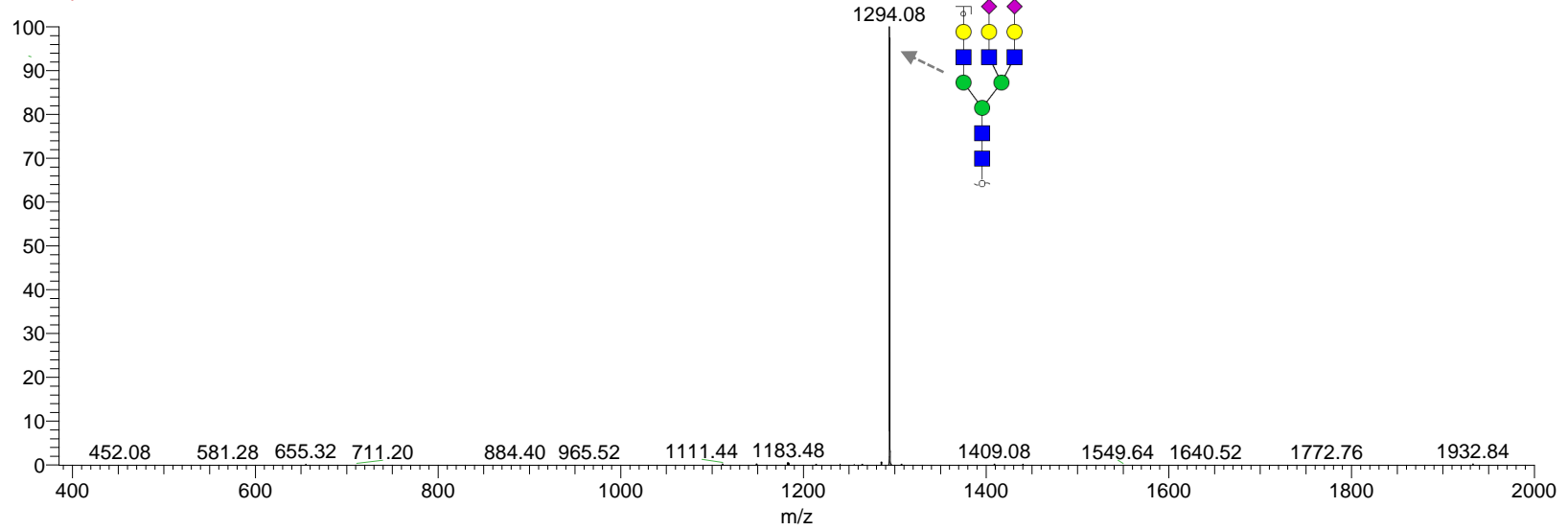
m/z 1439.57 (2-)

Retention time: 29 min

Theo mass [M-H] = 2880.14 Da



CC_220420_ID01_NG #1064-1125 RT: 28.94-29.48 AV: 2 NL: 7.45E2
F: ITMS - p ESI E d w Full ms2 1439.59

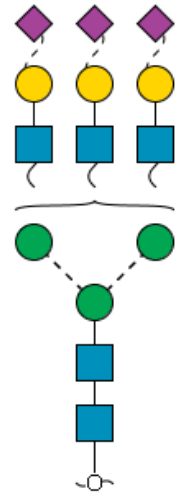


Glycan 50b

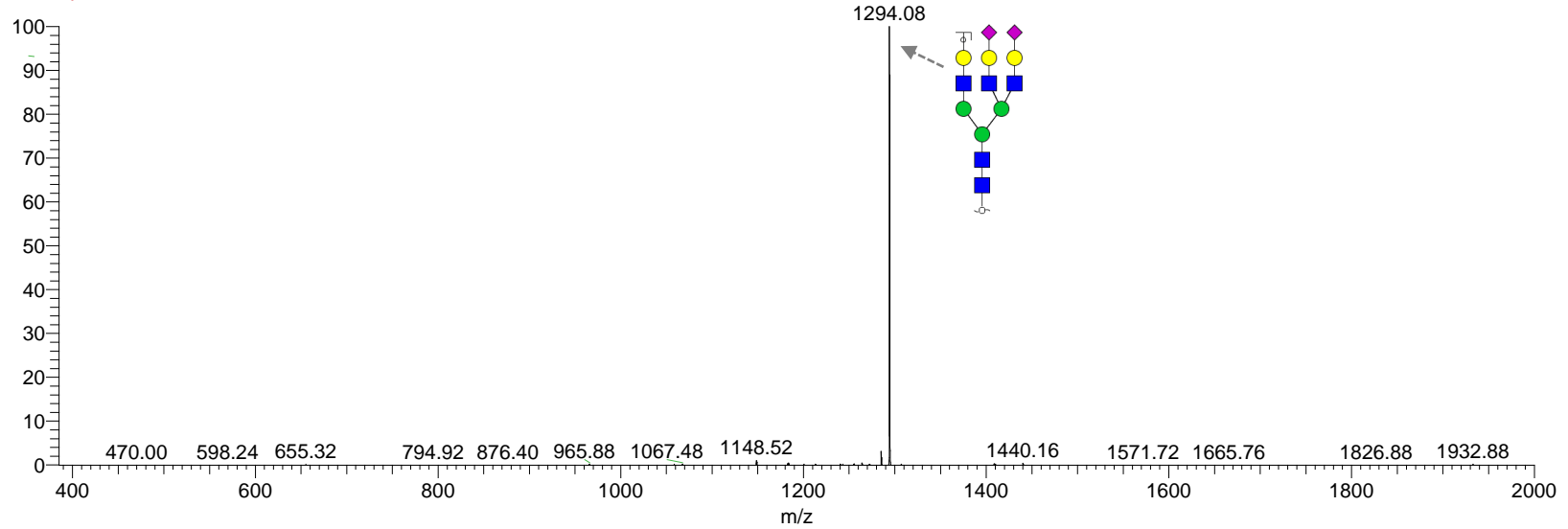
m/z 1439.57 (2-)

Retention time: 32.4 min

Theo mass [M-H] = 2880.14 Da



CC_220420_ID01_NG #1202-1261 RT: 32.82-33.72 AV: 3 NL: 4.81E2
F: ITMS - p ESI E d w Full ms2 1439.59



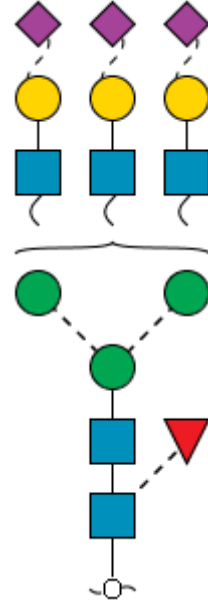
Note: No distinction intended between 3-arm/6-arm in glycan fragment scheme.

Glycan 51

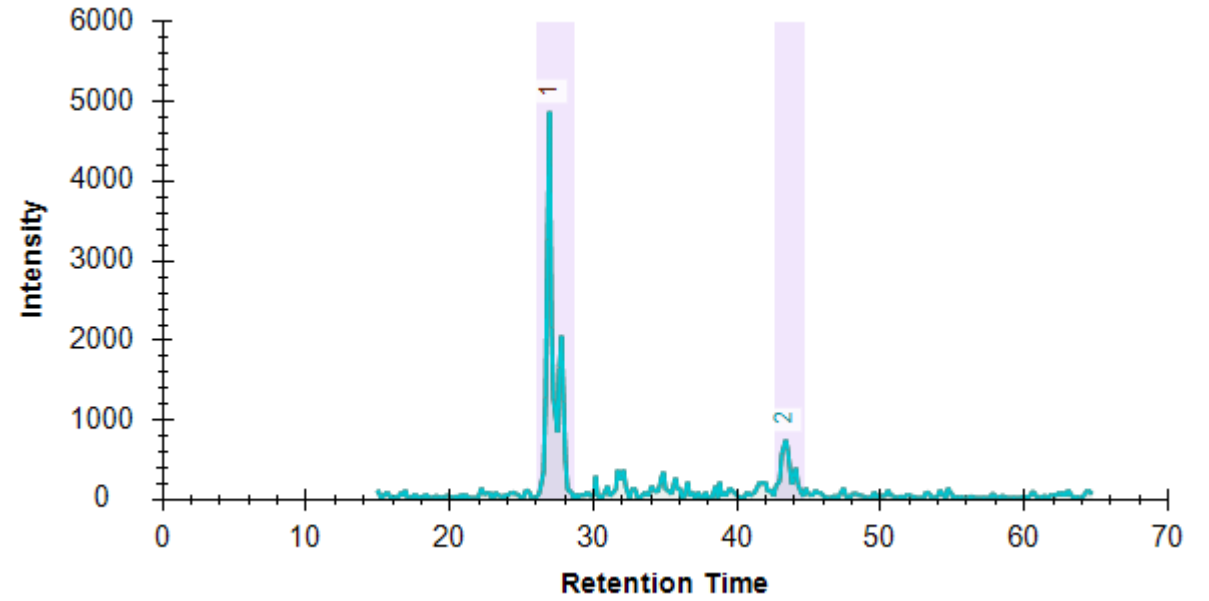
(Hex)3 (HexNAc)3 (Deoxyhexose)1 (NeuAc)3 + (Man)3(GlcNAc)2

m/z 1512.55 (2-)

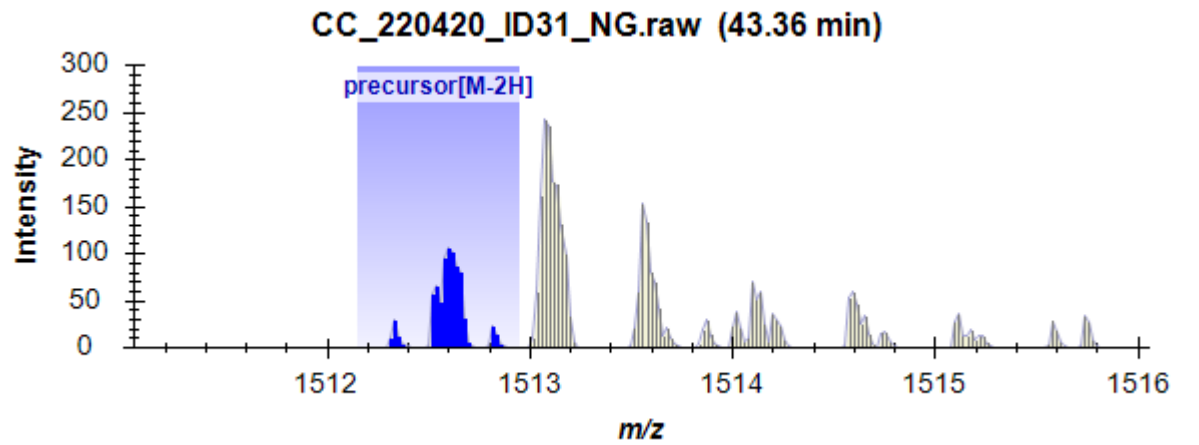
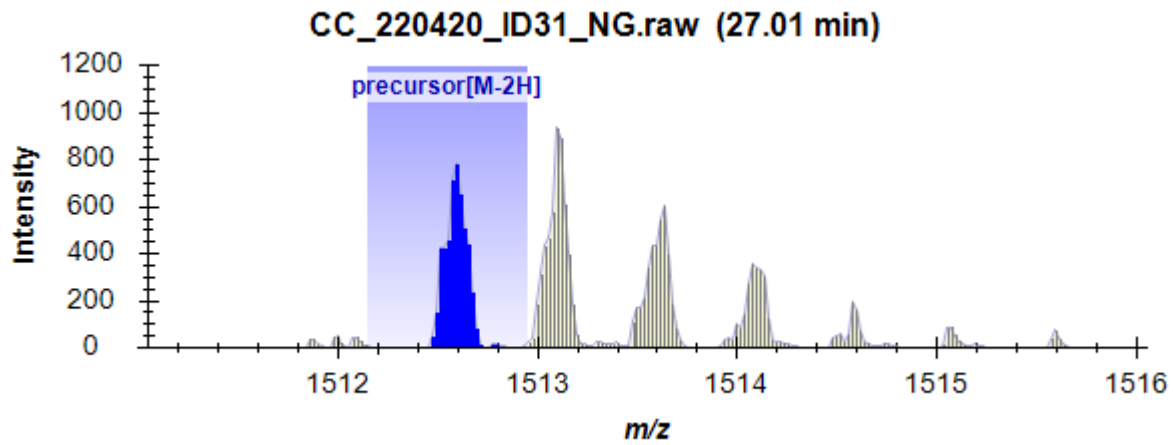
Theo mass [M-H] = 3026.1 Da



51a



51b

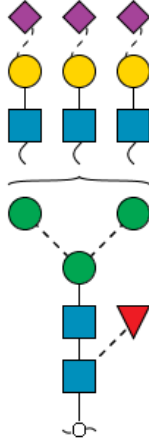


Glycan 51a

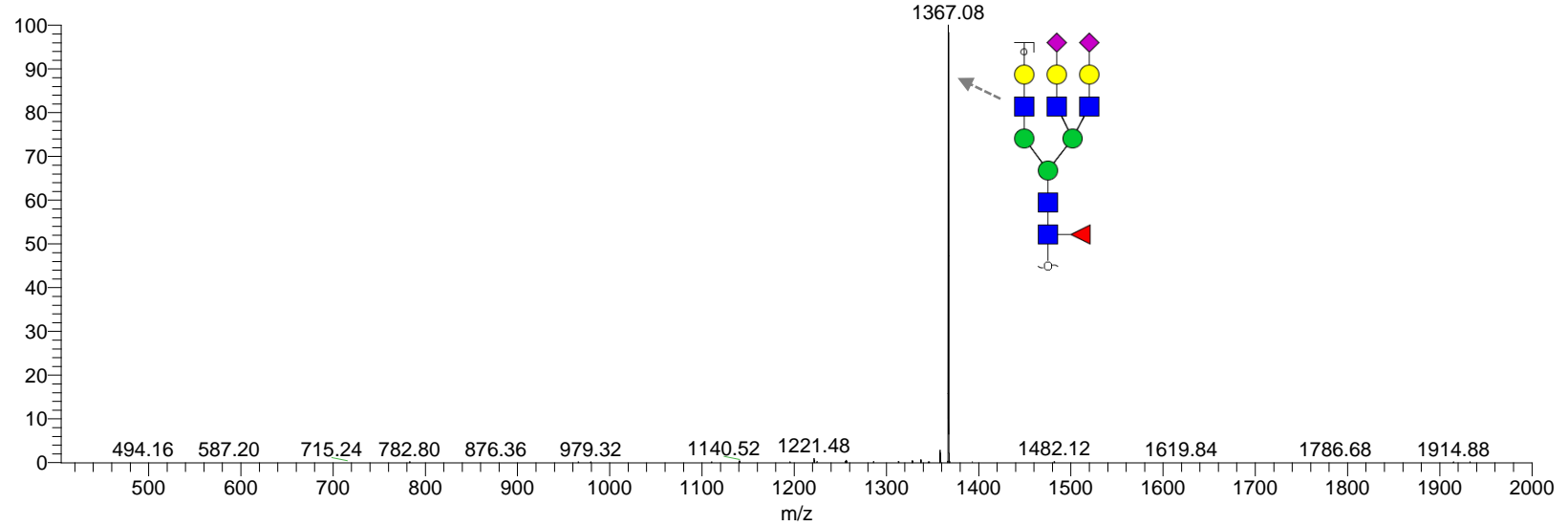
m/z 1512.55 (2-)

Retention time: 26.4 min

Theo mass [M-H] = 3026.1 Da



cc_220420_id31_ng #1014-1086 RT: 26.98-27.90 AV: 2 NL: 6.01E2
F: ITMS - p ESI E d w Full ms2 1512.60

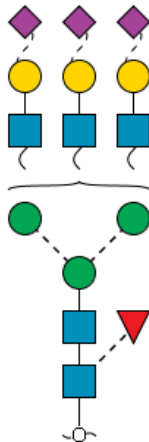


Glycan 51b

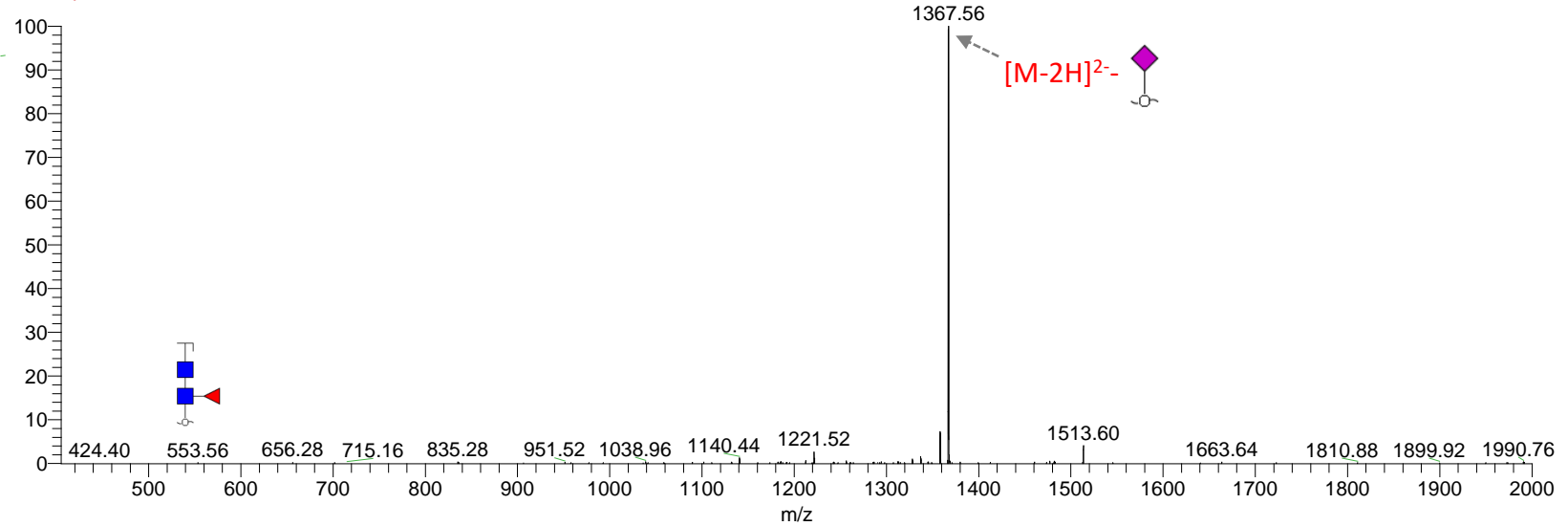
m/z 1512.55 (2-)

Retention time: 42.9 min

Theo mass [M-H] = 3026.1 Da



cc_220420_id40_ng #1551-1624 RT: 42.86-43.26 AV: 2 NL: 1.70E2
F: ITMS - p ESI E d w Full ms2 1512.55



Note: No distinction intended between 3-arm/6-arm in glycan fragment scheme.

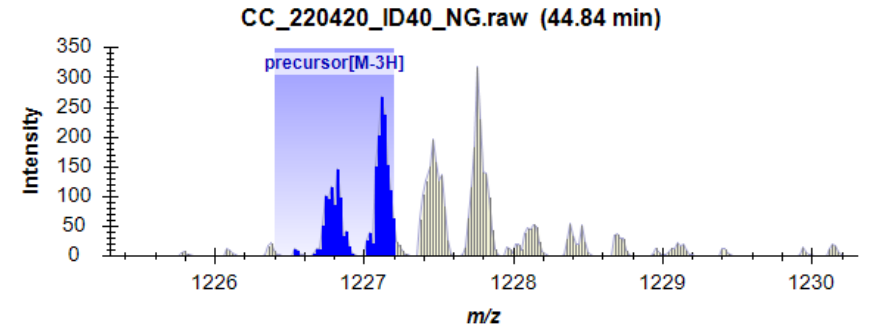
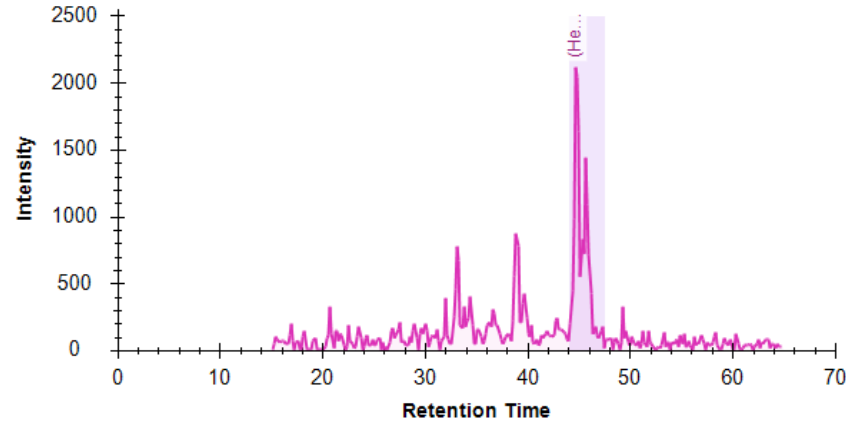
Glycan 52

(Hex)4 (HexNAc)4 (Deoxyhexose)1 (NeuAc)4 + (Man)3(GlcNAc)2

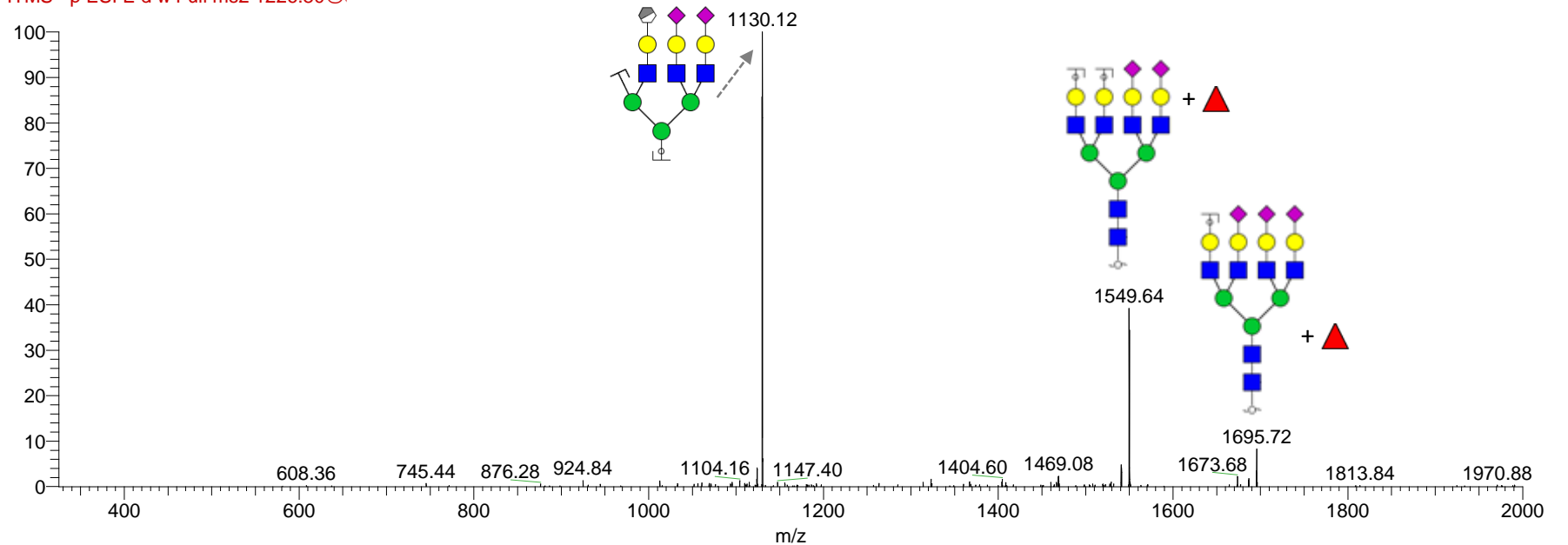
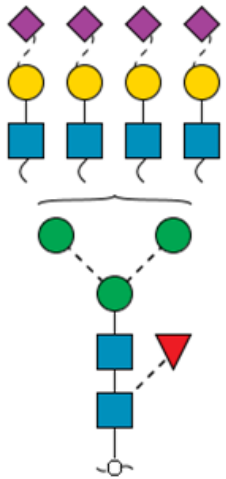
m/z 1226.80 (3-)

Retention time: 45 min

Theo mass [M-H] = 3682.4 Da



CC_220420_ID40_NG #1635 RT: 44.80 AV: 1 NL: 1.22E2
F: ITMS - p ESI E d w Full ms2 1226.80@



Note: No distinction intended between 3-arm/6-arm in glycan fragment scheme.